HIGHWAY RESEARCH **RECORD**

Number 145

Buried Circular Conduits
and
Behavior of Foundations

8 Reports

HIGHWAY RESEARCH BOARD

Department of Soils, Geology and Foundations

Eldon J. Yoder, Chairman
Joint Highway Research Project
Purdue University, Lafayette, Indiana

Chester McDowell, Vice Chairman
Supervising Soils Engineer
Texas Highway Department, Austin

HIGHWAY RESEARCH BOARD STAFF

A. W. Johnson, Engineer of Soils and Foundations
J. W. Guinnee, Assistant Engineer of Soils and Foundations

DIVISION B

H. Bolton Seed, Chairman
Department of Civil Engineering
University of California, Berkeley

Carl L. Monismith, Vice Chairman
University of California, Berkeley

COMMITTEE ON STRENGTH AND DEFORMATION CHARACTERISTICS OF PAVEMENT SECTIONS

(As of December 31, 1965)

Carl L. Monismith, Chairman
University of California, Berkeley

E. S. Barber, Consulting Engineer, Soil Mechanics and Foundations, Arlington, Virginia

Bonner S. Coffman, Department of Civil Engineering, Ohio State University, Columbus

B. E. Colley, Manager, Paving Development Section, Portland Cement Association, Skokie, Illinois

F. N. Finn, Chief Engineer, Materials Research and Development, Oakland, California

Raymond A. Forsyth, Senior Materials and Research Engineer, Materials and Research Department, California Division of Highways, Sacramento

W. S. Housel, University of Michigan, Ann Arbor

W. Ronald Hudson, Department of Civil Engineering, University of Texas, Austin

R. L. Kondner, Associate Professor of Civil Engineering, Department of Civil Engineering, Northwestern University, Evanston, Illinois

H. G. Larew, Department of Civil Engineering, University of Virginia, Charlottesville

T. F. McMahon, U. S. Bureau of Public Roads, Washington, D. C.

B. P. Shields, Research Council of Alberta, Edmonton, Alberta, Canada

Eugene L. Skok, Jr., Department of Civil Engineering, University of Minnesota, Minneapolis

J. E. Stephens, Professor of Civil Engineering, University of Connecticut, Storrs

Aleksandar S. Vesić, Duke University, Durham, North Carolina

Foreword

The several authors furnishing papers for this RECORD bring together phases of soil mechanics ranging from a basic numerical approach through design of conduits to layered systems of pavement structures. These papers are of interest to soils, foundations, and design engineers.

Watkins proposes a method for the structural design of buried flexible conduits based on the assumption that the conduit ring is just one component of a soil-structure interaction system. He considers the soil as not only exerting a pressure on the flexible conduit, but also contributing structural strength as determined by the relative stiffness of the soil and conduit ring. By this approach rigid conduits are but a limiting case of flexible conduits and may be analyzed by the same method.

Goodman et al present the results of studies of plate sinkage in sands and clays. The importance of size effects and scaling considerations are discussed in relation to vehicle sinkage problems. The fundamental soil properties which influence plate sinkage are of importance to highway soils engineers in relation to soil strength for pavement design as well as off road mobility.

Perloff et al describe the relationships between pressure on model footings and penetration of these footings into saturated cohesive soils. Empirical relations are developed and conclusions based on these are presented. This presentation will be of interest to bridge design engineers and foundation engineers.

De Barros presents two papers, one dealing with a deflection factor chart for layered elastic systems and the other with an application of the three-layer system method to an evaluation of soil-cement bases. These methods are of importance to a rational design or analysis of pavement systems. Kirk presents tables of radial stresses in the top layer of a three-layer elastic system as an additional contribution to the "art" of pavement design and analysis as do Kondner et al in the abridgment of their paper on load-deflection responses.

Schimming et al make a valuable contribution to the field of soil mechanics in this presentation of a numerical determination of stresses in earth masses. Rigid boundary effects and both spatial and time variations in material properties are treated by techniques based on finite difference approximations to the governing differential equations. A brief discussion of the development of slip-line patterns for stability problems utilizing numerical techniques concludes this paper.

Contents

Structural Design of Buried Circular Conduits

REYNOLD K. WATKINS
Professor and Head, Mechanical Engineering Department,
Utah State University

•THE FIRST attempts to structurally design buried circular conduits were limited to rigid conduits such as clay pipe and concrete pipe. Analysis started with the conduit ring as a free-body diagram (1). The vertical soil load was calculated, and kept less than a three-edge bearing load which developed a 0.01-in. crack in a laboratory sample ·of the same conduit. The procedure was only approximate, but adequate. The basic principles are still in use. These methods were not adequate for flexible conduits such as corrugated metal conduits, however, and a modification was proposed (1). Again, the analysis started with a free-body diagram of the conduit ring with soil loads acting on it, but the horizontal support of the soil which resists lateral deflection of the conduit was also considered. The basis for design was either a maximum allowable change in diameter or a maximum allowable stress in the conduit wall. Although rational, the method is based on a hard-to-measure soil modulus of passive resistance, and has not been useful in average design.

This paper proposes a practical method for the structural design of buried flexible conduits, based on the assumption that the conduit ring is just one component of a soil-structure interaction system. The soil exerts pressure on the flexible conduit, but it also contributes structural strength which is determined by the relative stiffness of the soil and conduit ring. According to this approach, the rigid conduit is simply a limiting case of flexible conduit, and may be analyzed by the same method.

SCOPE

The following analysis does not apply to bored-into-place conduits in which soil pressures may be relieved at the soil-conduit interface.

It is assumed that the soil is homogeneous and of great extent all about the conduit. This implies that a soil fill is placed up around the conduit rather than backfilled into a trench. Experience shows that this same assumption applies with less than 10 percent error for trench installations if the trench width is greater than twice the diameter of the conduit. A simple factor adapts the method to narrow trench installations (2).

Soil displacements are assumed so small that no major localized shear failure planes develop in the soil. This approach applies most accurately if conduit ring deflections are small, perhaps less than 10 percent. This limitation is not critical, however, and the procedure can be modified to account for gross soil displacements.

Soil cohesion is not included specifically. This is conservative and reasonable for highway installations because the soil is usually granular.

In the cases presented in this paper, friction between soil and conduit is neglected, the soil is assumed to be elastic, and the conduit ring configuration remains elliptical. These restrictions are not imperative, but make the mathematics simple yet sufficiently accurate for average design.

ANALYSIS

Analysis of a buried conduit requires a knowledge of the conduit ring (stiffness, yield strength, etc.), and also of the properties of soil and of the performance of soil as a structure. Often the soil is more important structurally than the conduit, and in extreme cases may be so structurally strong that it can retain a passageway without support from the conduit. The principle was used in ancient brick sewers of Paris—

the brick being simply well-compacted, well-placed soil. Under such circumstances, a conduit would serve merely to prevent raveling and erosion of the passageway. For most installations, however, the soil and conduit ring both contribute strength to the soil-conduit structure.

Analysis must be based on a rational criterion for failure. Failure of the soil-conduit system is defined as excessive deformation of the conduit ring; that is, the ring deforms so much that either (a) the conduit cannot perform its transport function, or (b) the soil cannot perform its support function. Failure may be excessive ring deflection (i. e., flattening down of the ring), or it may be crippling of the conduit wall. Crippling may occur as crushing of the wall or as reversal of curvature (snap-through).

Crippling failures are incipient at some maximum ring-compression stress in the conduit wall. Analysis amounts to the prediction of that ring-compression stress. Tests indicate that in some soils the conduit can actually withstand a greater load than the crippling failure load because as the conduit deforms more and more, it simply transmits more and more of its load to the soil. This case is not considered here. Crippling failure is analyzed in the following paragraphs for the ideal limiting case of noncompressible soil, and for compressible soil.

Crippling Failure

Noncompressible Soil (Idealized Limiting Case). — For soil-conduit systems in which the soil compressibility is zero (i. e., the soil modulus E' from a confined compression test is infinity), reasonable methods of analysis are available. For the limiting high soil friction angle, $\phi \rightarrow 90$ deg, a ring-compression method of analysis is proposed (3). If the conduit is perfectly flexible (like a watchband), and if it is assumed that no shearing stresses act between the soil and conduit, the radial soil pressure against the conduit is

$$p = \frac{T}{r} \qquad (1)$$

where

p = radial soil pressure;

T = tangential thrust or ring-compression force in conduit wall (constant if shearing stresses are neglected and ring is perfectly flexible); and

r = radius of curvature for conduit (constant if conduit ring is circular).

Taking the top half of the conduit as a free-body diagram (Fig. 1), the ring-compression stress in the conduit wall is T/A. The strength is simply yield point stress S_{yp},

where

T/A = tangential or ring-compression stress (if conduit is perfectly flexible, no flexural stresses develop);

A = tangential thrust in conduit wall = $p_V D/2A$ for noncompressible soil and noncompressible conduit perimeter;

p_V = calculated vertical soil pressure at level of conduit (height of fill times unit weight plus influence of surface loads);

A = cross-sectional area of conduit wall per unit length of conduit; and

S_{yp} = yield point strength of conduit wall.

For design, the stress T/A must be less than yield point by a factor of safety.

In Figure 1, the allowable stress, S_{yp}, plots as a horizontal straight line. Of course, everything is noncompressible and the soil friction angle is high.

On the same diagram is a plot of ring-compression strength for soil with a zero friction angle, $\phi \rightarrow 0$ deg. Because the soil is still assumed to be noncompressible, this is tantamount to hydrostatic pressure for which critical pressure, p, is related by the following dimensionless form (4):
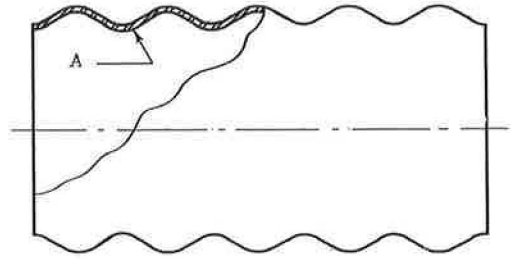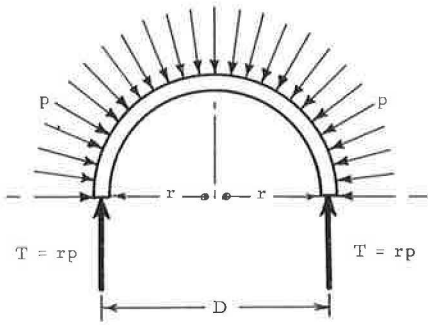
T = compression thrust in conduit wall,
D = mean diameter of conduit,
E = modulus of elasticity of conduit,
p = soil pressure on the conduit,
r = radius of curvature at thrust point.

A = cross sectional area of conduit wall per
    unit length of conduit,
k = radius of gyration of the wall cross
    sectional area.

$$\text{RING COMPRESSION STRESS} = \frac{T}{A}$$
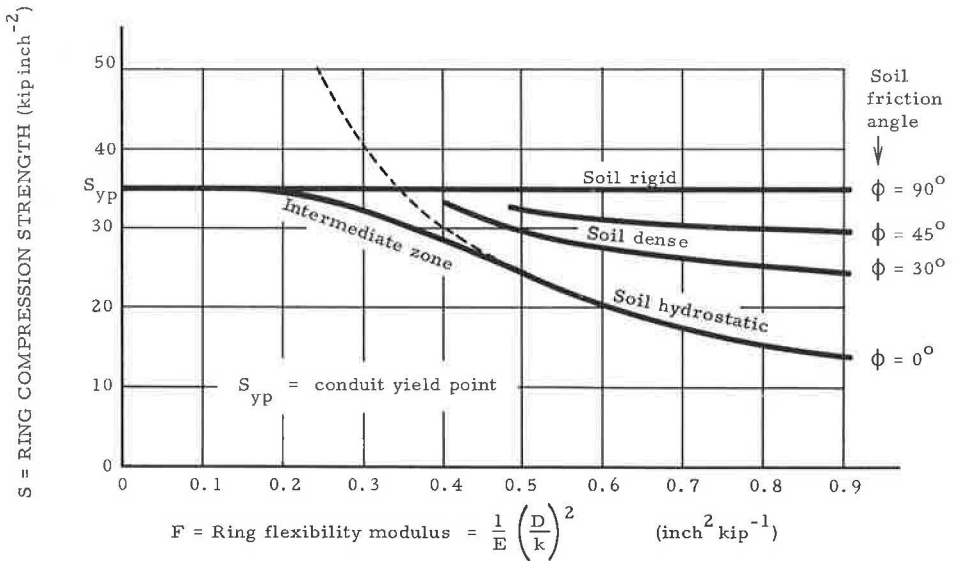
Figure 1. Ring compression stress and ring compression strength at incipient crippling failure of buried circular conduit.

$$\frac{pD^3}{EI} = 24$$

or rewritten, the ring-compression strength is

$$S = \frac{12}{\frac{1}{E}\left(\frac{D}{k}\right)^2}$$

where

    p = hydrostatic pressure;
    D = mean diameter of conduit ring (unloaded);
    E = modulus of elasticity of conduit wall;

    I = cross-sectional moment of inertia of wall per unit length of conduit; and

    k = radius of gyration of conduit wall, i. e., $k = (I/A)^{1/2}$ (this is approximately constant for a given corrugation configuration regardless of thickness of conduit wall).

For design, the stress T/A must be less than this strength by some factor of safety.

In Figure 1 the hydrostatic ring-compression strength plots as a hyperbola with ring-flexibility modulus as the abscissa. This is precisely analogous to the classical Euler hyperbola for the design of a slender column in which the allowable stress is the ordinate, and slenderness ratio $(1/E)$ $(L/k)^2$ is the abscissa. The only difference is column length, L, in place of conduit diameter, D, in the abscissa. The hydrostatic hyperbola applies only if the ring-flexibility modulus (analogous to slenderness ratio) is high. If the flexibility modulus is very low, the ring-compression stress at buckling is a constant (yield point). This is analogous to the design of a short column in which the allowable stress is also a constant, yield point. There is an intermediate zone between the high-flexibility hyperbola and the low-flexibility horizontal line in which a transition curve (5) best represents stress at crippling.

The degree of variation of strength between hydrostatic and rigid is measured by the soil friction angle, ϕ. Empirical data available at the present time plot approximately as shown in Figure 1 for $\phi = 30$ deg and $\phi = 45$ deg.

Two different basic types of crippling failure have occurred in model studies. One is a localized reversal of curvature in the ring similar to classical failures of thin-
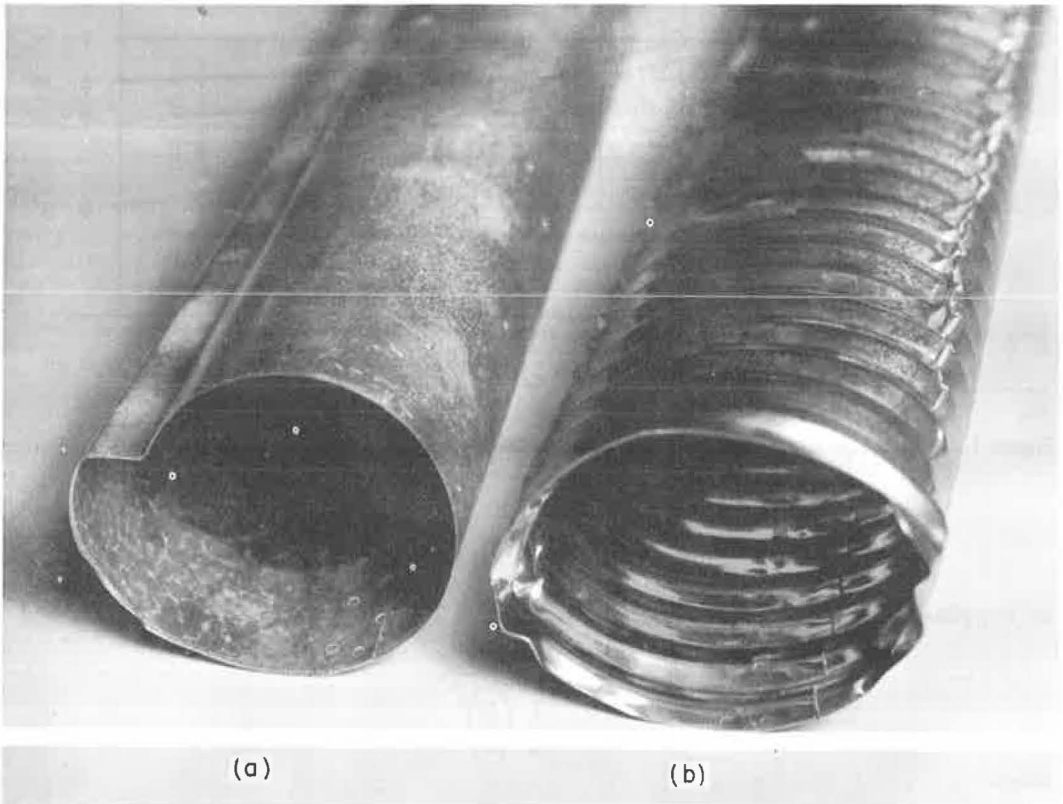
Figure 2. Failure by crippling of model sections of circular conduits buried in sand and loaded with vertical soil pressure: (a) comparatively flexible conduit failed by reversal of curvature, and (b) less flexible conduit failed by wall-crushing.

walled cylinder which buckle under external hydrostatic pressure (Fig. 2). Such failures occur in soil of low-friction angle with conduits of high ring-flexibility modulus (hyrostatic hyperbola in Fig. 1). The other type of crippling failure, wall crushing, has been observed in conduits of low-flexibility modulus buried in soil of high-friction angle (yield point line in Fig. 1). A critical ring-flexibility modulus may exist above which reversal of curvature occurs and below which wall-crushing failure occurs. This flexibility modulus is unstable and difficult to determine precisely. It is best represented by the intermediate zone. In any case, ring-compression strength is defined here as the ring-compression stress at which wall crippling starts, based on visual inspection.

The question logically arises concerning the effect on ring-compression strength when the conduit yield point is changed. If the soil is rigid (ϕ = 90 deg) as the yield point is increased, the allowable ring-compression stress increases proportionately. However, if the soil is hydrostatic (ϕ = 0) and the conduit is flexible, the allowable ring-compression stress being a function of ring-flexibility modulus only (independent of yield point), the original hydrostatic hyperbola applies.

If the friction angle of the soil is somewhere between ϕ = 0 and ϕ = 90 deg, increased conduit yield point causes a proportional rising of the ϕ-curves. For example, the curve for ϕ = 30 deg falls about half way between hydrostatic and rigid regardless of the yield point. For high soil-friction angles the increase in ring-compression strength is almost proportional to the increase in yield point. For low soil-friction angles, little is gained by the high conduit yield strength except when the ring-flexibility modulus is very low. Yield strength is increasingly important as wall crushing dominates failure.

Compressible Soil. —The foregoing concepts are based on noncompressible soil for which the soil pressure at the top of the conduit ring is assumed to be p_V, i. e., the unit weight of soil times the height of fill plus the influence of any surface loads. This assumption is not accurate for compressible soil for which the assumed vertical soil pressure must be modified to account for pressure concentrations.

Most soil is compressible; if vertical pressure is applied to a soil-conduit system, the unit decrease in cross-sectional area of the soil is greater than the unit decrease in cross-sectional area of the conduit. The flexible conduit may decrease in vertical diameter, but in so doing it increases in horizontal diameter so that the unit decrease in area may be much less than the unit decrease in area of the surrounding soil. The result is a "hard spot" in the soil with pressure concentrations on the conduit ring greater than p_V. Conceivably, the opposite could also occur. If the conduit area is more compressible than the surrounding soil, the conduit becomes a "soft spot" and pressures on the conduit are less than p_V. The Appendix contains an analysis by means of which soil pressure on the conduit is determined (Fig. 3). The plots are based on the assumptions that the conduit remains elliptical in cross-section, shearing stresses are negligible between the conduit and the soil, and the soil is elastic, isotropic, and homogeneous—right up to the soil-conduit interface. If the conduit perimeter is not constant, it can only decrease due to ring compression and/or seam slippage; and if the soil is not homogeneous, it will undoubtedly be less dense in the corrugations or near the conduit wall, like a soft blanket. All of these influences would lower the curves of Figure 3; therefore, the solid lines (for a noncompressible ring perimeter; i. e., $E'D/AE = 0$) represent upper limits. The dotted lines represent a conduit whose perimeter is not constant; i. e., $E'D/AE = 0.1$ for a conduit with a relatively compressible perimeter. This is equivalent to a 12-gage corrugated steel conduit 66-in. diameter in a very dense sand.

For most designs, it is quick and conservative to assume a limiting pressure concentration factor of 1.5 for flexible conduits. Very little safety factor is needed beyond this except to cover errors in installation.

A better method of design is to bypass the pressure concentration factor and solve directly for tangential wall thrust, T, as a result of pressure concentrations. Accordingly, the influence of vertical soil strain is essentially zero and T can be determined directly from Figure 4. For quick, conservative design assume K = 1. This is approximately correct for well-compacted soil. Then T = $\frac{3}{4}$ p_VD for a very flexible con-

6

UNCOMPRESSED SOIL CROSS SECTION   COMPRESSED SOIL
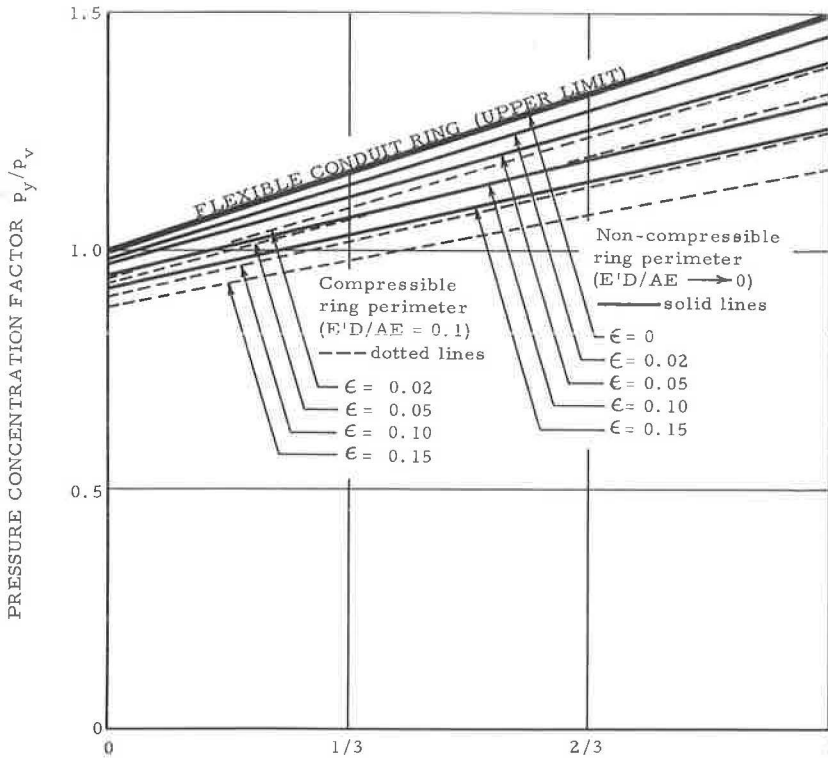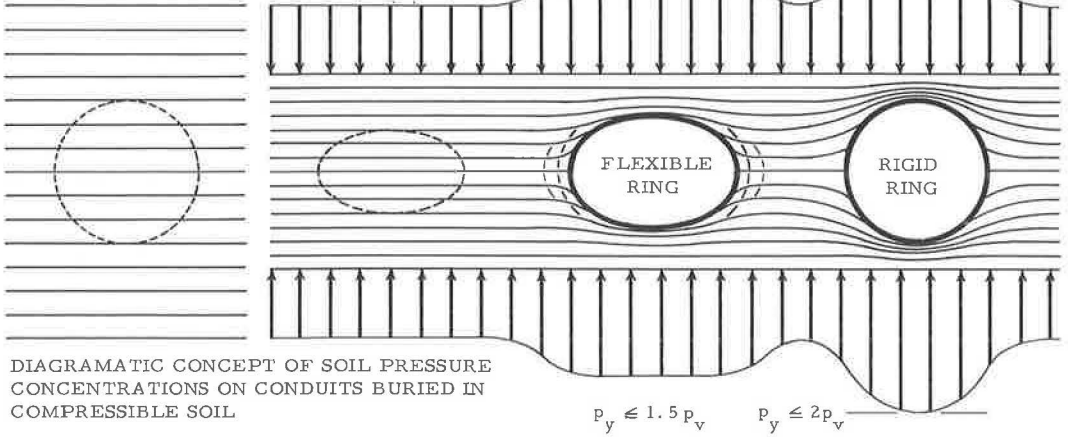
DIAGRAMATIC CONCEPT OF SOIL PRESSURE
CONCENTRATIONS ON CONDUITS BURIED IN
COMPRESSIBLE SOIL

Figure 3. Pressure concentration factor as a function of K, and vertical soil strain ϵ for maximum vertical pressure on a buried circular conduit.
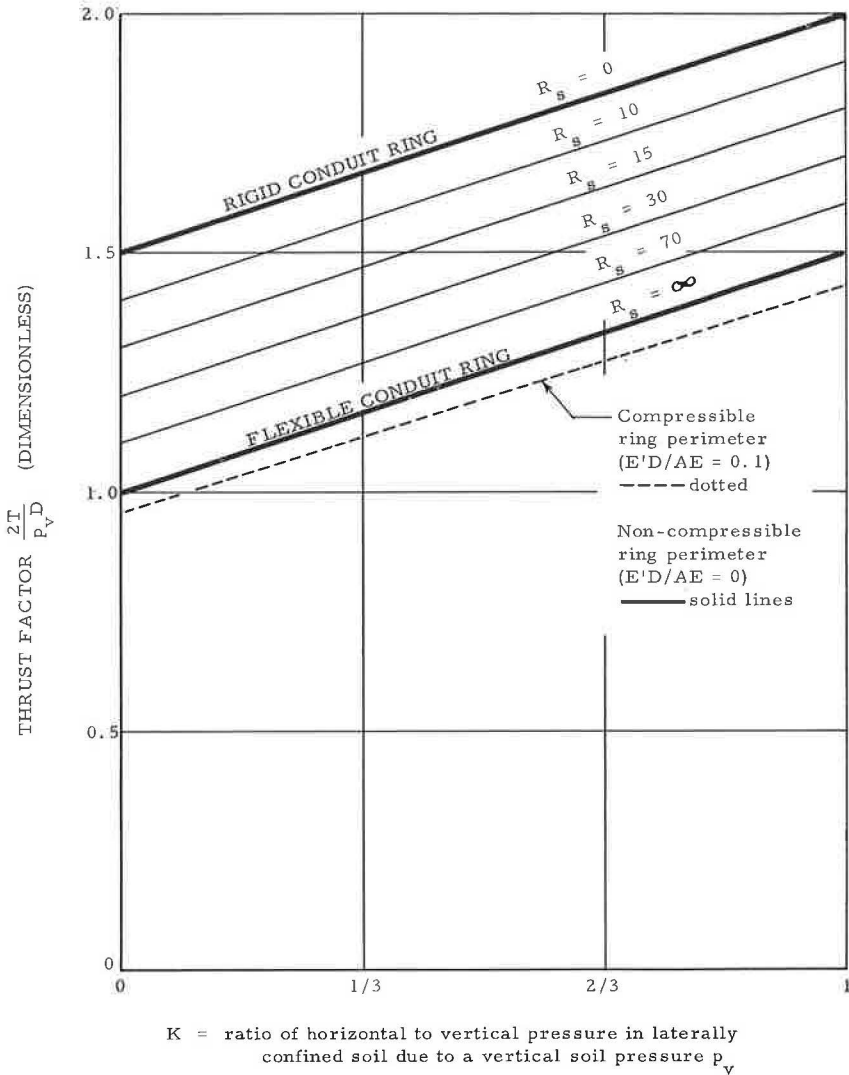
Figure 4. Thrust factor as a function of K for determining the tangential wall thrust in buried conduits.

duit and $T = p_v D$ for a rigid conduit. The estimated values between are based on limited empirical data for which the stiffness ratio R_s is the controlling parameter. For noncompacted, nonconfined soil, a limiting low value of K is $(1 - \sin \phi)/(1 + \sin \phi)$. For a soil-friction angle of $\phi = 30$ deg, $K = \frac{1}{3}$. It is doubtful that K would ever be so low. The solid lines (Fig. 4) apply to the limiting case of a noncompressible conduit perimeter. For a compressible perimeter such as a 12-gage corrugated conduit 66-in. diameter in dense sand ($E'D/AE = 0.1$) the plot is shown dotted. Generally, the solid lines (upper limits) should be used.

Design to resist ring buckling is completed by Figure 1. Using a trial conduit section, the designer enters Figure 1 with the abscissa F-value. (This value should be published for all conduit sections.) He then reads the ring-compression strength, S, corresponding to the soil-friction angle (based on degree of compaction) to be specified. The ring-compression stress, T/A, must be less than this strength by some safety factor. If not, the analysis is repeated using a new trial conduit section. It is hoped that design tables eliminating trial methods will be published eventually. An appropriate

factor of safety should depend on the design engineer who presumably knows the quality of control during installation, unanticipated loads, etc.

Bedding of the conduit is important. Ideally, the subbase should be preshaped to the same shape as the conduit. Also, a loose granular soil pad of constant thickness might be placed between the subbase and the conduit to insure full surface contact and to provide a cushion to relieve slightly the concentrated soil pressure p_y on the conduit. If the subbase is not preshaped and the fill soil under the haunches is not compacted to the same stiffness E' as the subbase, the conduit may develop a point loading at the invert which may initiate premature crippling. Ideally, installers should try to have homogeneous soil all around the conduit.

A soft soil blanket adjacent to the conduit can be exploited to transfer a large fraction of the ring compression to the soil. Of course, the soil outside of the loose blanket must be sufficiently well-compacted to carry the additional load. This is practically the same thing as designing a conduit ring with a compressible perimeter or slip seam so that it will relieve itself of load. The loose blanket can be easily placed by specifying that compacting equipment remain a minimum distance from the conduit. One compactor foot width is suggested for hand-operated compactors, one track or dual tire width for tractors and trucks, etc. The soil then forms a "low-grade masonry arch" over the conduit-lined passageway. Actually, this loose blanket concept (or imperfect trench method) occurs to a certain degree in most installations because it is difficult to compact soil right up to the interface.

In the past, rigid and flexible conduits have been distinguished and designed by different methods. Rigid conduits are usually concrete, clay, and other materials which crack rather than bend under load on the ring. Flexible conduits, such as corrugated metal pipes, deform without cracking. Actually, all are flexible to varying degrees and so may be analyzed by these methods if failure is defined. Of course, these methods apply to conduits in the zone between rigid and flexible, i. e., mortar-lined and/or coated steel pipe and deeply corrugated metal pipe. For these conduits it may be advisable to measure (rather than calculate) values for ring flexibility modulus, F. An approximate method is the three-edge bearing test from which (6)

$$F = 58.8 \frac{A}{D} \frac{\Delta x}{P} \tag{2}$$

where

A = cross-sectional area of conduit wall per unit length of conduit;
D = diameter to centroid of wall; and
$\Delta x/P$ = slope of plot of vertical load, P, per unit length of conduit vs horizontal change in diameter Δx.

After cracking commences, or if the flexible conduit takes on a permanent set, the value of F will not remain constant. Nevertheless, it can be used because it is related to ring deflection $\Delta y/D$, and a designer only needs to estimate the ring deflection (by methods that follow) and then select the corresponding F from three-edge bearing data published by the conduit manufacturer.

Deflection of Conduit Ring

Deflection (flattening) of the conduit ring occurs if the soil is compressible. The conduit might collapse in noncompressible hydrostatic soil, but this case is specifically excluded here because it can be analyzed according to the snap-through type of crippling already discussed. For the present discussion, ring deflection is considered a function of soil compressibility (i. e., vertical soil strain ϵ).

The four-step rationale in the Appendix is useful in this discussion. Suppose conduit ring deflection is defined as $\Delta y/D$. Assuming homogeneous, elastic soil of great extent and assuming the conduit is flexible with no shearing stresses acting on it, approximate equations for ring deflection can be derived with results shown in Eqs. 12a and 12b (Appendix). One equation is plotted in Figure 5. For average flexible conduit design a very quick and conservative prediction is that the vertical ring deflection factor = 1,
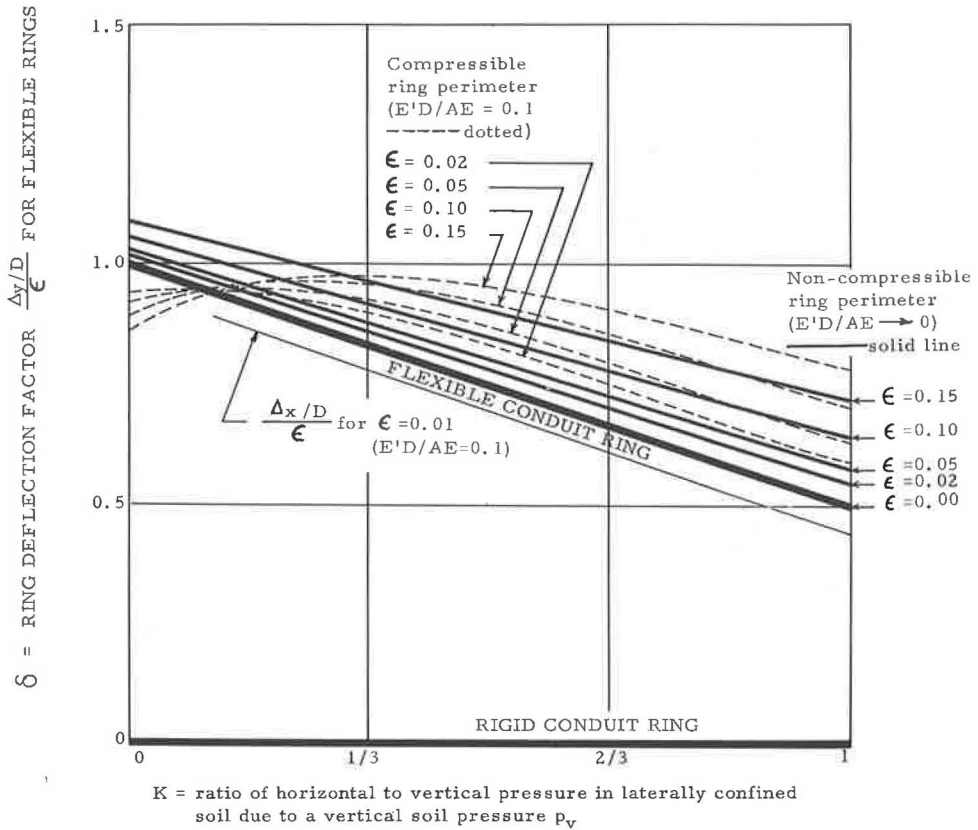
Figure 5. Ring deflection factor as a function of K, and vertical soil strain ϵ for flexible conduits.

i. e., $\Delta y/D$ will approximately equal the vertical soil strain ϵ caused by vertical soil pressure (K is generally greater than $\frac{1}{3}$). Horizontal ring deflection will be slightly less than vertical. For more accurate analysis, the vertical ring deflection factor can be picked off the graph of Figure 5, or solved by Eq. 12. Values of K increase with the amount of compaction effort during soil placement. If $\Delta x/D$ is required with greater accuracy, for a constant perimeter conduit, $\Delta x/D$ is the same as the vertical ring deflection $\Delta y/D$. For a compressible conduit perimeter, $\Delta x/D$ is less. (See curve for $E'D/AE = 0.1$ in Fig. 5.) This applies to a 66-in. diameter corrugated conduit of 0.1-in. steel buried in dense granular fill. Vertical soil strain ϵ can be determined from a load-deflection diagram using a vertical load of p_v. In the future it would be valuable to publish load-deflection diagrams for typical soil types at different degrees of compaction so that tests would not be needed for each specific installation.

The foregoing discussion applies to completely flexible conduits. If the conduit is not flexible it resists deflection, and if the conduit ring is rigid the ring deflection is zero. Empirical data indicate that the influence of the ring rigidity (or stiffness) on ring deflection can be included as a modification factor in the equation

$$\frac{\Delta y/D}{\epsilon} = \delta \left[e^{-2/R_S} \right] \tag{3}$$

where

δ = ring deflection factor from Figure 5 (varies from 0.5 and 1.0);

e = base of natural logarithms; and

$$\frac{\Delta y/D}{\epsilon} = \delta \left[\text{MODIFICATION FACTOR} \right]$$

R_S = STIFFNESS RATIO (SOIL TO RING)
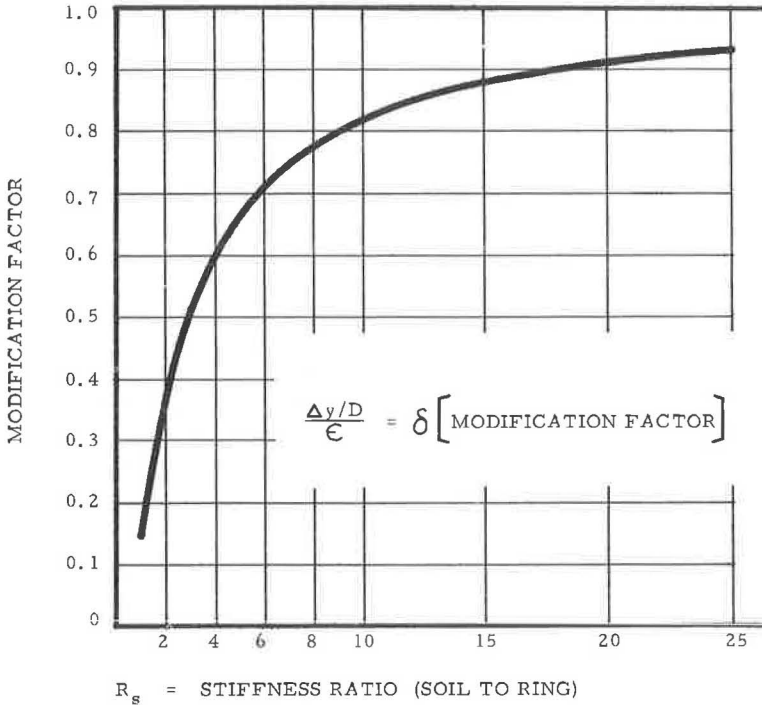
Figure 6. Modification factor for correcting ring deflection of flexible conduit to account for ring stiffness.

R_S = stiffness ratio (dimensionless) = ratio of soil stiffness $E'(= p_V/\epsilon)$ to conduit ring stiffness per unit length EI/D^3 (to be published by conduit manufacturers).

This relationship is plotted in Figure 6. To use Figure 6, the load-deflection data, p_V vs ϵ, for the soil must be available. The designer starts with the anticipated vertical soil pressure, p_V, for which the load-deflection diagram will provide the corresponding strain ϵ and the modulus E', i.e., slope of the chord from the origin to point (p_V, ϵ). He can calculate the stiffness ratio, R_S, if the data for an anticipated conduit section are known. He then determines the modification factor from Figure 6 and multiplies it by the ring deflection factor δ to determine $\Delta y/D$. The maximum allowable value of $\Delta y/D$ is often specified as 5 percent. There is little basis for this value, however, and additional research on reasonable limits is urgently needed. Ring deflection may be the major basis for design, although usually crippling is more important.

Conduit design may be further limited by the hazards of handling and installing conduit. If a concentrated load is applied to the ring, the pertinent ring flexibility criterion is D^2/EI which is sometimes referred to as a flexibility factor or handling factor. This factor has been effectively used by engineers of Armco Corp. who specify a maximum value depending on the method of handling and installing the conduit, and the method of compacting the soil. Mechanical compactors develop a load at the pipe-soil interface which is essentially a concentrated load.

The methods of design proposed here may be adapted to noncircular symmetrical sections by calculating the wall stress according to Eq. 1, $T = pr$. This wall stress must be everywhere less than the maximum allowable stress of Figure 1. More research is needed on deflection. In general, circular sections are most economical.

DESIGN

Practical structural design of circular conduits is based on conduit deformation which falls into two areas for consideration, wall crippling and ring deflection, with

additional limitations on flexibility for handling and placement, on bedding, possibly on blanketing, etc. Of course, other nonstructural factors, such as corrosion, erosion, infiltration of soil, end conditions, and camber, must be considered separately.

Crippling is limited by Figure 1 which shows the ring-compression strength as a function of conduit properties and the soil-friction angle. The maximum compressive stress, T/A, in the conduit wall is determined from the thrust factor of Figure 4, or for quick, conservative design, from the relationships $T = \frac{3}{4} p_V D$ for flexible conduits or $T = p_V D$ for rigid conduits. The ring compression strength must be reduced by a safety factor.

Ring deflection is quickly and conservatively estimated for flexible conduits by the conservative assumption that the ring deflection factor is $\Delta y/D = \epsilon$ where ϵ is the vertical soil strain from a consolidometer test. More accuracy is gained by using Figure 5 to determine the ring deflection factor.

Ring deflection for nonflexible conduits can be estimated by modifying the ring deflection factor for a flexible conduit by means of Figure 6.

REFERENCES

1. Spangler, M. G. Soil Engineering, pp. 431-437, International Textbook Co., 1960.
2. Watkins, R. K., and Loosle, David. Deflection of Cement-Mortar-Lined Spiral-Welded Steel Pipe Embedded in Soil. Armco Steel Corp., 1965.
3. White, H. L., and Layer, J. P. The Corrugated Metal Conduit as a Compression Ring. HRB Proc., Vol. 39, pp. 389-397, 1960.
4. Timoshenko, S. Strength of Materials, p. 188, D. Van Nostrand Co., 1956.
5. Brockenbrough, R. L. A Theoretical Evaluation of Two Corrugation Profiles for Corrugated Metal Pipe Culverts. Memo., U. S. Steel Corp., ARL Proj. 90. 12-017, Feb. 1962.
6. Spangler, M. G. The Structural Design of Flexible Pipe Culverts. Iowa Engineering Experiment Sta. Bull. 53, p. 14, 1941.
7. Murphy, Glenn. Advanced Mechanics of Materials, p. 120, McGraw Hill, 1946.

Appendix

PRESSURE CONCENTRATION FACTOR ON FLEXIBLE BURIED CIRCULAR CONDUITS

The actual vertical pressure p_y on a flexible buried conduit can be determined by a four-step rationale (Fig. 7).

1. Consider the unstressed, compacted soil cross-section (Fig. 7, step 1). No forces are acting, not even gravity. The outline of a flexible circular conduit ring is shown dotted, but the conduit has not been installed. This is an imaginary position only.

2. Next a uniform vertical soil pressure p_V is applied at infinity (Fig. 7, step 2). The imaginary ring outline becomes an ellipse. The major (horizontal) radius, b, is the same as the radius of the original conduit $D/2$ if the soil is restrained laterally at infinity. The minor (vertical) radius, a, is less than the radius of the original conduit because of the vertical compression in the soil due to p_V, i.e.,

$$a = \frac{D}{2}(1 - \epsilon)$$

where

    D = original diameter of conduit, and
    ϵ = vertical strain in soil due to vertical soil pressure, p_V.
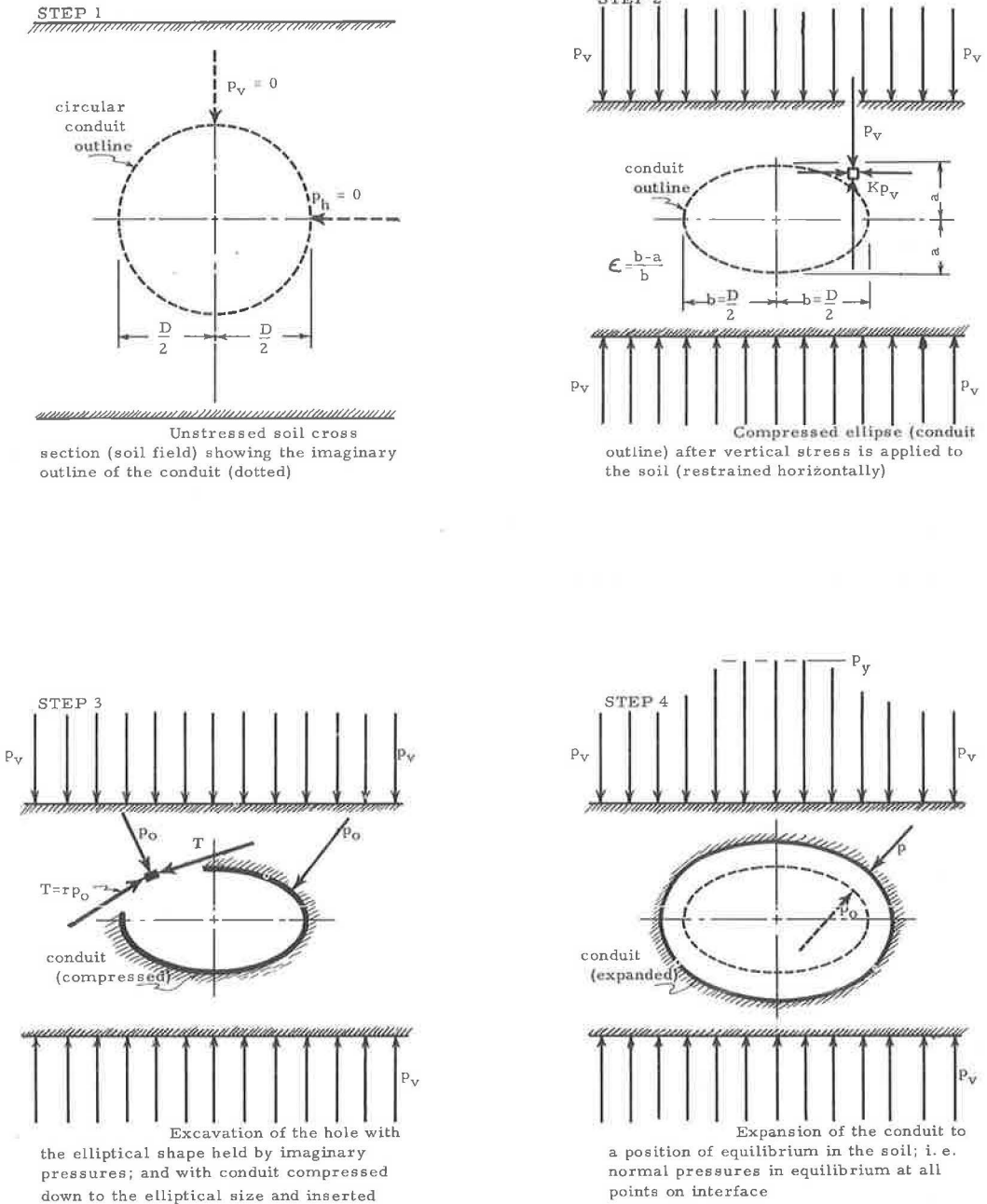
Figure 7. Four-step rationale for evaluating the deflection of, and the normal pressure against, a flexible circular conduit buried in homogeneous soil of great extent.

The value ϵ can be determined easily by a confined compression test on a sample of soil (at the proper compacted density) to which the vertical pressure p_v is applied. This test is adequate because soil in most soil-conduit systems is confined laterally.

3. The next step is the removal of soil from within the compressed ellipse (Fig. 7, step 2). To retain the elliptical shape of the hole, however, imaginary pressures must

be applied to the soil in such a fashion that the vertical component is everywhere equal to p_V and the horizontal component is everywhere equal to Kp_V. Now the conduit is compressed down by imaginary radial pressures p_O until it has exactly the shape of the elliptical hole. Then it is slipped into place in the soil with pressure p_O still acting on it (Fig. 7, step 3). Of course, imaginary pressure p_O may be very high because the perimeter of the conduit must be decreased significantly to fit into the elliptical hole.

4. Next, the radial compression pressure p_O is relaxed. The conduit expands (Fig. 7, step 4) until the restraining normal pressure, p, of the soil comes to equilibrium with the outward expansive pressure of the conduit. Shearing stresses also develop between the conduit and the soil. They may be considered, but are neglected in this example. Shearing stresses between soil and conduit are usually small because of a low coefficient of friction; because shearing stresses are not critical in carefully installed conduits; and because vibrations and temperature variations during construction tend to reduce shearing stresses.

From the foregoing four-step rationale, as the conduit is allowed to expand from step 3 to step 4, the normal pressure, p, on the conduit increases to something greater than the p_V and Kp_V components required to retain the elliptical hole (Fig. 7, step 3). Exceptions might occur if the horizontal support of the soil is very low, or if the p_V and Kp_V required to retain the elliptical hole are greater than the p_O required to compress the conduit. This is tantamount to a conduit with compressibility greater than the compressibility of the surrounding soil.

The basic equations for analysis are equations of deflection (Fig. 8.). The first deflection equations pertain to the soil.

Vertically,

$$\frac{\Delta y}{2} = \frac{D}{2} \epsilon - v \tag{4}$$

where

v = increase in radius of a cylindrical hole in an elastic material of great extent due to a change in pressure in the hole; i.e., (7):

D = Nominal diameter of conduit

ϵ = Vertical soil strain
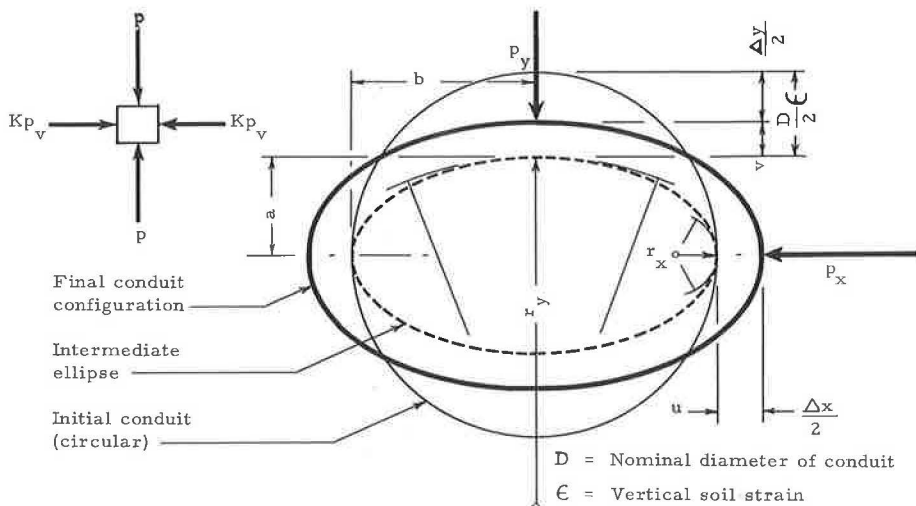
Figure 8. Deflections of conduit ring (steps 1-4 superimposed).

$$v = \frac{r_y (\Delta p)}{E'} (1 - \mu)$$

where

μ = Poisson's ratio, $\mu = 0$ (assumed) for soil;

$\Delta p = p_y - p_v$;

r = radius of curvature of compressed conduit ring; and

E' = soil modulus.

$$v = \frac{r_y (p_y - p_v)}{E'}$$

$$\frac{\Delta y}{2} = \frac{D}{2} \epsilon - r_y \frac{(p_y - p_v)}{E'} \tag{5}$$

Horizontally,

$$\frac{\Delta x}{2} = u$$

$$u = \frac{r_x (\Delta p)}{E'} (1 - \mu)$$

$$\mu = 0$$
$$\Delta p = p_x - Kp_v$$

$$\frac{\Delta x}{2} = r_x \frac{(p_x - Kp_v)}{E'} \tag{6}$$

The next deflection equation pertains to the conduit. For small deflections the final (equilibrium) configuration of the conduit may be assumed to be an ellipse for which the perimeter is approximately:

$$\text{Final conduit perimeter} = \pi (a + b)$$

where

$$a = \frac{D}{2} - \frac{\Delta y}{2} = \frac{D}{2} - \frac{D}{2} \epsilon + r_y \left(\frac{p_y - p_v}{E'} \right) \quad \text{from Eq. 5, or}$$

$$a = \frac{D}{2} (1 - \epsilon) + r_y \left(\frac{p_y - p_v}{E'} \right)$$

$$b = \frac{D}{2} + \frac{\Delta x}{2} = \frac{D}{2} + r_x \left(\frac{p_x - Kp_v}{E'} \right) \quad \text{from Eq. 6}$$

$$\text{Final conduit perimeter} = \pi \left[\frac{D}{2} (1 - \epsilon) + r_y \left(\frac{p_y - p_v}{E'} \right) + \frac{D}{2} + r_x \left(\frac{p_x - Kp_v}{E'} \right) \right]$$

Initial circle perimeter $= \pi D$

Δ perimeter = initial circle - final ellipse

$$= \pi D - \pi \left[D - \frac{D\epsilon}{2} + r_y \left(\frac{p_y - p_v}{E'} \right) + r_x \left(\frac{p_x - Kp_v}{E'} \right) \right]$$

$$\Delta perimeter = \pi \left[\frac{D\epsilon}{2} - r_y \left(\frac{p_y - p_v}{E'} \right) - r_x \left(\frac{p_x - Kp_v}{E'} \right) \right] \tag{7}$$

But

$$\frac{\Delta perimeter}{circle\ perimeter} = strain\ in\ conduit\ wall = \frac{stress}{E} = \frac{T}{AE} \tag{8}$$

where

E = modulus of elasticity of conduit wall;
T = tangential thrust in conduit ring; and
A = area of conduit wall per unit length of conduit.

Substituting Eq. 7 into Eq. 8

$$\frac{p_v}{2E'} - \frac{r_y}{D} \left(\frac{p_y - p_v}{E'} \right) - \frac{r_x}{D} \left(\frac{p_x - Kp_v}{E'} \right) = \frac{T}{AE} \tag{9}$$

In an approximate analysis, the following assumptions can be made:

1. The final configuration of the conduit is elliptical. (This has been observed empirically for conduits in homogeneous soil of great extent.)

2. $T = r_y p_y$ (actually the value r_y is slightly low because it pertains to the intermediate ellipse rather than the final ellipse; however, the difference is negligible.

3. $p_x = p_y \frac{r_y}{r_x}$ (r_y/r_x will be very nearly the same in the final ellipse as in the intermediate ellipse). Substituting in appropriate values:

$$p_y = p_v \left[\frac{D + 2r_y + 2Kr_x}{4r_y + 2E'Dr_y/AE} \right] \tag{10}$$

But the maximum and minimum radii of curvature for the intermediate ellipse are:

$$r_x = \frac{a^2}{b} = \frac{D}{2} (1 - \epsilon)^2$$

$$r_y = \frac{b^2}{a} = \frac{D}{2(1 - \epsilon)}$$

Now substituting values in Eq. 10:

$$\frac{p_y}{p_v} = \left[\frac{2 - \epsilon + K(1 - \epsilon)^3}{2 + E'D/AE} \right] \tag{11}$$

for flexible conduits buried in elastic soil with no shearing stresses on the interface, where the quantity in brackets is called the pressure concentration factor, and

where

p_y = maximum vertical pressure on buried conduit;
p_v = calculated vertical pressure in soil at level of top of conduit;

ϵ = vertical soil strain at level of conduit if no conduit were in place;

K = ratio of horizontal to vertical soil pressure in a laterally restrained soil field due to a vertical pressure p_v if no conduit were in place;

D = initial conduit diameter;

A = conduit wall area cross sectional per unit length;

E = modulus of elasticity of conduit material; and

E' = modulus of elasticity of soil. (The soil need not be assumed elastic, but if not, a numerical solution by computer would be necessary.)

In Eq. 11, p_v, ϵ, and E' are not independent; i.e., $E' = p_v/\epsilon$. Eq. 11 is left in this form, however, because the term $E'D/AE$ is very small for most conduit analyses, and may be neglected.

It is possible to substitute Eq. 11 and values of p_x, r_x and r_y into Eqs. 5 and 6 to calculate approximate values for the ring deflection factor $(\Delta/D)/\epsilon$. The results are as follows:

$$\frac{\Delta x/D}{\epsilon} = \frac{1}{1-\epsilon} \left[\frac{2 - \epsilon + K(1 - \epsilon)^3}{2 + E'D/AE} - K(1 - \epsilon)^3 \right] \tag{12a}$$

$$\frac{\Delta y/D}{\epsilon} = 1 - \frac{1}{1 + \epsilon} \left[\frac{2 - \epsilon + K(1 - \epsilon)^3}{2 + E'D/AE} - 1 \right] \tag{12b}$$

The foregoing equations are plotted in Figure 5.

The pressure concentration factor can be bypassed and the tangential wall thrust, T, solved directly by substituting the radii of curvature r_x and r_y and corresponding pressures p_x and p_y directly into Eq. 9. The result is as follows:

$$T = p_v \frac{D}{2} \left[\frac{2 - \epsilon + K(1 - \epsilon)^3}{(1 - \epsilon)(2 + DE'/AE)} \right]$$

This is plotted in Figure 4.

Scaling Considerations in Plate-Sinkage Tests

L. J. GOODMAN, Associate Professor of Civil Engineering, Syracuse
    University;
E. HEGEDUS, Soils Engineering, Herron Testing Laboratories, Inc.,
    Cleveland; and
R. A. LISTON, Chief, Land Locomotion Laboratory, U. S. Army Tank-
    Automotive Center, Warren, Michigan.

Experimental and analytical investigations of the vehicle sinkage
problem were conducted by means of plate-sinkage studies on
sand and clay soils. These studies were concerned with the in-
fluence of rates of plate penetration and size on the pressure-
sinkage relations of loose sands and remolded clays.

This paper covers the size effects of the small scale plate
studies, with attention given to scaling considerations. Ex-
perimental results are analyzed to predict pressure-sinkage
relations for large-scale footings based on laboratory models.
Sinkage rates as high as 1,750 in./min are included. Con-
trol measures involved constant soil density and water content
for each soil type used and an adequate ratio of soil bin to
footing size to eliminate interference from stresses induced
by the sides or bottom of the soil bin.

Physical characteristics of the soil-footing system relating
to pressure-sinkage relations are discussed. Dimensional
analysis is applied to determine the relationship between the
model and the prototype, with the results compared with model
test results.

•PLATE-LOADING tests are generally employed in many specialized fields of engineering
practice where it is either desirable to complement existing theories or where the com-
plexity of the relationships existing between the loading area and the loaded media re-
quires the use of semi-empirical or empirical approaches.

For example, plate-loading tests are often employed by the soils engineer to arrive
at a reasonable bearing value when adverse soil conditions are encountered. In high-
way engineering practice, plate-loading tests serve as a guide for evaluating subgrade
behavior and pavement requirements. Land locomotion mechanics, a relatively new
discipline, assumes that it is possible to predict vehicle performance on the basis of
plate-sinkage tests. To describe the behavior of wheel or track, it is necessary to
determine the work expended in compacting the soil to the depth of wheel or track sink-
age. These experiments are designed to simulate a particular condition. However,
it is common in most plate tests to extrapolate small plate data or assume that the in-
formation derived from a relatively small plate will be valid when applied to a larger
loading area, which may be of different geometrical shape than the model plate. It is
also common to assume that the loading rate and deformation rate have little or no in-
fluence on load deformation relationships.

The intention of this study was to analyze the pressure-sinkage curves obtained from
small-scale footing penetration tests in both sandy soils and remolded clay soils at
various rates of penetration, using different geometrical shapes and sizes of footings.
Some attention is also devoted to pressure-sinkage curves obtained in snow.

One of the objectives was to determine the influence of the rate of penetration on pressure-sinkage relationships. An alternate objective was to determine whether it is possible to predict the load-sinkage behavior of a large plate on the basis of model plate tests.

The penetration tests encompassed by the present investigation have been performed to a maximum of 7 in., because land locomotion problems require the study of relatively large deformations. During the penetration rate studies, however, particular attention was given to the initial portions of the pressure-sinkage curves to determine typical failure patterns and resulting bearing capacities. As far as model and prototype relationships are concerned, there is no reason to believe that the general principles employed in scaling considerations in relation to large deformations would not be applicable when only relatively small deformations are involved.

It is felt, therefore, that the results of this investigation should be of interest to both the highway and foundation engineer in providing information concerning subgrade behavior in pavement and shallow foundation design.

The use of small-scale footings to study stress-deformation characteristics of soil has been quite limited until recently and, therefore, represents a fairly new field of experimental and analytical investigation. The limited data in this field are summarized by J. E. Roberts (6) in an extensive review of past small-scale footing studies. This includes tests on sand by such investigators as Gilboy (2), Bekker (1), and Meyerhof (4), and tests on clay by Skempton (8) and Osterberg (5). Unfortunately, some of the investigations reported (6) did not contain data on significant control parameters such as moisture and density. Later, Selig and McKee (7) focused on load-displacement characteristics of footings when subjected to static and impulse loads.

EXPERIMENTAL PROGRAM

The test apparatus used in this investigation was the standard Land Locomotion Laboratory bevameter which is capable of inducing a constant rate of penetration and permitting the rate of sinkage to be varied from 0 to 1,750 in./min. Operational principles of the test apparatus are shown in Figure 1.

A similar device was also used for static load testing by constructing a platform to support and transmit the various load increments to the test footing. Relatively small load increments were applied, with each increment permitted to stand until plate sinkage was less than 0.001 in./hr.

Three different geometrical shapes of footings were used in the performance of load-sinkage tests: circular, rectangular, and square. At least four different sizes of plates were used in each category ranging approximately from 1 to 28 sq in., 1 to 25 sq in., and 4 to 72 sq in., in case of circular, square, and rectangular footings, respectively. The bottom of all footings was made rough for the sand tests.

The test materials consisted of dry Ottawa sand, wet Ottawa sand, remolded Boston blue clay, remolded Detroit clay, and snow. Classification characteristics and pertinent engineering indices of the materials tested are given in Table 1. Control parameters measured in each test
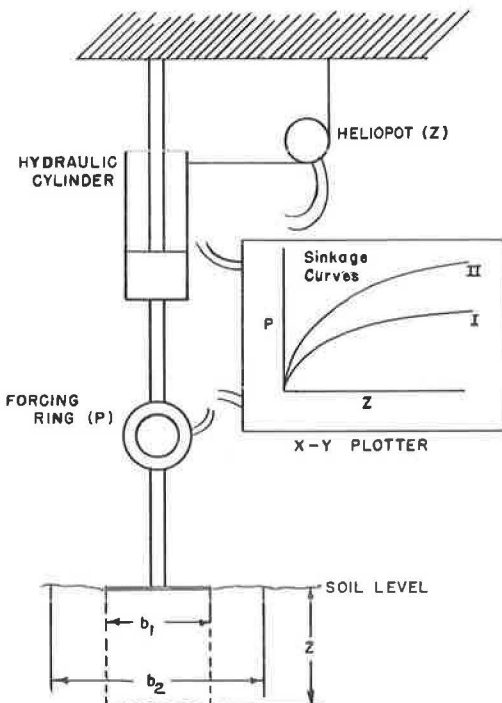
Figure 1. Load-sinkage bevameter diagram.

TABLE 1

CLASSIFICATION CHARACTERISTICS OF MATERIALS INVESTIGATED

Material	Description	Mechanical Analysis			Atterbergs		Natural Water Content (%)	Cohesion (tsf)		Density (pcf)
		Sand (%)	Silt (%)	Clay (%)	WL	IP		Undisturbed	Remolded	
Wet Ottawa sand	Medium rounded	100	—	—	—	—	2. 2[a]	0. 0144[b]	—	110. 0
Dry Ottawa sand	Medium rounded	100	—	—	—	—	—	—	—	105. 0
Boston blue clay	Silty with trace sand	7	42	51	36. 0	14. 6	29. 4	0. 31	0. 040	120. 5
Detroit clay	Silty with little sand	20	35	45	38. 0	16. 0	26. 0	—	0. 095	120. 0
Snow		—	—	—	—	—	—	0. 0072	—	17. 0

[a] Water content during test.
[b] Apparent cohesion owing to water content.

condition were moisture and density. Density readings for wet Ottawa sand reproduced within ± 1 pcf, and moisture content varied ± 0. 25 percent in consecutive test runs. The variation of moisture and density measurements for the Boston blue clay were ± 1 percent and ± 1. 8 pcf, respectively.

The footings employed in the clay tests were smooth because $\phi = 0$ deg was assumed for remolded clay. The soil bins used for the sand and clay tests were sufficiently large to eliminate both side or bottom interference.

At least three or more trial runs were conducted with each plate in each type of soil tested. The results presented in the paper are the averages of several measurements.

The effects of rate of penetration on load-sinkage curves were studied in wet Ottawa sand and remolded Boston blue clay. Plate size effect studies utilized all soil materials encompassed by the present investigation.

RESULTS OF INVESTIGATION

Influence of Rate of Sinkage

Sand. — Figures 2 and 3 show the pressure-sinkage curves for varying rates of deformation for two footing sizes in wet Ottawa sand. The deformation rates were varied in each curve from 0. 6 in. /min to 1, 750 in. /min, which means a speed multiplication factor of over 2, 900. With increased rates of penetration, the strength of the sand increased, and the mode of initial failure changed from local to general shear. Comparing the resulting bearing capacities with Terzaghi's equation (9), the measured bearing capacities at sinkage rates higher than 120 in. /min were approximately twice as high as expected from a static test. The computed bearing capacity values, designated by q, are shown in the figures. Although not verified analytically, it is felt that the general increase in resistance to penetration can at least be partially attributed to the inertia effect of the failing soil mass and to the change in the mode of failure encountered.

Clay. — All the footings tested at sinkage rates at or below 540 in. /min failed in a manner similar to that of local shear, which is the case in which there is not a definite ultimate limit to the curve until relatively large settlements or sinkages are reached.

Figure 4 shows the influence of the rate of footing sinkage for some of the smaller footings with the rate of sinkage varied between static and 540 in. /min. The influence of sinkage rates for two footing sizes in remolded Boston blue clay are shown, with six rates of sinkage in excess of static being considered. This family of curves indicates that an increase in the strength of the clay generally resulted with increased rates of sinkage, commencing with the 2. 25-in. /min rate. There is no definite ultimate limit to the static pressure-sinkage curves. It appears that the static clay strength is in excess of the strength obtained from the increased sinkage rates up to 540 in. /min. The shapes of the curves may be explained by the fact that a 2-week time period was necessary for the static tests, resulting in significant thixotropic regain of strength in

PRESSURE = p (psi.)
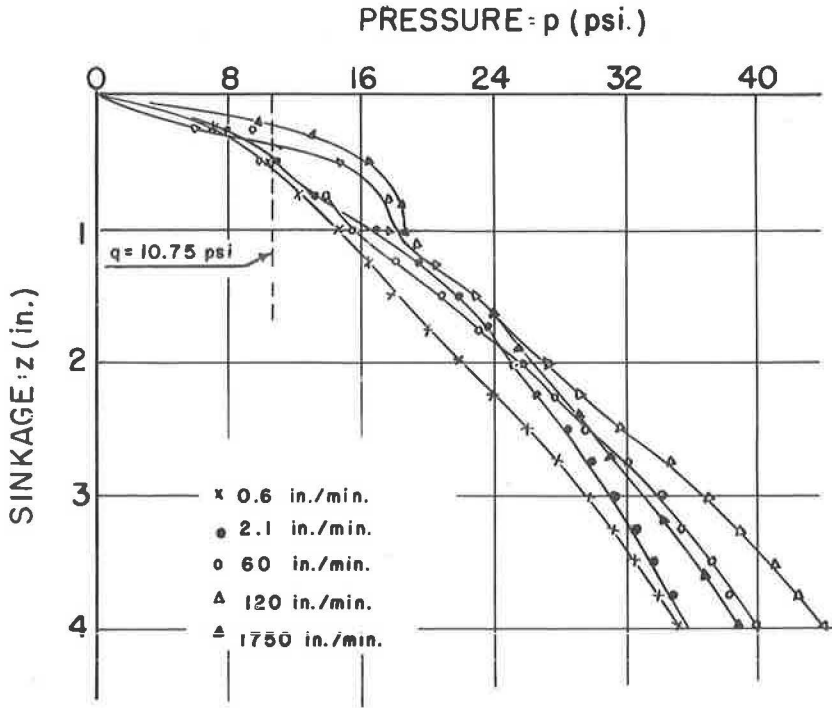
Figure 2. Pressure-sinkage curves for 2-in. diameter footing in wet Ottawa sand.

PRESSURE: p (psi.)
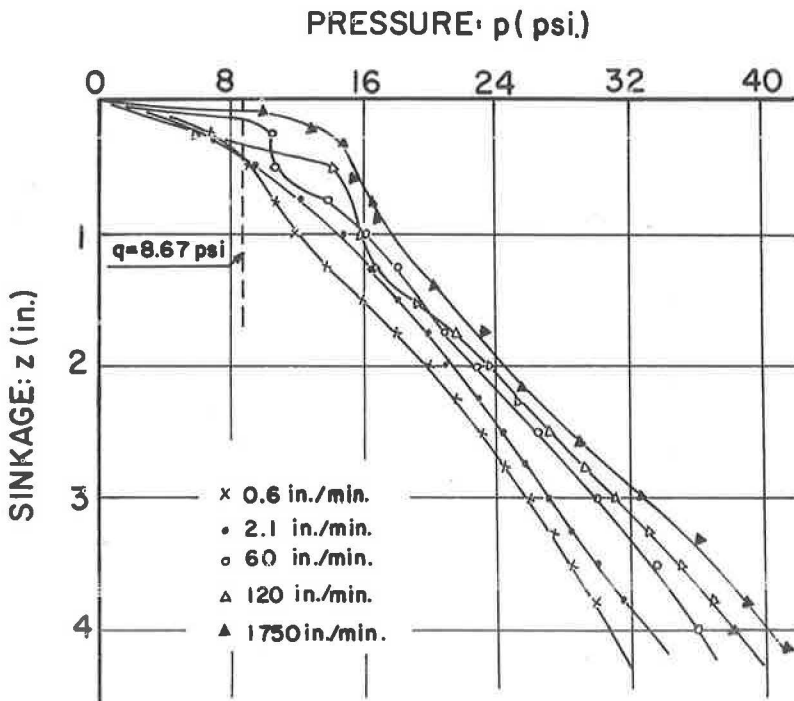
Figure 3. Pressure-sinkage curves for 2- by 4-in. footing in wet Ottawa sand.

PRESSURE: p (psi)
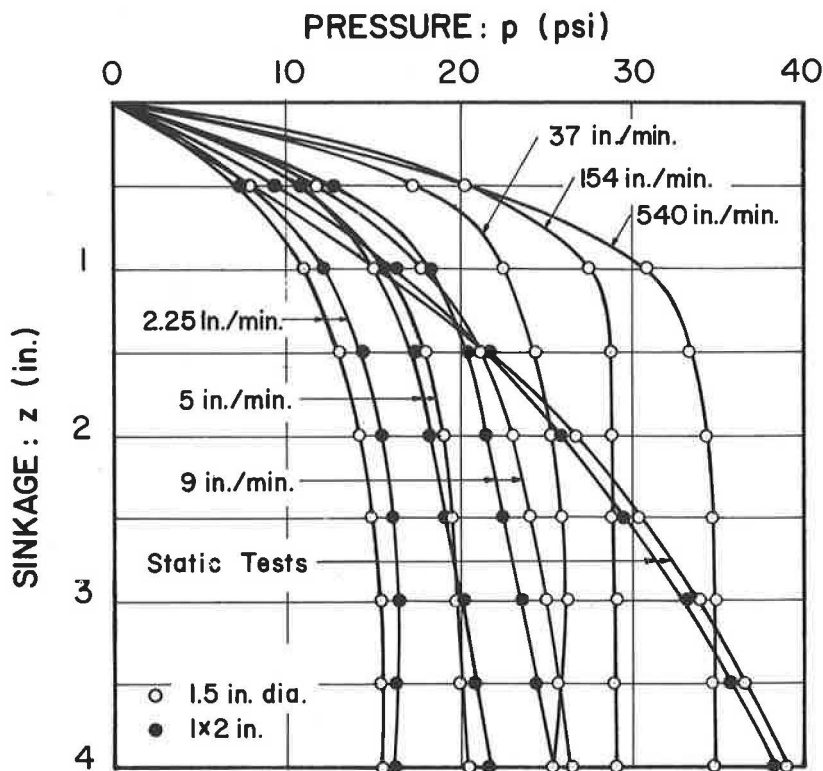
Figure 4. Pressure–sinkage curves at seven rates of loading for remolded Boston blue clay.

this time period after complete remolding. The increased strength with increasing rate of sinkage beyond the static case would indicate that plastic resistance becomes significant at the higher rates of sinkage. Another possible source of the increase in resistance may be due to inertia effects.

Influence of Plate Size

It is of considerable interest to examine the plate-sinkage problem from a dimensional analysis viewpoint. Can a small plate be considered a model of a larger prototype plate with any hope of success if we do not use model soils?

To investigate this proposition, it was assumed that the pressure-sinkage (p-z) relationship in soils is governed by the following variables: the circumference of the plate (s), characteristic length of the plate (ℓ), bulk density of the soil (γ), cohesion (c) and the angle of internal friction (ϕ).

Additional variables considered, but not included in the dimensional analysis were the coefficient of friction between plate and soil (μ), depth of the soil layer (h), and the velocity of penetration (v).

Because the soil type, plate material, and the velocity of penetration were to be kept constant, and the soil was taken as having a depth producing semi-infinite conditions, μ, h, and v were eliminated at the outset.

The application of standard dimensional analysis (3) techniques resulted in the following functional relationships for fixed plate geometries (ℓ/s = constant):

$$\frac{z}{s} = f_1\left[\frac{(\gamma \ell)}{p}, (\phi)\right] \tag{1}$$

$$\frac{z}{s} = f_2 \left[\frac{(\gamma \ell)}{p}, \frac{(c)}{p}, \frac{(c)}{s\gamma}, (\phi) \right] \qquad (2)$$

Eq. 1 is for frictional soils and Eq. 2 is for soils having both cohesion and friction.

Eq. 1 reveals that if one uses plates of several different lengths and circumferences in a cohesionless soil (c = 0 = constant, ϕ = constant), then for a given ℓ/p ratio, the z/s ratios must be constant; in other words z/s vs $\gamma\ell/p$ curves must collapse. If actual test results support this conclusion, then a pressure-sinkage equation can be found by describing the collapsed curves analytically. Eq. 1 in turn will take size effects into account, and it will be dimensionally consistent.

Eq. 2 shows that it is impossible to apply the preceding analysis to cohesive soils without referring to model soils if one wishes to be exact. For example, the c/sγ ratio cannot be kept equal for both the model and the prototype plate if the experiments are performed in the same soil. It is possible to devise a scaled soil, but the effort does not appear to justify the result, because each natural soil of interest would demand a model soil. The selection of variables associated with the dimensionless coefficients can best be justified by an examination of test results.

Sands and Snow. —The z/s vs $\gamma\ell/p$ relationship has been successfully applied to load-sinkage data obtained with footing sizes ranging from about 3 to 72 sq in. in dry sands, wet sand, and in snow. Typical pressure-sinkage relationships for dry Ottawa sand obtained with various sizes of rectangular plates having constant aspect ratios are shown in Figure 5. Circular plate tests included footings from 2 to 8 in. in diameter.
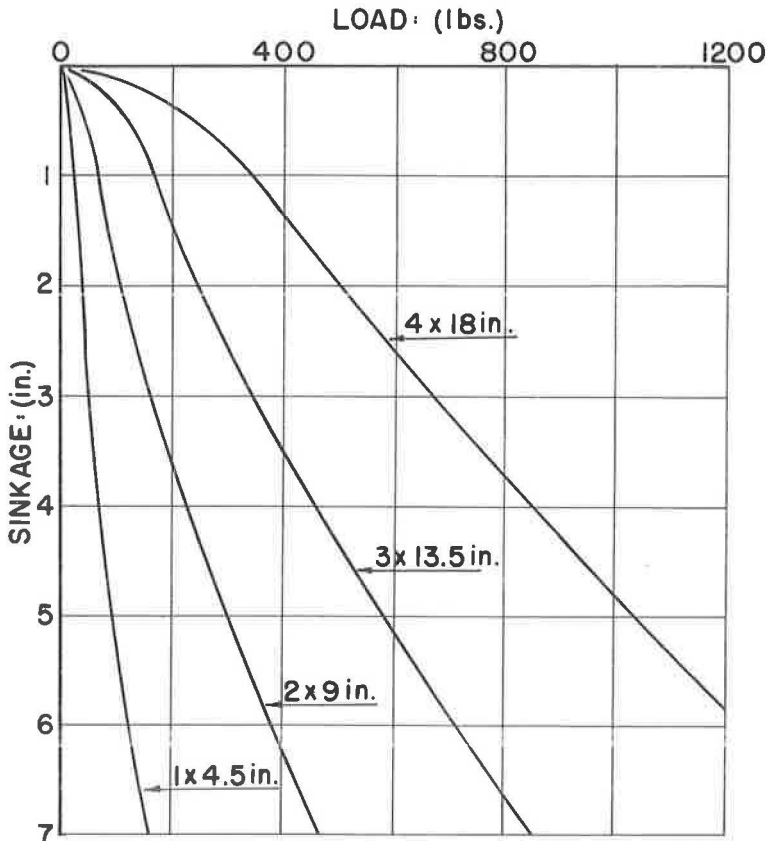
Figure 5. Rectangular plate-sinkage tests in dry Ottawa sand (60 in./min).
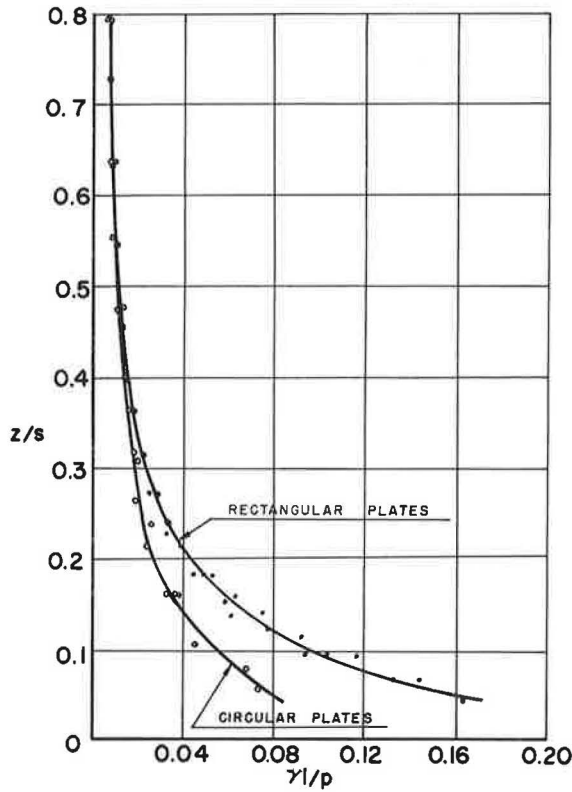
Figure 6. Dimensionless plot of pressure vs sinkage for dry Ottawa sand.

Converting the pressure-sinkage curves obtained for dry Ottawa sand in terms of dimensionless parameters (z/s and $\gamma\ell/p$), the curve shown in Figure 6 resulted; nearly all points are situated along an experimental curve for plates of a given geometrical shape.

Pressure-sinkage curves obtained in soils having a fair amount of cohesion have also been plotted in terms of dimensionless parameters. For example, a compacted wet Ottawa sand with an apparent cohesion of 0.2 psi also showed a remarkable collapse into a single curve for load-sinkage data obtained with plates of different sizes (Fig. 7).

Similar results were obtained in a snow material having cohesion of 0.1 psi (Fig. 8).

Plotting z/s vs $\gamma\ell/p$ relationships on log-log paper, a well-defined straight-line function resulted for sands and snow tested. Figure 9 shows a typical log-log plot of dimensionless parameters for dry Ottawa sand. Writing an equation for any of these straight lines the following pressure-sinkage equation results:

$$p = \frac{\gamma\ell}{A^{-\frac{1}{m}}B}\left(\frac{z}{s}\right)^{-\frac{1}{m}} \tag{3}$$

where A and B are the ordinate and abcissa, respectively, of any point along the straight line and m is the slope of the straight line. Constants associated with Eq. 3 are dimensionless parameters associated with soil properties and plate geometry.

Theoretically, only one load-sinkage curve is necessary for the evaluation of parameters in Eq. 3 and for the prediction of the load-sinkage behavior of a loading area
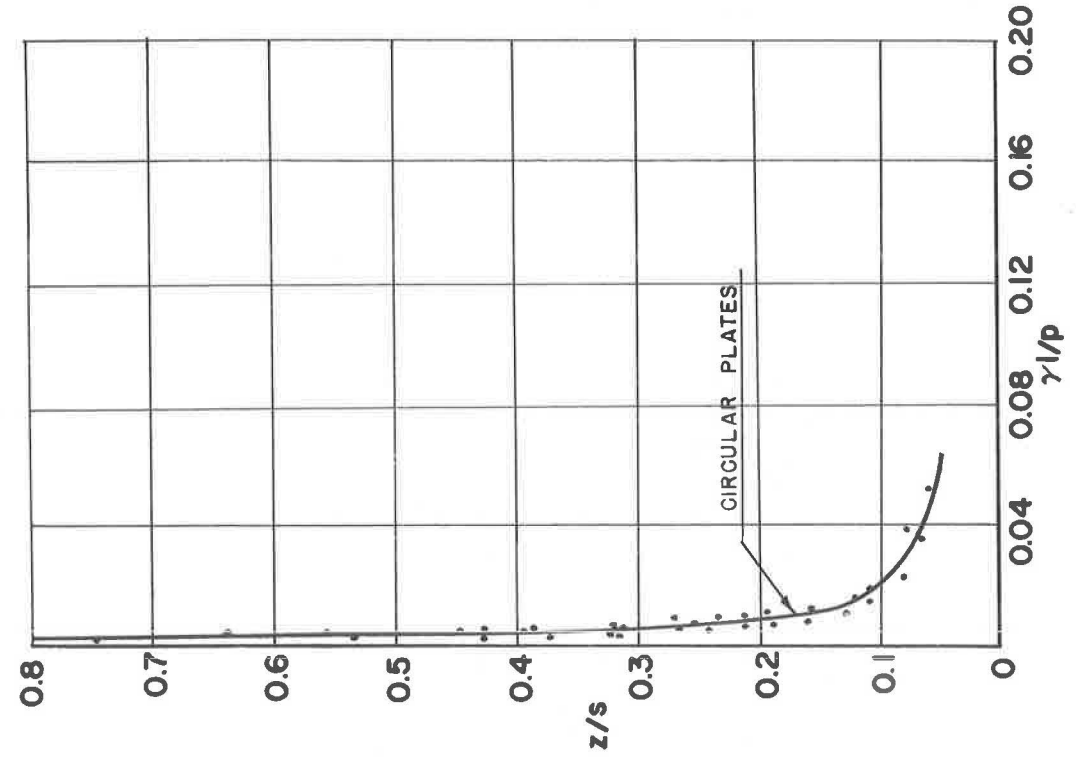
Figure 8. Dimensionless plot of pressure vs sinkage for snow.
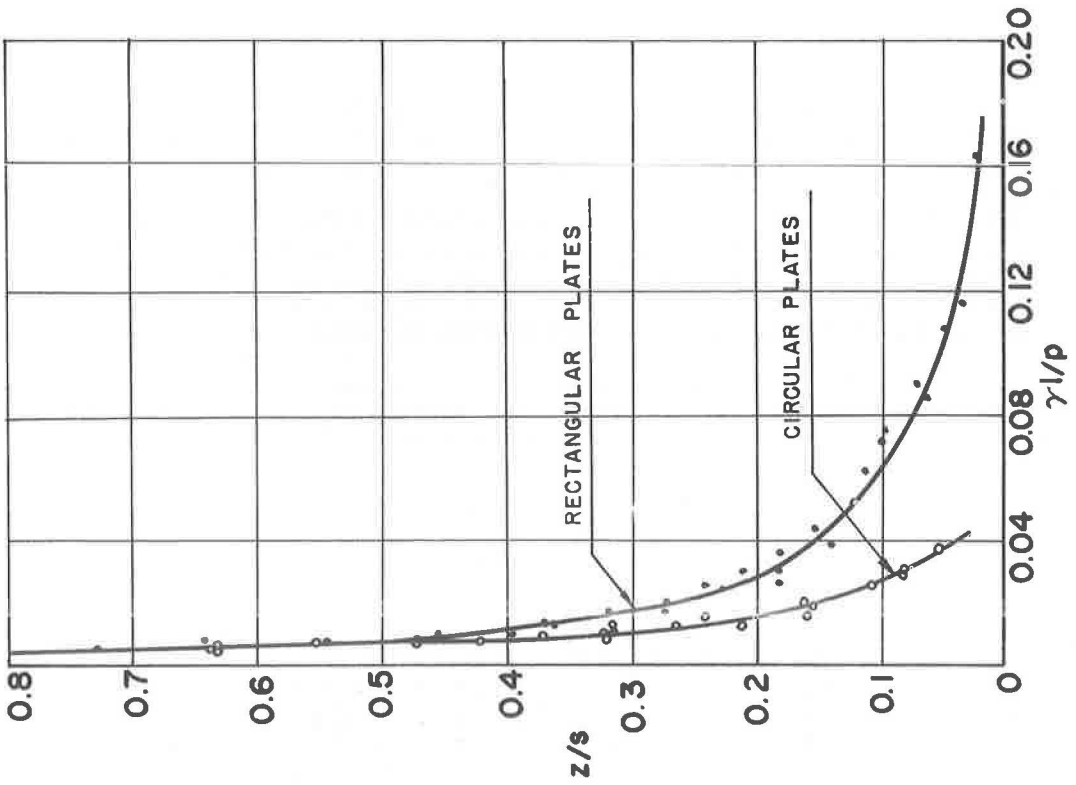
Figure 7. Dimensionless plot of pressure vs sinkage for wet Ottawa sand.

Figure 10. Dimensionless plot of pressure vs sinkage for clay soils.

Figure 9. Log-log plot of dimensionless parameters for dry Ottawa sand.
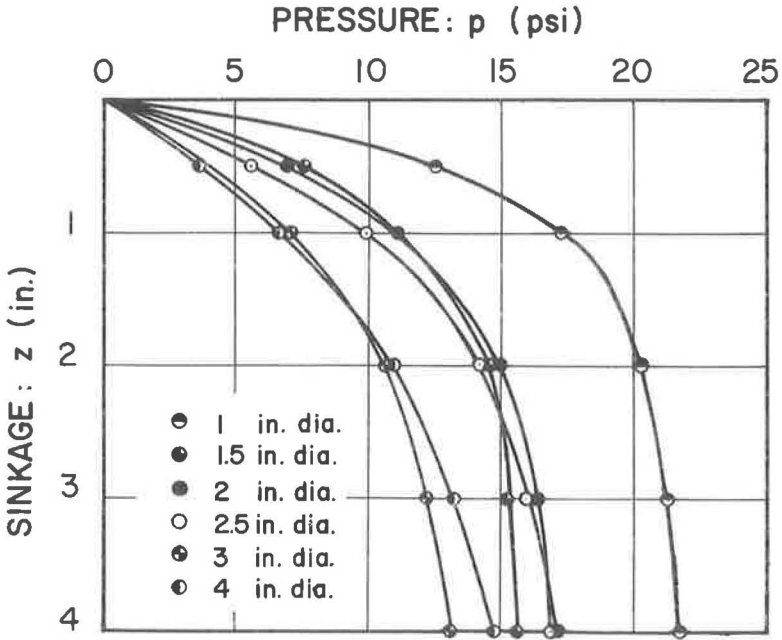
Figure 11. Circular-plate sinkage tests in Boston blue clay (2.25 in./min).
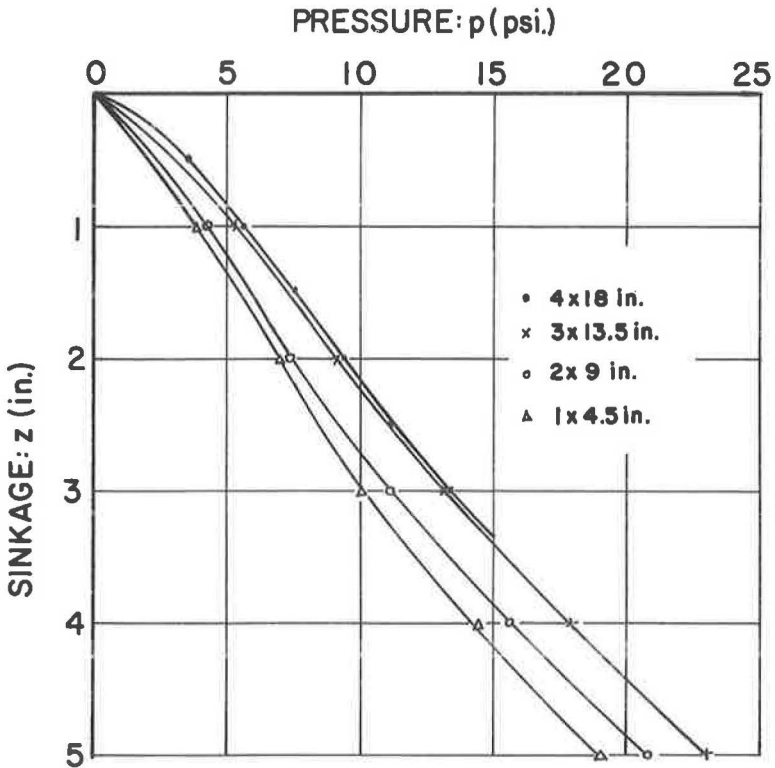
Figure 12. Rectangular-plate sinkage tests in Detroit clay (60 in./min).

from a small plate test, provided that the upper limit of extrapolating model footing data to prototype footings is known. Available experimental data indicate that a 1- × 4.5-in. footing is adequate to predict the load-sinkage behavior of a 4- × 18-in. footing. In this case, the prototype footing has 16 times greater contact area than the model footing.

Clay.—The resulting dimensionless relationships for clays are not encouraging. If small plate-sinkage tests are to be useful in predicting the behavior of large plates in cohesive soils, it will be necessary to resort to model soils. The experimental results support this conclusion.

In analogy to the sand experiments, z/s vs $\gamma\ell$/p relationships were established and plotted (Fig. 10). Typical load-sinkage curves obtained with circular plates in remolded Boston blue clay and with a set of rectangular plates in Detroit clay are shown in Figures 11 and 12, respectively.

The dimensionless plot shows that the resulting relationships are scattered, and do not reduce to a single curve for a given plate geometry. In connection with the "stronger" Detroit clay, having a cohesion of 1.3 psi as compared to 0.55 psi of the blue clay, the dimensionless parameters resulted in a well-defined curve for each plate size tested.

CONCLUSIONS

The conclusions of this investigation are somewhat negative in character. The rate effects in both sand and clay indicate an increase in bearing strength with an increase in loading rate. However, the magnitude of the increase in strength is not great enough to be considered significant for mobility purposes. If bearing capacity were the point of interest, the increase in strength could, however, be significant. It is assumed that if the loading rate were increased to the point of being considered as impact loading, the effect would be much more pronounced; but such a rate would be outside the range of interest to mobility research.

The results of this investigation show that the approach based on dimensional analysis is applicable in connection with frictional type of soils.

For clay soils, as shown by dimensional analysis, the effect of size does not reduce to a single general expression, implying that, except for predominantly frictional soils, an experimental relationship would have to be developed for each soil of interest.

REFERENCES

1. Bekker, M. G. Photographic Method of Determining the Soil Action Beneath Footings. Proc. 2nd Internat. Conf. on Soil Mech. and Found. Eng., Vol. 3, p. 193, 1948.
2. Gilboy, G. Bearing Capacity of Sands. Unpublished Rept. to Corson Construction Corp., 1930.
3. Langhaar, H. L. Dimensional Analysis and Theory of Models. John Wiley, New York, 1951.
4. Meyerhof, G. G. An Investigation of the Bearing Capacity of Shallow Footings on Dry Sand. Proc. 2nd Internat. Conf. on Soil Mech. and Found. Eng., 1948.
5. Osterberg, J. O. Symposium on Load Tests of Bearing Capacity of Soils. ASTM Spec. Tech. Publ. No. 79, p. 128, 1948.
6. Roberts, J. E. Small Scale Footing Studies: A Review of the Literature. Dept. of Civil Eng., M.I.T., 1961.
7. Selig, E. T., and McKee, K. E. Static and Dynamic Behavior of Small Footings. Jour. of Soil Mech. and Found. Div., ASCE, Vol. 87, No. SM6, 1961.
8. Skempton, A. W. An Investigation of the Bearing Capacity of a Soft Clay Soil. Jour. Inst. of Civil Eng., 1942.
9. Terzaghi, K. Theoretical Soil Mechanics. John Wiley, New York, 1957.

A Study of the Pressure-Penetration Relationship
For Model Footings on Cohesive Soil

W. H. PERLOFF and K. S. A. RAHIM
Respectively, Associate Professor of Soil Mechanics, Purdue University; and
Research Associate, Department of Civil Engineering,
Ohio State University

This paper describes a study of the relationship between the
pressure on model footings and the penetration of these footings
into saturated cohesive soils. Experimental results demon-
strate the influence of soil water content, rate of footing pene-
tration, type of testing, and roughness of the footing base on
this relationship. An empirical expression has been developed
to describe the pressure-penetration relationship. At this
time, the empirical equation represents the data satisfactorily
for square, rectangular, circular, and elliptical model footings
of various sizes.

•THE RESULTS of small-scale footing penetration tests are frequently utilized
to predict the sinkage of off-road vehicles traveling on soft soils. Inasmuch as the
resistance which the soil offers to motion is intimately related to the vehicle sinkage,
an adequate description of cross-country mobility depends on the ability to predict
sinkage of the prototype vehicle. However, to do this, it must be possible to express
the pressure-penetration relationship for a loaded area on the soil in terms of appro-
priate scale factors.

The problem is somewhat different from that often considered by foundation engi-
neers, because the magnitude of sinkage experienced by vehicles on soft soils is greatly
in excess of that which can be tolerated by most civil engineering structures. One
relationship commonly used in the field of land locomotion mechanics is that suggested
by Bekker (2):

$$p = \left(\frac{k_c}{b} + k_\phi\right) z^n \tag{1}$$

where k_c is the cohesive modulus of deformation of the soil, k_ϕ is the frictional mod-
ulus of deformation of the soil, b is the width of the loaded area, z is the sinkage of the
area, n is a dimensionless exponent, and p is the pressure applied to the area. Many
efforts have been made to verify this equation and to correlate the parameters k_c and k_ϕ
to soil type (9, 28, 29).

However, Eq. 1 can be questioned on several counts. Theoretical analyses of
rigid (3) and flexible (23, 30, 31) loaded areas on semi-infinite elastic media, as well as
experimental results for rigid loaded areas on both sands and clay (4, 7, 10, 11)
indicate that the displacement of a loaded plate on a soil is a function not only of
the width of the plate but of the shape as well. In addition, the interpretation of k_c and
k_ϕ as meaningful soil behavior parameters is hampered by the fact that the dimensions
of these constants are a function of the exponent n, which is a function of plate size
and soil type. Hence, even for a given soil, the deformation moduli will have different
dimensions. Furthermore, it would seem appropriate to examine critically the form

of the equation. Osterberg (17) found a straight-line load-sinkage relationship on a logarithmic plot, for load tests on clay, only in the range of small penetrations. Kondner and Krizek (11) suggest a hyperbolic relationship as most appropriate to fit their own data as well as those of other investigators. However, there is some question that the magnitude of deformation in the tests which they examined was sufficiently large to apply to a mobility problem. Vincent et al (29) suggested that Eq. 1 was valid for model plate studies on sand within a range of sinkage from 0.5 to 4.5 in. They found the exponent n to have a magnitude of approximately unity in this range, thus suggesting that the pressure-penetration relationship is linear! If such were the case over a meaningful range of pressures, the equations relating the pressure on a loaded area to the penetration of that area into the soil could be derived from finite elasticity theory. Clearly, the pressure-penetration relationship for soils is hardly this simple.

Based on the foregoing discussion, it seems that there is no presently available description of the pressure-penetration relationship for model footings on soil which is sufficiently general to encompass all of the significant factors involved. It was the specific objective of this study to examine this relationship for saturated cohesive soils, to elucidate the factors which influence it, and to seek an empirical description of the relationship.

PRELIMINARY ANALYSIS

In studying a problem in which so many factors affect the results, it is often convenient to group the factors into non-dimensional ratios. The standard method by which this is accomplished, dimensional analysis, has, in general, two benefits: first, it permits reduction in the number of variables studied; and second, it can assist the investigator in establishing dimensionless parameters of more significance to the problem than the individual factors themselves.

The variables thought to influence the pressure-penetration relationship for a purely cohesive soil ($\phi = 0$) are given in Table 1. Not all of the factors listed are independent. For example, the geometry of a footing can be described by the area, A, the circumference, C, and combinations of C, the width, B, and the length, L. Hence, when the independent variables have been chosen, they can be expressed in a variety of ways as non-dimensional ratios. Application of dimensional analysis procedures (12) yields functional relationships of the following general type:

$$f\left(\frac{z}{\sqrt{A}}, \frac{P}{Aq}, \frac{B}{L}, \frac{Pt}{A\eta}\right) = 0 \qquad (2)$$

TABLE 1

VARIABLES AFFECTING PRESSURE-
PENETRATION RELATIONSHIP FOR
SATURATED COHESIVE SOIL

Variable	Symbol	Dimensions
Footing width (or minor axis)	B	L
Footing length (or major axis)	L	L
Footing circumference	C	L
Footing area	A	L^2
Footing penetration	z	L
Force on footing	P	F
Soil water content	w	$F^0 L^0 T^0$
Soil strength parameter	q	FL^{-2}
Friction or adhesion coefficient between footing and soil	δ	$F^0 L^0 T^0$
Viscosity of soil	η	$FL^{-2}T$
Time of loading	t	T

One of the difficulties in a dimensional analysis approach is the choice of the most physically meaningful arrangement of variables. For example, the footing penetration can be represented in dimensionless form by any one of the following quantities:

$$\frac{z}{\sqrt{A}}, \frac{z}{B}, \frac{z}{C}, \frac{z}{L}, \frac{z}{\sqrt{CL}}, \frac{z}{\sqrt{CB}}$$

Similarly, the footing pressure can be expressed in a variety of ways, among which are

$$\frac{\sigma}{q}, \frac{\sigma t}{\eta}$$

where σ is the unit pressure on the footing (P/A).

The most useful parameters are determined from experimental results, and are discussed later.

EXPERIMENTAL PROCEDURES

Soil Used

The cohesive soil used in the majority of the tests was received as a dry, powdered, water-washed kaolin mined by the Edgar Plastic Kaolin Company of Edgar, Fla., and referred to herein as EPK. The clay is white, odorless when mixed with distilled water, and possesses the following classification properties:

Liquid limit: 58.5 percent
Plastic limit: 36.5 percent
Plasticity index: 22.0 percent
Shrinkage limit: 27.4 percent
Specific gravity of solids: 2.597
Percent clay size (<0.002 mm): 78 percent

Preparation of Soil Material for Testing

The powdered EPK was mixed in the as-received condition with a sufficient quantity of distilled water to bring the water content to approximately 45 to 48 percent. Initial mixing to insure homogeneity was performed with a Blakeslee power mixer. The soil was then passed through a Vac-Aire sample extruder which forces the soil through small openings into an evacuated chamber, thus removing air trapped in the voids. This feature is very important, because the use of unsaturated soil would further complicate the problem. The soil was passed through the extruder a minimum of three times to insure complete saturation and promote homogeneity, and was then extruded through a 2-in. square die. A complete description of the extruder and its operation is presented by Matlock et al (13).

Samples were cut precisely to desired lengths to fit tightly into four testing bins ranging in size from 10 in. wide by 18 in. long by 10 in. deep to 30 in. wide by 36 in. long by 36 in. deep. The extruded soil prisms were placed side by side in the bin to form a single 2-in. thick layer. The box dimensions are arranged so that the soil prisms will fit tightly together to form a uniform mass. When each layer was completed it was tamped with a spring loaded 2-in. square tamper, to insure that the soil truly formed a continuous mass. The spring tamper exerts a pressure approximating 2 psi on the soil. By this method, a mass of reasonably homogeneous, fully saturated cohesive soil can be prepared. The degree of saturation of the soil was checked on several occasions, and the soil was saturated in all cases.

The required number of layers of soil were placed in the bin, tamped, and covered with several sheets of waterproof plastic. The bin of soil was stored for at least 12 hr in a humid room before testing, to permit any minor internal adjustments of water content, and to promote further uniformity.

Model Footings

The plan dimensions of the model footings tested range in size from 1 by 1 in. to 3 by 9 in. They include squares, rectangles, circles, and ellipses. Some of the 1- and 2-in. square footings were made of brass. All other footings were made of polished, case-hardened, cold-rolled steel. The sides of all footings were polished to a smooth finish. The bases of the smooth footings were also polished to a smooth surface, whereas the bases of the rough footings were grooved in two directions at right angles to each other.

The footings were rigidly attached to the loading device in such a way as to prevent any rotation during testing.

Testing Procedure

The footings were loaded by an Instron Model TT-BM-L, Universal Testing Machine. Footing loads and penetrations were continuously recorded by the Instron on a 10-in.

Figure 1. Penetration test in progress.

wide strip chart. Figure 1 shows the Instron Testing Machine with a model footing mounted on the load cell under the crosshead at the inception of a test.

Before the start of each test, the soil underneath the model footing was leveled, and the model footing was lubricated on all sides and the base with Dow-Corning 200 silicone fluid with a viscosity of 1,000 centipoise, except in the case of the rough base footings, where only the sides were lubricated. During the course of the test the surface of the soil was covered with a plastic sheet at all times, except in the immediate vicinity of the footing, to inhibit loss of moisture through evaporation.

When more than one footing was tested in a bin, the spacing between the footings was never less than three times the footing width.

During the course of this research, a total of 247 model footing tests were performed (20). The majority of the tests were performed at constant rates of penetration of 0.50 or 2.0 cm/min. However, some tests were run as slowly as 0.01 cm/min and others were performed as rapidly as 8 cm/min. In the case of the constant rate of loading tests, the loading rate was either 12.5 or 25 kg/min. As it was necessary to vary the rate of penetration continuously to maintain a constant rate of loading, the rate of loading was chosen so that the penetration rates encountered would cover approximately the range of rates studied in the constant penetration rate tests. The constant rate of loading tests were carried out with a special load pacing attachment for the Instron which permitted a continuous loading rather than requiring application of discrete load increments.

Figure 2 shows a 1- by 16-in. model footing which has penetrated the soil to a depth of approximately 5 in. For illustrative purposes, the load cell and mounting plate have
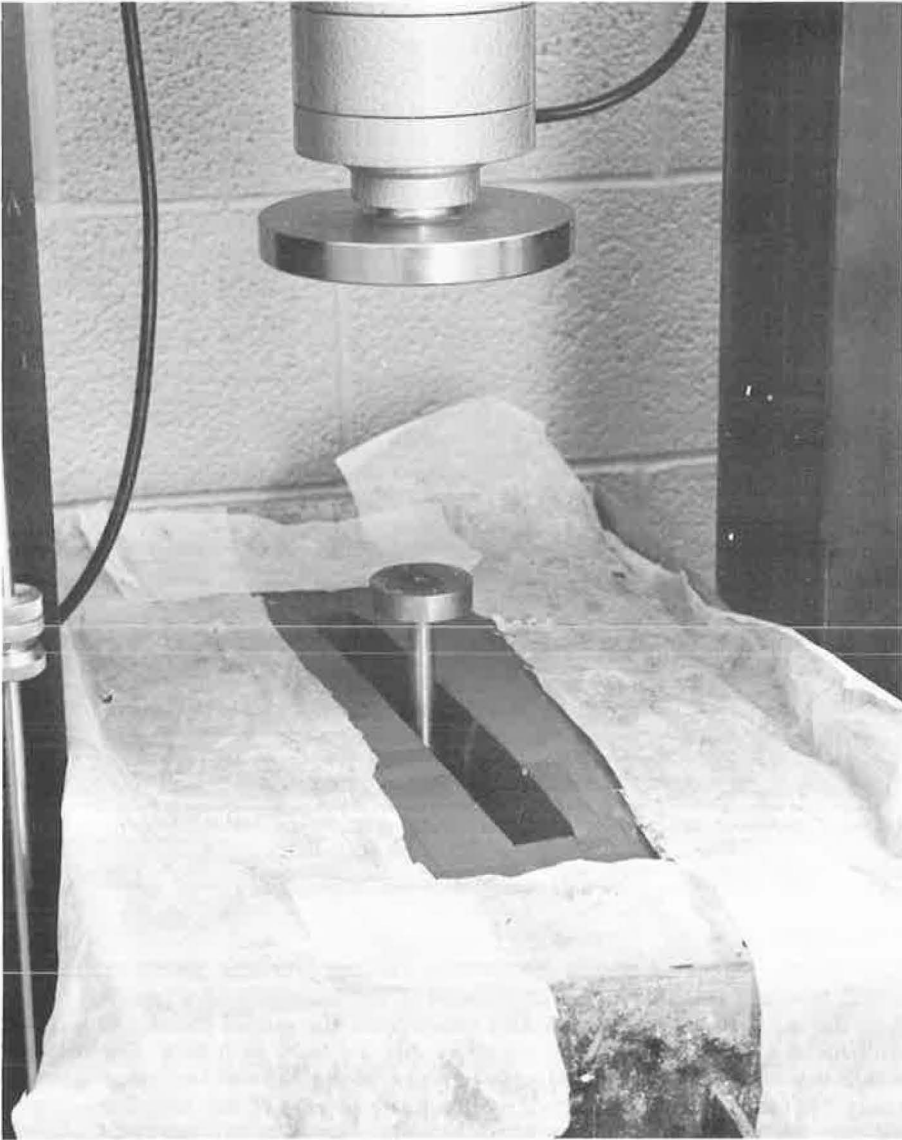
Figure 2. Model 1- by 16-in. footing at completion of penetration test.

been removed, and the footing has been left embedded in the soil.   Bulging of the ground surface has occurred in the vicinity of the footing.

At the completion of each model footing test, small soil specimens were removed from the area immediately under the center and sides of the footing indentation, and the water content of these specimens was determined.   At the completion of each series of footing tests, a 2-in. diameter cylindrical specimen was removed from the soil bin and an unconfined compression test performed on this specimen.   Both ends of the uncon-fined test specimen were lubricated with silicone grease to minimize the influence of end restraint.

When each series of tests was completed, the remaining soil from the test bin was removed and thoroughly remixed with a sufficient quantity of freshly mixed soil to fill the test bin.   The soil was then extruded once more, and a new test series prepared.

During the process of remixing, extrusion, and preparation of sample, approximately 1 to 2 percent of water was lost by evaporation. Thus, it was most convenient to prepare an initial batch of soil at a high water content and have subsequent batches at successively lower water contents.

FACTORS INFLUENCING EXPERIMENTAL RESULTS

In addition to the primary factors of footing shape and size, the following variables were felt to have a potentially significant influence on the pressure-penetration relationship: (a) water content of the soil, (b) rate of footing penetration, (c) type of testing, i.e., controlled rate of penetration or controlled rate of loading, and (d) roughness of the footing base.

Effect of Water Content

For most of the presently available results of model footings tests on cohesive soil, virtually no mention is made of the influence of water content. This seems to be the case because large batches of cohesive soil are usually tested in the unsaturated condition, and the problem is avoided by performing all tests under approximately identical conditions. In the writers' opinion, neglect of water content effects can lead to experimental errors which may obscure other effects being examined.

Figure 3 shows pressure-penetration curves for 2-in. square model footings on EPK at a variety of water contents. To some extent the shape, and certainly the ordinates of these curves, depend in an important way on the water content. These results are not surprising because the strength of EPK tested is greatly influenced by the water content. Since a model footing test is really only one form of strength test of the soil, it is to be expected that the pressure-penetration curves would be highly dependent on
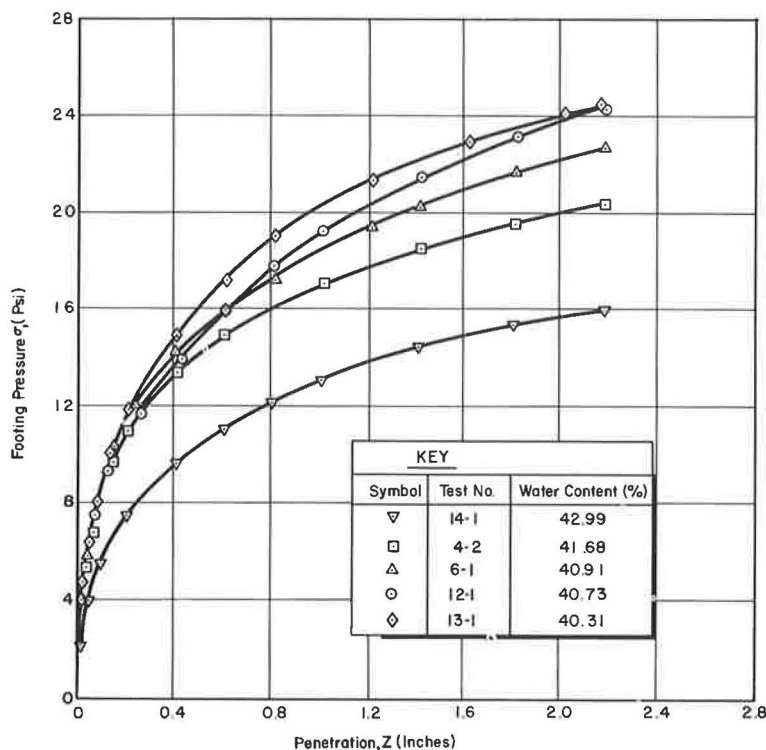
Figure 3. Effect of water content on pressure-penetration relationship for 2-in. square footings on EPK.
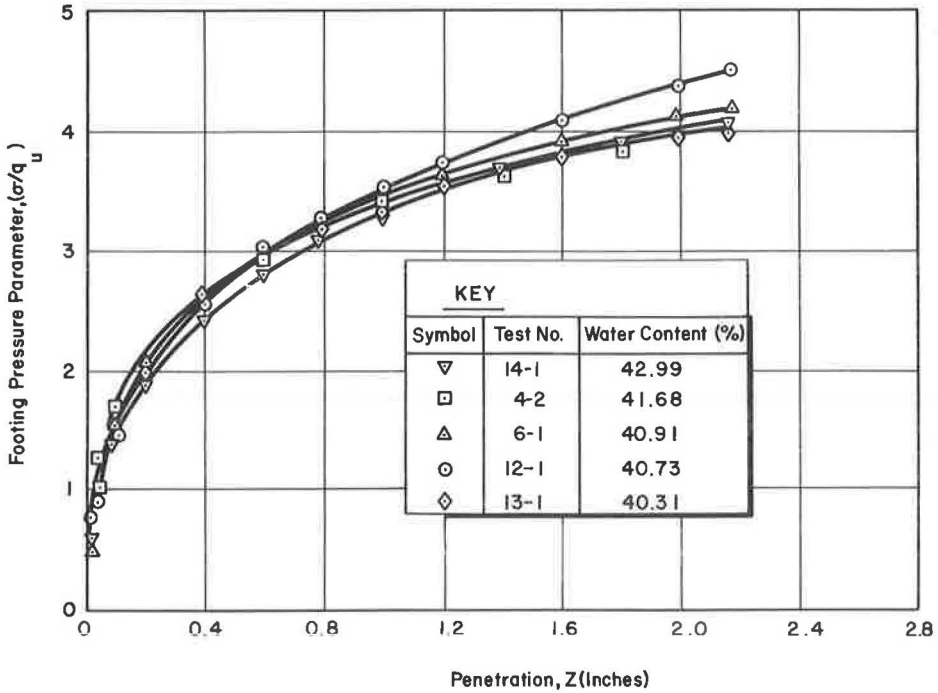
Figure 4. Effect of water content on pressure parameter-penetration relationship for 2-in. square footings on EPK.

water content effects. One way to assist in reducing the influence of water content on test results is suggested by the dimensional analysis previously described and by Kondner and Krizek (11). Inasmuch as the strength might be expected to depend on water content in the same general way as the pressure a model footing can sustain, it seems reasonable to consider, instead of the pressure, a pressure parameter equal to the magnitude of the average pressure on the model footing divided by the unconfined compressive strength of the soil at the water content of the footing tests (σ/q_u). The dimensional analysis suggests that such a parameter should include some measure of soil strength, but it does not indicate what strength measure is most appropriate. The unconfined compressive strength is a useful quantity for two reasons: first, because the unconfined compression tests can be performed quite readily, and second, because the unconfined compressive strength represents the actual in-situ strength of the soil, thereby bypassing consideration of such complicating factors as stress history effects.

The utility of the pressure parameter is shown in Figure 4, in which the results of Figure 3 are replotted in terms of σ/q_u. The curves from Figure 3 are drawn much closer to each other in Figure 4. The scatter in this figure is felt to be due to the variation in water content which occurs within the soil bin for a given test series. There are two ways in which this variation can affect test results. First, zones of increased or decreased water content in the vicinity of the footing test result in a footing pressure, at a given penetration, which may be higher or lower than representative values for average conditions. Second, variability in the unconfined compression results is bound to occur as a result of inhomogeneity, water content variations, nonparallel ends of the test specimen, and other minor experimental difficulties which inevitably arise.

To improve the utility of the pressure parameter, an attempt has been made to correct in part for the variability in the unconfined compressive strength. Figure 5 shows the unconfined compressive strength determined for each test series plotted as a function of the average water content of the unconfined compression specimen. These points lie along a straight line on the semi-logarithmic plot within a range of water
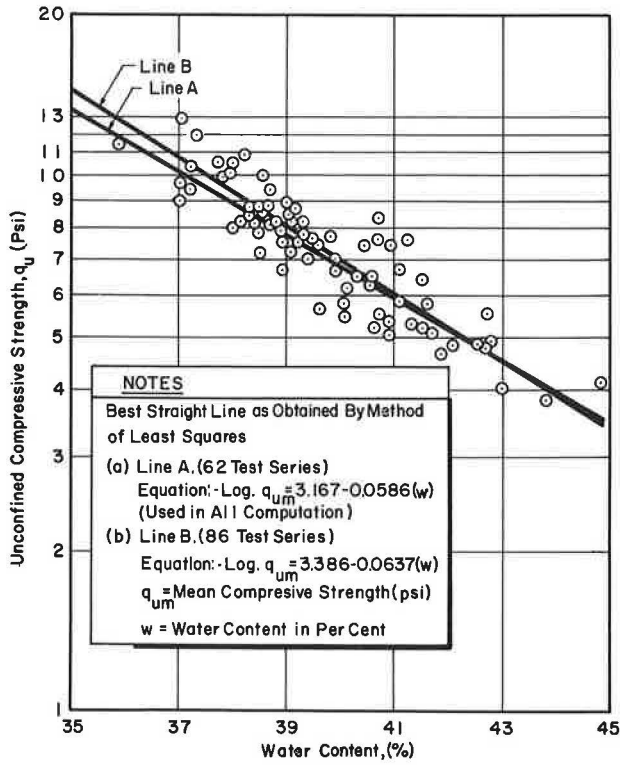
Figure 5. Water content vs unconfined compressive strength for EPK.
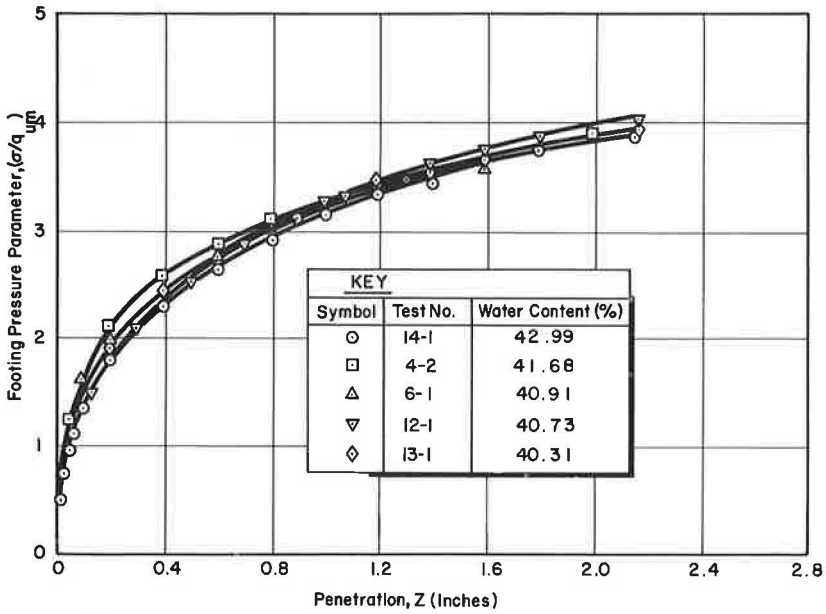
Figure 6. Effect of water content on pressure parameter-penetration relationship for 2-in. square footings on EPK.

contents from approximately 36 to 45 percent. The best straight-line fit of the plotted points (Fig. 5) was determined by the method of least squares. The value of the unconfined compressive strength indicated by this line at a particular water content is designated as the mean unconfined compressive strength, q_{um}. It appears that some experimental errors may be eliminated in the analysis by redefining the pressure parameter as the pressure on the model footing divided by the q_{um} corresponding to the water content of the soil. Figure 6 shows the data from Figures 3 and 4 with the footing pressure parameter recomputed as σ/q_{um}. Additional improvement can be noted in the approach of these data to a single curve, even though the unconfined compressive strength of the soil represented by these tests varies by a factor of approximately 1.5.

The relationship shown in Figure 5 is also of use in preparing soils of a given consistency or strength. Utilizing this figure, it is possible to estimate quite closely the water content at which a given strength will be obtained.

Effect of Penetration Rate

Tests were performed at various rates of penetration to examine the effect of penetration rate on the pressure-penetration relationship. The tests were carried out at penetration rates from 0.01 to 8.0 cm/min on square, rectangular, and circular footings. Results of the tests on 2-in. square footings, which are typical of all the test data, are shown in Figure 7. These results indicate that, at large penetrations, the pressure parameter is substantially larger for the slowest test than for the fastest test. Also, at small penetrations the reverse is true. To interpret these results in a meaningful manner, it is perhaps useful to review a few well-established concepts about the influence of testing rate on the behavior of cohesive soils.

As noted previously, a model footing test on a cohesive soil is really only one of many possible forms of strength tests. Similarly, the pressure-penetration relationship is simply a type of stress-strain curve of the soil. Hence, insight into the effect of testing rate on the pressure-penetration relationship can be obtained by considering the ordinary stress-strain relationships obtained from laboratory strength tests. The influence of testing rate on the results of stress-strain tests on cohesive soils seems to be three-fold in nature:

1. The most significant effect of testing rate, by far, is to determine whether, and how much, drainage of pore fluid occurs during the course of the test. Drainage can be prevented by performing a test so rapidly that essentially no drainage occurs due to the relationship between the permeability of the soil and the speed of testing, or, in the case of strength tests in which a soil specimen can be completely enclosed, all
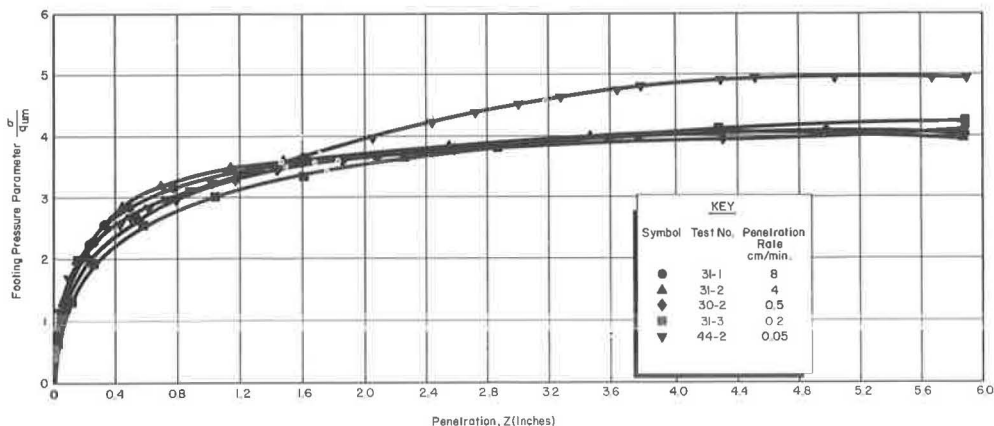
Figure 7. Effect of penetration rate on pressure-penetration relationship for 2-in. square footings on EPK.

drainage outlets are simply shut. If partial drainage occurs during loading, it may be difficult to compare test results.

2. Another important effect is that of soil creep (14, 18, 24). This effect is much more pronounced in some soils than others, and can be observed most strongly in sensitive and thixotropic soils. From the point of view of vehicle mobility, it hardly seems likely that stresses will be imposed on the soil at such a low rate that creep will become an important factor. Hence, it is important to perform the model footing tests in such a manner that creep is essentially eliminated. However, in the results shown in Figure 7 the soil appears strongest, at large penetrations, in the slowest test.

3. Finally, in general one must consider the dynamic, or inertial effect. Inertial effects occur only at very large testing rates, greatly in excess of those considered herein. Hence, dynamic effects can hardly be expected to be observed in the test results discussed.

Based on the foregoing discussion, it seems likely that the first two effects mentioned may be acting and influencing the curves shown in Figure 7. Indeed, this seems to be the case. Notice that at small penetrations, the slower tests lie below the faster tests. This would seem to be a minor manifestation of the creep effect. However, at large
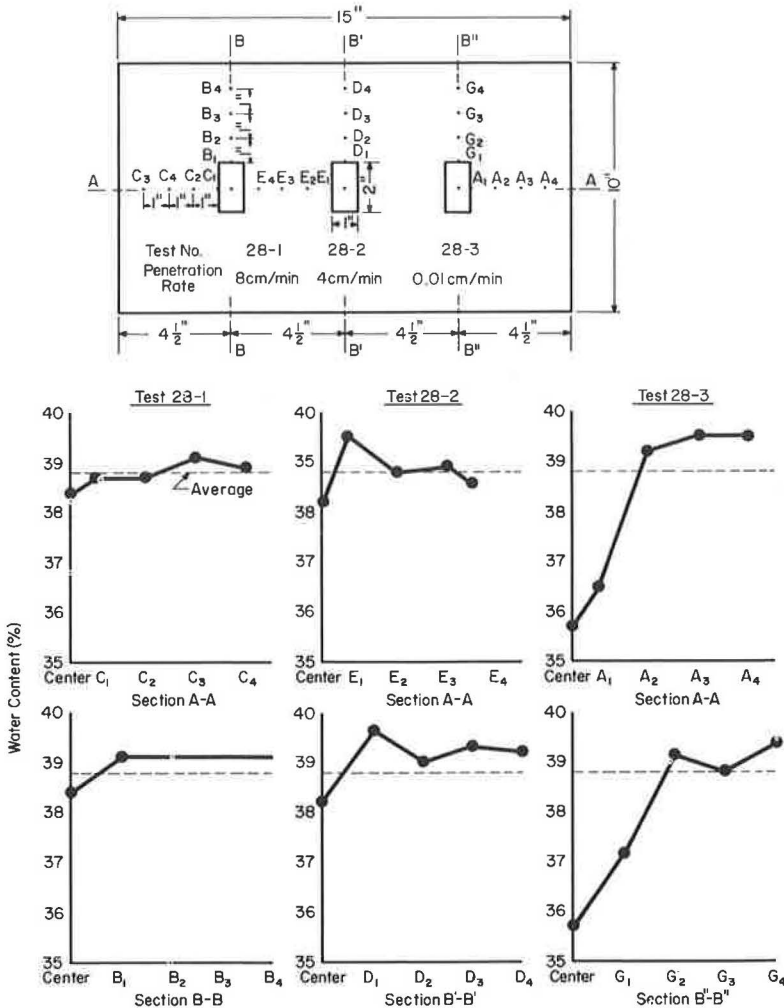
Figure 8. Effect of penetration rate on water migration under 1- by 2-in. model footings on EPK.
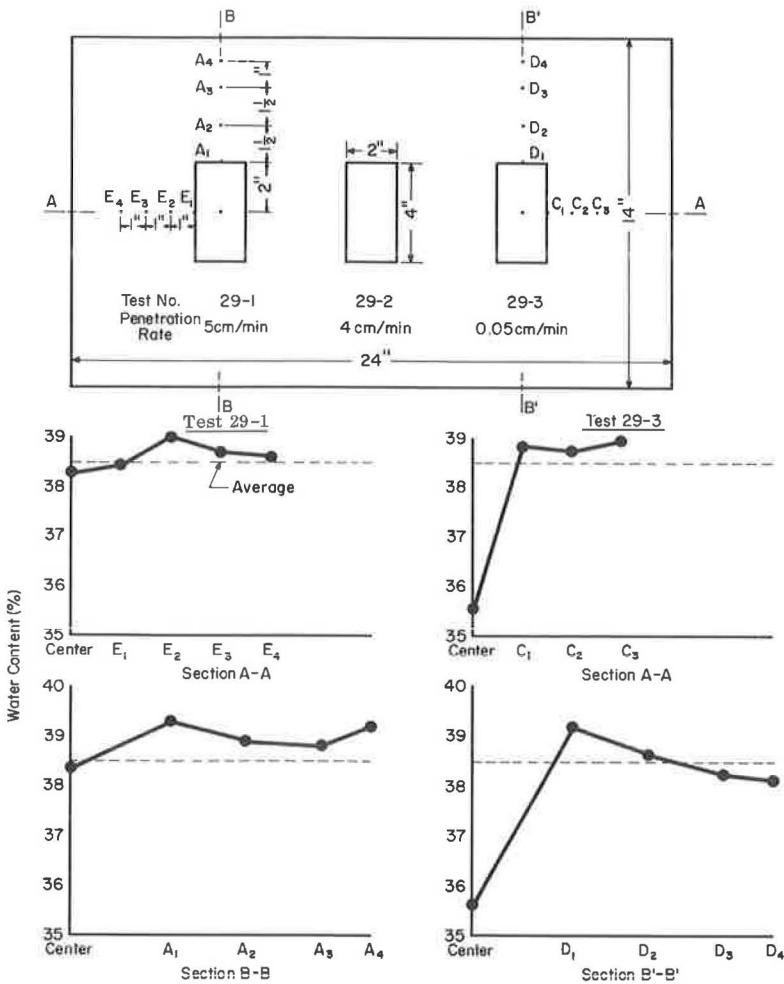
Figure 9. Effect of penetration rate on water migration under 2- by 4-in. model footings on EPK.

penetrations, and therefore, after longer times, the slower tests are stronger. This is probably due to migration of water away from the zones of high stress concentration underneath the footing permitted by the longer duration of the slower tests. If adequate time is provided for drainage to occur, the void ratio of the soil will decrease with a corresponding increase in strength.

The influence of penetration rate on moisture migration and the results for five model footing tests are shown in Figures 8 and 9. The locations of the model footings in the soil testing bins are shown in the upper part of the figures. At the completion of each test, the model footing was quickly removed and water content samples were taken from the elevation of the base of the footing at the locations shown in the upper part of the figures. The lower portions of Figures 8 and 9 show the variation in water content with distance from the center of each footing along the two principal axes. Several observations can be made about these results:

1. The water content immediately under the center of the footing is less than the average water content of the soil bin.

2. The loss in water content immediately under the center of the footing is quite clearly related to the rate of testing and/or the total time of testing. Thus in Figure 8,
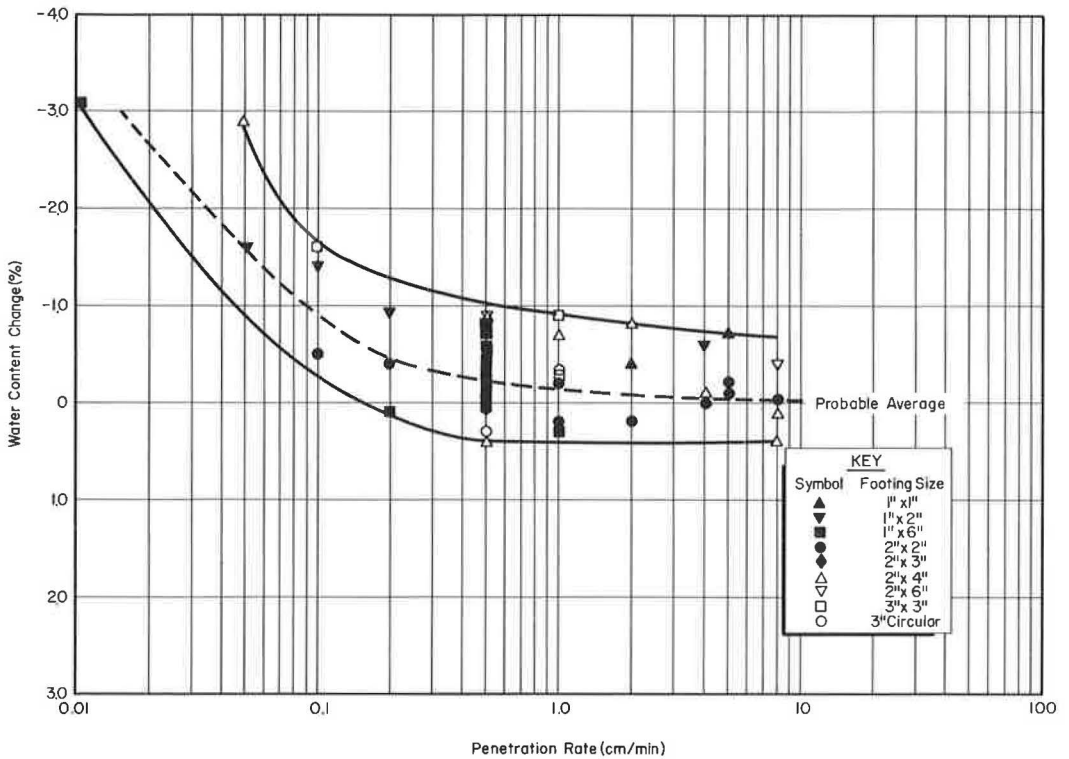
Figure 10. Effect of penetration rate on change in water content under model footing on EPK.

the water content under the center of the 1- by 2-in. footing tested at a penetration rate of 8 cm/min is only 0. 4 percent below the average water content of the box; whereas for the test performed at a penetration rate of 0. 01 cm/min, the water content under the center of the footing at the end of the test was 3. 1 percent below the average water content of the soil mass. A similar result is shown in Figure 9. A quantitative measure of the effect of penetration rate on moisture migration is shown in Figure 10. The figure shows the difference in water content between a point immediately under the center of the footings and the average for the soil bin, plotted as a function of the penetration rate. There are some points at the higher penetration rates for which there is actually a slight increase in water content under the footing. This is undoubtedly due to the unavoidable small nonuniformities which always occur. However, the average results of many tests show that the water content under the footing is essentially unchanged, as the penetration rate varies from 8 cm/min to approximately 0. 5 cm/min, and decreases sharply at lower penetration rates. It is important to remember, however, that the results obtained by measuring the water content immediately under the footing, and at points at the elevation of the base of the footing, will indicate changes in water content much larger than probably exist at some depth below the footing. Inasmuch as the pressure required to produce a given penetration depends on the resistance of the soil within a large zone under the footing, the results in Figures 8 and 10 indicate a limiting condition only, and not a result typical of this entire zone. Hence, it may be concluded from Figures 7 and 10 that penetration rates of the order of 0. 5 cm/min, and greater, are adequately high to prevent artifacts in the experimental results due to moisture migration underneath the footing.

3. In almost all cases the water content just outside the edge of the footing is higher than the average for the entire box. A theoretical analysis for a footing embedded within an elastic medium (21) shows that in the vicinity of the edge of the footing, tension
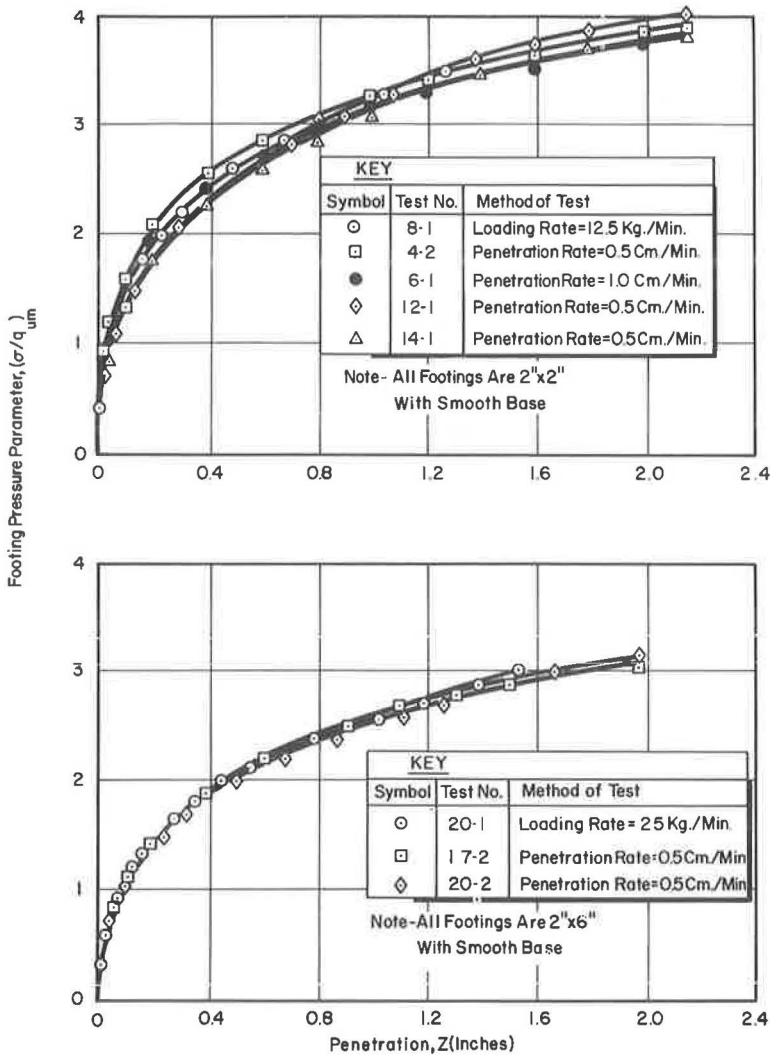
Figure 11. Effect of test method on pressure parameter–penetration relationship for EPK.

exists in the medium. In a cohesive soil, the tensile stress causes migration of pore water from the compressive zone immediately under the footing, and the relatively unstressed material outside the footing, into the zone which is in tension.

Effect of Type of Testing

The pressure-penetration relationship from model footing tests on cohesive soils will eventually be applied to the prediction of vehicle sinkage in similar soils. A vehicle imposes a load on the soil with penetration occurring as a function of the load. Therefore, it would seem appropriate to perform the model footing test with the same type of loading. However, it is experimentally simpler to use a constant rate of penetration method. Hence, the constant penetration rate type of test was compared with a constant loading rate type of test to determine whether the two tests are truly equivalent. Figure 11 shows the results of two such comparisons made on square and rectangular footings. These results indicate that the two types of tests produce virtually identical effects.
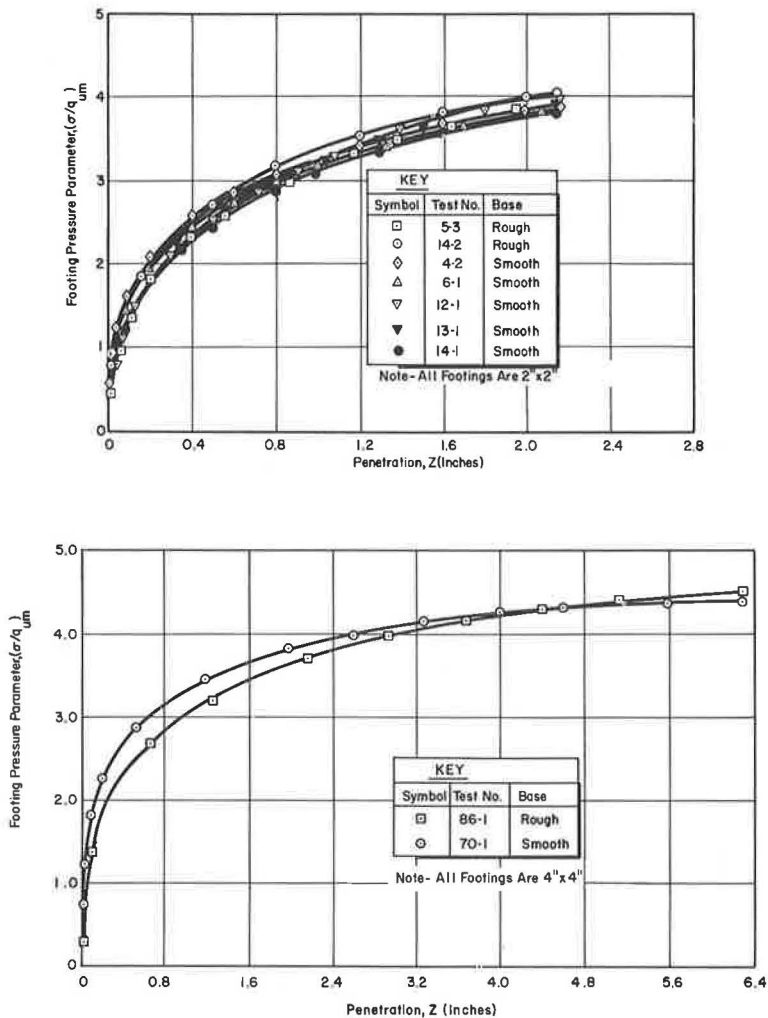
Figure 12. Effect of base roughness on pressure parameter-penetration relationship for square footings on EPK.

This result seems reasonable when the mechanism of constant rate of loading tests is considered. To carry out such tests, it is necessary to vary the penetration rate continuously to insure that the loading rate remains constant. Hence, at small penetrations the penetration rate required to maintain a constant loading rate is very small, whereas at large magnitudes of penetration, the penetration rate required is much higher. This is indicated in Table 2 which gives data from one test performed at a constant rate of loading on a 2-in. square footing. The penetration rate required to maintain a constant loading rate at the end of the test is approximately 50 times that required to maintain the same loading rate at the beginning of the test.

Therefore, the effect of test type is really quite similar to the effect of varying the rate of penetration, and the comments in the preceding section apply here as well. Thus, it seems that the type of testing does not influence results as long as the average rate of penetration is sufficiently high to prevent significant drainage of water from the zone beneath the footing.

Load Interval (kg)	Avg. Penetr. Rate During Load Interval (cm/min)	Ratio of Penetr. Rate to Initial Penetr. Rate
0-2.5	0.075	1
10-12.5	0.275	3.7
20-22.5	1.09	14.5
30-32.5	2.46	32.8
35-37.5	3.83	51.1

[a]Test number: 8-1; 2-in. square smooth base footing;
rate of loading: 12.5 kg/min.

Effect of Roughness of Footing Base

Theoretical analyses of the ultimate bearing capacity of purely plastic material being penetrated by a rigid punch indicate that a punch with a "perfectly rough" base will be capable of sustaining a pressure approximately 10 to 30 percent larger than a punch with a "perfectly smooth" base (15, 27) depending on the shape of the punch. Thus, it becomes important to determine what effect the condition of the base of the model footings will have on experimental results. Consequently, comparative tests were performed for a variety of footing sizes on "smooth" and "rough" base footings. The smooth base footings had polished sides and bases, and were lubricated with silicone fluid on all surfaces in contact with the soil. The rough base footings had polished sides, but the bases were roughened, as previously described. The sides were lubricated with silicone fluid, but the base was not. The results of such
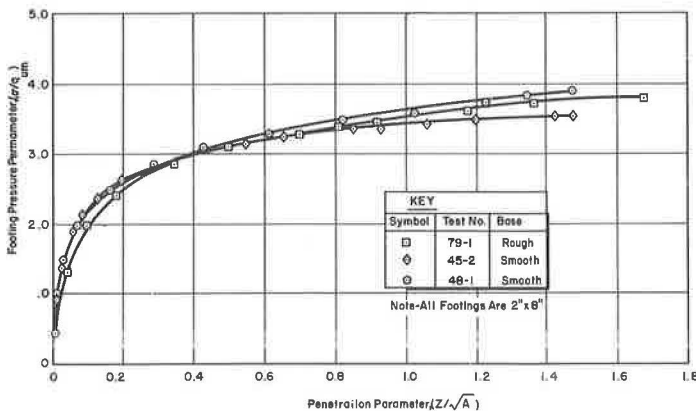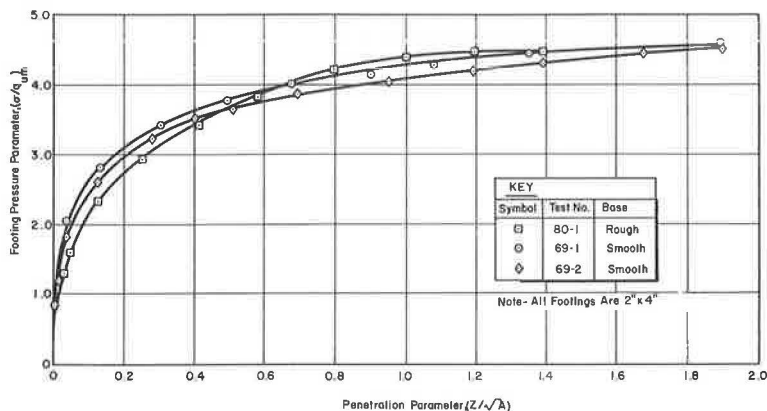
Figure 13. Effect of base roughness on pressure parameter-penetration relationship for rectangular footings on EPK.
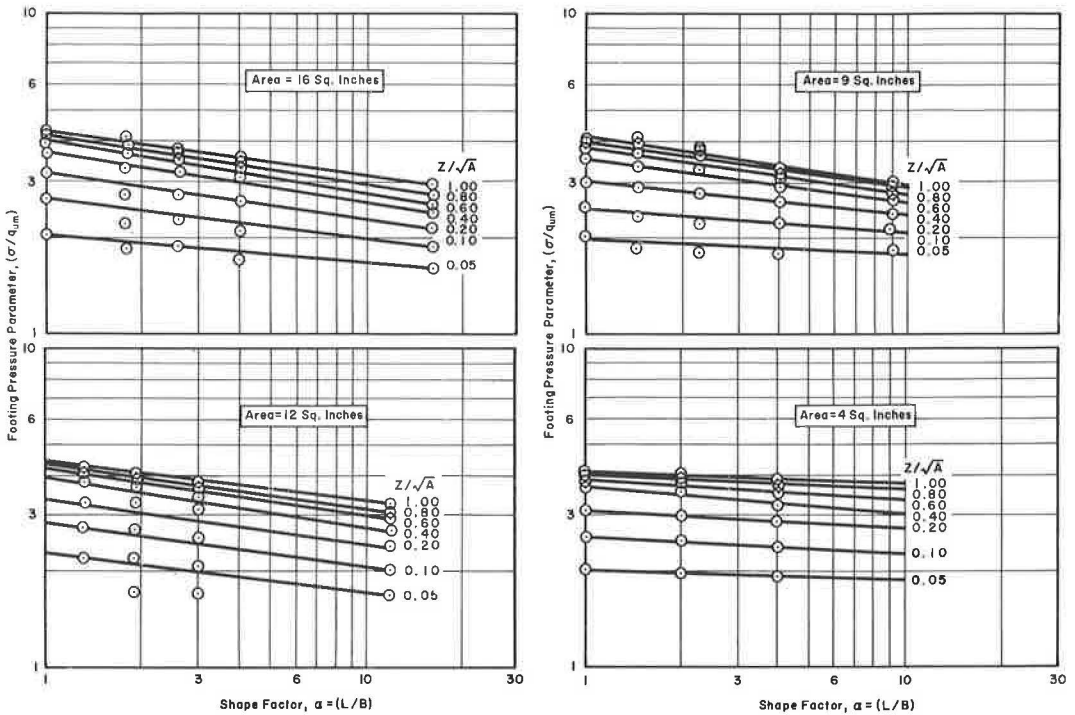
Figure 14. Effect of shape factor on pressure parameter for constant area footings on EPK.

comparative tests for square and rectangular model footings are shown in Figures 12 and 13. Surprisingly, these results suggest no effect of footing roughness on the pressure-penetration relationship. The reason for this appears to lie in the definition of "smooth base" and "rough base." In the theoretical analyses, a smooth base punch is mathematically characterized by the fact that no shear stress exists at the punch-soil interface. Similarly, the rough base punch is characterized by the fact that no relative horizontal displacement occurs between the punch and the soil at the punch-soil interface. Observation of the soil distortion underneath a footing after the removal of the footing at the end of a test suggests that even for the lubricated, so-called smooth base footings, some friction actually does develop due to the large normal pressures at the base of the footing. Hence, although a polished lubricated footing feels smooth to the touch, when it is pressed into the soil, its behavior can be characterized by the mathematical definition of a rough footing. Thus, for practical purposes, it appears impossible to prepare a model footing sufficiently smooth to prevent the development of shear stress between the footing and the soil.

Because it is simpler to prepare polished footings, the majority of the footings were constructed with polished surfaces.

PRESSURE-PENETRATION RELATIONSHIP

The previous sections have considered, and accounted for, a variety of factors which might influence the pressure-penetration relationship and obscure size and shape effects. After extraneous factors were eliminated, an examination of available pressure-penetration equations (1, 2, 5, 6, 11) was made. None of the suggested relationships was found to represent reasonably the data obtained in this study, or the published data of other investigators for a wide range of penetrations. Hence, a more meaningful relationship was sought.

The approach taken was to establish an empirical description of the pressure-penetration relationship, utilizing the observed relationship itself. When the various factors discussed in the preceding sections are held constant, the dimensional analysis suggests that the pressure should be a function of penetration, size, and shape of the model footing. A theoretical analysis by Schleicher (23) shows that penetration can be most appropriately represented in a dimensionless form by a penetration parameter, $z/\sqrt{A}$, and the shape effect can be represented by the ratio of length to width, L/B (herein designated α).

To elucidate the influence of shape, a number of model footing tests were carried out on footings of constant area with varying shape factors. Figure 14 shows the results of such tests for areas of 4, 9, 12, and 16 sq in. These results are shown in the form of footing pressure parameter plotted as a function of the shape factor, to logarithmic scales, for given values of penetration parameter. Except for very small values of penetration for the smaller footings, the slopes of these lines on logarithmic scales are approximately constant (Fig. 15). This figure shows the logarithmic slopes of these lines as a function of $z/\sqrt{A}$. Although there is considerable scatter apparent in Figure 15, the actual variation in slope of the lines in Figure 14 is not so large. It is not clear from Figure 15 whether or not there is a significant effect of area on these slopes. However, data for another soil, given below, suggest that, in fact, the slopes of the lines in Figure 14 are independent of area. Hence, it will be assumed here that the shape effect is independent of footing area and the magnitude of penetration.

The equation of these lines can be written as

$$\sigma/q_u = F\ (z/\sqrt{A})\ \alpha^{-D} \tag{3}$$

where $F\ (z/\sqrt{A})$ is the pressure corresponding to a given penetration for a square or circular footing (for which $\alpha = 1$) and D is the average absolute value of the logarithmic slopes of the lines in Figure 14. Eq. 3 states that, for a given size footing, the resistance to penetration decreases as the ratio of length to width increases. This result is in agreement with standard bearing capacity analyses for cohesive soils (26, 27). In fact, the numerical values of the shape effect term, α^{-D}, are close to those found experimentally by Meyerhof (15) for the effect of shape on the bearing capacity of model footings in clay.

The quantity $F\ (z/\sqrt{A})$ is actually the pressure-penetration relationship for square and circular footings, for which $\alpha = 1$. The relationship is shown in Figure 16 for 19 tests on square and circular footings with areas varying from 4 to 16 sq in. The penetration is represented by the penetration parameter, $z/\sqrt{A}$. The mean curve for all the tests is indicated by the dashed line. Examination of the plotted points shows that the scatter from the mean curve does not follow any consistent pattern, and can probably be attributed to the unavoidable variability always present in experimental results. Thus, the parameter $z/\sqrt{A}$ appears significant, because the pressure-penetration relationships for all of these square and circular footings reduce to the same curve when penetration is represented by this penetration parameter.

A variety of expressions by which the relationship shown in Figure 16 could be represented has been studied, and the two-constant rectangular hyperbola shown below appears to be the most applicable:

$$\sigma/q_u = \frac{z/\sqrt{A}}{M + Q\ z/\sqrt{A}} \tag{4}$$

where M and Q are constants.

To determine if the pressure-penetration relationships shown in Figure 16 can reasonably be represented by Eq. 4, a test plot can be constructed (8). Eq. 4 can be rewritten as

$$\frac{z/\sqrt{A}}{\sigma/q_u} = M + Q\ z/\sqrt{A} \tag{5}$$
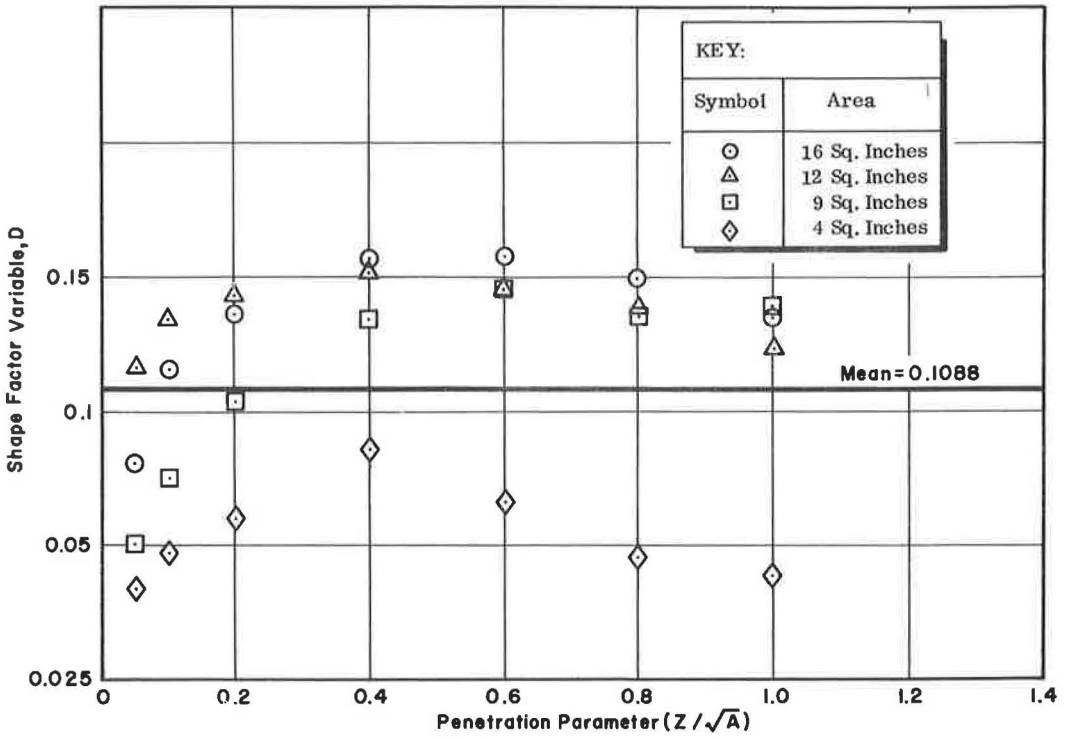
Figure 15. Effect of footing area and penetration on logarithmic slope of lines in Figure 14.
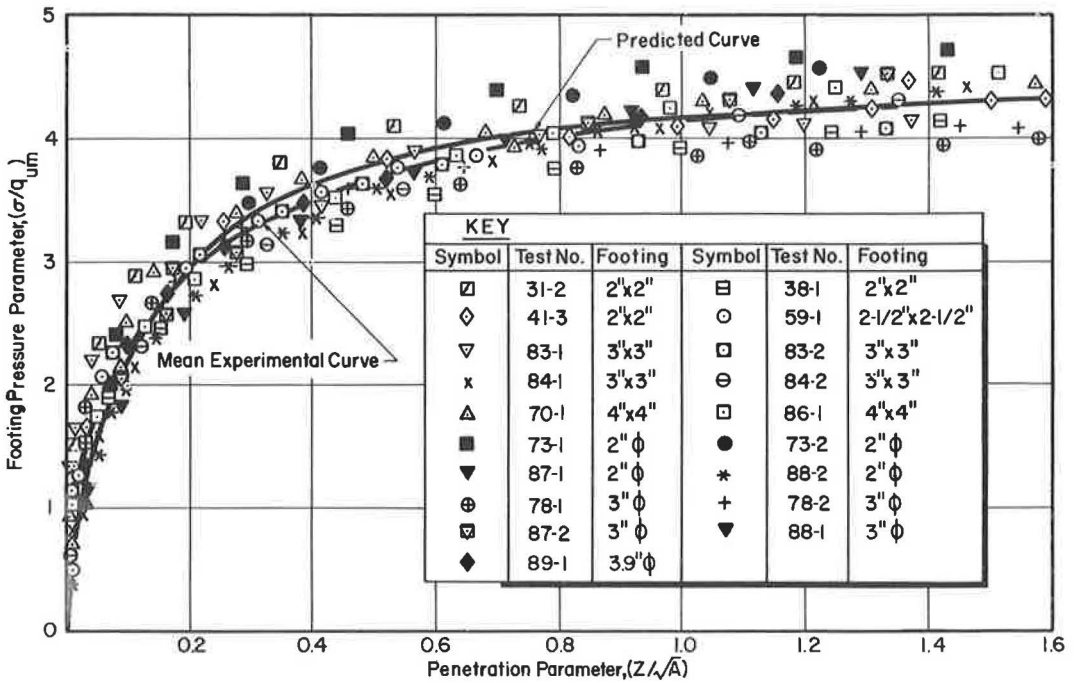
Figure 16. Pressure-penetration relationship for square and circular footings on EPK $(\alpha = 1)$.

KEY				
Symbol	Test No.	Footing	M	Q
○	41-3	2"x2"	0.022	0.219
△	70-1	4"x4"	0.022	0.214
◇	78-2	3"Dia.	0.020	0.230
□	83-2	3"x3"	0.024	0.222
▽	88-2	2"Dia.	0.024	0.219
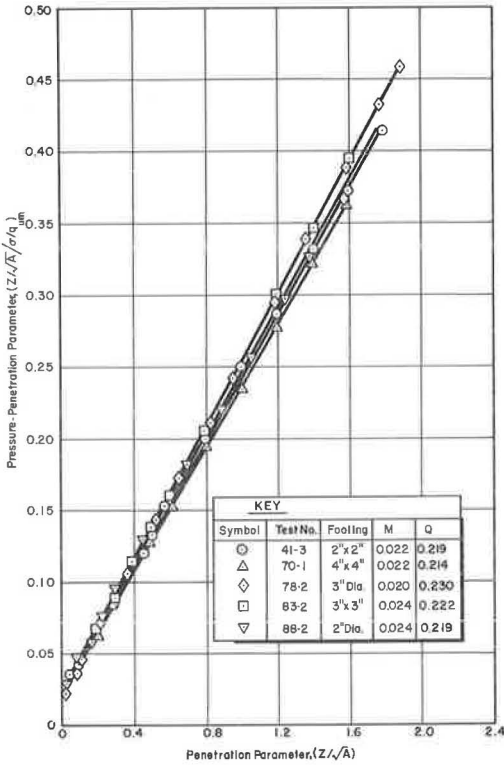
Figure 17. Hyperbolic pressure-penetration test plots for square and circular footings on EPK.

which is the equation of a straight line. Hence, if the data in Figure 16 can, in fact, be represented by Eq. 4, these data will appear as a straight line when plotted in the form of Eq. 5.

The typical test plots of this sort in Figure 17 show that Eq. 4 does satisfactorily represent the experimental data over a large range of penetrations. The constants in Eq. 4 are determined from the test plot: M is the σ/q_u intercept when $z/\sqrt{A} = 0$, and Q is the slope of the test plot line.

A physical interpretation can be ascribed to the constants M and Q in Eq. 4. By the appropriate substitutions it can be seen that $1/M$ is the initial tangent modulus (slope) of the hyperbolic curve. The quantity $1/Q$ is the magnitude of the pressure parameter to which the hyperbolic curve is asymptotic.

The test plot lines in Figure 17 all lie quite close to each other, and it is not surprising that the magnitudes of the constants M and Q are all quite close. The fact that there is no significant influence of area on the magnitude of these constants is shown by Figure 18, in which the constants M and Q have been plotted as a function of $1/\sqrt{A}$. Although some experimental scatter is present, there does not appear to be any consistent trend as a function of footing area.

Combining Eqs. 3 and 4 results in an empirical pressure-penetration relationship which should predict the behavior of model footings of various shapes and sizes:

$$\sigma/q_u = \frac{z/\sqrt{A}}{M + Q\ z/\sqrt{A}}\ \alpha^{-D} \tag{6}$$

where $D = 0.1088$, $M = 0.0232$, and $Q = 0.219$ for the cohesive soil (EPK) tested. Eq. 6 predicts that the relationship between σ/q_u and $z/\sqrt{A}$ for square and circular footings is unique for all size footings, and that the shape effect is independent of footing size.

The validity with which Eq. 6 represents the actual pressure-penetration data for model footings on EPK is shown in Figures 16 and 19 through 24. These figures show results for square, circular, rectangular, and elliptical footings with areas from 2 to 27 sq in. and length-to-width ratios from 1 to 16. The results of tests on square and circular footings of various sizes are shown in Figure 16. The solid line is the predicted curve, and inasmuch as it was determined essentially from these same points, it is not surprising that the predicted curve represents the data quite well. The results for both squares and circles ($\alpha = 1$) are indistinguishable from each other. Similar comparisons are made for values of α greater than one, and a variety of areas (Figs. 19-24). As the constants in the hyperbolic expression were determined from the data for square and circular footings (Fig. 16), the excellent representation of the data by the prediction equation is considered a demonstration of the validity of this approach.

Figures 20 and 21 show the results of tests on elliptical footings. It seems clear that rectangular and elliptical footings yield essentially the same results (which can be represented by the prediction equation) when the rectangle and ellipse being compared
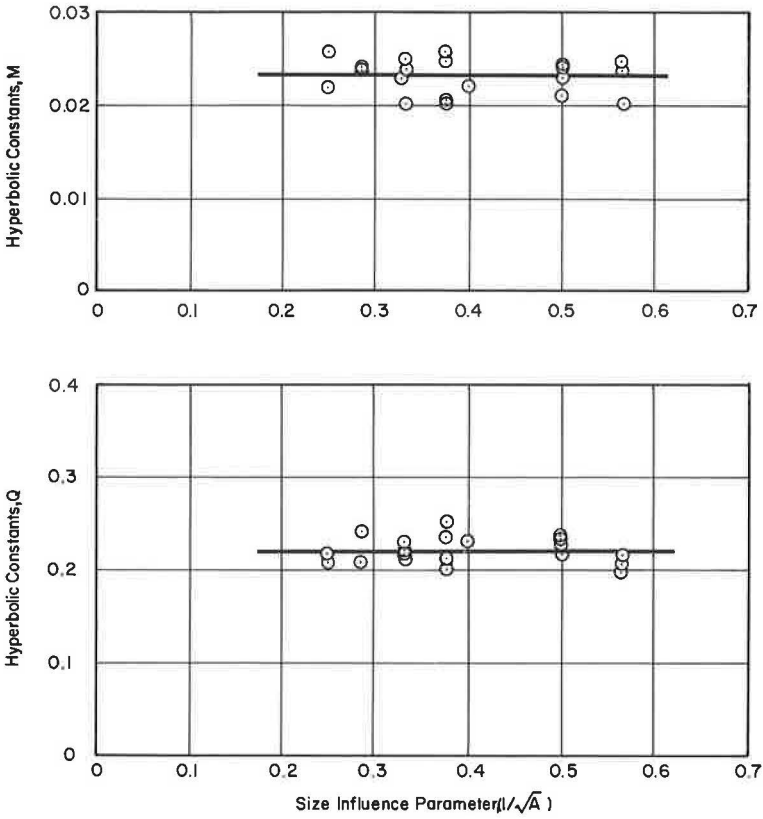
Figure 18. Relationship between the hyperbolic constants M and Q and footing area for EPK.
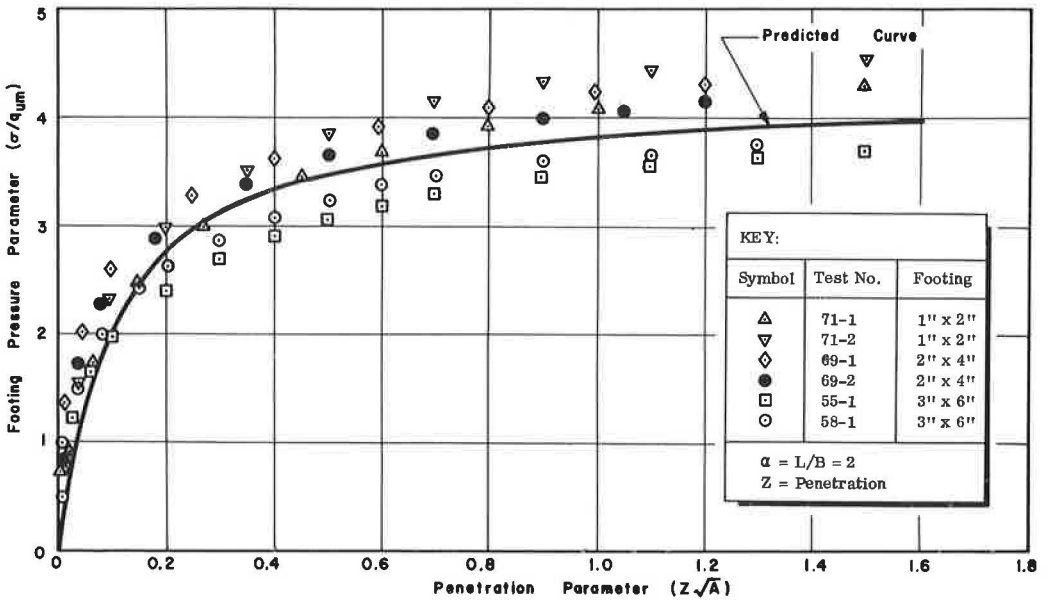
Figure 19. Pressure-penetration relationship for model footings on EPK ($\alpha = 2$).

48
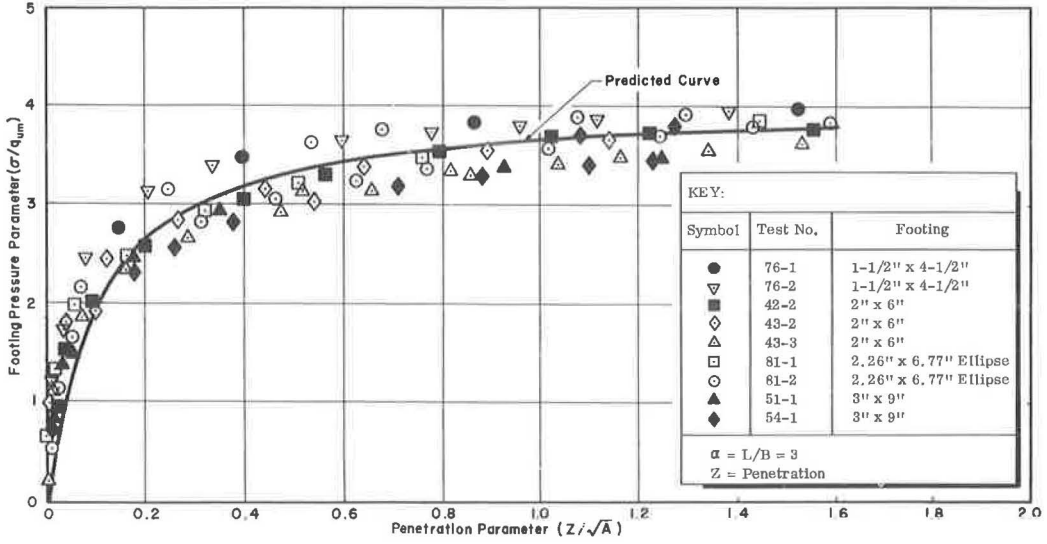
Figure 20. Pressure-penetration relationship for model footings on EPK ($\alpha = 3$).
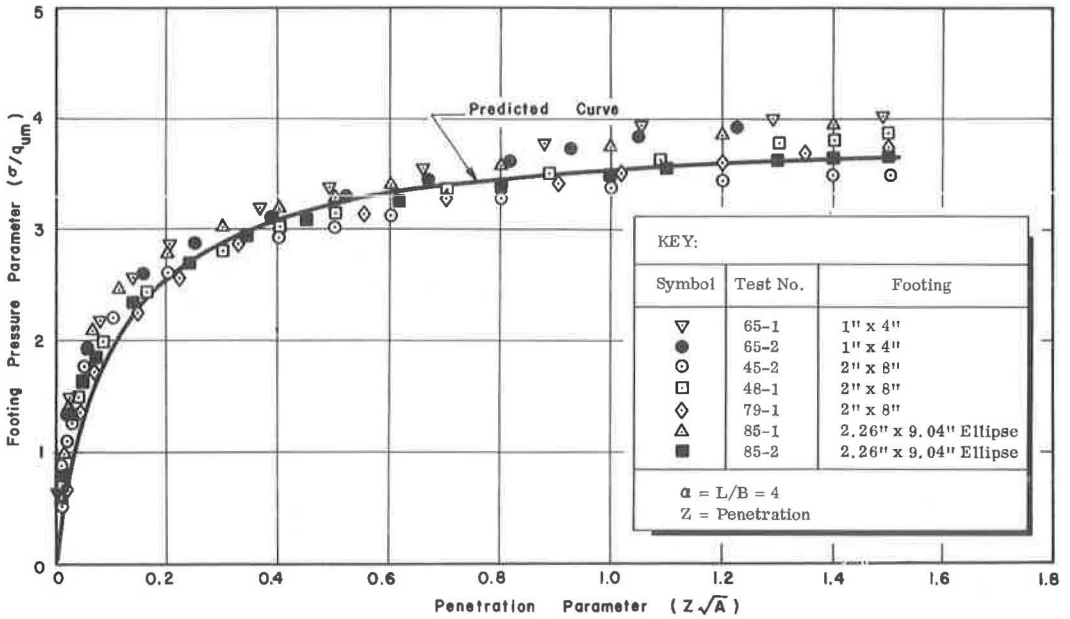
Figure 21. Pressure-penetration relationship for model footings on EPK ($\alpha = 4$).
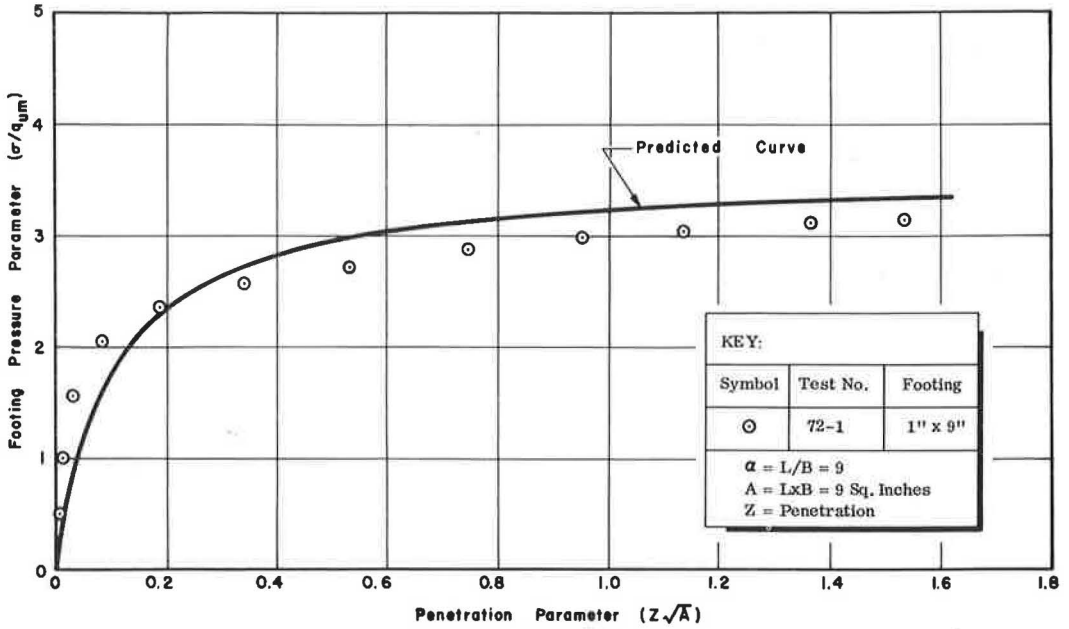
Figure 22. Pressure-penetration relationship for model footings on EPK ($\alpha = 9$).
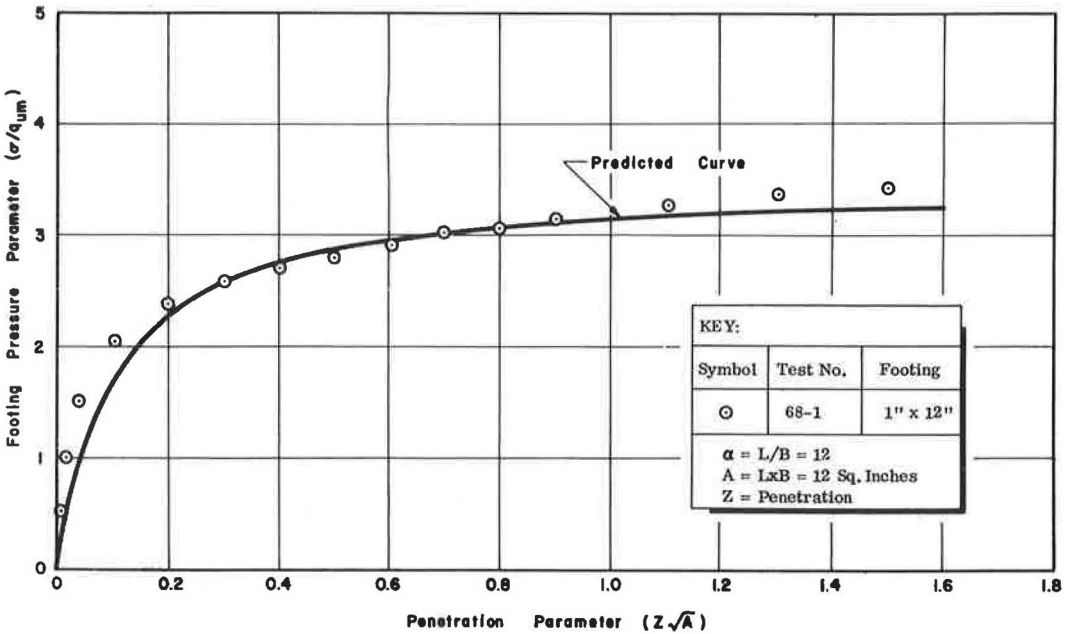
Figure 23. Pressure-penetration relationship for model footings on EPK ($\alpha = 12$).
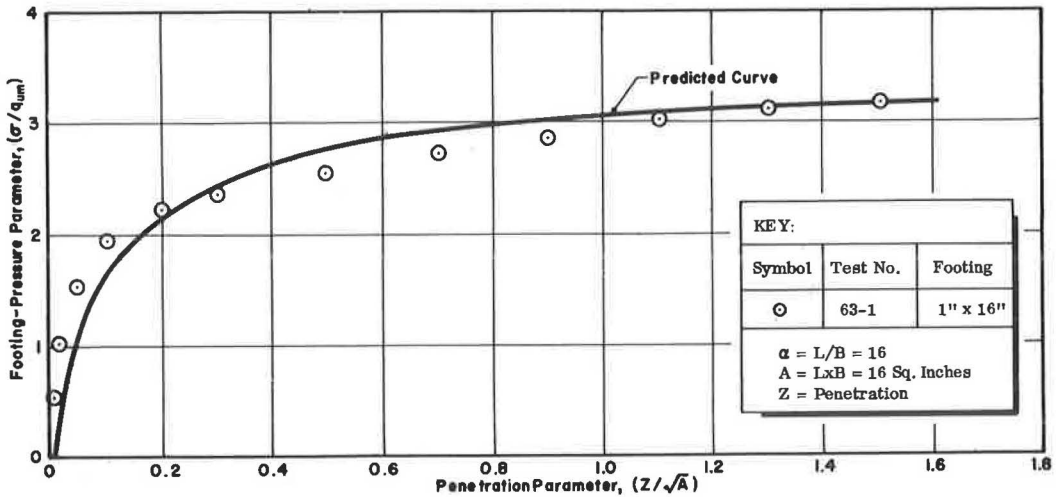
Figure 24. Pressure-penetration relationship for model footings on EPK ($\alpha = 16$).

have the same area and the same α. In the case of the ellipse, α is also considered to be the length-to-width ratio, i.e., the ratio of the length of the major and the minor axes. For example, Figure 20 shows results for rectangles and ellipses of 12 sq in. in area, with $\alpha = 3$. In this case, the rectangles were 2 in. wide by 6 in. long, and the minor and major axes of the ellipses were 2.26 in. and 6.77 in., respectively.

A similar series of tests was performed on a mined soil from Goose Lake County, Ill. The soil, called Grundite, is sold in dry powdered form, and is primarily an illite with approximately 15 percent fine quartz. Classification properties of Grundite are

Liquid limit: 55.6 percent
Plastic limit: 32.0 percent
Plasticity index: 23.6 percent
Specific gravity of solids: 2.84
Clay size fraction (<0.002 mm): 64 percent

The results of the tests on saturated Grundite are shown in Figures 25 through 35. Figures 25 and 26, for Grundite, are analogous to Figures 14 and 15 for EPK. They further suggest that the shape effect is essentially independent of the magnitude of penetration and the footing area. Figure 27 shows the results for square and circular footings ($\alpha = 1$). Again, the scatter is no more than can be expected from experimental results. The test plots for Eq. 4 are given in Figure 28 for several of the experimental curves. The agreement over a wide range of penetrations is evident, both in Figure 28 and in Figure 27 where Eq. 4, with the appropriate constants inserted, is shown. Figure 29 shows that the constants M and Q for Grundite, as for EPK, are not significantly affected by footing area.

Figures 30 through 35 show the results for footings on Grundite with α ranging from 1.77 to 16. The reliability of Eq. 6 is somewhat less for the Grundite than for the EPK (Figs. 19-24). This appears to be primarily due to the influence of the tests on the 4-sq in. footings (Fig. 26). Certainly the predicted curves are valid within expected experimental error.

Kondner and Krizek (11) have also suggested a two-constant hyperbolic expression for the pressure-penetration relationship. However, the similarity appears superficial, because they examined only penetrations of very small magnitude, and utilized a penetration parameter somewhat different from that considered herein. In addition, their test results for very small scale model footings (2 sq in. in area) indicate that as the ratio of length to width increases, the footing pressure required for a given penetration
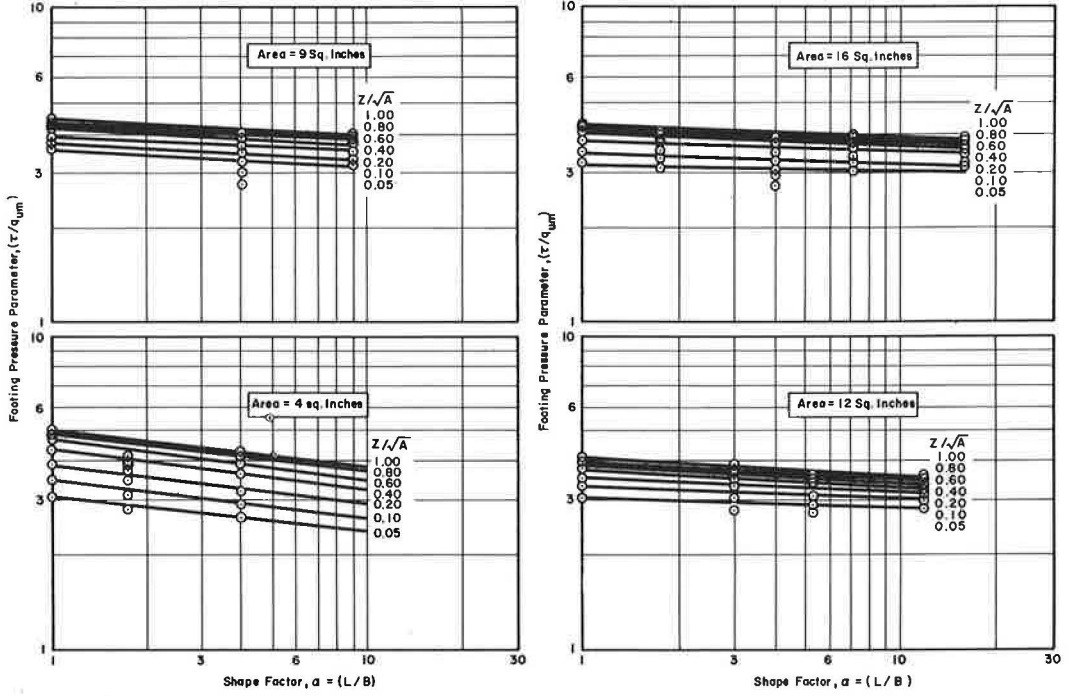
Figure 25. Effect of shape factor on pressure parameter for constant area footings on Grundite.
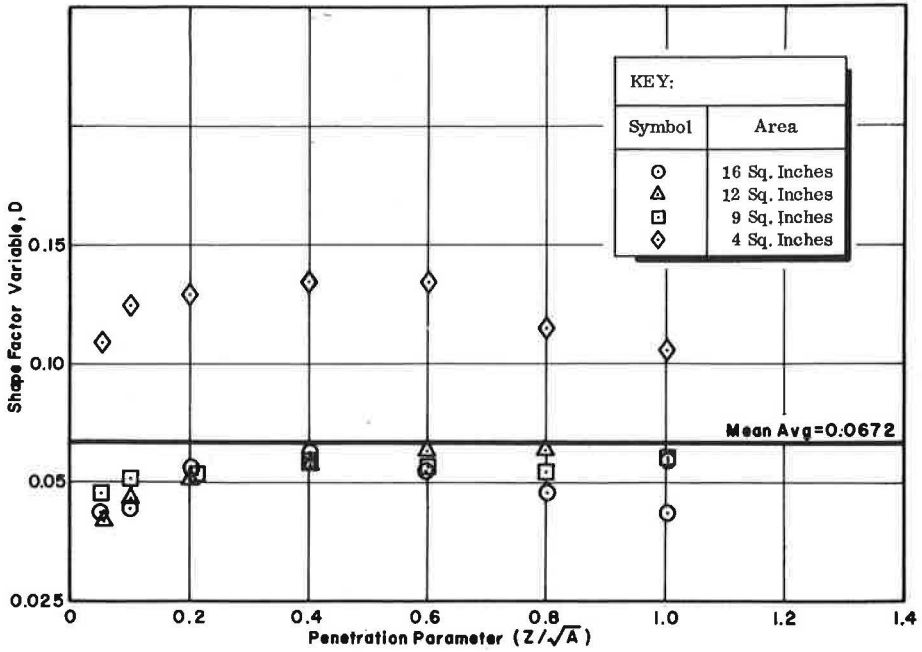
Figure 26. Effect of footing area and penetration on logarithmic slope of lines in Figure 25.
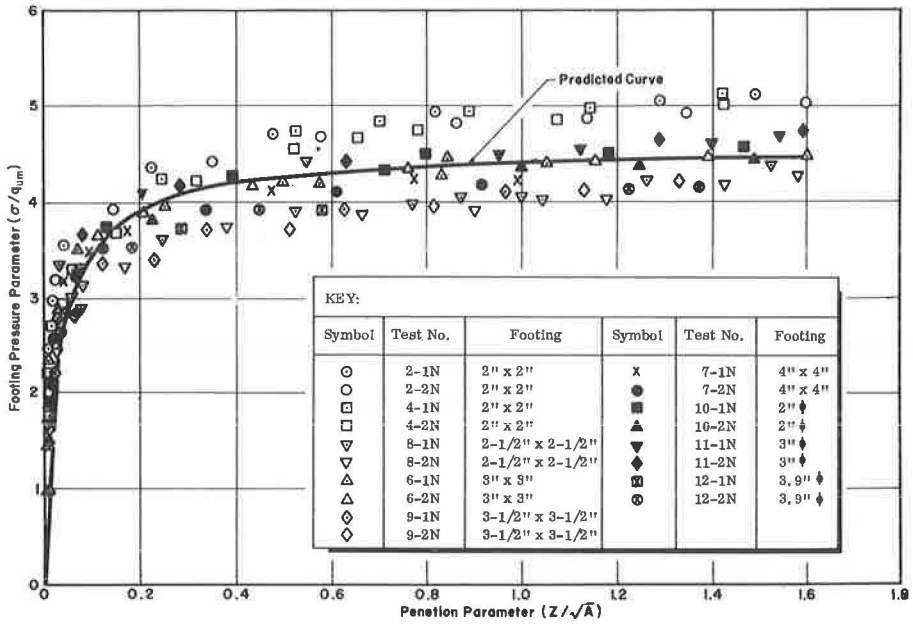
Figure 27. Pressure–penetration relationship for square and circular footings on Grundite ($\alpha = 1$).
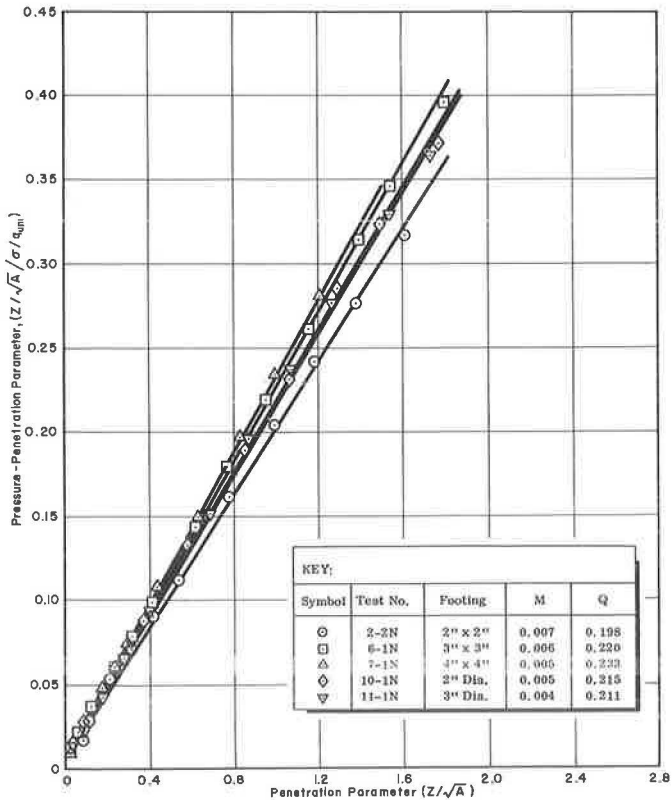
Figure 28. Hyperbolic pressure–penetration test plots for square and circular footings on Grundite.
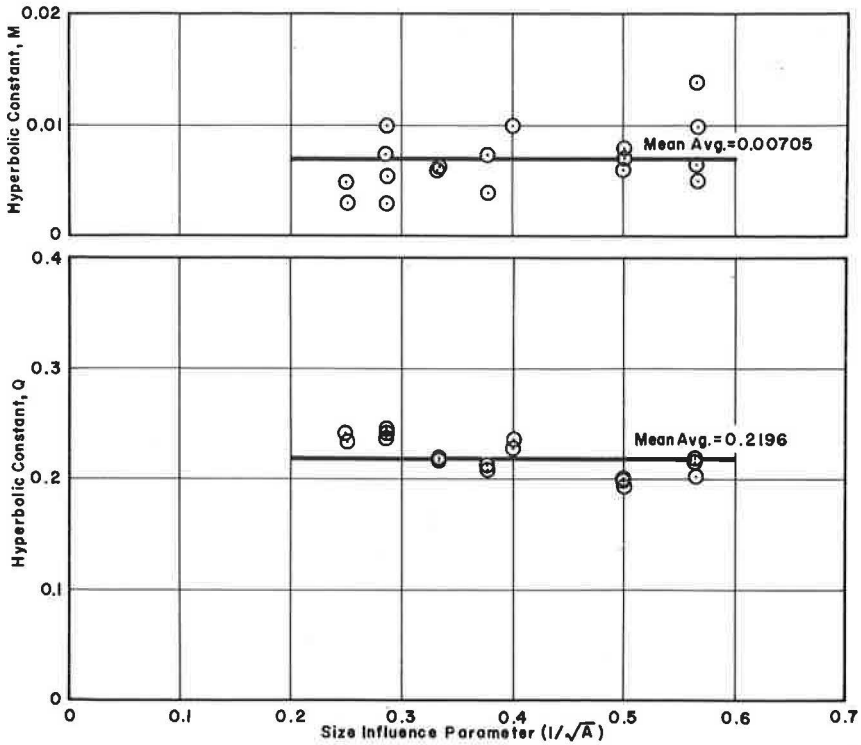
Figure 29. Relationship between hyperbolic constants M and Q and footing area for Grundite.
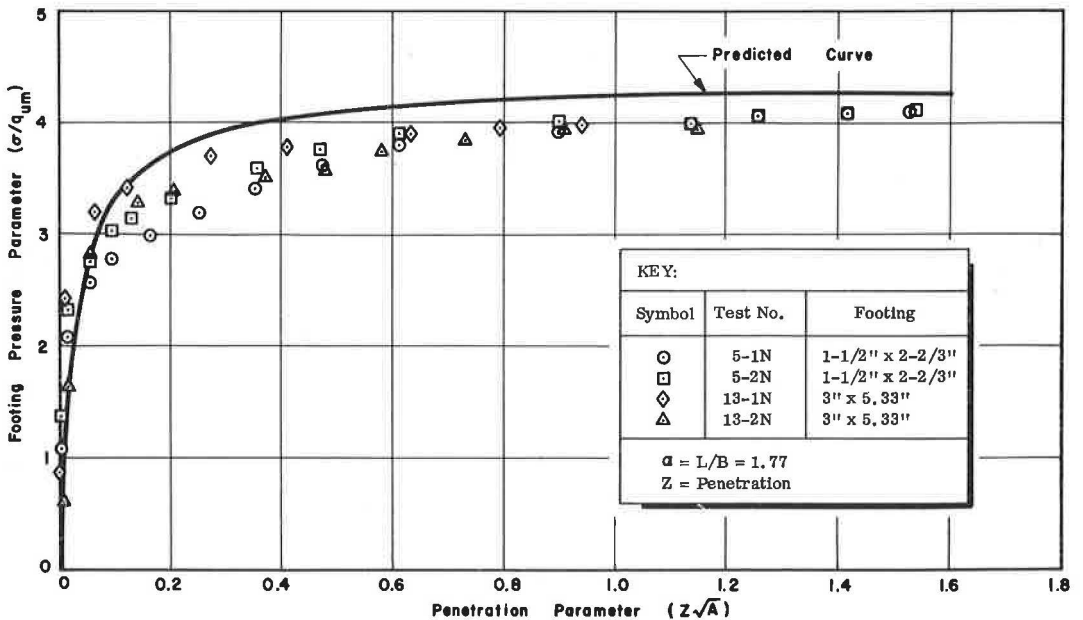
Figure 30. Pressure-penetration relationship for model footings on Grundite ($\alpha = 1.77$).
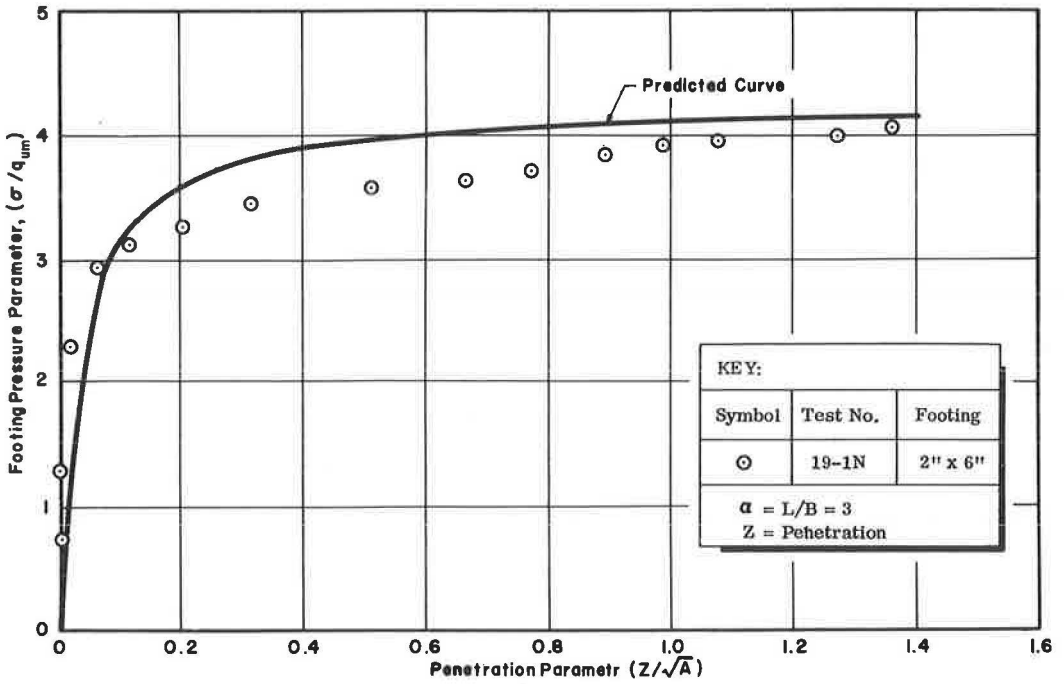
Figure 31. Pressure-penetration relationship for model footings on Grundite ($\alpha = 3$).
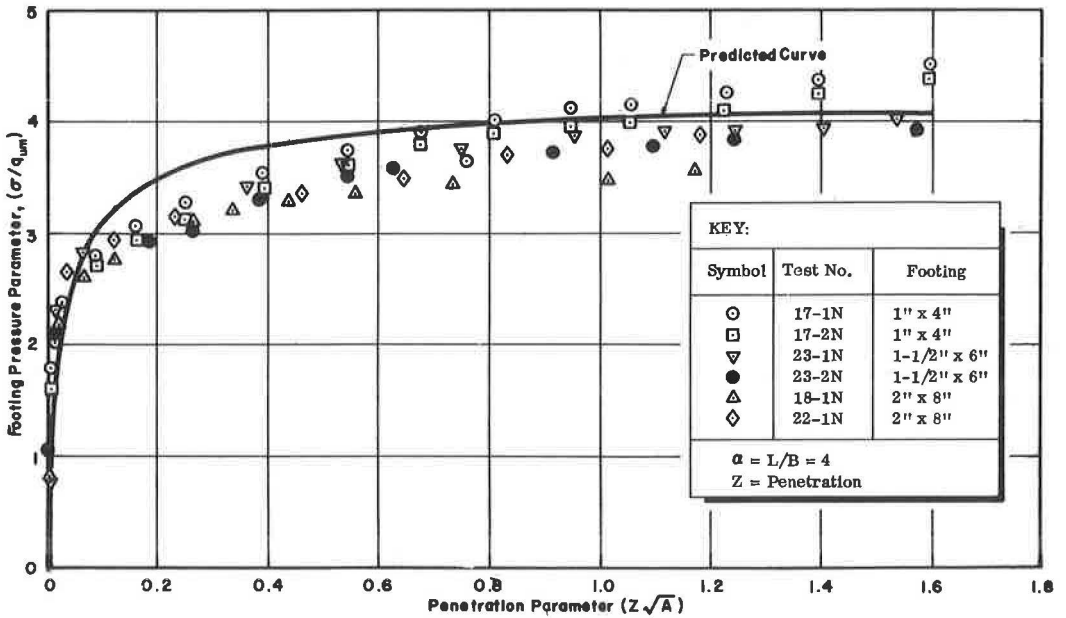
Figure 32. Pressure-penetration relationship for model footings on Grundite ($\alpha = 4$).
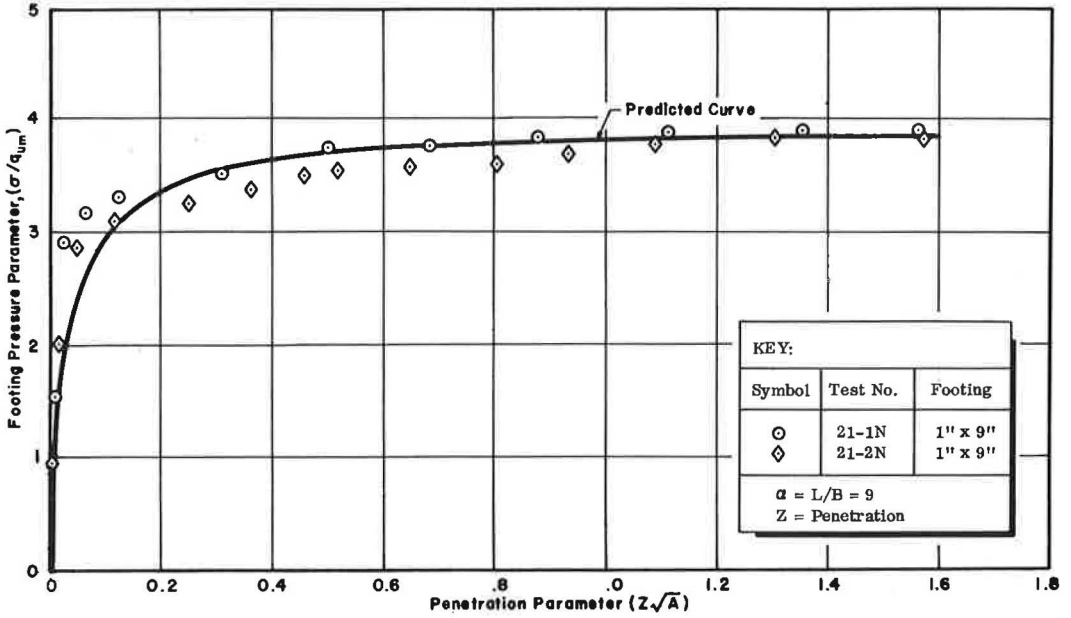
Figure 33. Pressure-penetration relationship for model footings on Grundite ($\alpha = 9$).
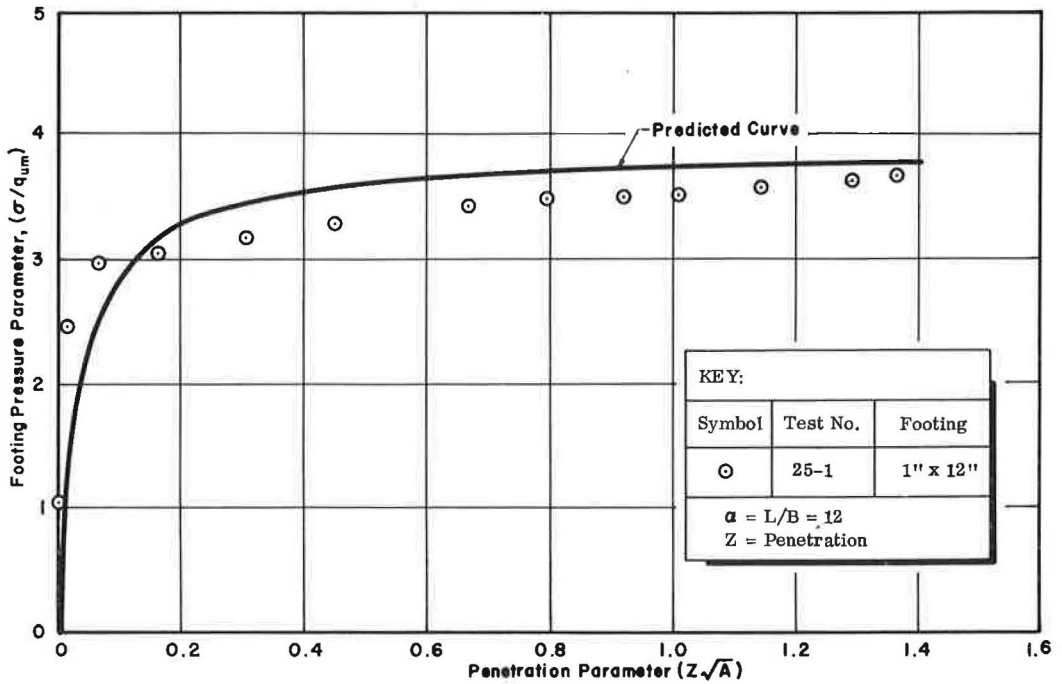
Figure 34. Pressure-penetration relationship for model footings on Grundite ($\alpha = 12$).

56

becomes greater. This is in direct contradiction to the data presented herein, as well as both theoretical and experimental bearing capacity results presented by many authors (15, 26, 27).

Reece (22) conducted a similar series of tests on circular and rectangular footings in a cohesive soil. There were several aspects of the study which make comparisons with the results presented herein less useful than one might hope:
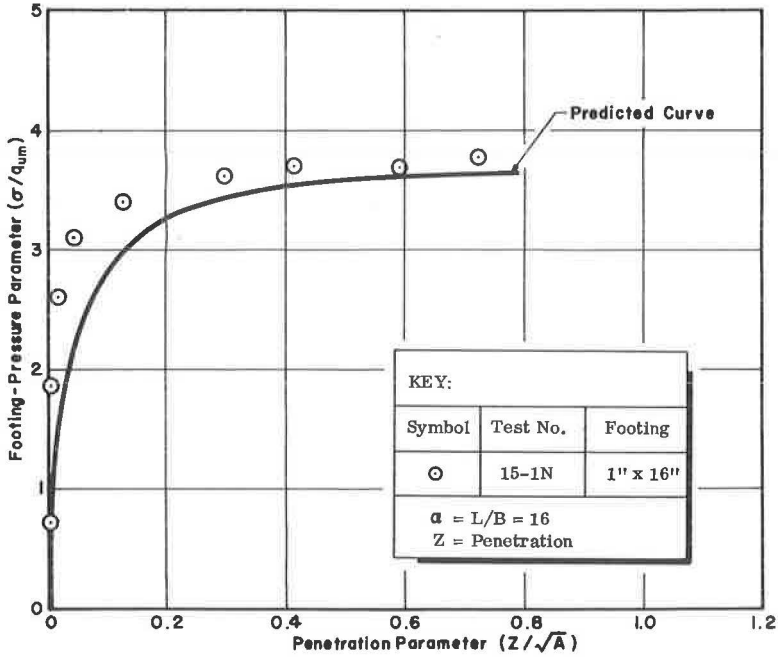
Figure 35. Pressure-penetration relationship for model footings on Grundite (α = 16).
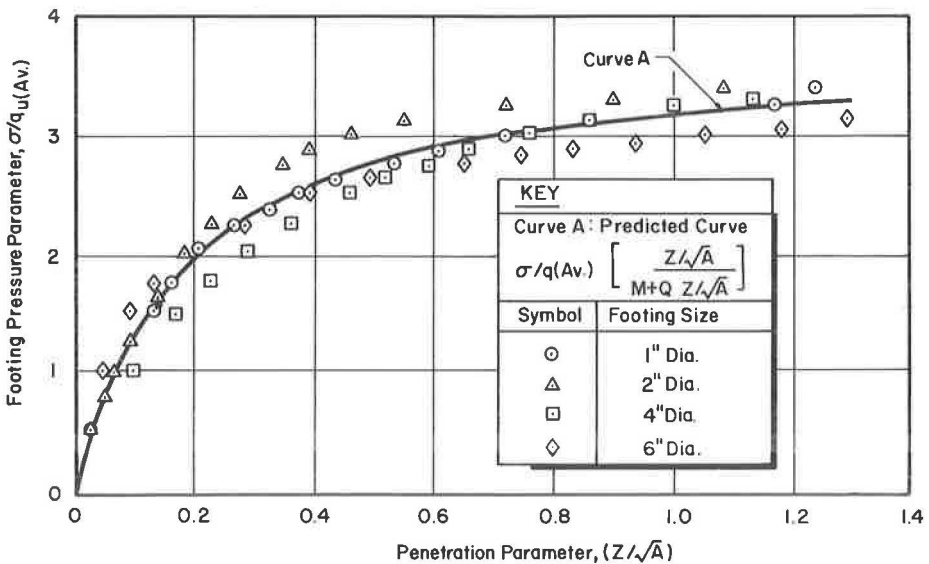
Figure 36. Pressure-penetration relationship for circular footings (data from Reece, 22).
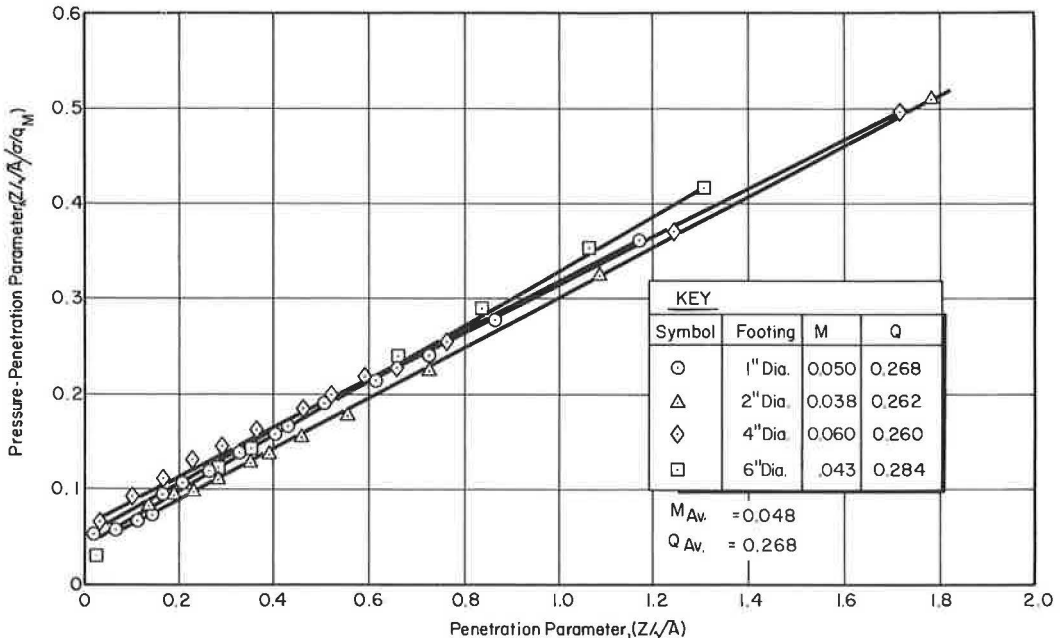
Figure 37. Hyperbolic pressure-penetration test plots for circular footings (data from Reece, 22).

1. The clay soil which Reece (22) used was not completely described, and it is difficult to assess its degree of saturation and other significant properties.

2. The preparation and storage procedures described by Reece (22) hardly seem likely to eliminate experimental scatter due to nonuniformity of the soil. No indication was given of the variability of the strength test results. Furthermore, it appears that the soil strength was not determined in connection with each test series.

3. According to Reece (22), the thickness of the clay layer tested was 13 in. The figures presented by him indicate penetrations of 8 in. and more. It seems almost certain that there was an insufficient depth of clay to prevent an artificial strengthening effect from the underlying sand for the tests on the larger (3- by 18-in., 4- by 18-in.) footings.

Pressure-penetration data for 1-, 2-, 4-, and 6-in. diameter model footings, from Reece (22), are shown in Figure 36. The pressure parameter is given in terms of the average unconfined compressive strength reported by Reece (22), as the individual test results were not presented. The hyperbolic test plot (Fig. 37) indicates the excellent representation of these data by Eq. 6. The solid line in Figure 36 is the plot of Eq. 6 with the constants determined from Figure 37. These results certainly suggest agreement with those presented previously for EPK and Grundite.

It was not possible to evaluate the shape factor variable D, since an adequate number of tests on footings of a given area with varying shape factor were not performed. However, had such data been presented, they would have been suspect because of the difficulty previously cited. To illustrate this point: the results given by Reece (22) for 2- by 9-in., 3- by 13 $\frac{1}{2}$-in., and 4- by 18-in. footings all substantially coincide with the results in Figure 36. That these curves should, in fact, lie below the data in Figure 36 is predicted by this report, bearing capacity theory (15), and Reece (22, pp. 45-46). This anomaly can readily be explained by the insufficient depth of clay provided.

SUMMARY AND CONCLUSIONS

This paper describes a study of the relationship between the pressure on model footings and their penetration into saturated cohesive soils. Experimental results

demonstrate the influence of soil water content, rate of footing penetration, type of testing, and roughness of the footing base on this relationship. An empirical expression has been developed to describe the pressure-penetration relationship. At this time the empirical equation represents the data satisfactorily for square, rectangular, circular, and elliptical model footings of various sizes.

Based on the results of this study, the following conclusions seem justified for the saturated cohesive soils and range of footing sizes and shapes tested:

1. The effect of water content on the pressure-penetration relationship can be greatly reduced, or eliminated, by expressing pressure in terms of a dimensionless pressure parameter, i.e., the footing pressure divided by the mean unconfined compressive strength of the soil, corresponding to the water content of the test.

2. Footing penetration is not, per se, a significant quantity. Rather, it is the penetration in relation to the footing size which is important.

3. The primary influence of the penetration rate on test results appears to stem from moisture migration from the area immediately underneath the footing. For the soils tested, penetration rates equal to or greater than 0.5 cm/min are sufficiently rapid to prevent significant migration of water from underneath the test footing.

4. The type of testing, i.e., constant rate of penetration or constant rate of loading, has no significant effect providing the average penetration rate is sufficiently rapid to prevent substantial migration of water from underneath the test footing.

5. The roughness of the footing base does not appear to influence the test results. In fact, both smooth and rough base footings seem to develop considerable frictional restraint at the footing-soil interface.

6. An empirical equation has been developed to describe the pressure-penetration relationship for model plate footings on the cohesive soils tested. This equation satisfactorily predicts the behavior of square, rectangular, circular, and elliptical footings of 2 to 27 sq in. in area over a wide range of penetrations. Results of another investigation tend to verify the applicability of the equation, at least for circular footings.

7. The behavior of elliptical footings is identical to that of rectangular footings of the same area with the same length-to-width ratio.

ACKNOWLEDGMENTS

REFERENCES

1. Assur, A. Locomotion Over Soft Soil and Snow. SAE Paper 782F, Automotive Eng. Cong., Detroit, Michigan, Jan. 1964.
2. Bekker, M. G. Theory of Land Locomotion, Univ. of Michigan Press. Ann Arbor.
3. Berardi, G. Piastra Rigidia Rettangolare, Caricata Simmetricamente E Appoggiata su un Semipazo Elastico. Giornale del Genio Civile, Vol. 99, No. 11, p. 853, Nov. 1961.
4. Brebner, A., and Wright, W. An Experimental Investigation to Determine the Variation in the Subgrade Modulus of a Sand Loaded by Plates of Different Breadths. Geotechnique, Vol. III, No. 8, Dec. 1953.
5. Carroli, W. F. Vertical Displacements of Spread Footings on Clay: Static and Impulsive Loadings. Unpublished PhD thesis, Univ. of Illinois, Urbana, 1963.
6. Dewhirst, D. L. A Comparison of Pressure Sinkage Size Equations. Chrysler Corp., preprint, May 1964.
7. Janbu, N., Bjerrum, L., and Kjaernsli, B. Veiledning ved løsning av fundamenteringsoppgaver. Norwegian Geotechnical Inst., Publ. No. 16, 1956.
8. Johnson, L. H. Nomography and Empirical Equations, p. 112, John Wiley and Sons, New York, 1952.

9. Karafiath, L.   An Analysis of New Techniques for the Estimation of Footing Sinkage in Soils.   Land Locomotion Res. Branch, Res. Dev. Div., OTAC, Rept. No. 18, Oct. 1957.

10. Kogler, F.   Disc. of Soil Mechanics Research by G. Gilboy.   Trans. ASCE, Vol. 98, p. 299, 1933.

11. Kondner, R. L., and Krizek, R. J.   Correlation of Load Bearing Tests on Soils. HRB Proc., Vol. 41, p. 557, 1962.

12. Langhaar, H. L.   Dimensional Analysis and Theory of Models, John Wiley and Sons, New York, 1951.

13. Matlock, H., Jr., Fenske, C. W., and Dawson, R. F.   Deaired Extruded Soil Specimens for Research and for Evaluation of Test Procedures.   ASTM Bull. No. 177, Oct. 1951.

14. Mitchell, J. K., and Campanella, R. G.   Creep Studies on Saturated Clays.   Symp. on Laboratory Shear Testing of Soils, ASTM Spec. Tech. Publ. No. 361, p. 90, 1963.

15. Meyerhof, G. G.   The Ultimate Bearing Capacity of Foundations.   Geotechnique, Vol. 2, p. 301, 1951.

16. Milne, W. E.   Numerical Calculus, Princeton Univ. Press, Princeton, New Jersey, 1949.

17. Osterberg, J. O.   Disc. of Symposium on Load Tests of Bearing Capacity of Soils. ASTM Spec. Tech. Publ. No. 79, p. 128, 1948.

18. Osterberg, J. O., and Perloff, W. H.   Stress-Strain Characteristics of Compacted Clay Under Varied Rates of Strain.   HRB Proc., Vol. 39, p. 605, 1960.

19. Parkes, E. W.   A Comparison of the Contact Pressure Beneath Rough and Smooth Rafts on an Elastic Medium.   Geotechnique, Vol. 9, p. 183, 1956.

20. Perloff, W. H.   A Study of the Pressure-Penetration Relationship for Model Footings on Cohesive Soil.   Ohio State Univ. Res. Found. Rept. RF 1745-4, 1964.

21. Rahim, K. S. A.   A Theoretical Investigation of Stress Distribution for a Strip Load Placed at Different Depths in an Elastic Half Space.   PhD Dissert., Ohio State Univ., 1965.

22. Reece, A. R.   Problems of Soil Vehicle Mechanics.   Rept. No. 8470, LL 97, U. S. Army Tank-Automotive Center, Warren, Mich., 1964.

23. Schleicher, F.   Zur Theorie des Baugrundes.   Der Bauingenieur, No. 48, p. 931, 1926.

24. Seed, H. B., Mitchell, J. K., and Chan, C. K.   The Strength of Compacted Cohesive Soils.   Res. Conf. on Shear Strength of Cohesive Soils, ASCE, p. 877, June 1960.

25. Skempton, A. W.   The Bearing Capacity of Clays.   British Building Res. Cong., p. 180, 1951.

26. Teng, W. C.   Foundation Design, Prentice-Hall, 1962.

27. Terzaghi, K.   Theoretical Soil Mechanics, John Wiley and Sons, New York.

28. Trask, P. D., Snow, D. T., et al.   Pressure Sinkage Tests on Synthetic and Natural Clay Soils.   Land Locomotion Lab., Res. and Eng. Directorate, OTAC, Rept. No. 75, April 1962.

29. Vincent, E. T., Hicks, H. H., Jr., Oktar, E. I., and Kapur, D. K.   Rigid Wheel Studies by Means of Dimensional Analysis.   Rept. No. 7841, LL 79, U. S. Army Tank-Automotive Center, Center Line, Michigan, 1963.

30. Newmark, N. M.   Stress Distribution in Soils.   Proc., Purdue Conference on Soil Mechanics and Its Applications, p. 295, 1940.

31. Newmark, N. M.   Influence Charts for Computation of Stresses in Elastic Foundations.   Bull., Univ. of Illinois Engineering Experiment Sta., No. 338, 1942.

Application of Three-Layer System Methods to Evaluation of Soil-Cement Bases

S. THENN DE BARROS, University of São Paulo, São Paulo, Brazil

A series of bearing tests on soil-cement pavements at several airports of the state of São Paulo, was made by the Instituto de Pesquisas Tecnologicas, University of São Paulo, Brazil, with the main objective of assessing the load capacity of the pavements. The findings and conclusions of this study have been reported in a previous paper. As a by-product of the study, an evaluation was made of the effective in-place elastic modulus of soil-cement bases by the application of the elastic layered theory. The pavements studied are basically three-layer structures composed of soil-cement base, granular soil subbase, and natural subgrade. A thin asphaltic-concrete wearing course was built after the bearing tests were performed. A first tentative analysis was made by two-layer methods, considering the two lower layers as a single layer of equivalent elastic properties, but this analysis gave erratic and unrealistic results. A new method of analysis was then developed for the interpretation of the bearing test data by the use of three-layer elastic theory, which yielded consistent and workable results. This paper reports the latter method of analysis.

A summary of the design and construction data of the airport pavements, characteristics of materials, details of tests, and reports of test data are given. The process of testing was incremental-repetitive loading, with rigid plates of three diameters. The soil-cement base modulus of reaction K (load-deflection ratio) was nearly constant and elastic for each plate for all loads after the first loading in every test. This load-deflection ratio was taken as a characteristic mechanical parameter of the pavement.

The load-deflection pattern of the pavements by the three-layer elastic theory is interpreted, and the soil-cement modulus of elasticity is evaluated. This paper presents a practical application of the three-layer deflection factor tables computed by Jones (2). The proposed method of analysis is believed to be accurate and dependable. It is, however, affected by the scatter of the field measurements. It was found that the effective elastic modulus of the subgrade underneath the pavement's structure is much greater than the value obtained by direct loading tests on the subgrade. The so-called "equivalent" single layer for substituting the two lower layers is not a valid concept for the three-layer structure. A reasonably good correlation was observed between theoretical and experimental curves of the load-deflection ratio against the inverse of plate radius. A nonlineal relationship was observed between the load and perimeter-area ratio, which follows the elastic theory.

•THE THEORY of elastic layered systems was proposed by Burmister in 1943 (1), and was subsequently developed by others. Burmister (1) presented numerical computation of the deflection factor for two-layered systems, for the usual values of the significant parameter, in graphic form. The numerical computation of the deflection factor for three-layered systems was presented in tabular form 20 yr later, by Jones (2). Table 1 gives some typical values taken from Jones' tables. At present there is no published

TABLE 1

VALUES OF DEFLECTION FACTOR FOR THREE-LAYERED
ELASTIC SYSTEMS WITH PERFECT CONTINUITY
AT INTERFACES[a]

$E_1/E_2 = n_1$	$E_2/E_3 = n_2$	$h_1/h_2 = H$	$h_2/r = \dfrac{1}{A}$	A	$\overline{F}$	F
20	20	0.25	1.25	0.8	139.3	0.232
			2.5	0.4	75.18	0.125
			5.0	0.2	39.50	0.066
20	20	1	1.25	0.8	67.97	0.113
			2.5	0.4	35.10	0.059
			5.0	0.2	18.46	0.031
20	2	0.25	1.25	0.8	36.69	0.612
			2.5	0.4	23.22	0.387
			5.0	0.2	13.44	0.224
20	2	1	1.25	0.8	15.75	0.263
			2.5	0.4	8.922	0.149
			5.0	0.2	5.362	0.089
2	20	0.25	1.25	0.8	16.98	0.283
			2.5	0.4	9.944	0.166
			5.0	0.2	6.015	0.100
2	20	1	1.25	0.8	10.92	0.182
			2.5	0.4	6.395	0.107
			5.0	0.2	4.083	0.068

[a]Data derived from Ref.2. All interpolations are to be computed graphically on
log-log paper.
[b]Poisson's ratio = 0.35;
   $\overline{F}$ = Jones deflection factor; and
   F = normal deflection factor.

Deflection:

$$D = \frac{1.5\,p\,r}{E_3} \cdot F \quad \text{or} \quad D = \frac{p\,r}{E_1} \cdot \overline{F}$$

Relationship between two deflection factors:

$$F = \overline{F} \cdot \frac{1}{1.5\,n_1\,n_2}$$

computation of the deflection factor for systems of more than three layers by the elastic
theory. Such computation would be exceedingly complicated because of the great num-
ber of significant parameters necessary in a general solution. To analyze pavements
of more than three layers by the elastic theory, it is necessary to reduce them to a
three-layer model, combining similar adjacent layers. This expedient affords a rea-
sonable degree of analogy between the theoretical model and the real multilayer sys-
tem. If a further reduction is made from a multilayer system to a two-layer model,
great discrepancies may arise, depending on the values of the parameters.

The deflection under load of a uniform elastic medium, which could be considered
as a one-layered system, is calculated by the Boussinesq-Love equations.

Figure 1 shows side-by-side the main equations used for deflection calculations of
uniform mediums, two-layered systems, and three-layered systems. These equations
together with the Burmister graph (Fig. 2) and the Jones tables given in Table 1 rep-
resent an abridgment of the theoretical information available on deflection computation

A - Uniform elastic medium

Rigid circular plate
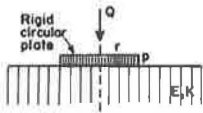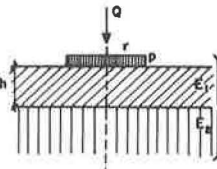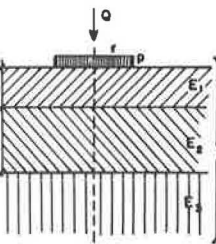
Poisson's Ratio = 1/2 (all layers)

B - Two-layered system

C - Three-layered system

Boussinesq:

$$D = \frac{1.18 pr}{E} \quad (1a)$$

$$K = \frac{p}{D} \quad (2a)$$

$$E = 1.18 rK \quad (3a)$$

Radius change:

$$K' = K \frac{r}{r'} \quad (4a)$$

Burmister:

$$D = \frac{1.18 pr}{E_2} F \quad (1b)$$

$$K_{eq} = \frac{p}{D} \quad (2b)$$

$$E_2 = 1.18 r K_{eq} F \quad (3b)$$

$$E_{eq} = 1.18 r K_{eq} \quad (4b)$$

$$E_{eq} = \frac{E_2}{F} \quad (5b)$$

If $E_2 = E$:

$$F = \frac{K}{K_{eq}} \quad (6b)$$

Solution for the problem:

$$F = f\left[\frac{E_1}{E_2}, \frac{h}{r}\right] \quad (7b)$$

(See Graphic of Fig. 2)

Approximate formulas:

$$E_1/E_2 = n \qquad h/r = H$$

$$F = F'\left(1 - \frac{1}{n}\right) + \frac{1}{n} \quad (8b)$$

$$F' = \frac{1}{\sqrt{1 + (H \sqrt[3]{n})^2}} \quad (9b)$$

Burmister - Jones:

$$D = \frac{1.18 pr}{E_3} F \quad (1c)$$

$$K_{eq} = \frac{p}{D} \quad (2c)$$

$$E_3 = 1.18 r K_{eq} F \quad (3c)$$

$$E_{eq} = 1.18 r K_{eq} \quad (4c)$$

$$E_{eq} = \frac{E_3}{F} \quad (5c)$$

If $E_3 = E$:

$$F = \frac{K}{K_{eq}} \quad (6c)$$

Solution for the problem:

$$E_1/E_2 = n_1 \qquad E_2/E_3 = n_2$$

$$n_1 n_2 = N$$

$$h_1/h_2 = H \qquad r/h_2 = A$$

$$F = f\left[n_1, n_2, H, A\right] \quad (7c)$$

(See values of F in Table 1)

NOTE: Table 1 was computed for Poisson's ratio = 0.35 in all layers.

IMPORTANT NOTE:

For flexible uniform load instead of rigid plate substitute coefficient 1.5 for 1.18 in all equations.

Q = total load (Kg)

r = plate radius (cm)

$p = \frac{Q}{\pi r^2}$ = average applied unit load (kg/cm²)

D = vertical deflection beneath the center of plate (cm)

E = modulus of elasticity of uniform medium (kg/cm²)

K = load/deflection ratio of uniform medium (kg/cm²/cm or kg/cm³)

h = thickness of first layer (cm)

E_1, E_2 = moduli of elasticity of layers (kg/cm²)

E_{eq} = composite modulus of elasticity of system (kg/cm²)

K_{eq} = load/deflection ratio of system (kg/cm³)

F = deflection factor of two-layer system (F_w in original Burmister's graph)

h_1, h_2 = thicknesses of first and second layers (cm)

E_1, E_2, E_3 = moduli of elasticity of layers (kg/cm²)

E_{eq} = composite modulus of elasticity of system (kg/cm²)

K_{eq} = load/deflection ratio of system (kg/cm³)

F = deflection factor of three-layer system (from Jones' tables)

Figure 1. Equations and symbols used in this paper.

of elastic layered systems. For justification of these formulas and equations, see Ref. 3. Figure 1 also includes a list of symbols and definitions as they are used in this study.

The deflection factor computed by Jones is somewhat different from the normal deflection factor used by Burmister and most authors. The Burmister deflection factor F (originally designated by F_w) for flexible uniform loading derives from the following equations:
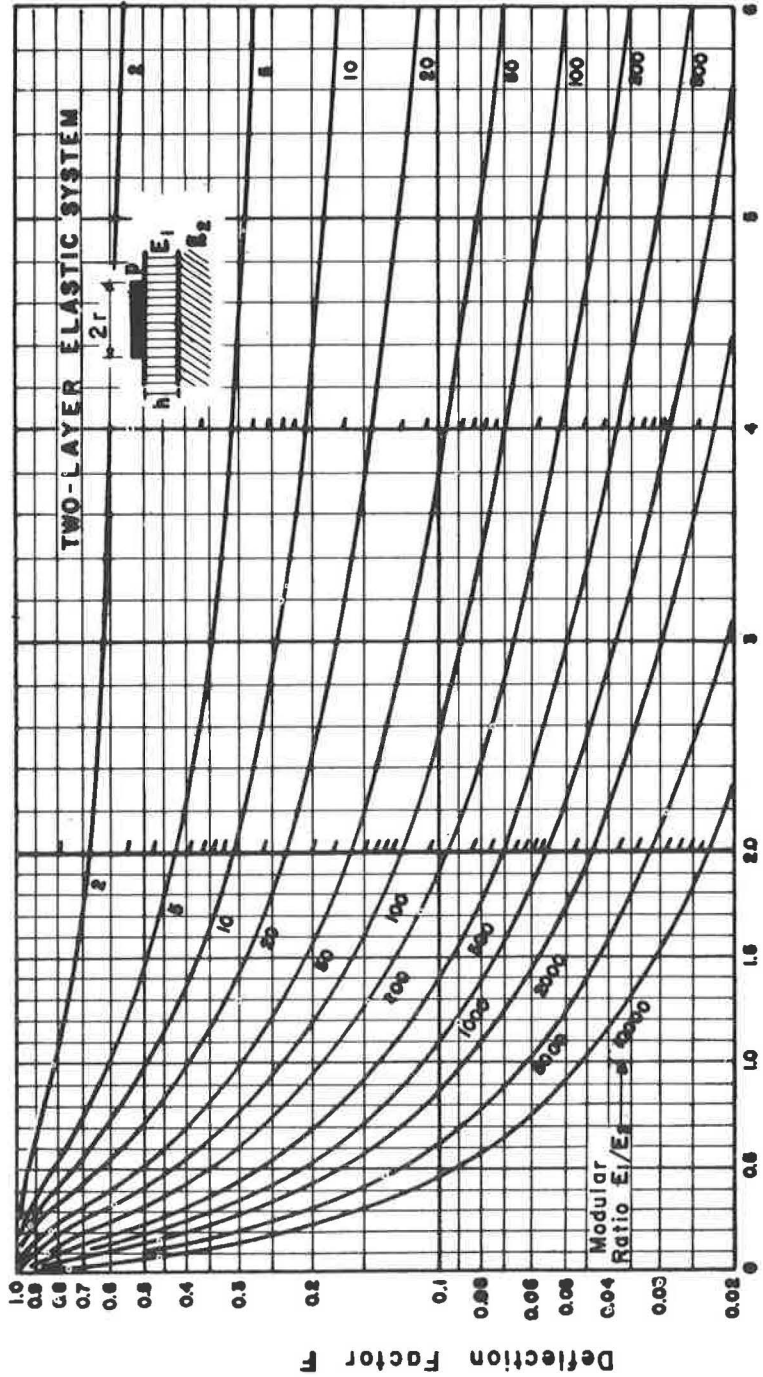
Figure 2. Two-layer system deflection factor as function of modular ratio and thickness-to-radius ratio (Burmister).

$$\text{Two-layer system} \quad D = \frac{1.5\,p\,r}{E_2} \cdot F$$

$$\text{Three-layer system} \quad D = \frac{1.5\,p\,r}{E_3} \cdot F$$

For rigid plate loading, substitute 1.18 for 1.5.
The Jones deflection factor $\overline{F}$ for uniform loading is defined by the equation:

$$\text{Three-layer system} \quad D = \frac{p\,r}{E_1} \cdot \overline{F}$$

where

D = deflection,
p = contact pressure,
r = radius,
E_1 = elastic modulus of top layer,
E_2, E_3 = elastic moduli of lower layers, and
$F, \overline{F}$ = deflection factors

The two factors are related by the equation:

$$F = \overline{F} \cdot \frac{1}{1.5\,n_1\,n_2}$$

$$n_1 = E_1/E_2$$
$$n_2 = E_2/E_3$$

Table 1 gives the deflection factors $\overline{F}$ as computed by Jones, and the corresponding deflection factors F, calculated by the foregoing relationship. In this study, we will use only the normal deflection factor F, with the usual definition. When recourse is necessary to the original Jones tables, factor $\overline{F}$ of these tables is transformed to factor F.

The Jones tables were computed for Poisson's ratio equal to 0.35[1]. Burmister, as most authors, computed his graph for a 0.5 Poisson's ratio. In the particular case of the soil-cement bases, the value of 0.35 would probably be closer to the truth than the value 0.5. The opposite situation would occur in the case of saturated untreated granular bases and subbases. However, the influence of Poisson's ratio on the deflection is known to be small, in all instances.

Jeuffroy and Bachelez (4) also presented a numerical computation of the deflection factor for three-layered systems in graphic form, for several values of the parameters. The Jeuffroy-Bachelez theory is based on simplifying assumptions (Navier hypothesis), but it gives results close to the more exact Jones theory, for the deflections. However, the Jones tables are easier to use and cover a wider range of parameters than the Jeuffroy-Bachelez graphs.

---

[1]The deflection coefficient for flexible uniform load to use in connection with Jones tables should actually be 1.755 and not 1.5, due to the value of Poisson's ratio. The correct deflection equations are

$$D = \frac{1.755\,p\,r}{E_3} \cdot F$$
$$F = \overline{F} \cdot \frac{1}{1.755\,n_1\,n_2}$$

$\overline{F}$ = value from Jones tables.

Evidently the numerical value of D remains unchanged. The writer mantains the coefficients 1.5 for flexible load and 1.18 for rigid plate to preserve a formal analogy between the equations of Figure 1 for all layered systems. The final results of the analysis are not affected by the substitution of 1.5 for 1.755, or 1.18 for 1.378, in all equations.

The application of layered system concepts and principles to the interpretation and evaluation of flexible pavements has been tried by many authors with variable success. Among others, Burmister (5) analyzed the Hybla Valley Test Track data and the WASHO Road Test data by two-layer methods. The results of this analysis are somewhat disappointing with respect to the consistency of the determination of the "in-place" moduli of elasticity of the pavement layers. Jeuffroy and Bachelez (4) analyzed the same WASHO Road Test data by three-layer methods and found more consistent results for the layers' moduli. Sowers and Vesić (6) measured the vertical stresses in subgrades beneath statically loaded flexible pavements and found great discrepancies between measured stresses and values computed by the elastic layered theory, for most types of pavements. However, for soil-cement pavements there is a good agreement between measured and theoretical computed values of the vertical stress. According to these findings, the elastic theory applies to soil-cement pavements better than to other types of flexible pavements, at least as far as the vertical stress.

The equations shown in Figure 1 are general equations, valid for any values of the parameters, except for Poisson's ratio. In the case of the three-layer systems, due to the great many parameters necessary, it is practically impossible to solve problems of deflection computation using only these general equations. To solve the specific problem of this study we have included a few graphs which are valid only for the range of parameters of our particular case, and which should not be extrapolated for other values of the parameters. However, the method of analysis outlined is believed to be general in scope, provided new graphs are drawn for the range of parameters in each particular case.

DESIGN AND CONSTRUCTION DATA

The São Paulo Institute for Technological Research performed a series of bearing tests on soil-cement pavements at eight airports in different cities of the state. Most of the airports were located in the northwestern part of the state, which is a great sedimentary basin composed of fine sandy soils of rather uniform texture. One airport was located outside this geological area, but the subgrade soil at this location is also a fine uniform sandy soil. The subgrade soils at all airports are remarkably alike. Table 2 gives the average physical characteristics of the subgrade soils. The reason for selecting soil-cement for all pavements was the ease of stabilizing these sandy soils with economical percentages of cement and the lack of granular aggregates at the airport locations.

A typical cross-section of the airport pavements (Fig. 3) is composed of asphaltic-concrete wearing course of 2.5 to 3 cm (1 to 1 ¼ in.) of thickness; soil-cement base course of 15 to 16 cm (6 to 6 ¼ in.); compacted soil subbase of 60 to 61 cm (24 in.); and noncompacted subgrade. The soils used in the soil-cement base and in the compacted subbase were taken from selected borrow pits to assure uniformity, but their general characteristics are the same as the subgrade soils indicated in Table 2. The "in-place" CBR of the uncompacted subgrade, which was only lightly compacted by the normal operation of the earthmoving equipment, was near 3 percent. The soil subbase was compacted near the optimum moisture to 95 percent of the standard Proctor maximum density. The compacted subbase CBR varied from 16 to 35 percent, with an average of 25 percent. The soil-cement base was designed and built according to Brazilian standards, which follow in general the procedures recommended by the Portland Cement Association. The designed cement content was a little under 10 percent by volume, but for safety and ease of control it was specified at 10 percent in all cases. The actual construction cement content was in general slightly over 10 percent by volume. The soil-cement base was also compacted at optimum moisture to 95 percent of standard Proctor maximum density. The thin asphaltic-concrete wearing course was primarily designed as a protection against traffic abrasion and moisture infiltration, with little structural influence. The bearing tests were performed on top of the soil-cement base, before the placing of the wearing course. The wearing course is not considered in this structural analysis. The pavement cross-section can therefore be considered as a three-layered system: the first layer is the soil-cement base,

TABLE 2

AVERAGE PHYSICAL CHARACTERISTICS OF AIRPORT SOILS

Characteristic	Range
Texture	
Coarse sand (2. 00-0. 42 mm)	0-5%
Fine sand (0. 42-0. 05 mm)	70-75%
Silt (0. 05-0. 005 mm)	10-15%
Clay (less than 0. 005 mm)	10-20%
Consistency	
Liquid limit	23-30%
Plastic index	6-12%
Classification	
HRB classification system:	
Generally	A 2-4 (0)
Eventually	A 2-6 (2)
Unified classification system	SC
Compaction tests (AASHO T 134-57)	
Optimum moisture	9-12%
Maximum density	1. 92-2. 00 g/cm^3 (120-125 pcf)
Strength tests	
CBR-Typical value for uncompacted subgrade	3%
CBR-Range of values for compacted subbase	16-35%
CBR-Average value for compacted subbase	25%
Soil-cement tests	
Compressive strength (7-day curing)	22-32 kg/cm^2 (315-460 psi)

the second layer is the compacted subbase, and the third layer is the uncompacted sub-grade. The first and second layers have definite thicknesses, and the third layer is theoretically considered to have infinite thickness.

BEARING TESTS

Forty-four bearing tests were made with circular rigid plates of diameters of 80, 45 and 30 cm (31 ½, 17 ¾, and 11 ¾ in., roughly). For economy's sake, and to get as much information as possible at every testing point, the three diameters of plates were successively used in every mounting of reaction load (Fig. 4). The reaction load was a box full of earth weighing up to 100 metric tons. The load was transferred to the plate by a calibrated hydraulic jack hinged to the truck frame. The loadings were measured by the calibrated pressure gage. The plate deflections were measured by two deflectometers located in diametrically opposite positions, mounted on an independent supporting beam, which rested on supports outside the deflection basin. The average of the readings of the two deflectometers was taken as the deflection at the center of the plate, for every loading. The 80-cm plate was used first at the center of the mounting. After the completion of this test, the load was removed, and new tests were made with the 45- and 30-cm plates at points to the right and left of the first test, using the same reaction load. The distance between the centers of the plates was approximately 1. 20 m (4 ft). It was later realized that this distance was not great enough to warrant independent results, i.e., the first test unfavorably influenced the second and third tests. A procedure was proposed to correct the results of the two

Cross-secction of airport pavements
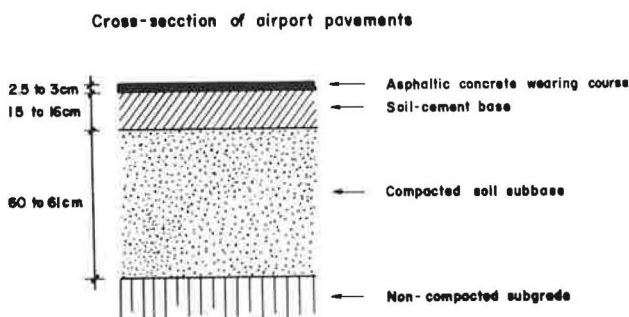
Figure 3. Airport pavement cross-section; bearing tests made on top of soil-cement base before placing of wearing course.
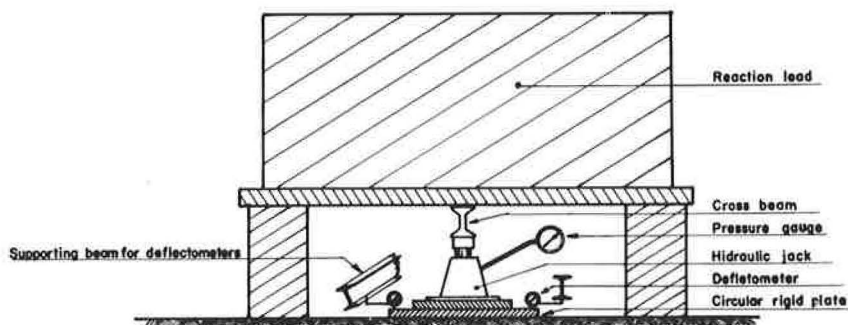
Figure 4. Mounting of bearing tests.

later tests for this influence. At one airport, a plate of 39 cm (15 ¼ in.) in diameter was used instead of the 45-cm plate. The results obtained with the 39-cm plate are comparable to those of the 45-cm plate. A bearing test was made on the top of the subbase at one of the airports, using a 80-cm plate.

About half the loading tests were performed according to the Asphalt Institute Process (7). This process is as follows. After seating the plate, a small load is applied and sustained until the increase of deflection is less than 0.02 mm/min. The deflection is recorded, and the load is removed. The plate is kept unloaded until the recovery of deflection is less than 0.02 mm/min. The same load is reapplied and removed three more times, with the deflection recorded every time. A greater load is then applied and removed four times, and the deflections are recorded. The same procedure is repeated with increasing loads, until the end of the test. The test is stopped when the pavement breaks, or when the deflections are very high (over 10 mm), or when all the reaction load is used.

The remaining loading tests were performed according to the International Civil Aviation Organization Process (8). This process is similar to that of the Asphalt Institute Process with one difference: every load is applied five times instead of four times.

The only loading test made directly on the subbase was performed according to the U. S. Corps of Engineers Process (9), which is a continuous loading procedure recommended for the determination of the subgrade modulus of reaction.

Load-deflection diagrams were drawn for all loading tests (Fig. 5). The soil-cement base modulus of reaction K (load-deflection ratio) was computed for every stage of loading in all loading tests. The load-deflection ratio was completely recoverable and
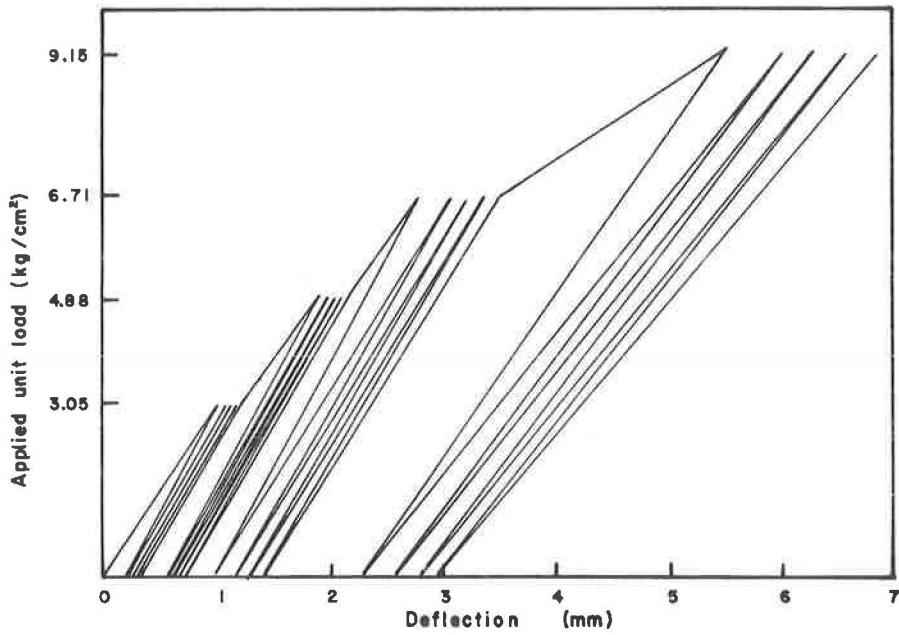
Figure 5. Typical load-deflection diagram of tests.

TABLE 3

TYPICAL VALUES OF LOAD-DEFLECTION RATIO
FOR TEST NO. 631

Applied Pressure (kg/cm²)	Loading Cycle	Load-Deflection Ratio (kg/cm²/cm)	
		Initial	Elastic
3. 05	1	30. 8	
	2		37. 2
	3		35. 5
	4		36. 8
	5		38. 2
4. 88	1	36. 9	
	2		38. 4
	3		40. 3
	4		39. 3
	5		39. 3
7. 32	1	36. 4	
	2		39. 8
	3		39. 5
	4		39. 5
	5		40. 2
12. 20	1	27. 2	
	2		33. 7
	3		34. 5
	4		34. 8

TABLE 4

AVERAGE VALUES OF ELASTIC LOAD-DEFLECTION RATIO
FOR ALL TESTS ON SOIL-CEMENT BASES

Series (Airport)	Test No.	Load-Deflection Ratio (kg/cm^2cm or kg/cm^3)		
		$\phi = 80$ cm	$\phi = 45$ cm	$\phi = 30$ cm
1	111	37		
2	211	25		
	221	27		
	231	37		
	Mean	(29.7)		
3	311	32		
4	410	25	54[a]	67
	420	34	56[a]	93
	Mean	(29.5)	(55.0)[a]	(80.0)
5	510	30	71 (61)	140
	520	36	51	120
	532a		100	
	532b		82 (91)	
	542a		87	
	542b		95	
	Mean	(33.0)	(81.0)	(130.0)
6	610	40	98	177
	620	40	102	123
	630	39	122	233
	Mean	(39.7)	(107.3)	(177.7)
7	710	31	49	97
8	810	25	80	193
	820	34	44	87
	830	34	31	136
	Mean	(31.0)	(51.7)	(138.7)
	Overall mean	32.9	74.8	133.3
	Std. Dev.	5.3	26.3	50.2
	Coeff. of variation	16%	35%	38%

[a]Results measured with plate of $\phi = 39$ cm; numbers between parentheses are series averages.

nearly constant for all loads after the first stage of loading, in every test. The initial load-deflection ratio for the first stage of loading was non-recoverable, and its value was of the order of 85 percent of the later deflection ratio. Table 3 gives typical values for one test. The average of the elastic load-deflection ratios for all loads after the first stage of loading, for every test, was taken as a characteristic mechanical parameter of the pavement. This average elastic load-deflection ratio is referred to as the load-deflection ratio, and indicated by the letter K, in the present analysis. It is contemplated that the elastic load-deflection ratio is the most significant parameter for the evaluation of the structural behavior of pavement under the action of repetitive loadings, such as traffic loads.

TABLE 5

SELECTED VALUES OF LOAD-DEFLECTION RATIO FOR
COMPARABLE TESTS ON SOIL-CEMENT BASES (kq/cm³)

Series	φ = 80 cm		φ = 45 cm		φ = 30 cm	
	Avg. of Tests	Avg. of Series	Avg. of Tests	Avg. of Series	Avg. of Tests	Avg. of Series
4	25	29. 5	54[a]	55. 0[a]	67	80. 0
	34		56[a]		93	
	30		71		140	
5		33. 0		61. 0		130. 0
	36		51		120	
7	31	31. 0	49	49. 0	97	.97. 0
8	25		80		193	
	34	31. 0	44	51. 7	87	138. 7
	34		31		136	
Partial mean		31. 1		54. 3		111. 5
Standard deviation		1. 4		5. 2		27. 6
Coeff. of variation		5%		10%		25%
Corrected load/deflection ratio (K_{eq})		31. 1		54. 3 × 1. 5 = 81. 5		111. 5 × 1. 5 = 167. 3
Ratio K_r/K_o		1		81. 5/31. 1 = 2. 62		167. 3/31. 1 = 5. 38

[a]Results measured with plate of φ = 39 cm.

LOAD-DEFLECTION RATIOS

Table 4 gives the load-deflection ratios measured in all tests. Each series of results corresponds to one airport (10, 11). The measured load-deflection ratios show great scatter of values. The statistical coefficient of variation is 16 percent for the 80-cm plate, 35 percent for the 45-cm plate, and 38 percent for the 30-cm plate. This large dispersion of values indicates that the results in Table 4 cannot be considered homogeneous, and therefore the overall mean is not significant. Also, there is some dispersion within the data pertaining to each airport. However, the gathering of data summarized in Table 4 required a considerable expense of energy, time, and money. It would be regretable if all this effort should be wasted. The load-deflection ratios, as experimental measurements obtained under definite conditions, are not readily useful for the design of other pavements in different conditions, unless they are analyzed, interpreted and generalized under the light of a suitable theoretical framework. It was then decided to extract a set of homogeneous and comparable data from Table 4 and to analyze these data by the elastic layered theory. The resulting numerical figures are to be regarded as tentative, as they are affected by the dispersion of field data, but the proposed theoretical method of analysis is believed to be entirely valid.

Table 5 gives the selected values of the load-deflection ratio for comparable tests on soil-cement bases. The justification for transferring data from Table 4 to Table 5 was as follows:

1. Tests of series 1, 2, and 3 were not used because these series contained data for only one diameter of plate, all for the same thickness of pavement. These data are not enough to solve the mathematical problem of layered systems.

2. Series 5 contains tests no. 510 and 520, performed according to the normal three-plate procedure, and test no. 532-a to 542-b, performed with the 45-cm plate alone. The latter group of results, obtained by a non-normal testing procedure, was not included in Table 5.

3. Results of series 6 were abandoned because they were much higher than results from all other series, for all three plates. Not only the load-deflection ratios, but also the total loads were much higher in series 6, whereas the final deflections were smaller. The causes of these differences were not readily apparent, and were not further investigated, but it is evident from the test results that series 6 represents a pavement of better quality than the other series.

4. The remaining tests of series 4, 5, 7 and 8 were considered comparable in quality of pavement and procedure of testing, and were included in Table 5. The data in Table 5 were not specifically chosen, but, rather, remained after tests which were non-typical in one respect or another were eliminated. These data are homogeneous in the sense that all tests were performed by the same procedure and the pavements tested are of comparable strength.

The data in Table 5 show marked improvement in statistical consistency over the previous table. The coefficient of variation is only 5 percent for the 80-cm plate, and 10 and 25 percent for the 45-cm and 30-cm plates, respectively. The variation of 5 percent for the largest plate was considered purely accidental, and compatible with the accuracy of experimental measurements. The average of the 80-cm plate results is statistically significant. The larger variation of the two smaller plates is attributed to the detrimental influence of the first test on the following tests, at each location. It can be concluded that the large plate data warrant a high degree of confidence, the intermediate plate data allow lesser confidence, and the small plate data deserve very little confidence. Unfortunately, three diameters of plates are needed for the mathematical solution of a three-layered system of uniform thickness. Whenever possible, the 80-cm plate data are used as the primary basis for theoretical analysis. The two smaller plates are mostly used for cross-checking the hypothesis of calculus. The averages of the results in Table 5, for each diameter of plate, are called "partial means" and represent a homogeneous type of pavement.

The data of series 5 permit the establishment of a criterion for correcting the results of the two smaller plates. The average of tests no. 510 and 520 (normal three-plate procedure) is 61 kg/cm^3. The average of tests no. 532-a to 542-b (intermediate plate alone) is 91 kg/cm^3. These results indicate that the first test (80-cm plate), caused a weakening of the pavement, possibly due to cracking, so that the second test, (45-cm plate) produced a smaller load-deflection ratio than it should if the second test were performed over virgin pavement. The ratio between the two values gives the correction factor

$$\text{Correction factor} = 91/61 \cong 1.5$$

In a first approximation, all results of the two smaller plates are multiplied by this empirical factor, 1.5, to obtain the corrected load-deflection ratio, K_{eq}. The values of the 80-cm plate do not need correction, of course. The corrected values agree with the theoretical curves developed in the analysis, whereas the uncorrected values fall completely out of line. This agreement between corrected and theoretical values confirms to a certain degree the validity of the correction. Nevertheless, this empirical correction is only an expedient to arrive at some tentative conclusions from a mass of experimental data that would otherwise be lost.

The following theoretical analysis shows that it is useful to study the relationship between the corrected load-deflection ratios for the three diameters of plates. The load-deflection ratio for the 80-cm diameter plate, which is always the lowest, is taken as the basic parameter K_{80}. The load-deflection ratios for the 45-cm and 30-cm
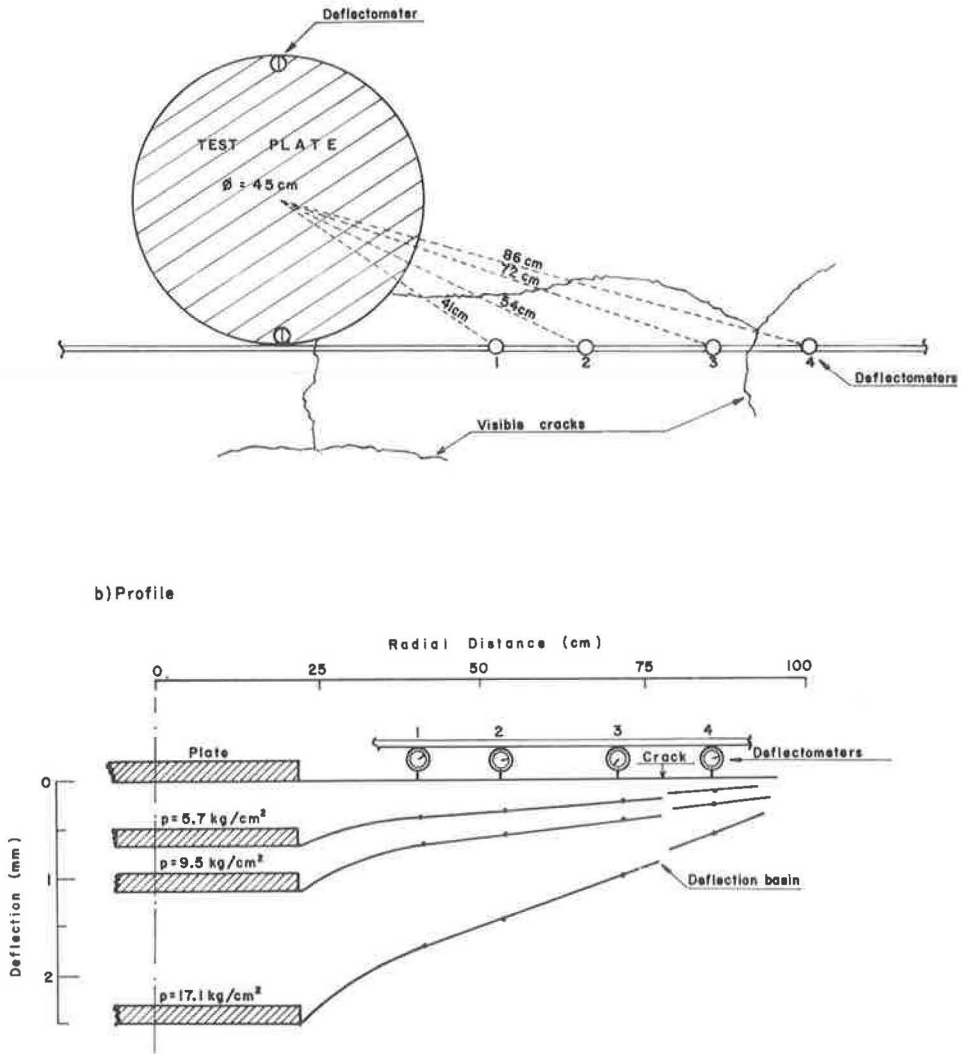
Figure 6. Slab effect of soil-cement bases as shown by survey of deflection basin: (a) mounting of test (plan); (b) pattern of deflection basin for three loadings (profile).

diameter plates are designated by K_{45} and K_{30}, respectively. These three values yield two relationships K_{45}/K_{80} and K_{30}/K_{80}, indicated in general terms by K_r/K_0. Evidently this ratio is equal to unity for the basic 80-cm diameter plate. Table 5 gives the K_r/K_0 ratios for the partial means.

SLAB EFFECT OF SOIL-CEMENT BASES

One of the most discussed characteristics of soil-cement bases is slab effect, i.e., the ability to distribute loads by acting as an effective rigid slab. All soil-cement bases present an irregular pattern of hair-cracking due to shrinkage and thermal variations. These cracks conceivably alleviate flexural stresses induced by applied loads, but retain the ability to transmit vertical stresses. It was not known how the cracking pattern would influence the effectiveness of the slab effect. A special series

of measurements was devised to check the slab effect through the study of the deflection basin.

At the location of test no. 630, with the 45-cm plate, four additional deflectometers were installed, in addition to the two normal deflectometers located over the plate. The extra deflectometers were mounted at regular intervals on the supporting beam, with the probe point resting directly on the pavement. The farthest deflectometer was located at a distance from center of plate almost four times the radius of plate. Figure 6a shows the mounting of the special test, and the pattern of cracking before testing. Fortunately, deflectometers 3 and 4 were located on opposite sides of a visible crack. Figure 6b shows the pattern of the deflection basin for several loadings, as measured by the deflectometers. At a distance of the perimeter of the plate equal to the plate diameter, the deflection was 44 percent of the plate deflection, for the highest load. At a distance four times the plate diameter, on the opposite side of a visible crack, the deflection was 20 percent of the plate deflection. The recovered deflections were also proportional to the plate recovered deflections. New cracks showed up under loading that were not apparent before loading. The conclusion was that soil-cement bases maintain an appreciable degree of slab effect, in spite of the cracking pattern.

INTERPRETATION OF TEST DATA

A tentative analysis was made of the test data by the theory of the two-layered elastic systems, considering the subgrade and subbase as a single layer of equivalent elastic properties. This analysis gave erratic and unrealistic results, producing values too high for the soil-cement modulus of elasticity. Two causes were thought to be responsible for the failure of the two-layer theory to explain the load-deflection pattern of the pavement structures:

1. The pavement structures are basically three-layered systems. Combining the two lower layers as a single layer is not merely a question of greater or lesser detail in the analysis; this unwarranted simplification markedly affects the computed values of the elastic modulus, in different ways for the different plate diameters.

2. The Burmister graph (Fig. 2) is not accurate enough, particularly in the region of h/r less than unity. The writers were unable to locate published tables of deflection factor values for two-layered systems. Also, the method of analysis proposed by Burmister (1), based on the shape and concavity of trial deflection factor curves, was somewhat erratic.

A new method of analysis was then developed for the interpretation of the bearing test data by the use of three-layer elastic theory. This analysis puts forward a practical application of the three-layer deflection factor tables published by Jones (2). The proposed method of analysis is believed to be accurate and dependable. Its results depend, however, on the accuracy of the measured data.

It is believed that the proposed method, particularly the analysis of the K_r/K_0 ratio, can be successfully extended to the analysis of truly two-layered systems, to avoid the difficulties discussed in the foregoing item 2.

ANALYSIS OF TEST ON SUBBASE

The only bearing test made directly on the soil subbase with the 80-cm plate was at Airport 5; it yielded a load-deflection ratio of 7 kg/cm^3. The pavement structure tested is a two-layer system, namely the soil subbase and the uncompacted subgrade. The system parameters are

Known Data		Unknown Data
K_{eq} = 7 kg/cm^3		E_1 = ?
r = 40 cm	h/r = 1.5	E_2 = ? E_1/E_2 = ?
h = 60 cm		

The mathematical problem involved is indeterminate for the known data only. The solution of the problem would require knowledge of the values of E_{eq} for other diame-
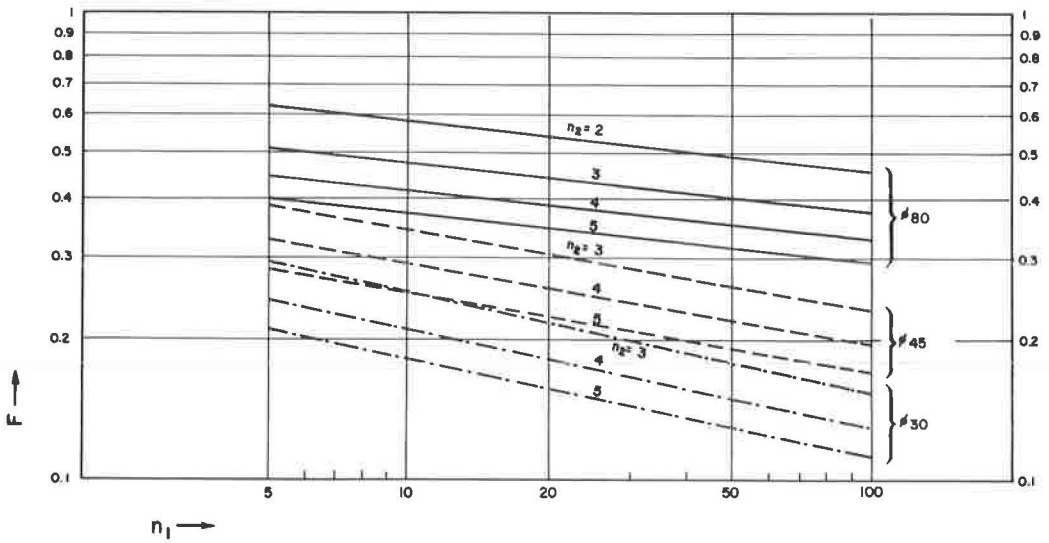
Figure 7. Three-layer deflection factor $\overline{F}$ as function of modular ratios n_1 and n_2 and plate diameter ϕ (graph valid only for thicknesses indicated in Figure 3).
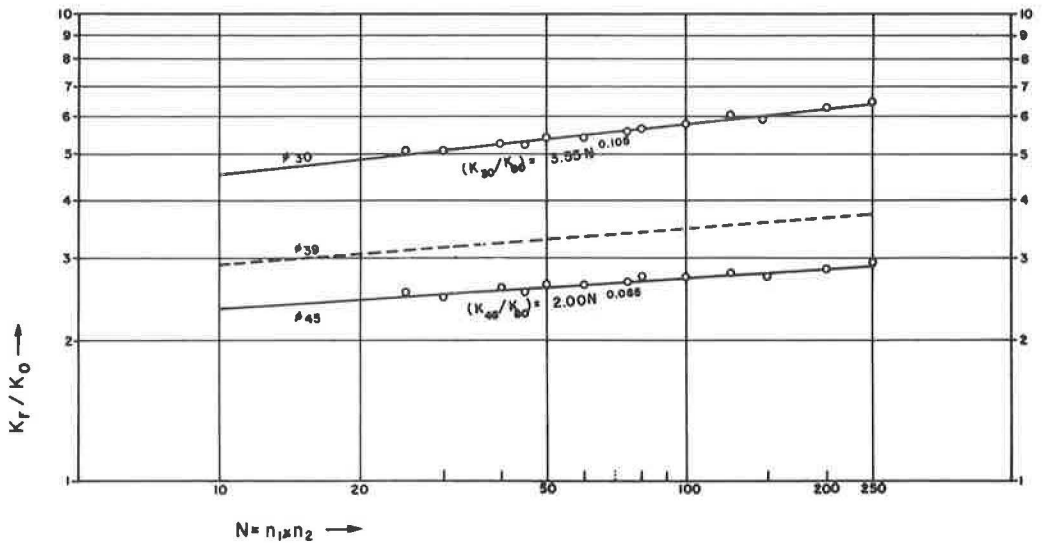
Figure 8. Ratio K_r/K_O as function of modular ratio N and plate diameter for considered three-layer system.

ters of plates, or else the value of the modular ratio E_1/E_2. Many authors, including Peattie (12), Dormon (13), and Heukelom (14), have found that the effective modular ratio for granular non-cemented materials is always between 2 and 5. For instance, if the ratio $E_1/E_2 = 4$, from Eq. 7b (Fig. 1) and the graph in Figure 2 we have:

$$h/r = 1.5 \left.\begin{cases} \\ \end{cases}\right. \quad \therefore \quad F = 0.54$$
$$E_1/E_2 = 4$$

From Eq. 3b

$$E_2 = 1.18 \times 40 \times 7 \times 0.54 \cong 180 \text{ kg/cm}^2$$
$$E_1 = 4 \times 180 = 720 \text{ kg/cm}^2$$

The same result would be found computing F by the approximated Eqs. 8b and 9b, instead of taking F from Figure 2.

Eq. 5b gives the following value for E_{eq}:

$$E_{eq} = 180/0.54 \cong 330 \text{ kg/cm}^2$$

The same value of E_{eq} would be found if the two-layer system were considered as a uniform medium of modulus E and L/D ratio K = 7 kg/cm³. From Eq. 3a we have:

$$E = 1.18 \times 40 \times 7 = 330 \text{ kg/cm}^2$$

If the calculated values of E_1, E_2, or E could be used in the solution of the three-layer system, the problem would be much simplified. Unfortunately this substitution is not valid, even if the modular ratio $E_1/E_2 = 4$ is supposed to hold true. A multilayer system (Fig. 1 B and 1 C) can be replaced by an equivalent uniform medium (Fig. 1 A) for the condition of K = K_{eq}, but this substitution is valid only once for the entire system. It is not valid to replace the two lower layers by one supposedly "equivalent" single layer within the three-layer system; and neither is it correct to use data measured on the two-layer system in the calculation of the three-layer system. The main reasons are (a) the stress and strain distribution would not be the same in the two cases, and the theoretical equations would not apply after the replacement; (b) the confining effect of the top layer is not present in the two-layer structure alone; (c) the compaction of the top layer is partially transmitted to the lower layers, producing an increase in the density and in the value of the effective modulus. This last effect is very important at the airport pavements tested, due to the sandy nature of the soil and the use of vibratory rollers, in the compaction of the soil-cement base. Consequently, the three-layer system moduli should be computed from measurements made on the complete structure. Tests made on the lower layers alone are of no avail for this purpose.

ANALYSIS OF SERIES 5 TESTS

Series 5 is analyzed first because it contains much useful data in addition to the test on the subbase. The pavement structure is a three-layered system (Fig. 3).

Geometric Parameters

	Test $\phi 80$	Test $\phi 45$	Test $\phi 30$
r =	40	22.5	15
h_1 =	15	15	15
h_2 =	60	60	60
H = h_1/h_2 =	0.25	0.25	0.25
A = r/h_2 =	0.67	0.37	0.25

Bearing Test Results

	$\phi 80$	$\phi 45$	$\phi 30$
K_{eq} (measured) =	33	61	130
K_{eq} (corrected) =	33	61 × 1.5 ≅ 91	130 × 1.5 = 195
K_r/K_0 =	1	91/33 = 2.76	195/33 = 5.91

Unknown Elastic Parameters

$E_1 = ?$

$E_2 = ?$ $E_1/E_2 = n_1 = ?$

$E_3 = ?$ $E_2/E_3 = n_2 = ?$ $n_1 n_2 = N = ?$

As previously mentioned, the modular ratio n_2 is always between 2 and 5. It is shown later that the selection of any value for n_2 between 2 and 5 is not too critical for the computed value of the base modulus E_1, which is the primary objective of this analysis. We have two independent equations relating the unknown parameters to the known data:

Eq. 3c: $E_3 = 1.18\, r\, K_{eq}\, F$

Eq. 7c: $F = f\,[n_1, n_2, H, A]$

The symbol f in Eq. 7c represents an extremely complex differential function, but it has been computed in tabular form (2). Some typical values are given in Table 1. As factor F is also unknown, it can be eliminated reducing the two foregoing equations to one:

$$E_3 = 1.18\, r\, K_{eq} \cdot f\,[n_1, n_2, H, A]$$

Applying this equation to the test results, with three plate diameters we have a system of three equations with three variables:

Known Data	Variables
$K_{80}, K_{45}, K_{30}, r, H, A$	E_3, n_1, n_2
$H = h_1/h_2$	$n_1 = E_1/E_2$
$A = r/h_2$	$n_2 = E_2/E_3$

The mathematical problem is therefore determinate. However, due to the complexity of function f of Eq. 7c, the system must be solved by trial methods. A set of values of E_3, n_1, and n_2 are sought that simultaneously satisfy the three equations of the system. A practical way to do this is to adopt tentative values for n_1 and n_2, and compute the corresponding values of E_3. When the three values of E_3 given by the three equations are equal, the trial values n_1 and n_2 plus the computed value E_3 are a solution for the system. The base modulus E_1 can then be easily calculated. A difficulty of the trial method of solution is that the measured values of the L/D ratio K_{80}, K_{45}, and K_{30} are affected by an experimental error. The computed values of E_3 are never equal, but show a dispersion as the L/D ratios. The best solution must be found by statistical criteria.

After a few trials, the following solution was found adequate for series 5:

$$n_1 = 30 \quad\quad n_2 = 4 \quad\quad N = 120$$

Let us check this solution, to demonstrate the trial method employed. First, the values of F corresponding to these values of n_1 and n_2 are computed for the three diameters by interpolation in Jones tables (2). Next, the corresponding values of E_3 are calculated by Eq. 3c:

$\phi 80$ $E_3 = 593\ \mathrm{kg/cm}^2$

$\phi 45$ $E_3 = 581\ \mathrm{kg/cm}^2$

$\phi 30$ $E_3 = 576\ \mathrm{kg/cm}^2$

The three values of E_3 are close enough to justify the given solution. The dispersion of values of E_3 is less than the dispersion of L/D ratios. Now calculate E_2 and E_1 using the average value of E_3, or better the value for the $\phi 80$ plate:

$$E_1 = 120 \times 593 \cong 71,000 \text{ kg/cm}^2$$
$$E_2 = 4 \times 593 \cong 2,400 \text{ kg/cm}^2$$
$$E_3 \cong 600 \text{ kg/cm}^2$$

Let us check the influence of the modular ratio n_2 on the computed value of E_1, maintaining constant the overall ratio N = 120. Repeating all calculations gives

$$n_1 = 40 \qquad n_2 = 3 \qquad E_1 = 77,000 \text{ kg/cm}^2$$
$$n_1 = 30 \qquad n_2 = 4 \qquad E_1 = 71,000 \text{ kg/cm}^2$$
$$n_1 = 24 \qquad n_2 = 5 \qquad E_1 = 64,000 \text{ kg/cm}^2$$

The variation of E_1 for the possible values of n_2 is of the same order of the dispersion of measured L/D ratios. This conclusion warrants a simplifcation of the calculus. If an intermediate value is adopted for n_2, the problem will be reduced to the calculation of two variables, namely N and E_3.

The value of the subgrade modulus $E_3 = 600 \text{ kg/cm}^2$ measured on the three-layered system is much greater than the value measured in the test made directly on the subbase (180 kg/cm^2), even higher than the equivalent modulus corresponding to the subgrade-subbase ensemble (330 kg/cm^2). This increase in the subgrade modulus value can be explained by the three causes mentioned in the analysis of the test on the subbase.

If the base modulus E_1 is computed from the subbase L/D ratio K = 7 kg/cm^2, and the base L/D ratio $K_{eq} = 33 \text{ kg/cm}^2$ by Eqs. 6b and 7b, assimilating the pavement structure to a two-layered system, the value $E_1 = 726,000 \text{ kg/cm}^2$ will be found. This latter value is evidently highly unrealistic for soil-cement bases. This computation proves again that the supposedly equivalent single layer for substituting the two lower layers is not a valid concept in the three-layered structure.

The trial method described, using Jones tables directly (2), is extremely tedious because of the great number of interpolations necessary. Each value of F, corresponding to a pair of values of n_1, and n_2, for every diameter, requires at least eight interpolations on log-log paper. To avoid this difficulty, a simplified method of analysis was developed, based on Jones tables (Figs. 7, 8). Figure 7 shows the three-layer deflection factor F as function of modular ratios n_1 and n_2, for the three plate diameters. Figure 8 shows the value of ratio K_r/K_0 as function of modular ratio N and plate diameter. For the particular values of the geometric parameters of the pavement structures of this study, the ratio K_r/K_0 is a function of N, but it is practically independent of the individual values of n_1 and n_2. The graphs in Figures 7 and 8 apply only to the range of parameters of the particular problem under study, and should not be extrapolated. For other values of the parameters, new graphs should be drawn up, from the original tables.

The problem is now solved as follows:

Known Data

$$K_{80} = 33 \text{ kg/cm}^2$$
$$K_{45}/K_{80} = 2.76$$
$$K_{30}/K_{80} = 5.91$$

Unknown Parameters

$$N = ? \qquad E_3 = ?$$

From Figure 8, the two values of K_r/K_0 give two values of N:

$$N_{45/80} = 130 \qquad N_{30/80} = 110$$

The two values of N are close enough to warrant the adoption of its average as the most probable value. Adopting an intermediate value for n_2 gives

$$N = 120 \qquad n_1 = 30 \qquad n_2 = 4$$

TABLE 6

VALUES OF SOIL-CEMENT MODULUS OF
ELASTICITY FOUND IN SERIAL ANALYSIS (kg/cm²)

Series	$n_1 \times n_2$	N	E_1 (kg/cm²)	Data
1	20 x 3	60	46,600	$\phi 80$
2	20 x 3	60	37,400	$\phi 80$
3	20 x 3	60	40,300	$\phi 80$
4	5 x 2	10	8,700	$\phi 80, \phi 39$
5	30 x 4	120	71,200	$\phi 80, \phi 45, \phi 30$
6	30 x 4	120	88,000	$\phi 80$
7	6 x 2	12	10,700	$\phi 80, \phi 45, \phi 30$
8	11 x 3	33	22,900	$\phi 80, \phi 45$
General avg.			$E_1 = 40,700$ kg/cm²	

From Figure 7, comes the value of F for the $\phi 80$ plate:

$$F_{80} = 0.380$$

Eq. 3c gives the value of E_3:

$$E_3 = 1.18 \times 40 \times 33 \times 0.380$$
$$= 592 \text{ kg/cm}^2$$

Knowing E_3, the other moduli E_2 and E_1 are calculated as before.

The proximity between the two values of N confirms the validity of the correction factor of 1.5 previously suggested. The value N = 130 is based on measured data only, as series 5 contains test data on virgin points of pavement both for $\phi 80$ and $\phi 45$ plates. The value N = 110 is based on corrected data for the $\phi 30$ diameter. If the uncorrected test data were
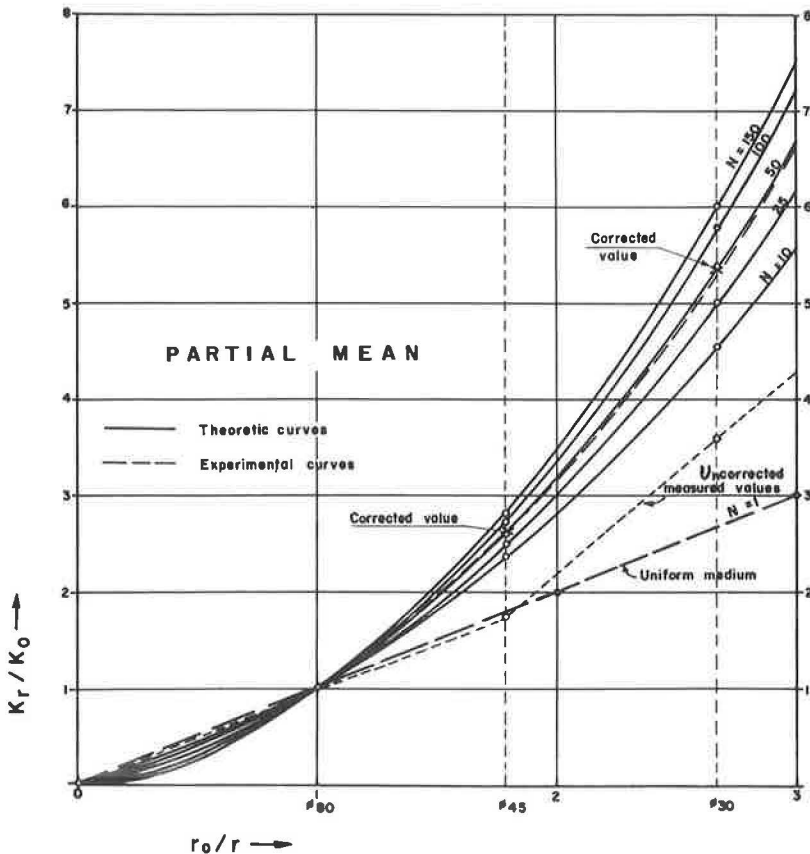
Figure 9. Ratio $K_r K_o$ as function of radial ratio r_o/r for partial mean values for the considered three-layer system (curves are accurate at plotted points, only approximate between points).

used, it would not be possible to find a value of N satisfying simultaneously the two values of K_r/K_o.

ANALYSIS OF SERIES 6 TESTS

As previously noted, series 6 test data indicate a pavement considerably stronger than the other series. When analyzed by the same method used in series 5, series 6 data produced incompatible results. There is no value of N simultaneously satisfying the two values of K_r/K_o, neither for the corrected nor for the uncorrected data. This incompatibility indicates that some of the hypotheses assumed in the theoretical formulation are not met in series 6. The causes of these discrepancies were not further investigated.

Using only the L/D ratio for the 80-cm plate $K_{80} = 39.7$ kg/cm^2, and adopting the same modular ratios found in series 5, we have for series 6:

$$N = 120 \qquad n_1 = 30 \qquad n_2 = 4 \qquad E_1 = 88.000 \text{ kg/cm}^2$$

ANALYSIS OF ALL SERIES

The same method used in series 5 was used in analyzing test data from all eight series (Table 6).

For the three first series, comprising results for the $\phi 80$ plate only, the modular ratio of the partial mean (N = 60) was adopted. For series 4 and 8 the result of the $\phi 30$ plate was abandoned because it was too much out of line with all others. The proposed method of analysis yielded consistent results for the three plate diameters both for series 5 and series 7, where the modulus values are very high and very low, respectively. The average of all values of the base modulus is 40,700 kg/cm^2, but this average is not significant because the series data are not homogeneous. The most important information of Table 6 is the range of values of the soil-cement base modulus of elasticity in the pavements studied, which goes from 10,000 to 70,000 kg/cm^2 (150,000 to 1,000,00 psi). It is likely that the modulus is higher than this latter value in series 6.

ANALYSIS OF THE PARTIAL MEAN DATA

The partial mean refers to a homogeneous group of test data given in Table 5. The analysis of the partial mean data is aimed at finding a significant mean value for the base modulus. As the test data on Table 5 are more refined, so is the method of analysis. The basic concepts remain the same, however.

	Computation of modular ratio N		
K_{eq} (measured) =	31.1	54.3	111.5
K_{eq} (corrected) =	31.1	81.5	167.3
K_r/K_o =	1	2.62	5.38
N (Fig. 8) =	-	64	48

The two values of N are close enough, as computed modular ratios go, to justify adopting its average as the best value. But, as the $\phi 45$ data deserve more confidence than the $\phi 30$ data, the most probable value of N is closer to 64 than to 48. Let us adopt: N = 60.

Let us try several combination of n_1 and n_2, keeping constant the product $n_1 \times n_2 = 60$. Every pair of values of n_1 and n_2 correspond to one value of F from Figure 7 and to one value of E_3 computed by Eq. 3c:
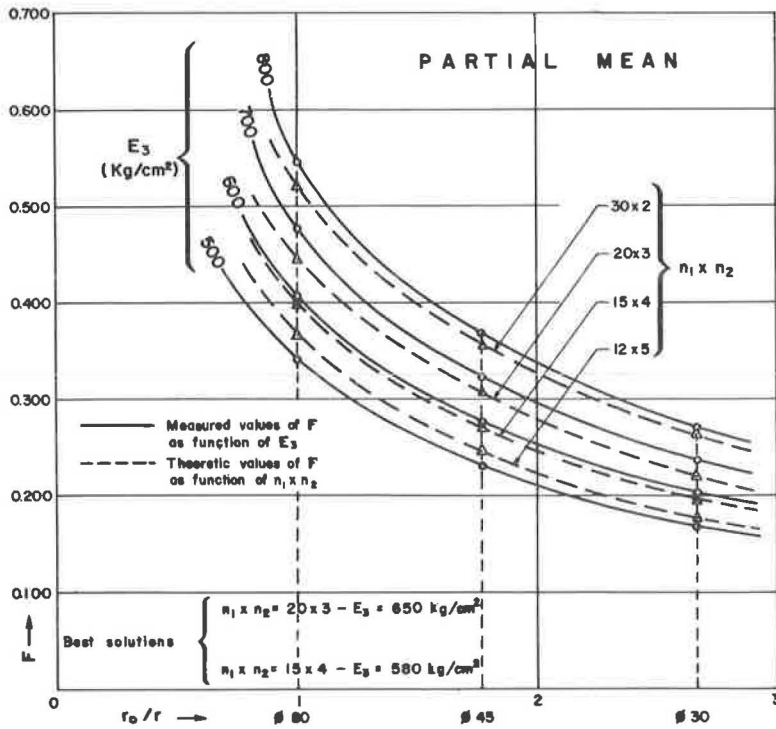
Figure 10. Deflection factor of considered three-layer system as function of radial ratio, modular ratio, and subgrade elastic modulus (trial method solution).

$n_1 \times n_2$	Computed values of E_3 (kg/cm^2)		
	$\phi 80$	$\phi 45$	$\phi 30$
30 × 2	763	790	773
20 × 3	653	662	651
15 × 4	584	589	580
12 × 5	539	532	521

In theory, the equality of computed values of E_3 for one given combination of n_1 and n_2 would indicate that the system of equations was simultaneously satisfied, and this combination is a solution for the problem. However, in practice the absolute equality of values of E_3 is never attained because of the dispersion of measured values of K_{eq}. Practically any of these combinations would be acceptable. The values of E_3 for the $\phi 80$ plate are the most reliable. Let us take as representative values the following:

$$n_1 \times n_2 = 20 \times 3 \qquad N = 60$$
$$E_3 \cong 650 \text{ kg/cm}^2$$
$$E_2 = 3 \times 650 \cong 2,000 \text{ kg/cm}^2$$
$$E_1 = 60 \times 650 = 39,000 \text{ kg/cm}^2$$

The method of analysis is shown in Figures 9 and 10. Figure 9 is a graph of ratio K_r/K_0 as function of radial ratio r_0/r for the partial mean values. The curves are accurate at plotted points, and only approximate between points. The K_r/K_0 ratio was chosen as a significant parameter because it is dependent on N but practically independent

of the values of n_1 and n_2, within the range of parameters of our particular case. The ratio r_0/r was chosen as the geometric parameter referring to plate diameter. The basic radius is $r_0 = 40$ cm ($\phi 80$ cm).

The graph of K_r/K_0 as function of r_0/r is similar to the graph of load vs perimeter-area ratio. The r_0/r ratio, being proportional to the perimeter-area ratio, is a non-dimensional number, whereas the perimeter-area ratio is numerically equal to $2/r$ and has the dimension of cm^{-1}. The r_0/r ratio is therefore a more adequate parameter for drawing influence curves. McLeod (15) found an empirical lineal relationship between load and perimeter-area ratio, for a given deflection, for flexible pavements with granular and asphaltic bases. Figure 9 shows a curved relationship, nearly parabolic for the three diameters, for the semiflexible soil-cement bases. According to the layered system elastic theory, this relationship should be nonlineal, as it was found to be. In theory, the concavity of the curves is inverted for diameters less than $\phi = 30$ cm, if the basic radius $r_0 = 40$ cm is kept constant. There is no experimental evidence to confirm the shape of the curves beyond $\phi = 30$ cm.

The solid lines of Figure 9 are theoretical curves for several values of N. The broken line (long dashes) is the curve of measured values, with the correction already referred to. The pointed line (short dashes) is the curve of uncorrected measured values. The shape and curvature of the corrected curve closely follow the set of theoretical curves, indicating a value of N close to 60. The uncorrected curve falls completely out of line with the theoretical curves. The shape of the corrected curve again confirms the validity of the adopted correction. The straight line for $N = 1$ represents the variation of K_r/K_0 as function of r_0/r for the uniform medium. Theoretically, this relationship should be lineal, according to Eq. 4a. Experimental measurements reported by Stratton (16) have shown a moderate deviation from the theoretical lineal relationship. According to Stratton, the load-deflection ratio of a uniform medium (modulus of subgrade reaction) is independent of the plate diameter for diameters over 75 cm (30 in.). This finding justifies the selection of $r_0 = 40$ cm as the basic radius.

Figure 10 shows the trial method for the simultaneous solution of E_3, n_1 and n_2 values. The solid lines are experimental curves of F as function of r_0/r, for tentative values of E_3 and measured values of K_{eq}, computed by Eq. 3c. The broken lines are theoretical curves of F as function of r_0/r, for several values of $n_1 \times n_2$, independent of E_3. Comparing the empirical and theoretical curves, the best fitting line is found, yielding the simultaneous values of the three variables. Two theoretical curves corresponding to 20 x 3 and 15 x 4 are practically parallel to the empirical curves, whereas the outside curves run in opposite directions (Fig. 10). Figure 10 yields the two best solutions:

$$n_1 \times n_2 = 20 \times 3 \quad E_3 = 650 \text{ kg/cm}^2$$
$$n_1 \times n_2 = 15 \times 4 \quad E_3 = 580 \text{ kg/cm}^2$$

Any one of the foregoing solutions is within the accuracy of the measured data. The first one was taken as a typical value for the soil-cement bases.

The values of K_{eq} used in drawing the empirical curves of Figures 9 and 10 represent the final refinement of hundreds of direct measurements of pressures and deflections. The remarkable similarity between the theoretical and empirical curves on both figures points to a significant cause and effect relationship. It indicates that the theoretical interpretation of the measured data is correct, within the accuracy of the measurements.

CONCLUSIONS

The main conclusions of the study are as follows:

1. The theory of elastic layered systems is adequate for intepreting the load-deflection pattern of soil-cement bases.

2. The modulus of elasticity of soil-cement bases in the pavements studied is in the range of 10,000 to 70,000 kg/cm^2 (150,000 to 1,000,000 psi). There is some indication that the modulus can be higher than this value when the soil is very good.

3. The value 40,000 kg/cm^2 (550,000 psi) can be taken as a typical value for soil-cement made with soil of 25 percent CBR and 10 percent of cement, built following sound construction practices.

ACKNOWLEDGMENTS

REFERENCES

1. Burmister, D. M. The Theory of Stresses and Displacements in Layer Systems and Application to the Design of Airport Runways. HRB Proc., Vol. 23, pp. 126-149, 1943.

2. Jones, A. The Calculation of Surface Deflection for Three-Layer Elastic Systems. Proc. Symp. on Road Tests for Pavement Design, Lisbon, 1962.

3. de Barros, S. Thenn. O Cálculo das Tensões e dos Recalques do Pavimento Flexivel Inst. de Pesquisas Rodoviárias, Rio de Janeiro, 1964.

4. Bachelez, J., and Jeuffroy, G. Note on a Method of Analysis for Pavements. Proc. Ann Arbor Conf., 1962.

5. Burmister, D. M. Application of Layered System Concepts and Principles to Interpretations and Evaluations of Asphalt Pavement Performances and to Design and Construction. Proc. Ann Arbor Conf., 1962.

6. Sowers G. F., and Vesić, A. B. Vertical Stresses in Subgrades Beneath Statically Loaded Flexible Pavements. HRB Bull. 342, pp. 90-123, 1962.

7. Manual on Airfields. The Asphalt Institute, 1947.

8. Aerodrome Manual. International Civil Aviation Organization.

9. Rigid Airfield Pavements (EM 1110-45-303), U. S. Corps of Eng., 1958.

10. Pinto, Sousa C. Interpretacão de Provas de Carga Especiais em Pavimentos Flexiveis. 5a Reunião Anual de Pavimentacão, Rio de Janeiro, 1964.

11. de Barros, S. Thenn. Pesquisa del Modulo de Elasticidad de Bases de Suelo-Cemento. Quinto Congreso Argentino de Vialidad y Transito, Embalse Argentina, 1964.

12. Peattie, K. R. The Significance of the Surface Deflection of Flexible Pavements. Proc. Symp. on Road Tests for Pavement Design, Lisbon, 1962.

13. Dormon, G. M. The Extension to Practice of a Fundamental Procedure for the Design of Flexible Pavements. Proc. Ann Arbor Conf., 1962.

14. Heukelom, W., and Klomp, A. J. G. Dynamic Testing as a Means of Controlling Pavements During and After Construction. Proc. Ann Arbor Conf., 1962.

15. McLeod, N. W. Relationships Between Applied Loads, Surface Deflections, Traffic Volumes, and Thicknesses of Flexible Pavements. Proc. Fifth Internat. Conf. on Soil Mech. and Found. Eng., Paris, 1961.

16. Pavement Design for Roads and Airfields. Road Research Lab., T. P. No. 20, 1951.

Deflection Factor Charts for Two- and Three-Layer Elastic Systems

S. THENN DE BARROS, Consulting Engineer, São Paulo, Brazil

Tables of deflection factor values for three-layer elastic systems loaded with uniform circular loads have been published by A. Jones of the Thornton Research Center, in connection with the development of a fundamental method of pavement design. For convenience in the design and analysis of pavement structures, these factors should be presented in graphic form. The analytical expression of the deflection factor was modified, and the determining parameters were transformed to permit an easier and more direct process of deflection analysis. Two-layer factors were also computed as a particular case of three-layer systems. This paper presents a series of deflection factor charts for two- and three-layer systems, for a wide range of parameter values, based on Jones' tables. Several examples were computed to show the practical application of the charts.

•THE deflection beneath the center of a uniform load, p, applied on a circular, flexible bearing area of radius r (Fig. 1) resting on the surface of a uniform elastic medium of semi-infinite depth, of elastic modulus E and Poisson's ratio μ, after Boussinesq is

$$W = \frac{2(1 - u^2)\,p\,r}{E}$$

$$\text{for } \mu = 0.5 \quad W = \frac{1.5\,p\,r}{E}$$

$$\text{for } \mu = 0.35 \quad W = \frac{1.75\,p\,r}{E}$$

The reduction of Poisson's ratio from 0.5 to 0.35 increases the deflection of the uniform medium by 17 percent.

If the load is applied by a rigid plate instead of a flexible bearing area, the deflection of the uniform medium computed by the foregoing formulas should be multiplied by the factor $\pi/4$ or 0.785. For instance

$$\text{For } \mu = 0.5 \quad W_r = \frac{1.18\,p\,r}{E}$$

Let us now compute the deflection of the uniform medium below a certain depth, considering the layer above this depth as incompressible. The deflection at any depth is equal to the term $\frac{p\,r}{E}$ multiplied by a deflection factor F. Figure 1 shows the values of the deflection factor at various depths for flexible and rigid bearing areas. The two curves show that the influence of the type of bearing area depends on the depth at which the deflection is computed. At the surface, the deflection factor is 1.5 for a flexible
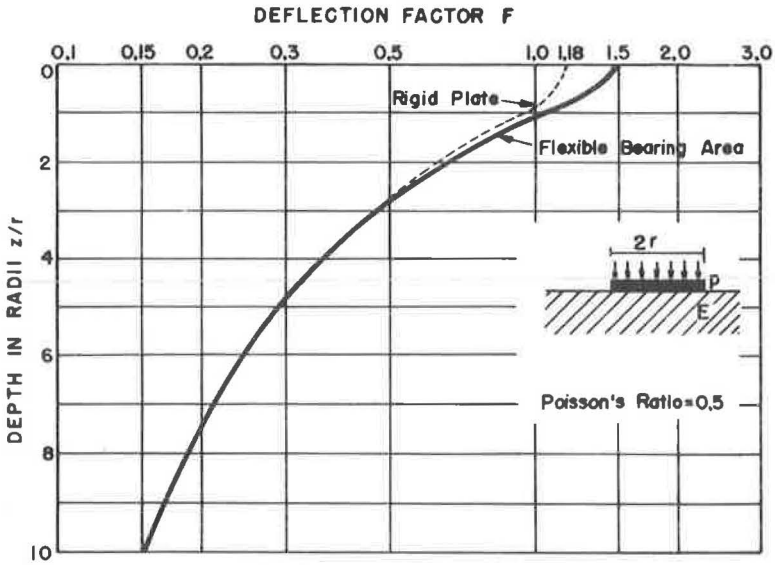
Figure 1. Deflection factor of uniform medium.
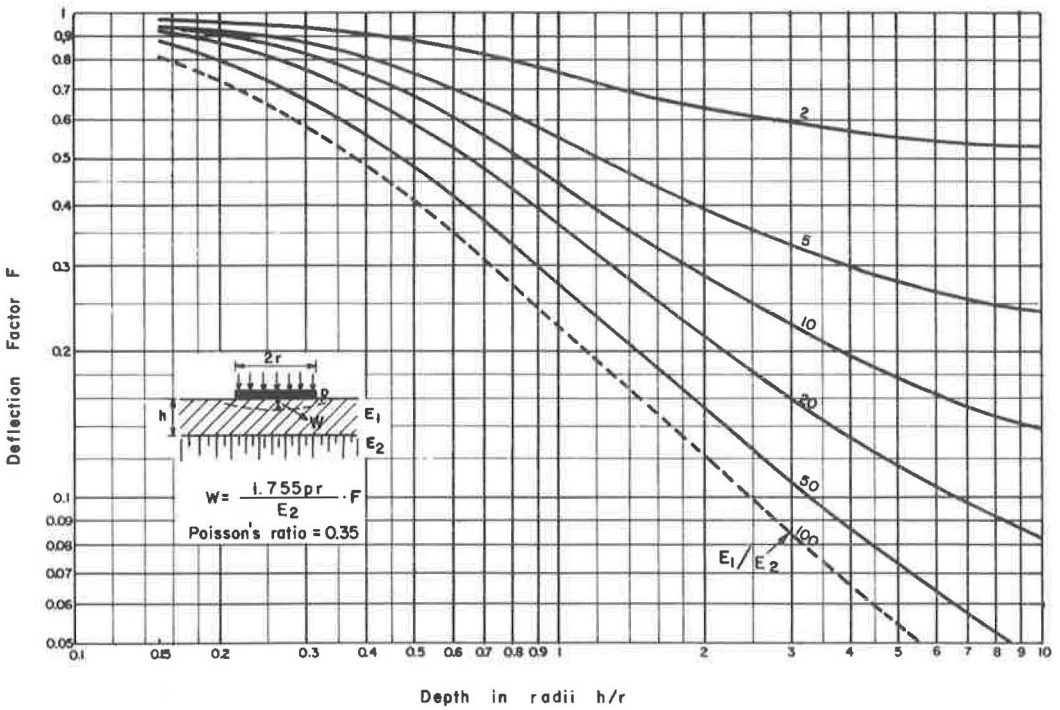
Figure 2. Deflection factor chart for two-layered elastic systems.

bearing area and 1.18 for a rigid plate (for $\mu = 0.5$). At depths greater than three times the radius the two factors are practically equal.

The deflection of a two-layer elastic system can be expressed in a form similar to the deflection of the uniform medium, but affected by an appropriate deflection factor. Assume a two-layer system such as that in Figure 2, in which the first layer is of thickness h, elastic modulus E_1, and Poisson's ratio μ, and the second layer is of semi-infinite depth, elastic modulus E_2 and the same Poisson's ratio μ, with perfect continuity between the two layers. The deflection, after Burmister (1), is

$$W = \frac{1.5\,p\,r}{E_2} \cdot F_W \qquad (\mu = 0.5)$$

The deflection factor F_W, for $\mu =$ constant, depends on the parameters E_1/E_2 and h/r. The Burmister graph (1) gives the values of the factor F_W for several values of the parameters, but allows little accuracy in the readings of F_W, especially in the region of $h/r < 1$. Moreover, the range it covers is too small for the parameter h/r (up to 6) and too large for the parameter E_1/E_2 (up to 10,000).

Jones (2) published a series of tables of deflection factor values for three-layer elastic systems loaded with a uniform circular load, in connection with the development of a fundamental method of pavement design. The Jones' deflection factors were computed for a value of Poisson's ratio of 0.35 in each layer. Two-layer systems are a particular case of three-layer systems, in which one modular ratio is equal to one. Hence, two-layer factors were computed from Jones' tables by a proper selection of parameters. For convenience and uniformity of presentation, the two-layer factors were transformed to comply with the equation

$$W = \frac{1.75\,p\,r}{E_2} \cdot F \qquad (\mu = 0.35)$$

The deflection factor F depends on the same parameters E_1/E_2 and h/r, for $\mu =$ constant. The numerical value of factor F is different from factor F_W, for the same values of the parameters, but the deflections computed by the two last equations are very close. The reduction of Poisson's ratio from 0.5 to 0.35 increases the deflection of layered systems by less than 10 percent, for the practical range of the parameters. The average increase is about 7 percent. The actual value of Poisson's ratio of pavement structures is not known, but it is likely to be between 0.35 and 0.5. This difference can be ignored in practical applications.

The second equation may be put under another form, more adequate for the determination of the moduli by load bearing tests:

$$E_2 = 1.75\,r\,\frac{p}{W}\,F$$

But $p/W = k$ is the unit load per unit deflection or "modulus of reaction." Hence

$$\therefore \ E_2 = 1.75\,r\,k\,F \qquad (\mu = 0.35)$$

The deflection factor F varies from 0 to 1. It is inversely proportional to the load spreading ability or reinforcing effect of the pavement over the bare subgrade.

Table 1 and the graph of Figure 2 give the values of the deflection factor F for several practical values of the parameters. Parameter h/r varies logarithmically from 0.15 to 10, and parameter E_1/E_2 varies from 2 to 100. The curves for modular ratios from 2 to 50 were computed from Jones' tables. The curve for $E_1/E_2 = 100$, not computed by Jones, was drawn by logarithmical extrapolation and is accurate enough for practical applications. The graph should not be further extrapolated. All interpolations for intermediary values of E_1/E_2 should be computed logarithmically.

Jones' original deflection factors (2) for three-layer systems conform with the equation

TABLE 1

DEFLECTION FACTOR VALUES FOR TWO-LAYERED
ELASTIC SYSTEMS
(Poisson's ratio = 0. 35)

$E_1/E_2 \rightarrow$ h/r	1	2	5	10	20	50
0.156	1.000	.966	.939	.925	.908	.869
0.312	1.000	.930	.867	.818	.756	.654
0.625	1.000	.839	.693	.600	.512	.405
1.25	1.000	.711	.494	.388	.307	.227
2.5	1.000	.614	.356	.250	.183	.126
5	1.000	.558	.279	.176	.117	.0732
10	1.000	.529	.240	.138	.0836	0.466

$$W = \frac{1.755\,p\,r}{E_3} \cdot F$$
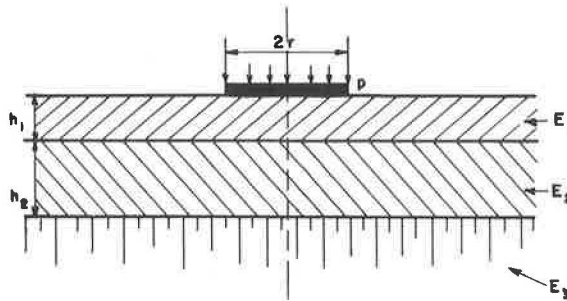
Poisson's ratio = 0.35

$$\frac{E_1}{E_2} = n_1 \qquad \frac{E_2}{E_3} = n_2 \qquad n_1 \cdot n_2 = N$$

$$F = f\ (h_1/r,\ h_2/r,\ n_1,\ n_2)$$

W = deflection beneath the center of circular uniform load
r = radius   p = unit load
h_1, h_2 = thicknesses of layers
E_1, E_2, E_3 = elastic modulii of layers
F = deflection factor

Figure 3. Deflection parameters of three-layered elastic systems.

$$W = \frac{p\,r}{E_1} \cdot \overline{F}$$

$$\overline{F} = \int_0^\infty \frac{1 + \sum_{i=1}^\infty p_i(x)\,\exp q_i(x)}{1 + \sum_{i=1}^\infty r_i(x)\,\exp q_i(x)} \cdot \frac{J_1(Ax)}{x}\,dx$$

The functions $p_i(x)$, $q_i(x)$ and $r_i(x)$ are polynomials with coefficients depending on the non-dimensional parameters, J_1 is a Bessel function, $A = r/h_2$ and the other parameters are shown in Figure 3. The factor $\overline{F}$ as such has no immediate physical meaning. Jones computed and tabulated the factor $\overline{F}$ in function of the parameters

$$E_1/E_2 = k_1,\ E_2/E_3 = k_2,\ h_1/h_2 = H,\ r/h_2 = A$$

For convenience and ease of application, Jones' three-layer factors were also transformed to comply with the following equation, similar to the two-layer equation

$$W = \frac{1.75\,p\,r}{E_3} \cdot F \qquad (\mu = 0.35)$$

The three-layer deflection factor F, for $\mu = $ constant, depends on the parameters defined in Figure 2

$$E_1/E_2 = n_1,\ E_2/E_3 = n_2,\ h_1/r,\ h_2/r$$

The tables and graphs in Figures 4 to 18 give the values of the three-layer deflection factor F for all combinations of the following parameter values

$$n_1 = 2, 5, 10, 20, 50$$
$$n_2 = 2, 5, 10$$
$$h_1/r = 0.15 \text{ to } 5$$
$$h_2/r = 0.3 \text{ to } 5$$

Combining the graphs in Figures 4 to 18 with the graph of Figure 2 it is possible to interpolate for values of n_1 or n_2 between 1 and 2.

Jeuffroy and Bachelez (3) proposed an approximate method of three-layer system deflection calculation. The deflections computed by the Jeuffroy-Bachelez method are close to the values computed by the Jones method.

All deflection factors given for two- and three-layer systems were computed for the case of a flexible bearing area. For the case of a rigid plate, the computed deflections should be multiplied by a "bearing factor." The exact value of this factor cannot be determined at this time. It can be safely stated that for the layered systems of interest in pavement design the bearing factor must be between $\pi/4$ and 1, probably closer to 1. From analogy with the uniform medium (Fig. 1), it is evident that the surface layers have a greater influence on the difference between deflections of rigid and flexible bearing areas. If the surface layers are relatively stiff, this difference should be small. Taking into account the overall inaccuracies of modeling the pavement by an elastic layered system, it is suggested that the same deflection factors should be tentatively used in deflection analysis of pavement systems loaded with rigid plates.

An approximate formula is now proposed to calculate an "equivalent modulus" $E_{1,2}$ that can be substituted for moduli E_1 and E_2, for the same deflection. The three-layer system is thus reduced to an equivalent two-layer system, composed of one layer of
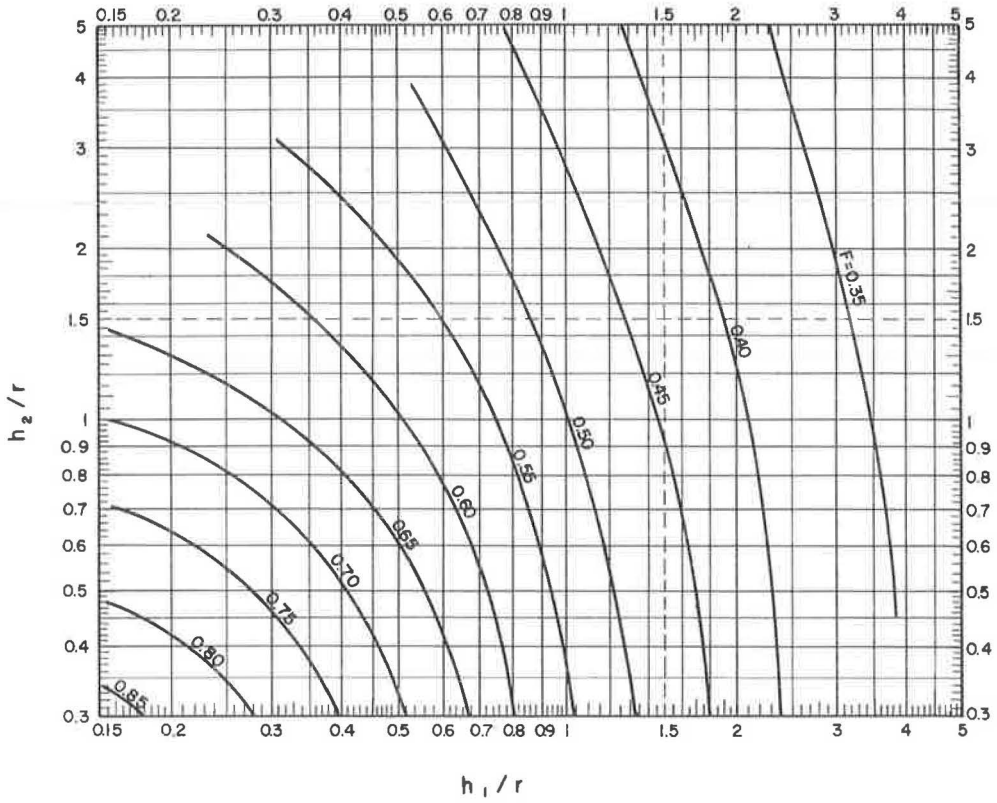
Figure 4.

h₂/r \ h₁/r	0,156	0,312	0,625	1,25	2,5	5
0,312	.858	.789	.662	.510	.394	———
0,625	.772	.717	.616	.489	.387	.323
1,25	.669	.633	.560	.460	.375	.319
2,5	———	.564	.508	.428	.360	.314
5	———	———	.470	.400	.343	.306

Figure 5.

Figure 6.

Figure 7.

h_1/r h_2/r	0,156	0,312	0,625	1,25	2,5	5
0,312	.830	.733	.556	.372	.246	—
0,625	.745	.669	.522	.359	.242	.174
1,25	.648	.593	.476	.339	.235	.172
2,5	—	.528	.430	.313	.224	.168
5	—	—	.394	.289	.211	.163

Figure 8.

$n_1 = 5$
$n_2 = 5$
$N = 25$
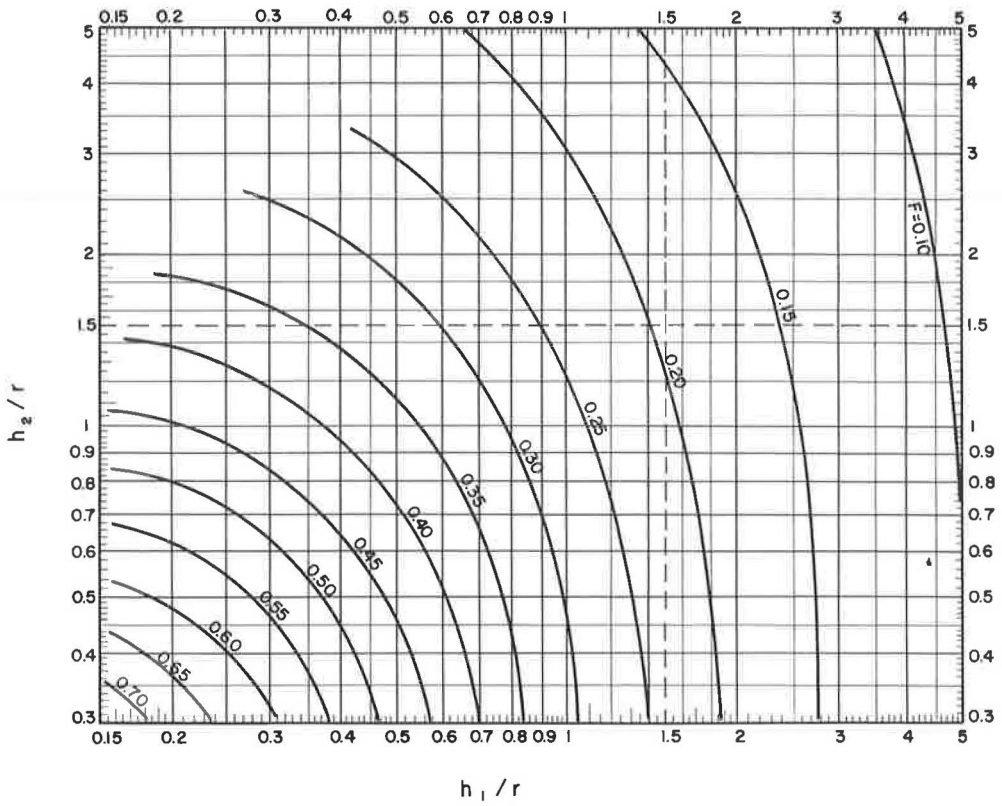
h_1/r h_2/r	0,156	0,312	0,625	1,25	2,5	5
0,312	,713	,598	,427	,268	,162	—
0,625	,572	,497	,378	,250	,157	,101
1,25	,429	,387	,312	,223	,148	,0989
2,5	—	,299	,249	,188	,134	,0944
5	—	—	,202	,155	,116	,0871

$n_1 = 5$
$n_2 = 10$
$N = 50$
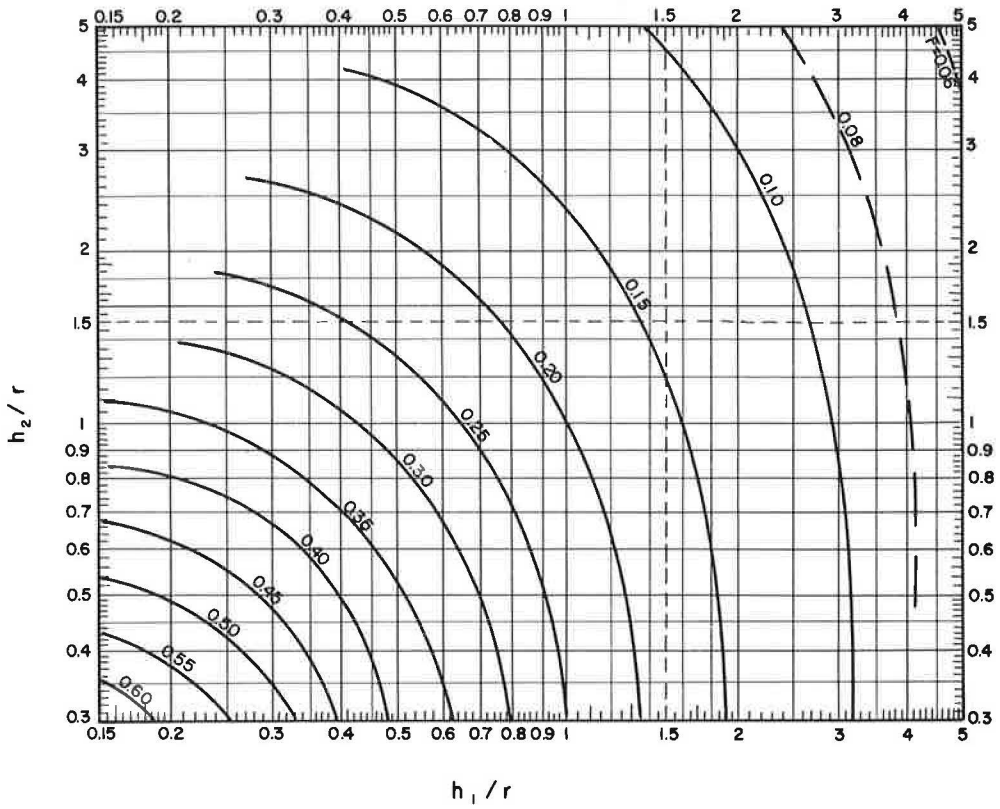
h_1/r h_2/r	0,156	0,312	0,625	1,25	2,5	5
0,312	.626	.508	.350	.211	.122	—
0,625	.469	.401	.301	.195	.118	.0712
1,25	.325	.291	.236	.168	.109	.0691
2,5	—	.206	.174	.134	.0954	.0649
5	—	—	.130	.102	.0779	.0579

Figure 9.

Figure 10.

The chart contains the following labels:

$n_1 = 10$
$n_2 = 2$
$N = 20$

Axis labels: h_2/r (vertical), h_1/r (horizontal)

Contour labels: F=0.15, 0.20, 0.25, 0.30, 0.35, 0.40, 0.45, 0.50, 0.55, 0.60, 0.65, 0.70, 0.75, 0.80
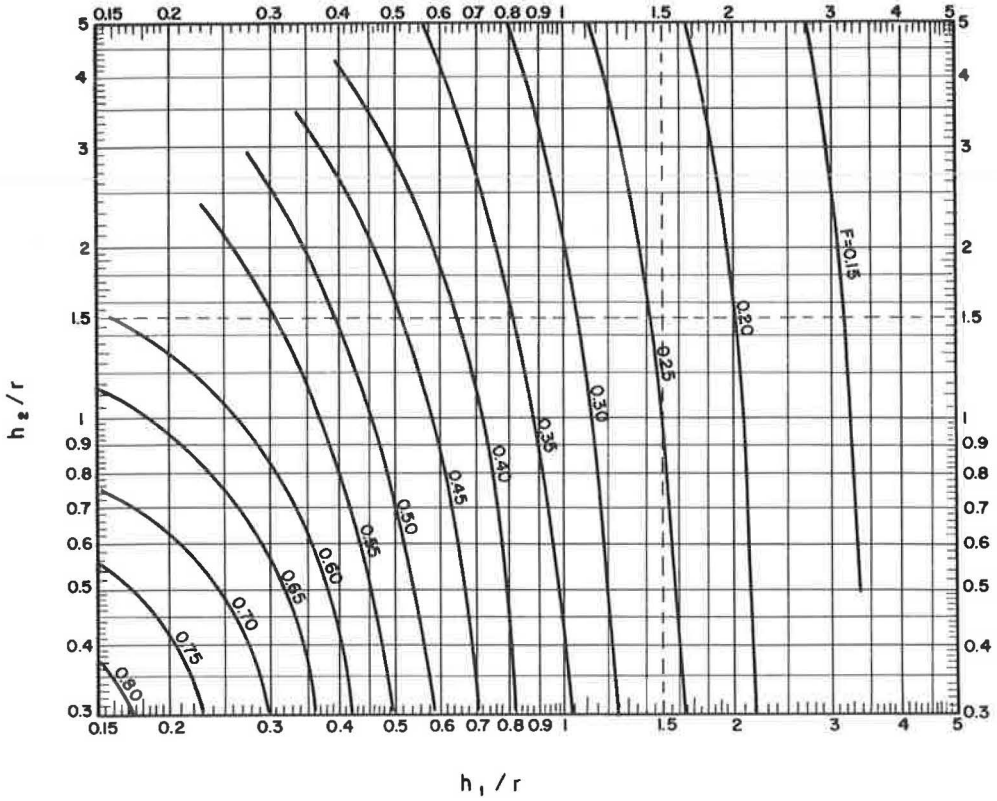
h_1/r ⟍ h_2/r	0,156	0,312	0,625	1,25	2,5	5
0,312	.811	.687	.483	.298	.181	—
0,625	.729	.630	.457	.290	.178	.116
1,25	.634	.561	.420	.275	.174	.115
2,5	—	.499	.379	.255	.166	.112
5	—	—	.346	.234	.156	.109

Figure 11.
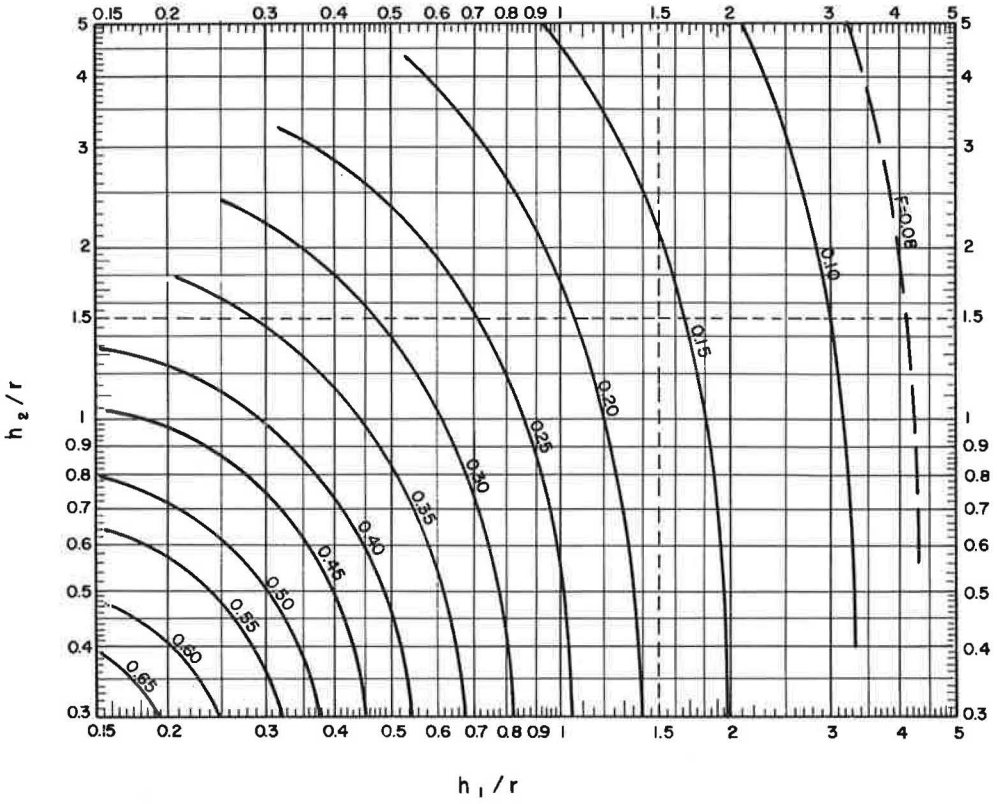
h₂/r \ h₁/r	0,156	0,312	0,625	1,25	2,5	5
0,312	.689	.553	.369	.217	.123	—
0,625	.553	.467	.334	.207	.121	.0720
1,25	.416	.367	.281	.187	.115	.0706
2,5	—	.284	.225	.160	.105	.0679
5	—	—	.181	.130	.0912	.0629

n₁ = 10
n₂ = 10
N=100
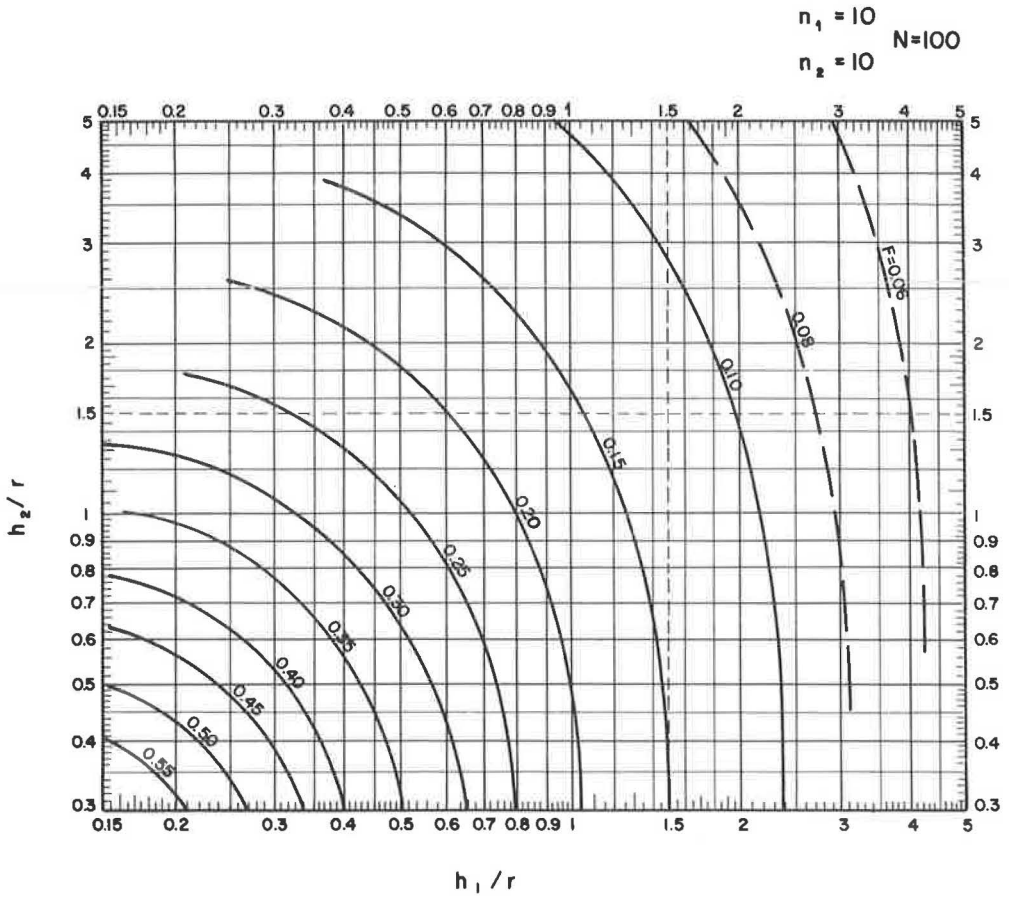
Figure 12.

h₁/r ＼ h₂/r	0,156	0,312	0,625	1,25	2,5	5
0,312	.601	.467	.302	.172	.0946	—
0,625	.450	.376	.267	.163	.0924	.0525
1,25	.312	.275	.214	.144	.0876	.0514
2,5	—	.195	.159	.117	.0782	.0489
5	—	—	.117	.0885	.0642	.0442
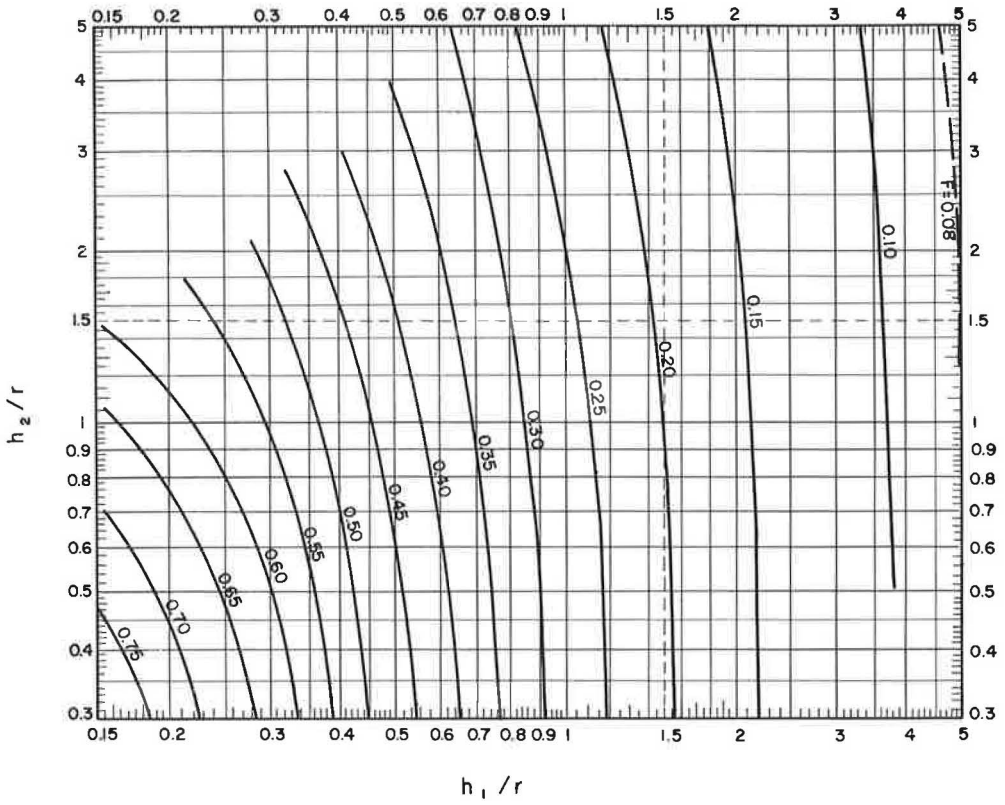
$n_1 = 20$
$n_2 = 2$
$N = 40$

h_1/r ╲ h_2/r	0,156	0,312	0,625	1,25	2,5	5
0,312	.789	.629	.411	.239	.136	—
0,625	.711	.583	.394	.234	.135	.0809
1,25	.621	.523	.365	.224	.132	.0802
2,5	—	.465	.331	.209	.127	.0788
5	—	—	.300	.191	.120	.0764

Figure 13.

$n_1 = 20$
$N = 100$
$n_2 = 5$
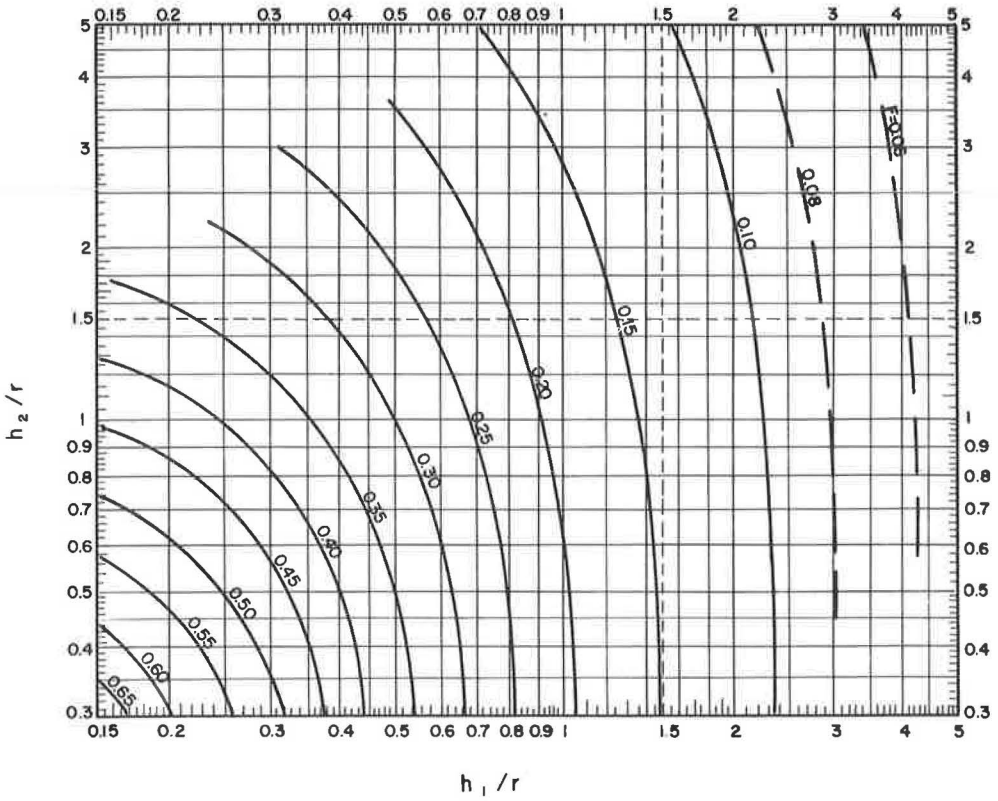
h_2/r \ h_1/r	0,156	0,312	0,625	1,25	2,5	5
0,312	.662	.501	.313	.175	.0953	——
0,625	.535	.433	.290	.169	.0939	.0528
1,25	.404	.345	.250	.157	.0909	.0521
2,5	——	.267	.202	.136	.0846	.0506
5	——	——	.161	.112	.0742	.0475

Figure 14.

$n_1 = 20$
$n_2 = 10$
$N = 200$

h_2/r

h_1/r
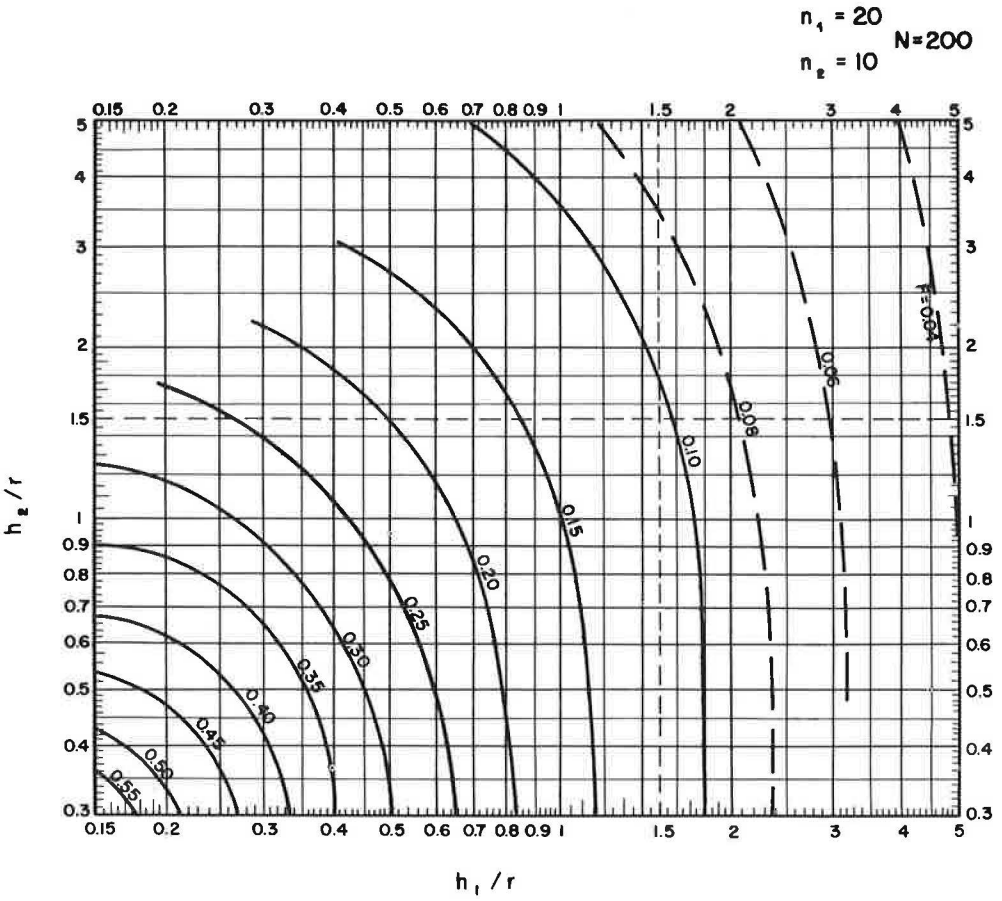
Figure 15.

h_1/r h_2/r	0,156	0,312	0,625	1,25	2,5	5
0,312	.573	.419	.254	.139	.0740	—
0,625	.434	.349	.232	.134	.0729	.0396
1,25	.301	.260	.193	.123	.0703	.0390
2,5	—	.184	.145	.102	.0645	.0377
5	—	—	.106	.0779	.0542	.0348

Figure 16.
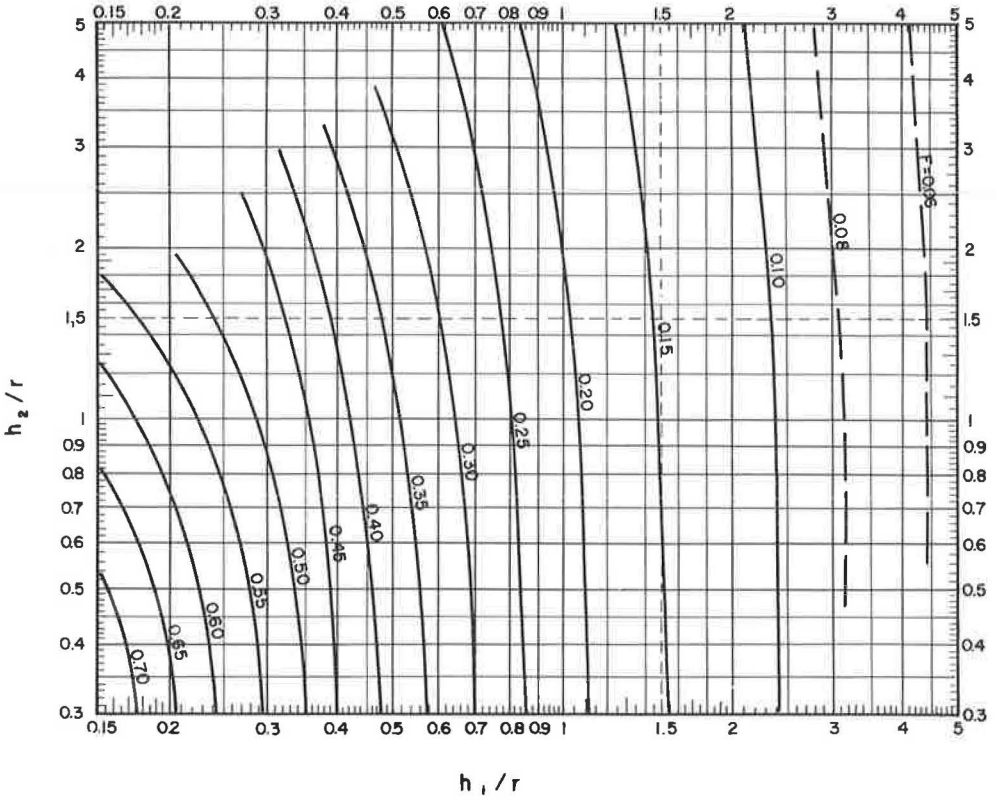
h_2/r \ h_1/r	0,156	0,312	0,625	1,25	2,5	5
0,312	.744	.538	.324	.178	.0960	——
0,625	.677	.508	.314	.175	.0953	.0532
1,25	.594	.461	.297	.170	.0940	.0528
2,5	——	.411	.271	.161	.0915	.0522
5	——	——	.245	.148	.0868	.0509

Figure 17.

$n_1 = 50$

$N = 500$

$n_2 = 10$
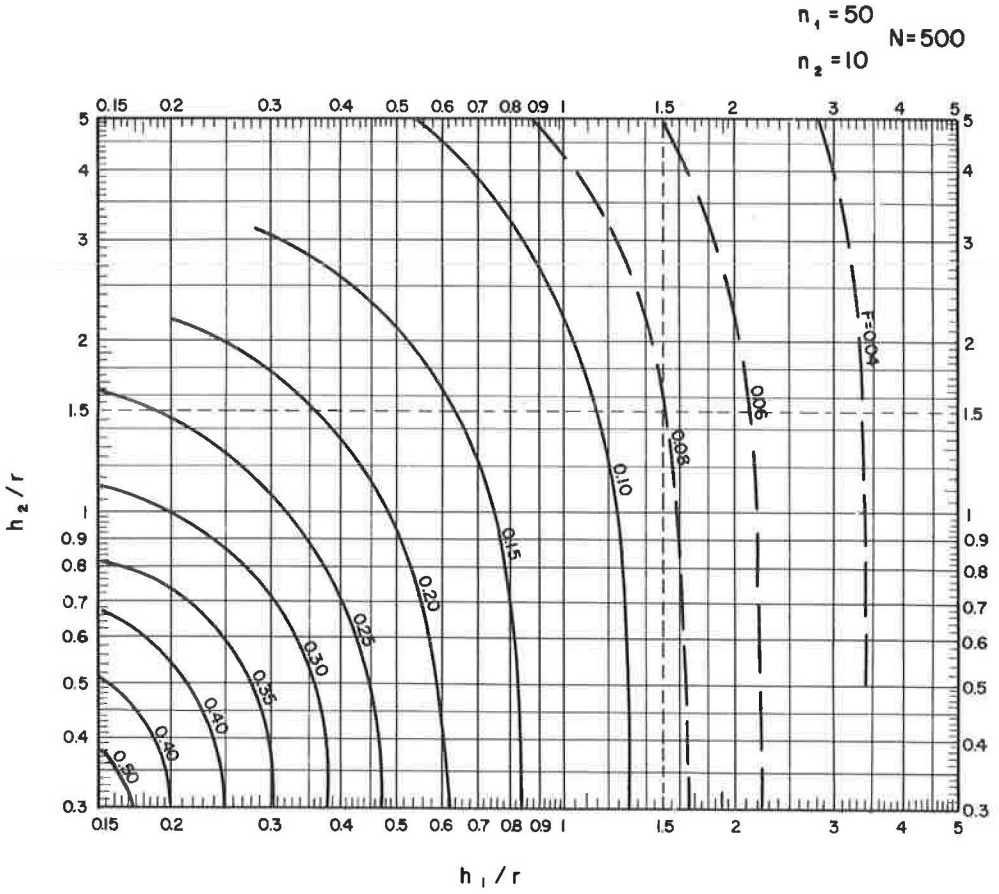
h_1/r h_2/r	0,156	0,312	0,625	1,25	2,5	5
0,312	.524	.348	.197	.104	.0539	—
0,625	.410	.305	.187	.102	.0534	.0280
1,25	.288	.237	.164	.0966	.0523	.0277
2,5	—	.169	.128	.0847	.0496	.0272
5	—	—	.0926	.0664	.0436	,0258

Figure 18.

modulus $E_{1,2}$ and thickness $h_1 + h_2$ supported by the same subgrade of modulus E_3. The approximate formula is

$$E_{1,2} = \left[\frac{h_1 \sqrt[3]{E_1} + h_2 \sqrt[3]{E_2}}{h_1 + h_2} \right]^3$$

The term $h_i \sqrt[3]{E_i}$ is called the layer rigidity factor. The approximate formula is exact within 10 percent of the computed deflection for h_2/r not greater than 1, and within 15 percent for h_2/r not greater than 2. This formula is not indicated for h_2/r greater than 2. Making n' the modular ratio of the equivalent two-layer system and $h_1/h_2 = H$, it follows

$$n' = \frac{E_{1,2}}{E_3} = n_2 \left[\frac{H \sqrt[3]{n_1} + 1}{H + 1} \right]^3$$

The deflection of the equivalent two-layer system may be calculated by the graph in Figure 2 with the parameters n' and $(h_1 + h_2)/r$.

An analogous expression has been proposed by Palmer and Barber (4) to reduce the two-layer system to an equivalent uniform medium. Barber demonstrated that his approximate formula yielded deflections very close to Burmister's two-layer analysis (1). The validity of the rigidity factor concept both for two-layer and three-layer systems lends support to its tentative extension to multilayer systems. It is suggested that intermediate layers may be modified if the rigidity factor is kept constant. It is also suggested that multilayer systems can be reduced to equivalent three-layer systems for the purpose of deflection calculation, aggregating similar adjacent layers and computing their equivalent modulus by the foregoing formula. The subgrade should not be altered, in any case, and neither should it be included in the equivalent modulus calculation, due to its infinite depth. Further research is needed on these points.

The modular ratio E_1/E_2 for two-layer flexible pavement structures is always below 100, being closer to 100 for semiflexible soil-cement pavements (5, 6, 7, 8). The modular ratio for rigid pavements is always well above 100. Therefore, the graph in Figure 1, including values of E_1/E_2 from 2 to 100 is adequate for the structural analysis of flexible and semiflexible two-layer pavements. Rigid pavement design is based on a stress criterion and not on deflection limits. Accordingly, surface deflection computation is of little use for rigid pavement analysis, and it is not necessary to include in the graph the higher values of the modular ratio.

In the case of three-layer pavement structures, there is normally a marked difference between modular ratios n_1 and n_2. For technical and economical reasons n_1 and n_2 are always greater than one, and n_1 is usually greater than n_2. The effective modular ratio for granular non-cemented materials is always between 2 and 5 (9, 10, 11). Hence, the value of n_2 is usually between 2 and 5. The value of n_1 for flexible and semiflexible pavements is usually between 5 and 50. The three-layer deflection charts in Figures 4 to 18 provide an adequate range of modular ratios for the design and structural analysis of flexible and semiflexible pavements.

The elastic moduli to be used in the structural analysis should be measured by load bearing tests or other field tests conducted on the full pavement section. Laboratory tests on small samples or molded specimens do not correlate well with field values. Great care should be exercised in the determination of the layers moduli, for the moduli values have a critical effect on the deflections.

It is not correct to measure the subgrade modulus by load bearing tests on the subgrade alone, and then to measure the pavement layers' moduli by new tests on each superimposed layer, using in the calculations the subgrade modulus previously determined. This process gives too high and erratic values for the pavement moduli, as reported elsewhere (12). The effective in-place subgrade modulus is much higher than the modulus of the subgrade alone. The main reasons are (a) an increase in compaction of the lower layers caused by the compaction of the top layers; (b) the confining effect of the top layer; (c) the nonlinearity of the soil stress-strain curve; (d) the load

spreading ability of the pavement, allowing lower stresses on the subgrade; (e) possibly, lack of agreement between the theoretical elastic model and actual pavement response. All these factors contribute in varying degrees to an increase of the effective subgrade modulus. The saturation of the subgrade by capillarity after the construction of the pavement acts in the opposite direction, but this effect is smaller than the sum of the others. Consequently, the modulus of the subgrade alone is of no avail for the calculation of the pavement moduli. All moduli should be measured simultaneously by tests conducted at the surface of the complete pavement. This determination is possible with load bearing tests with several plate diameters or several pavement thicknesses. Theoretically, the solution of a two-layer system requires at least two plate diameters (or two thicknesses) and the solution of a three-layer system requires at least three diameters (or thicknesses). The calculation of the moduli requires the solution of a system of simultaneous equations. For greater precision, the deflection factor values should be interpolated in the tables below each graph, instead of reading the values on the graphs. The problem is further complicated by the scatter of test results. A study of three-layer system moduli determination has been published (12).

A few examples of application are included to illustrate the use of the deflection factor charts.

PRACTICAL EXAMPLES

1. Suppose a pavement is composed of penetration macadam base course and light surface treatment, with total thickness of 15 cm (6 in.), resting directly on the subgrade. Assume the following values for the elastic moduli: subgrade soil 500 kg/cm^2 (7,140 psi); base and surfacing considered as a single layer 30,000 kg/cm^2 (429,000 psi). The basic wheel load is 5 long tons (11,200 lb), with contact pressure of 7 kg/cm^2 (100 psi) and contact radius of 15.1 cm (6 in.). Calculate the elastic deflection.

$$h/r = 15/15.1 \cong 1$$
$$E_1/E_2 = 30,000/500 = 60$$
$$W = ?$$

The graph in Figure 2 gives the value of F by interpolation between the curves of E_1/E_2 = 50 and 100, for h/r = 1. For better accuracy, several values of F should be taken from the graph, at the intersections of the curves of E_1/E_2 with the vertical line of h/r = 1. An auxiliary graph should be made on log-log paper, plotting values of F vs respective values of E_1/E_2, and connecting the plotted points by a continous curve. This auxiliary graph gives the value of F for E_1/E_2 = 60

$$F = 0.26$$

$$\therefore W = \frac{1.75 \times 7 \times 15.1}{500} \times 0.26 \cong 0.1 \text{ cm} \qquad (0.04 \text{ in.})$$

2. Design the thickness of the same pavement of Example 1 for the condition of the deflection being less than 0.05 cm (0.02 in.).

$$E_1/E_2 = 60$$
$$W = 0.05 \text{ cm}$$
$$h/r = ?$$

The required deflection factor is

$$F = \frac{0.05 \times 500}{1.75 \times 7 \times 15.1} = 0.13$$

Inasmuch as the deflection factor is proportional to the deflection, this value of F could be obtained taking half of the previous value. Now it is necessary to draw the complete curve of E_1/E_2 = 60 on the graph in Figure 2 interpolating between the curves of 50 and

100. The points near the probable solution, i.e., between h/r = 2 and 3, should be plotted by logarithmical interpolation, as in the previous example. The point at the intersection of the curve of $E_1/E_2 = 60$ with the horizontal line of F = 0.13 gives the solution

$$h/r = 2.3$$

$$\therefore\ h = 2.3 \times 15.1 = 35\ cm \qquad (13.8\ in.)$$

It was necessary to increase the thickness to more than double the previous value to reduce the deflection in half.

3. Compute the elastic moduli of the same pavement, with 35 cm (13.8 in.) of thickness, from the following results of load bearing tests

Diameter		Modulus of Reaction	
cm	in.	kg/cm^3	pci
80	31.5	24.6	888
20	7.9	317.5	11,462

The equation is

$$E_2 = 1.75\ r\ k\ F$$

For ϕ 80 h/r = 35/40 = 0.875
$$k = 24.6\ kg/cm^3$$
$$F' = ?$$
$$E_2 = 1.75 \times 40 \times 24.6 \times F' = 1722\ F'$$

For ϕ 20 h/r = 35/10 = 3.5
$$F'' = ?$$
$$k = 317.5\ kg/cm^3$$
$$E_2 = 1.75 \times 10 \times 317.5 \times F'' = 5556\ F''$$

Comparing the two values of E_2

$$1722\ F' = 5556\ F''$$
$$\therefore\ F'/F'' = 3.22$$

Take from the graph in Figure 2 several values of F, at the intersections of the curves of E_1/E_2 with the vertical lines of h/r = 0.875 and h/r = 3.5, and calculate their respective ratios

E_1/E_2	F' (h/r = 0.875)	F'' (h/r = 3.5)	F'/F''
2	0.78	0.58	1.34
5	0.59	0.31	1.90
10	0.49	0.21	2.33
20	0.40	0.14	2.86
40	0.328	0.106	3.10
50	0.305	0.096	3.18
60	0.290	0.090	3.22
70	0.278	0.085	3.27
100	0.250	0.075	3.33

The points near the probable solution (E_1/E_2 more than 40) should be computed by logarithmical interpolation, as in the first example.

The computed value of F'/F'' equals the required value of 3.22 at the point $E_1/E_2 = 60$ or $F' = 0.290$. The moduli sought are

$$E_2 = 1722 \times 0.290 = \quad 500 \text{ kg/cm}^2 \quad (7,140 \text{ psi})$$
$$E_1 = \quad 60 \times \quad 500 = 30,000 \text{ kg/cm}^2 \ (429,000 \text{ psi})$$

4. Calculate the deflection of the following three-layer pavement. The wheel load is 5 long tons (11,200 lb), the contact pressure is 7 kg/cm^2 (100 psi) and the contact radius is 15.1 cm (6 in.).

Layer	Thickness		Modulus	
	cm	in.	kg/cm^2	psi
1. Asphaltic-concrete surface course	15	6	50,000	714,300
2. Stabilized base course	20	7.9	2,500	35,700
3. Subgrade	—	—	500	7,140

$$n_1 = 50,000/2,500 = 20 \qquad h_1/r = 15/15.1 \cong 1$$
$$n_2 = 2,500/500 = 5 \qquad h_2/r = 20/15.1 = 1.32$$
$$E_3 = 500 \text{ kg/cm}^2$$

From the graph in Figure 14 : $\quad$ F = 0.185

$$\therefore \ W = \frac{1.75 \times 7 \times 15.1}{500} \times 0.185 = 0.07 \text{ cm} \qquad (0.027 \text{ in.})$$

5. Modify the thickness of the pavement of Example 4 so that the deflection is less than 0.05 cm (0.02 in.). The required deflection factor is

$$F = \frac{0.05 \times 500}{1.75 \times 7 \times 15.1} = 0.13$$

A new curve for F = 0.13 should be interpolated between the curves of 0.10 and 0.15 in the graph of Figure 14. All points on this curve correspond to thicknesses h_1 and h_2 satisfying the required condition of W = 0.05 cm. Possible combinations are as follows.

h_1/r	h_2/r
1	4.7
1.25	3
1.5	1.7
1.6	1.32

The best combination of h_1 and h_2 should be selected by considering economic and engineering aspects, taking into account the unit costs of surface and base courses. In most cases, it is cheaper to increase the base thickness. Suppose the first combination is selected

$$h_1/r = 1 \qquad h_1 = 1 \times 15.1 \cong 15 \text{ cm}$$
$$h_2/r = 4.7 \qquad h_2 = 4.7 \times 15.1 \cong 71 \text{ cm}$$

Total thickness: $\quad$ 15 + 71 = 86 cm $\quad$ (33.9 in.)
If the fourth combination were preferred

$$h_1/r = 1.6 \qquad h_1 = 1.6 \times 15.1 = 24 \text{ cm}$$
$$h_2/r = 1.32 \qquad h_2 = 1.32 \times 15.1 = 20 \text{ cm}$$

Total thickness: $24 + 20 = 44$ cm   (17.3 in.)

Increasing the surface course from 15 to 24 cm permits reducing the total thickness from 86 to 44 cm. In this particular case, 1 cm of surface course is equivalent to 5.7 cm of base course.

The deflection of the latter combination may be checked by the approximate formula, since h_2/r is less than 2.

$$H = 1.6/1.32 = 1.22$$

$$n' = 5\left[\frac{1.22\sqrt[3]{20} + 1}{1.22 + 1}\right]^3 = 36.2$$

$$n'/r = \frac{24 + 20}{15.1} = 2.91$$

Entering the graph of Figure 2 with parameters n' and h'/r F = 0.128

$$\therefore \quad W = \frac{1.75 \times 7 \times 15.1}{500} \times 0.128 = 0.047 \text{ cm}$$

The result is close enough to the specified deflection of 0.05 cm.

6. If the given modular ratios are intermediate between the values of the graphs in Figures 4 to 18, it is necessary to construct an auxiliary graph of similar aspect, by a series of logarithmical interpolations between the given graphs. Consider for instance the following case.

$$n_1 = 15 \qquad h_1/r = 1$$
$$n_2 = 4 \qquad h_2/r = 1.5$$

The deflection factor is bracketed by the following values

$n_1 \times n_2$	F
20×5	0.175
20×2	0.265
10×5	0.210
10×2	0.315

The deflection factor, obtained by three interpolations on log-log paper, is

$$F = 0.208$$

If an analysis of several thicknesses is required, it is necessary to trace the auxiliary graph corresponding to $n_1 = 15$, $n_2 = 4$ for the whole range of thicknesses.

REFERENCES

1. Burmister, D. The Theory of Stresses and Displacements in Layer Systems and Applications to the Design of Airport Runways. HRB Proc., Vol. 23, pp. 126-149, 1943.
2. Jones, A. The Calculation of Surface Deflection for Three-Layer Elastic Systems. Proc. Symp. on Road Tests for Pavement Design, Lisbon, 1962.
3. Jeuffroy, G., and Bachelez, J. Note on a Method of Analysis for Pavements. Proc. Ann Arbor Conf., 1962.
4. Palmer, L. A., and Barber, E. S. Soil Displacement Under a Circular Loaded Area. HRB Proc., Vol. 20, pp. 279-286, 1940.

5. Harris, F. A.   Selection and Design of Semi-Flexible and Conventional Type Pavements.   HRB Proc., Vol. 35, pp. 110-138, 1956.
6. Baker, R. F., and Papazian, H. S.   The Effect of Stiffness Ratio on Pavement Stress Analysis.   HRB Proc., Vol. 39, pp. 61-85, 1960.
7. Sowers, G. F., and Vesić, A. B.   Vertical Stresses in Subgrades Beneath Statically Loaded Flexible Pavements.   HRB Bull. 342, pp. 90-123, 1962.
8. Vesić, A. B.   Disc., Proc. Ann Arbor Conf., 1962.
9. Peattie, K. R.   The Significance of the Surface Deflection of Flexible Pavements. Proc. Symp. on Road Tests for Pavement Design, Lisbon, 1962.
10. Dormon G. M.   The Extension to Practice of a Fundamental Procedure for the Design of Flexible Pavements.   Proc. Ann Arbor Conf., 1962.
11. Heukelom, W., and Klomp, A. J. G., Dynamic Testing as a Means of Controlling Pavements During and After Construction.   Proc. Ann Arbor Conf., 1962.
12. de Barros, S. Thenn.   Application of Three-Layer System Methods to the Evaluation of Soil-Cement Bases.   Highway Research Record 145, 1966.

Numerical Determination of Stresses in Earth Masses

B. B. SCHIMMING and H. J. HAAS
Respectively, Acting Head and NSF Trainee, Department of Civil Engineering, University of Notre Dame, Notre Dame, Indiana

General numerical techniques are developed for the purpose of analyzing stress distributions in commonly encountered foundation conditions. These conditions include the effect of rigid boundaries, mixed boundary conditions, nonhomogeneous materials, and time-dependent material characteristics. The numerical development is oriented toward computer utilization. Typical results for the various problem categories are included.

●THE IMPACT of the computer revolution on contemporary society is self-evident to most observers. In the area of research, new disciplines have emerged in the computer environment which already offer great promise. The more traditional disciplines have been able to develop refined techniques of solution for classical problems. The latter topic is pursued in this presentation.

The calculation of stresses in earth masses is beset with numerous difficulties. It would do well to elucidate these difficulties to appraise the potential contribution of numerical methods in conjunction with the computer.

Of fundamental importance to any stress analysis problem is the description of the mechanical behavior of the material involved, together with a complete description of the shape of, and conditions at, the boundaries, and any spatial or time variations in material characteristics which may occur in the regions under consideration.

With respect to an adequate description of the mechanical behavior of soil, the computer has little to offer except in a supplementary role. Only patient work in the soil mechanics laboratory will eventually unwind the mysterious nonlinearities of soil. Until this is accomplished, the traditional assumptions concerning elastic, viscoelastic or plastic behavior will have to be judiciously utilized.

The incorporation of environmental realities into the stress analysis of a particular earth mass problem can, however, be greatly enhanced by the use of the computer. Nonhomogeneities, so prevalent in nature, and irregularly shaped boundaries subjected to mixed stress and displacement conditions are typical of the types of problems which can now be analyzed with relative ease. The relative importance of these effects is discussed before the suggested techniques of solution.

A final comment for the benefit of the reader is that this paper is presented in the spirit of "how to" rather than the "results of."

ENVIRONMENTAL BOUNDARY EFFECTS

Rigid Base Beneath a Layer of Soil

Figure 1 (Terzaghi, 1) demonstrates the effect on the vertical stress distribution of a rigid base beneath a layer of elastic soil subjected to a surface load. The significant

feature is that the departure from the semi-infinite case is a function of the depth or position of the rigid base with respect to the applied load.

Rigid Vertical Boundary

Figure 2 shows the difference between measured values of horizontal stress along a rigid vertical boundary and the calculated values, assuming an elastic half space as given by Spangler (2). The departure is again a function of the relative position of the applied load with respect to the vertical constraint.

Friction Along a Rigid Boundary

The increase in vertical stress along a rigid horizontal boundary due to lateral restraint provided by friction along that boundary is shown in Figure 3 (1). Thus, resist-
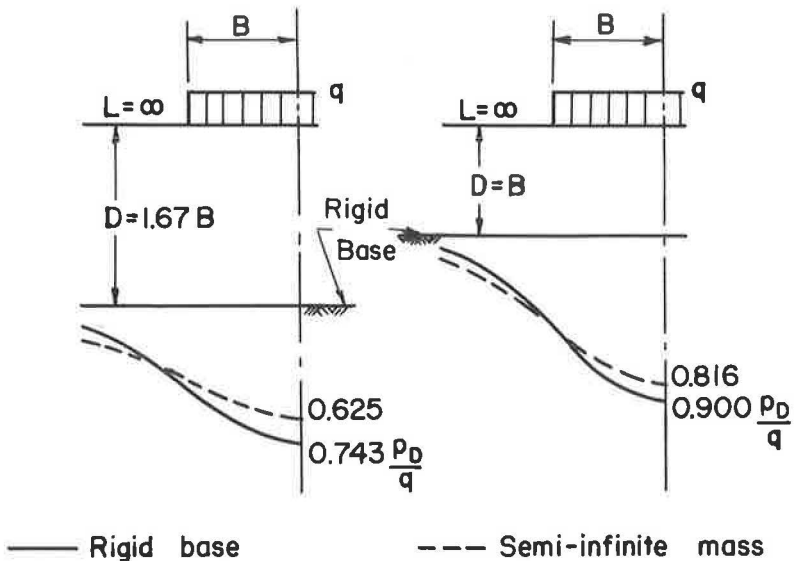
Figure 1. Pressure distributions at indicated depths.
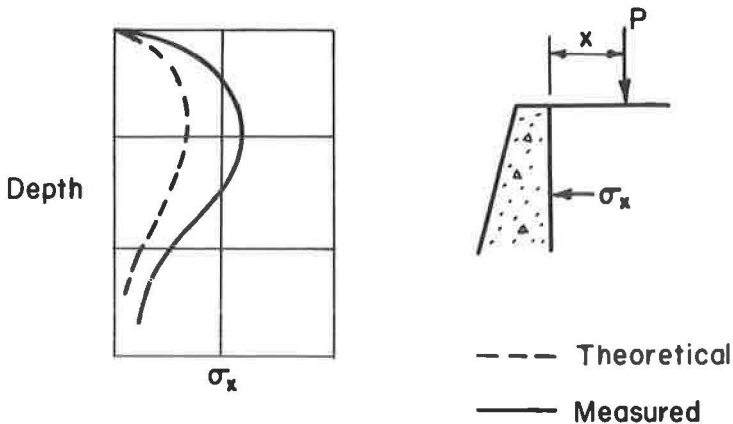
Figure 2. Horizontal pressures on retaining walls due to concentrated surface loads.
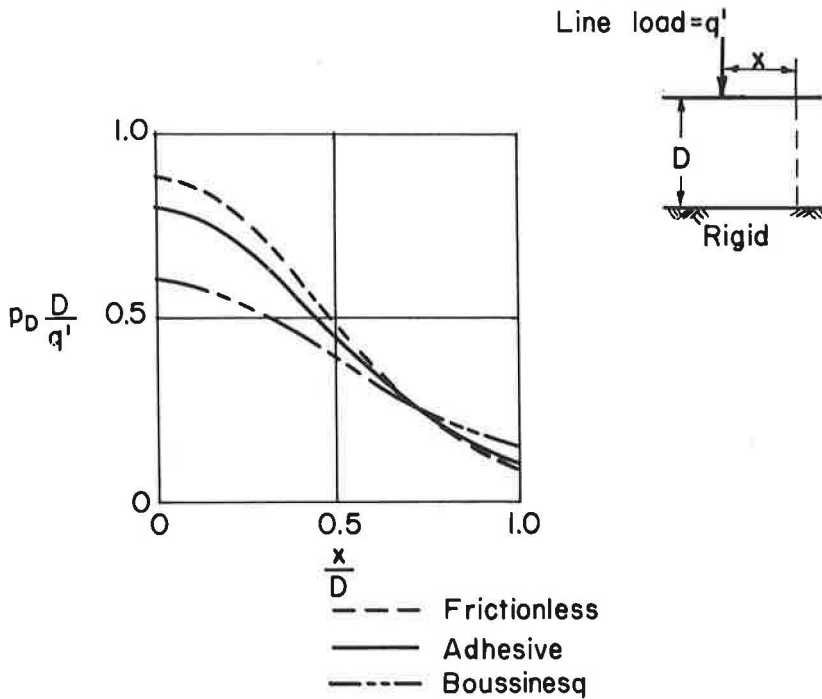
Figure 3. Distribution of normal pressure on rigid base of elastic layer acted on by line load.

ance to displacement in a direction parallel as well as perpendicular to a rigid boundary may have a significant effect on stress distribution.

VARIATIONS IN MATERIAL PROPERTIES

Spatial Variation in Elastic Modulus

The effect of spatial variations in mechanical properties as typified by an elastic modulus which is a function of position, $E(r, z)$, is shown in Figure 4 (3). The stress distributions are forced in the direction of the stiffer material, resulting in a considerable modification of the Boussinesq solution.

Anisotropy

Directional variations in elastic properties as well as spatial variations may alter stress distributions, as shown in Figure 5 (1). The extent of the modification is, of course, dependent on the magnitude of the ratio of the moduli in the principal directions.

Time-Dependent Material Characteristics

Rather radical redistributions of stress as a function of time may occur in time-dependent or viscoelastic materials. Figure 6 (4) shows such a redistribution for a Maxwell type material.

METHODOLOGY

Many numerical techniques exist for obtaining approximate solutions to differential systems. Probably the most widely accepted approach involves the use of finite differences. Basically, a finite difference approximation simply does not allow a derivative to be taken to the limit. Thus a difference is "discrete" and therefore compatible with the digital computer.
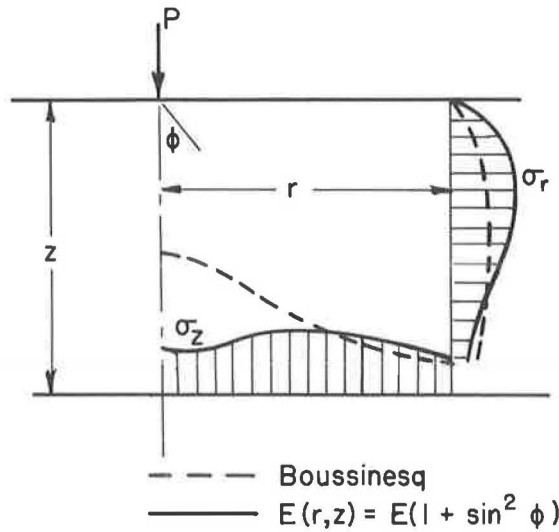
Figure 4. Stress distributions with and without spatial variations in elastic modulus (E).
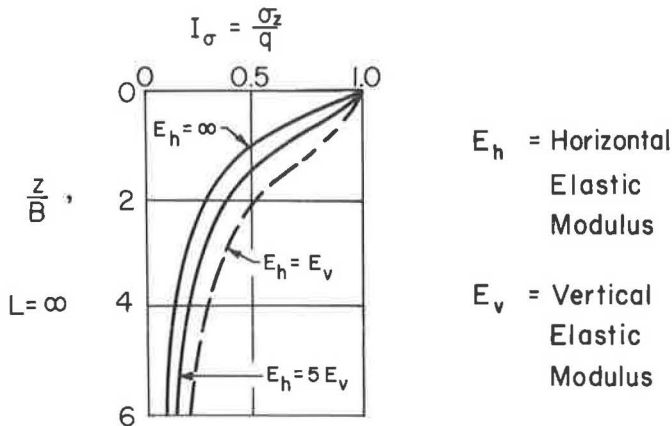
Figure 5. Relation between depth and vertical unit pressure beneath center line of flexible strip load with $E_h \geq E_v$.

The common finite difference approximations (Table 1) have been formulated according to the grid notation shown in Figure 7. The value of w_n is the magnitude of the function at the nth grid point.

Utilizing these algebraic approximations to derivatives, it is possible to replace a differential field equation describing the stress distribution in a region by a set of algebraic equations. The solution of this set of equations yields numerical values for the dependent variable at the nodes (intersection of the mesh lines).

The choice of the dependent variable (stress or displacement) cannot be divorced from the circumstances surrounding a particular problem. For example, if all the boundary conditions are of the stress variety, then stress would be a probable solution variable. If the boundary conditions are mixed, displacement may be a more convenient choice. This situation is analogous to the force and displacement alternatives which occur in the matrix analysis of structures.

Each approach is presented along with some applications.
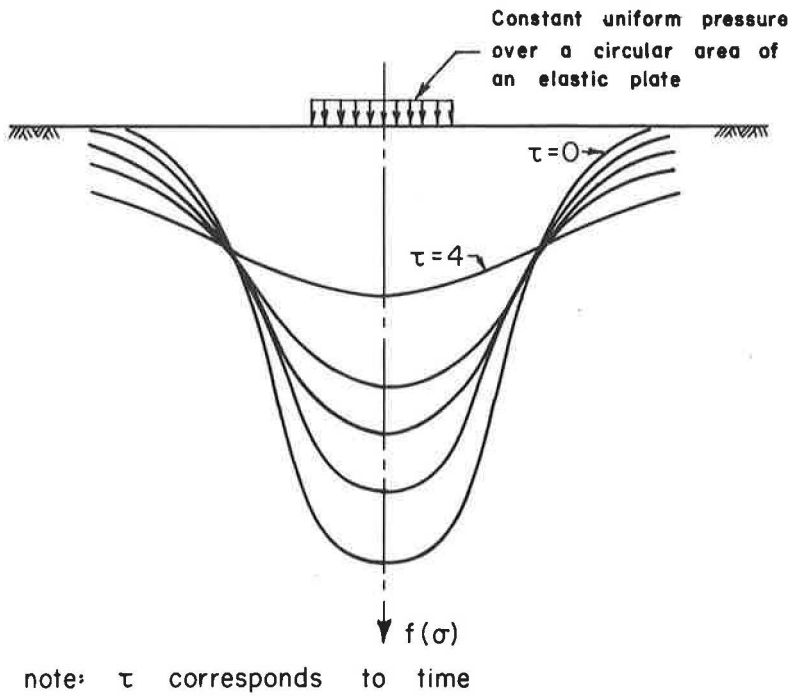
Figure 6. Reactive pressure distribution for plate on Maxwell foundation at various times τ.
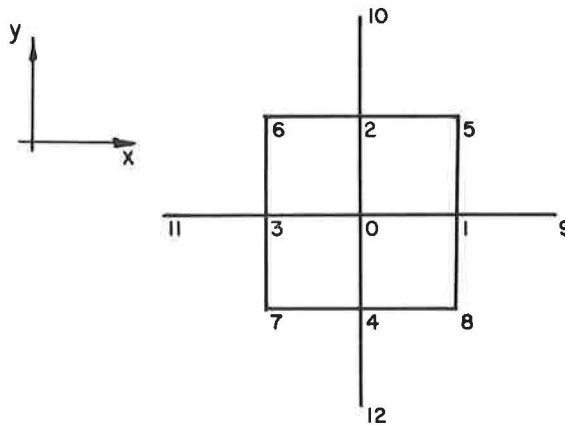
Figure 7. Finite difference grid notation.

Force Method

The governing field equation describing the stress distribution in a linearly elastic body is the biharmonic

$$\nabla^4 \phi = 0 \tag{1}$$

114

TABLE 1

$$\left[\frac{\partial w}{\partial x}\right]_0 \;=\; \frac{w_1 - w_3}{2h}$$

$$\left[\frac{\partial w}{\partial y}\right]_0 \;=\; \frac{w_2 - w_4}{2h}$$

$$\left[\frac{\partial^2 w}{\partial x^2}\right]_0 \;=\; \frac{w_1 + w_3 - 2w_0}{h^2}$$

$$\left[\frac{\partial^2 w}{\partial y^2}\right]_0 \;=\; \frac{w_2 + w_4 - 2w_0}{h^2}$$

$$\left[\frac{\partial^2 w}{\partial x\,\partial y}\right]_0 \;=\; \frac{w_5 - w_6 + w_7 - w_8}{4h^2}$$

$$\left[\frac{\partial^3 w}{\partial x^3}\right]_0 \;=\; \frac{w_9 - 2w_1 + 2w_3 - w_{11}}{2h^3}$$

$$\left[\frac{\partial^3 w}{\partial y^3}\right]_0 \;=\; \frac{w_{10} - 2w_2 + 2w_4 - w_{12}}{2h^3}$$

$$\left[\frac{\partial^4 w}{\partial x^4}\right]_0 \;=\; \frac{6w_0 - 4w_1 - 4w_3 + w_9 + w_{11}}{h^4}$$

$$\left[\frac{\partial^4 w}{\partial y^4}\right]_0 \;=\; \frac{6w_0 - 4w_2 - 4w_4 + w_{10} + w_{12}}{h^4}$$

$$\left[\frac{\partial^4 w}{\partial x^2\,\partial y^2}\right]_0 \;=\; \frac{4w_0 - 2\,\Sigma\,w_1 + \Sigma\,w_5}{h^4}$$

where ϕ is the Airy stress function describing all stresses in either a plane strain or plane stress situation. The extension of the biharmonic to include spatial variations in material properties is (5):

$$\frac{\partial^2}{\partial x^2}\left[A\frac{\partial^2\phi}{\partial x^2}\right] + \frac{\partial^2}{\partial y^2}\left[A\frac{\partial^2\phi}{\partial y^2}\right] + \frac{\partial^2}{\partial x\,\partial y}\left[2A(1+B)\frac{\partial^2\phi}{\partial x\,\partial y}\right]$$

$$-\frac{\partial^2}{\partial x^2}\left[AB\frac{\partial^2\phi}{\partial y^2}\right] - \frac{\partial^2}{\partial y^2}\left[AB\frac{\partial^2\phi}{\partial x^2}\right] \tag{2}$$

$$-\nabla^2\left[A(1-B)V\right] + \nabla^2(C\alpha T) = 0$$

where:

$$A = \frac{1-\nu^2}{E}$$

$$B = \frac{\nu}{1-\nu}$$

$$C = 1+\nu$$

$V = $ potential of body forces

$\alpha T = $ thermal expansion term

For the elastic case with $\nu = \frac{1}{2}$, $B = 1$, and neglecting the thermal expansion term, Eq. 2 reduces to the relationship indicated in Eq. 3.

$$A(\nabla^4\phi) + 2\frac{\partial A}{\partial x}\left[\frac{\partial^3\phi}{\partial x^3} + \frac{\partial^3\phi}{\partial x\,\partial y^2}\right] + 2\frac{\partial A}{\partial y}\left[\frac{\partial^3\phi}{\partial y^3} + \frac{\partial^3\phi}{\partial x^2\,\partial y}\right]$$

$$+\left[\frac{\partial^2 A}{\partial y^2} - \frac{\partial^2 A}{\partial x^2}\right]\left[\frac{\partial^2\phi}{\partial y^2} - \frac{\partial^2\phi}{\partial x^2}\right] + 4\left[\frac{\partial^2 A}{\partial x\partial y}\cdot\frac{\partial^2\phi}{\partial x\partial y}\right] = 0 \tag{3}$$

The value of the modulus at the point as well as its first, second, and cross derivatives appear as coefficients of the unknown stress function. Thus, these quantities must be initially calculated numerically from the known variations in modulus. They can then be substituted as numerical coefficients into the following finite difference approximation to Eq. 3.

$$\phi_0(20A) + \phi_1(-8A - 4A_x - A_{yy} + A_{xx}) +$$

$$\phi_2(-8A - 4A_y + A_{yy} - A_{xx}) + \phi_3(-8A + 4A_x - A_{yy} + A_{xx}) +$$

$$\phi_4(-8A + 4A_y + A_{yy} - A_{xx}) + \phi_5(2A + A_x + A_y + A_{xy}) +$$

$$\phi_6(2A - A_x + A_y - A_{xy}) \quad + \quad \phi_7(2A - A_x - A_y + A_{xy}) \quad +$$

$$\phi_8(2A + A_x - A_y - A_{xy}) \quad + \quad \phi_9(A + A_x) \quad + \quad \phi_{10}(A + A_y) +$$

$$\phi_{11}(A - A_x) + \phi_{12}(A - A_y) \quad = \quad 0$$

where: $\quad A_x = \dfrac{\partial A}{\partial x} \cdot h$; $\quad A_y = \dfrac{\partial A}{\partial y} \cdot h$; $\quad A_{xx} = \dfrac{\partial^2 A}{\partial x^2} \cdot h^2$;

$$A_{yy} = \dfrac{\partial^2 A}{\partial y^2} \cdot h^2 \qquad \text{and} \qquad A_{xy} = \dfrac{\partial^2 A}{\partial x \partial y} \cdot h^2$$

This difference approximation is formulated at every interior grid point of the region. The boundary conditions are introduced into those equations which contain points on or outside of the boundary (6). A typical statement of boundary conditions is shown in Figure 8. The homogeneous solution refers to the known stress function solution for a homogeneous half space.
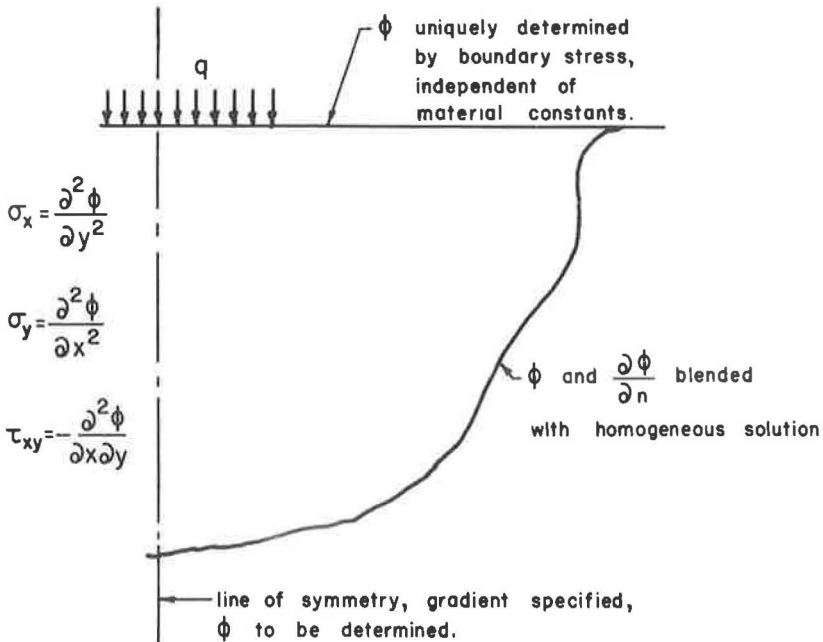
Figure 8. Statement at boundary conditions.

The resulting set of algebraic equations can be stated in the following matrix form.

The B matrix is a diagonal matrix whose coefficients are determined by the spatial variations in material properties; C is the unknown stress function column vector, and D is a known column vector dictated by the values of stress at the boundaries. Performing a matrix inversion yields values for the stress function and thus stresses at the interior grid points.

The results of a rather unusual application of this technique are shown in Figure 9.
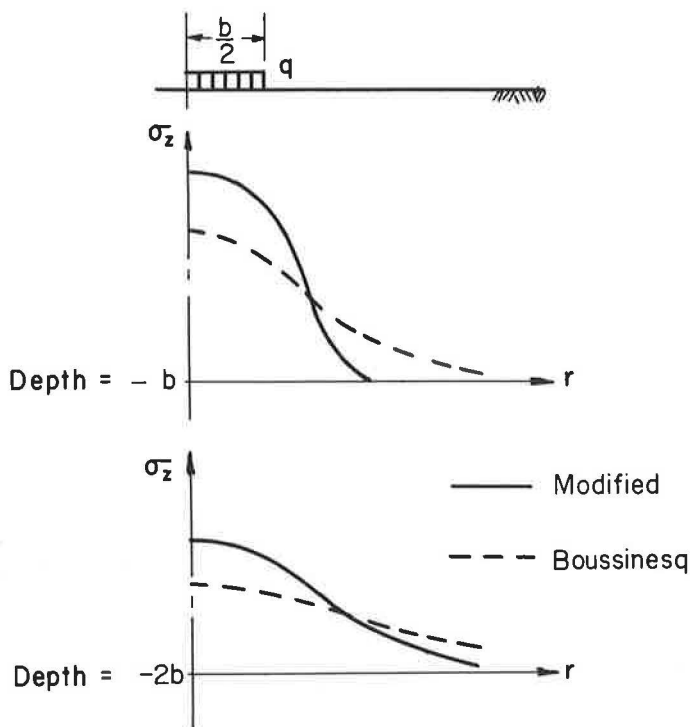
Figure 9. Comparison of homogeneous and nonhomogeneous cases.

In this case the modulus was assumed to vary as the first stress invarient $\left[\dfrac{\sigma_x + \sigma_y + \sigma_z}{3}\right]$ thus imposing a nonlinearity which required iteration of the previous technique.

For the particular case of a discontinuity in modulus, such as a layered system, the biharmonic would apply in each of the homogeneous layers; however, compatibility of stress and strain would have to be insured (5) according to the following relations.

$$\phi = \bar{\phi}$$

$$\frac{\partial \phi}{\partial y} = \frac{\partial \bar{\phi}}{\partial y}$$

stress requirements

$$A_1\left[\frac{\partial^2 \phi}{\partial y^2} - B_1\frac{\partial^2 \phi}{\partial x^2}\right] = A_2\left[\frac{\partial^2 \bar{\phi}}{\partial y^2} - B_2\frac{\partial^2 \bar{\phi}}{\partial x^2}\right]$$

strain requirements

$$-A_1\left[\frac{\partial^3 \phi}{\partial y^3} + (2 + B_1)\frac{\partial^3 \phi}{\partial x^2 \partial y}\right] = -A_2\left[\frac{\partial^3 \bar{\phi}}{\partial y^3} + (2 + B_2)\frac{\partial^3 \bar{\phi}}{\partial x^2 \partial y}\right]$$

$$\nabla^4 \phi = 0$$

$$\nabla^4 \bar{\phi} = 0$$

where: A and B are material constants

These equations expressed in finite difference form allow the elimination of points outside each of the respective regions as indicated in Figure 10 whereupon ϕ and $\bar{\phi}$ can be determined as usual.

Displacement Method
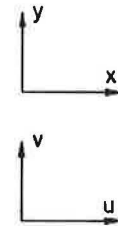
In contrast to the single fourth order field equation in the force method, the displacement method requires the simultaneous satisfaction of two second order differential equations (6) which are

$$(\lambda + 2\mu)\frac{\partial^2 u}{\partial x^2} + \mu \frac{\partial^2 u}{\partial y^2} + (\lambda + \mu)\frac{\partial^2 v}{\partial x \partial y} = 0$$

(4)

$$\mu \frac{\partial^2 v}{\partial x^2} + (\lambda + 2\mu)\frac{\partial^2 v}{\partial y^2} + (\lambda + \mu)\frac{\partial^2 u}{\partial x \partial y} = 0$$

where:
$$\lambda = \frac{E \nu}{(1 + \nu)(1 - 2\nu)}$$

$$\mu = \frac{E}{2(1 + \nu)}$$

Discretizing (finite difference conversion) these equations causes them to assume the following form:

$$\frac{(\lambda + 2\mu)}{h^2}(u_3 - 2u_0 + u_1) + \frac{\mu}{h^2}(u_2 - 2u_0 + u_4)$$

(5)

$$+ \frac{(\lambda + \mu)}{4h^2}(v_5 - v_6 + v_7 - v_8) = 0$$

$$\frac{\mu}{h^2}(v_3 - 2v_0 + v_1) + \frac{(\lambda + 2\mu)}{h^2}(v_2 - 2v_0 + v_4)$$

(6)

$$+ \frac{(\lambda + \mu)}{4h^2}(u_5 - u_6 + u_7 - u_8) = 0$$
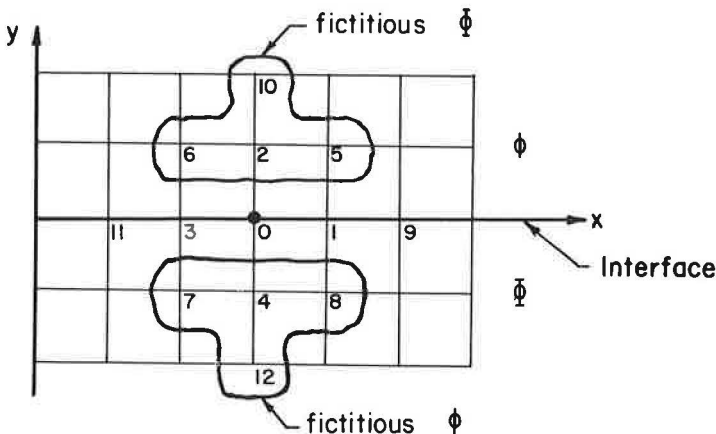
Figure 10. Finite difference notation at interface.

The application of these difference equations is probably best explained with a specific example. Consider the region EFGH in Figure 11 and assume the displacements u and v are completely specified on the boundary. Thus eight unknowns must be determined, the horizontal and vertical displacements at nodes 6, 7, 10 and 11. Application of Eqs. 5 and 6 to these nodes yields the following set of equations in matrix notation.

Again, matrix inversion gives the solution for the unknown displacements.

When stress conditions as well as displacements are imposed on the boundary, the use of the displacement approach requires the conversion of the stress condition to a displacement condition via the stress strain relation for the material. For an elastic material, the following equations provide the conversion.

$$\sigma_x = \lambda \left[\frac{\partial u}{\partial x} + \frac{\partial v}{\partial y} \right] + 2\mu \frac{\partial u}{\partial x}$$

$$\sigma_y = \lambda \left[\frac{\partial u}{\partial x} + \frac{\partial v}{\partial y} \right] + 2\mu \frac{\partial v}{\partial y}$$

$$\tau_{xy} = \mu \left[\frac{\partial u}{\partial y} + \frac{\partial v}{\partial x} \right]$$

The displacements at a stressed boundary as well as interior displacements must be determined. Application of the field equations at the boundary involves mesh points outside the region as shown in Figure 12. However, these fictitious points are eliminated using the known values of stress at the boundary and the stress strain relation. The results for a typical mixed boundary condition problem of this type are given in Figure 13.

This problem can be considered as a fill in a rigid (rock) valley subjected to a uniform load. The increase in vertical stress near the rigid boundary at the lower section is quite evident.

Viscoelasticity and the Displacement Method

The incorporation of a viscoelastic assumption in a two-dimensional stress analysis increases the number of independent variables from two to three. Thus a solution must be obtained at a given time, t, as a function of the spatial coordinates x and y and then "marched" to a new t as dictated by the governing equations.
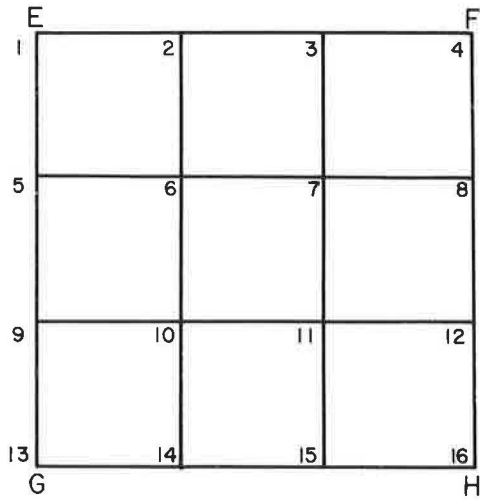
note: u and v specified on EFGH

Figure 11. Region considered in displacement method example.
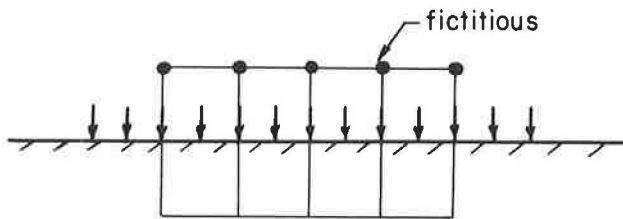
Figure 12. Location of fictitious grid points at boundary.
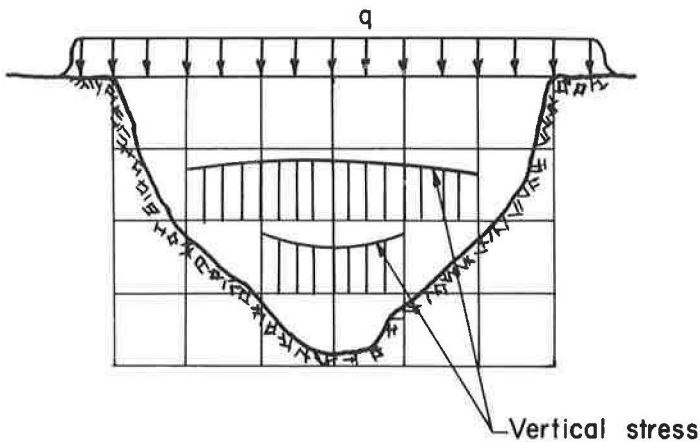
Figure 13. Plot of vertical stress distribution in irregular cross-section.

Again, a particular case may best serve to demonstrate the technique. The displacement field equations for a Voigt solid (7) are

$$(\lambda + 2\mu)\frac{\partial^2 u}{\partial x^2} + (\lambda' + 2\mu')\frac{\partial}{\partial t}\left[\frac{\partial^2 u}{\partial x^2}\right] + \mu\frac{\partial^2 u}{\partial y^2}$$

$$+ \mu'\frac{\partial}{\partial t}\left[\frac{\partial^2 u}{\partial y^2}\right] + (\lambda + \mu)\frac{\partial^2 v}{\partial x \partial y} \tag{7}$$

$$+ (\lambda' + \mu')\frac{\partial}{\partial t}\left[\frac{\partial^2 v}{\partial x \partial y}\right] = 0$$

$$\mu\frac{\partial^2 v}{\partial x^2} + \mu'\frac{\partial}{\partial t}\left[\frac{\partial^2 v}{\partial x^2}\right] + (\lambda + 2\mu)\frac{\partial^2 v}{\partial y^2}$$

$$+ (\lambda' + 2\mu')\frac{\partial}{\partial t}\left[\frac{\partial^2 v}{\partial y^2}\right] + (\lambda + \mu)\frac{\partial^2 u}{\partial x \partial y} \tag{8}$$

$$+ (\lambda' + \mu')\frac{\partial}{\partial t}\left[\frac{\partial^2 u}{\partial x \partial y}\right] = 0$$

where λ' and μ' are the viscous components of the material behavior.

With the grid notation shown in Figure 14 the algebraic expression of these equations takes the indicated form where the Crank-Nicolson technique of averaging the space derivatives at either end of the time increment is employed for reasons of mathematical stability.

$$A_1(u_3 - 2u_0 + u_1)_{t_0 + \Delta t} + B_1(u_2 - 2u_0 + u_4)_{t_0 + \Delta t}$$
$$+ A_2(v_5 - v_6 + v_7 - v_8)_{t_0 + \Delta t} = A_3(u_3 - 2u_0 + u_1)_{t_0}$$
$$+ B_2(u_2 - 2u_0 + u_4)_{t_0} + A_4(v_5 - v_6 + v_7 - v_8)_{t_0}$$

where:
$$A_1 = (\lambda\Delta t + 2\mu\Delta t + 2\lambda' + 4\mu')$$
$$A_3 = (-\lambda\Delta t - 2\mu\Delta t + 2\lambda' + 4\mu')$$
$$A_2 = (1/4)(\lambda\Delta t + \mu\Delta t + 2\lambda' + 2\mu')$$
$$A_4 = (1/4)(-\lambda\Delta t - \mu\Delta t + 2\lambda' + 2\mu')$$
and $B_1 = \mu\Delta t + 2\mu'$ $B_2 = -\mu\Delta t + 2\mu'$
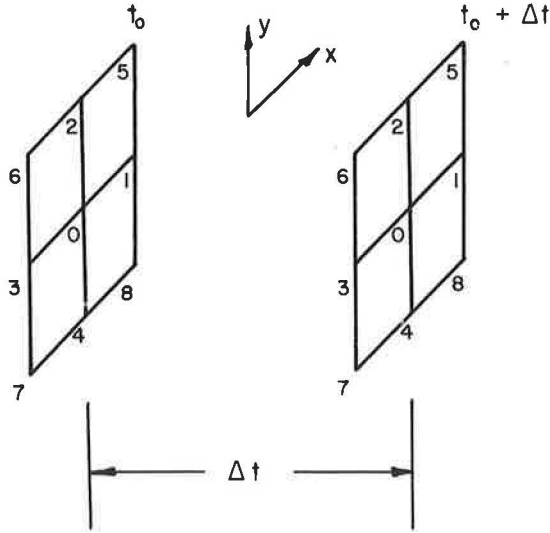
Figure 14. Grid notation for spatial and time coordinates.

The viscoelastic solution is similar to a repeated elastic solution in that a set of simultaneous equations must be solved at the end of each finite time increment.

A typical set of results using this approach is shown in Figure 15, which essentially describes the time-dependent displacement of the surface of a Voigt foundation material subjected to a uniform line load.

CRITICAL EQUILIBRIUM OF EARTH MASSES

The previous discussion has been confined to continuous behavior assuming small strains satisfying equilibrium and compatibility requirements.

In the case of discontinuous behavior which occurs when failure or slip planes develop in an earth mass, equilibrium must still be satisfied at impending failure; however, the yield or failure criterion for the material replaces the compatibility require-
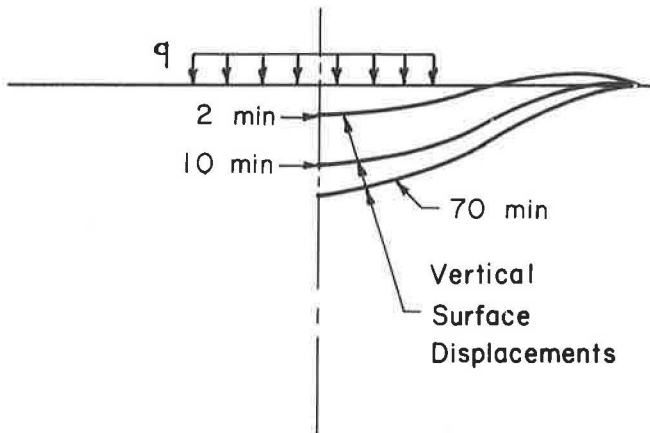
Figure 15. Typical viscoelastic surface displacements.

ment.   The failure criterion for a material with cohesion and internal friction as given by Scott [8] is

$$\left.\begin{array}{c}\sigma_x \\ \\ \sigma_z\end{array}\right\} = \sigma\,(1 \mp \sin\phi\,\cos 2\theta) - H$$

$$\tau_{xz} = \sigma\,\sin\phi\,\sin 2\theta$$

where: ϕ = angle of internal friction,

θ = defined in Figure 16,

$H = c \cdot \cot\phi$, and

$\sigma = 1/2\,(\sigma_x + \sigma_z + 2H) = 1/2(\sigma_1 + \sigma_3 + 2H)$

with the various angles shown in Figure 16.   The failure criterion can be combined with the equations of equilibrium,

$$\frac{\partial\sigma_x}{\partial x} + \frac{\partial\tau_{xz}}{\partial z} = 0$$

$$\frac{\partial\tau_{xz}}{\partial x} + \frac{\partial\sigma_z}{\partial z} = \gamma$$

to form a set of nonlinear equations which by the following transformations,

$$\chi = \frac{\cot\phi}{2}\,\log_e \frac{\sigma}{\sigma_0}$$

$$\xi = \chi + \theta$$

$$\eta = \chi - \theta$$

yield the ordinary differential equations,

$$\frac{d\xi}{dz} = - \frac{\gamma\,\sin(\theta - \alpha)}{2\sigma\,\sin\phi\,\cos(\theta + \alpha)}$$

$$\frac{d\eta}{dz} = \frac{\gamma\,\sin(\theta + \alpha)}{2\sigma\,\sin\phi\,\cos(\theta - \alpha)}$$

(9)
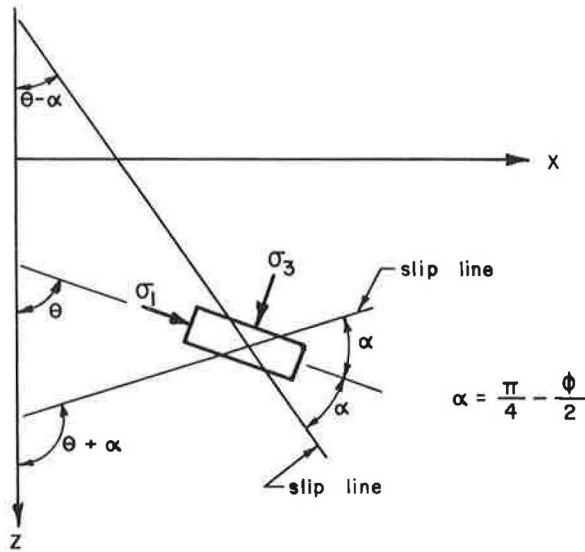
Figure 16. Slip line formation in real space.

as valid relationships along the "slip" lines. Thus starting at a boundary where ξ and η are defined, the family of slip lines within the earth mass can be developed by integrating Eq. 9.

Again utilizing difference techniques the expression for ξ typically becomes

$$\xi_C = \xi_A - \frac{(z_C - z_A)\, \gamma\, \sin(\theta - \alpha)}{2\,\sigma_A\, \sin\phi\, \cos(\theta + \alpha)}$$

which, in conjunction with the assumption of a straight-line approximation to short segments of a slip line, allows the discrete development of the slip line grid. The repetitive nature of this process is particularly well adapted to the computer.
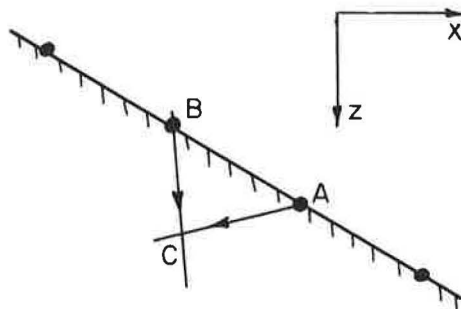
Figure 17. Reference diagram for beginning solution at a boundary.

Sokolovski (9) has improved the numerical process by developing the following expressions for the coordinates of the intersection of slip lines (Fig. 17).

$$x_C = x_B + (z_C - z_B) \tan(\theta_B - \alpha)$$

$$z_C = \frac{z_B \tan(\theta_B - \alpha) - x_B - z_A \tan(\theta_A + \alpha) + x_A}{\tan(\theta_B - \alpha) - \tan(\theta_A + \alpha)}$$

CONCLUSIONS

The purpose of this somewhat cursory excursion into the realm of numerical techniques as related to foundation problems has been to stimulate awareness of the current availability of tools that may allow the job to be done better.

Independent of this presentation, the future will record that its purpose has been realized.

REFERENCES

1. Terzaghi, K.   Theoretical Soil Mechanics, John Wiley and Sons, New York, 1956.
2. Spangler, M. G.   Horizontal Pressures on Retaining Walls Due to Concentrated Surface Loads.   Iowa Eng. Experiment Sta. Bull. 140, Iowa State College.
3. Hruban, K.   The Basic Problem of a Non-Linear and Nonhomogeneous Half-Space. In Non-Homogeneity in Elasticity and Plasticity, Ed. by W. Olszak, Pergamon Press Ltd., 1959.
4. Lee, E. H.   Stress Analysis for Viscoelastic Bodies. In Viscoelasticity-Phenomenological Aspects, Ed. by J. T. Bergen, Academic Press, New York, 1960.
5. Zienkiewicz, O. C., and Holister, G. S.   Two-Dimensional Stress Analysis and Plate Flexure by Finite Difference. In Stress Analysis, pp. 20-21, John Wiley and Sons, New York, 1965.
6. Allen, D. N.   Relaxation Methods, McGraw-Hill, New York, 1954.
7. Kolsky, H.   Stress Waves in Solids, Dover Publications, New York.
8. Scott, R. F.   Principles of Soil Mechanics, Addison-Wesley Inc., 1963.
9. Sokolovski, V. V.   Statics of Soil Media, Butterworths Scientific Publications, London, 1960.

Load-Deflection Response of Layered Flexible Pavement Sections Under Rigid Bearing Plates

ROBERT L. KONDNER, RAYMOND J. KRIZEK, and EIICHI YAMAMOTO
Northwestern University

ABRIDGMENT

●NON-DIMENSIONAL techniques are employed to analyze data from rigid plates bearing on flexible pavement sections. Response equations are developed to describe pavement load-deflection behavior under a variety of different conditions. Deflections are considered at the surface, base course, and subgrade of the layered system. The data were obtained from the Hybla Valley Test Program, and include effects of different test procedures, temperature, and limited repetitive loading (up to 75 repetitions). Empirical equations are proposed to describe the response trends observed, and specific coefficients are determined for the particular conditions of this test program.

Temperature decrease has the effect of increasing the stiffness of the soil-pavement system. Also, the load-deflection response of deflection-controlled and load-controlled tests is found to differ. This indicates that caution must be used when attempting any correlation with rigid plate bearing tests. The total deflections from original datum due to repetitive loading increase substantially (up to 80% or more for 75 load applications) compared to single application deflections. The expression of surface, base course, and subgrade deflections by analytic equations permits an investigation of the effect of layer deflections. Surface deflection alone may be misleading in some cases unless the layer contributing the largest portion of the deflection is known. Layer deflections take on added significance when it is noted that some studies have indicated no correlation between serviceability parameters and surface deflections. However, others have observed that crack frequency is related statistically to the subbase modulus, and have deduced that subbase deformations, regardless of season, contributed to the occurrence of surface cracks. They also concluded that deflection measurements of the individual layers are useful in showing the relationship between pavement cracking and the properties of each layer.

Tables of Radial Stresses in Top Layer of Three-Layer Elastic System at Distance From Load Axis

J. M. KIRK, The Danish Asphalt Industries' Road Research Laboratory

For a load distributed over a circular area, numerical values of radial stresses in the top layer of a three-layer elastic system have been calculated, not only under the center of the load but also for radial distances from the load axis up to four times the radius of the loaded area, and for different values of Poisson's ratio.

Tables are included which indicate that, for the same axle load, the radial stresses caused by dual wheels can be considerably smaller than the stresses caused by single wheels, when the thickness of the layer is greater than the radius of one of the dual wheel load areas.

Furthermore, the tables indicate that for layers with a thickness less than the radius of one of the dual wheel load areas, the maximum radial stress is found as the radial stress under a single wheel load equal to one-fourth of the axle load.

A few examples of the important influence of Poisson's ratio on the radial stresses are also given.

●THE LIFE of a sound road structure depends mainly on the stresses in the subgrade and on the tensile stresses in the pavement caused by the wheel loads. Knowledge of these stresses is, therefore, important. In 1951 Acum and Fox (1) published tables for the stresses on the axis of a single wheel load in a three-layer system, and these tables were later extended by Jones (2).

Practically all heavy axle loads are transmitted to the road surface by dual wheels, and it is necessary to evaluate the combined stresses caused by two wheel loads placed closely together.

Normally, there is only an unimportant difference between the stresses in the subgrade caused by an axle load, transmitted by two single wheels, and the stresses caused by the same axle load, transmitted by two pairs of dual wheels. However, this is not the case when the tensile stresses in the top layer of road structure are considered. Therefore, the radial stresses were calculated for radial distances up to four times the radius of the loaded area.

PARAMETERS

The numerical values given in the tables were calculated by use of Burmister's theory (3), after correction of a printing error in Eq. 36e, where a factor of $(1 - K)/(1 - I)$ has been omitted in the first term in the fifth line of the second bracket. The values in the tables are the radial stresses caused by unit load, and a negative sign indicates compression. Poisson's ratio is assumed equal to 0.5 for all three layers for all values in Appendix A. In Appendix B values are given for Poisson's ratio equal
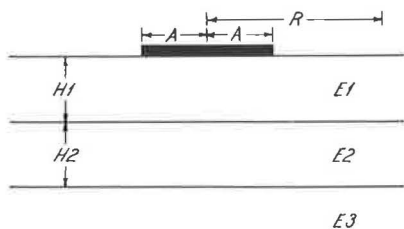
Figure 1. Notation used for parameters in a
three-layer system.

to 0. 4, and Appendix C gives values for Poisson's ratio equal to 0. 3. The notation follows from Figure 1, where E stands for modulus of elasticity. The center for the coordinate system has been chosen at the first interface under the center of the loaded area.

As the radial stresses have been calculated both at the bottom and at the surface of the top layer, six parameters are necessary. The following parameters and parameter values have been chosen, and the tables state the radial stresses for all combinations of these values:

$$H1/A = 0.25, 0.50, 1.00, 1.50, 2.00$$
$$H2/A = 1.00, 2.00, 3.00$$
$$Z/H1 = 0.00, 1.00$$
$$E1/E2 = 2, 5, 10, 20, 50, 100, 500$$
$$E2/E3 = 5, 10$$
$$R/A = 0.0, 0.5, 1.0, 1.5, 2.0, 2.5, 3.0, 3.5, 4.0$$

Z is the vertical distance from the first interface, and R is the radial distance from the load axis. As the number of combinations of parameter values are rather high, the calculated stresses are given with only two decimals, which should be sufficient for most purposes.

The calculations are based on the usual assumptions that the materials are perfectly homogeneous, isotropic and elastic; the two topmost layers are weightless and of finite thickness but of infinite extent horizontally; the bottom layer is of infinite thickness and extent; there is perfect interaction between the layers at the interfaces; there is zero stress and displacement at infinite depth; and, finally, the load acts normal to the road surface and is distributed uniformly over a circular area.

For some of the combinations of parameter values, the radial stresses are also found in Acum and Fox's tables, as well as in Jones' tables. These stresses are stated in Table 1, and the disagreement is very small.

TABLE 1

RADIAL STRESS

H1/A	H2/A	E1/E2	E2/E3	Acum and Fox	Jones	AOV
0. 25	1. 00	5	5	0. 3230	0. 30868	0. 3084
0. 25	1. 00	50	5	12. 0880	12. 095563	12. 0955
2. 00	1. 00	5	5	0. 6319	0. 63161	0. 6317
2. 00	1. 00	10	5	0. 8790	0. 87867	0. 8782
2. 00	1. 00	50	5	1. 3413	1. 34590	1. 3460
0. 50	2. 00	5	5	1. 1490	1. 15327	1. 1529
0. 50	2. 00	50	5	7. 1620	7. 16480	7. 1648

EXAMPLES

As an example of the use of the tables, Figure 2 shows the combined radial stress at the first interface for $E1/E2 = 10$, $E2/E3 = 5$, $H1/A = 2$, and $H2/A = 2$ for a contact pressure of 7 kg/cm^2. Poisson's ratio is equal to 0. 5 in all three layers. The two
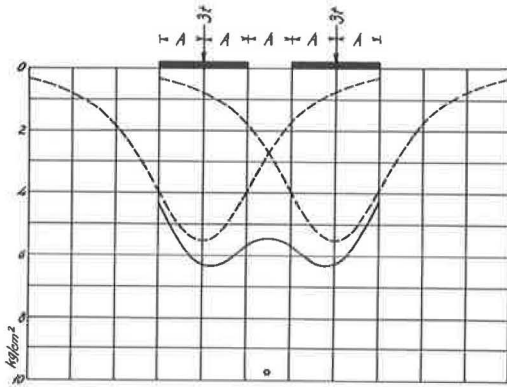
Figure 2. Effect of single wheel load of 3 tons (dotted line); combined effect of dual wheels (solid line); stress resulting from single wheel load of 6 tons (small circle).

dotted lines show the effect of a single wheel load of 3 tons, and the solid line shows the combined radial stress from dual wheels of 3 tons each. Even for a layer of this thickness (approximately 10 in.) the combined effect of the dual wheels of 3 tons each is only about 15 percent greater than the stress caused by a single wheel load of 3 tons. If, as is usually done in calculations, a single wheel load of 6 tons is used as an approximation for dual wheels, and the radial stress is calculated for this load, the result is a stress indicated in Figure 2 with a circle, which is about 50 percent too high in this example.

Table 2 gives the maximum tensile stress at the bottom of the top layer for a road structure with H1/A = 0.5, H2/A = 2.0 for a load of 6-ton single wheel, 2- × 3-ton dual wheels and 3-ton single wheel, all with a contact pressure of 7 kg/cm^2.

Similar examples are given in Tables 3, 4 and 5.

From the tables it follows that for pavements with a thickness less than about the radius in the load area for one of the dual wheels, the maximum tensile stress is found by taking a single wheel load equal to one-fourth of the axle load. For pavements with a thickness greater than about the radius in the load area for one of the dual wheels, the maximum tensile stress is found as the combined effect of the two dual wheels.

INFLUENCE OF POISSON'S RATIO

To evaluate the influence of Poisson's ratio on the radial stresses in the pavement, calculations were carried out for a road with a thin top layer and for a road with a thick top layer, loaded with dual wheels as shown in Figure 2, and with different values of Poisson's ratio in the layers. The contact pressure is again 7 kg/cm^2. The values given in Tables 6 and 7 are the maximum stresses at the first interface in the top layer. These two tables show that Poisson's ratio for the top layer has an important influence on the stresses in the two examples investigated, and that the Poisson's ratio for the

TABLE 2

MAXIMUM TENSILE STRESS AT BOTTOM OF TOP LAYER

H1/A	H2/A	E1/E2	E2/E3	6 t	2 × 3 t	3 t
0.5	2.0	5	5	5.6	8.0	8.0
0.5	2.0	10	5	15.7	17.6	17.6
0.5	2.0	20	5	35.0	30.0	30.0

TABLE 3

MAXIMUM TENSILE STRESS AT BOTTOM OF TOP LAYER

H1/A	H2/A	E1/E2	E2/E3	6 t	2 × 3 t	3 t
1.0	3.0	5	5	8.8	7.1	7.1
1.0	3.0	10	5	17.7	11.6	11.6
1.0	3.0	20	5	24.6	16.5	16.5

TABLE 4

MAXIMUM TENSILE STRESS AT BOTTOM OF TOP LAYER

H1/A	H2/A	E1/E2	E2/E3	6 t	2 × 3 t	3 t
1.5	2.0	10	5	14.0	8.7	8.3
1.5	2.0	20	5	17.3	12.3	10.9
1.5	2.0	50	5	21.0	17.4	14.2

TABLE 5

MAXIMUM TENSILE STRESS AT BOTTOM OF TOP LAYER

H1/A	H2/A	E1/E2	E2/E3	6 t	2 × 3 t	3 t
2.0	2.0	10	5	9.7	6.3	5.5
2.0	2.0	20	5	11.5	8.7	7.2
2.0	2.0	50	5	13.4	11.8	9.1

TABLE 6

MAXIMUM STRESS AT FIRST INTERFACE IN TOP LAYER

H1/A	H2/A	E1/E2	E2/E3	NY1 = 0.5 NY2 = 0.5 NY3 = 0.5	NY1 = 0.5 NY2 = 0.3 NY3 = 0.5	NY1 = 0.3 NY2 = 0.5 NY3 = 0.5	NY1 = 0.3 NY2 = 0.3 NY3 = 0.5	NY1 = 0.3 NY2 = 0.3 NY3 = 0.3
0.5	3	5	5	7.8	5.8	6.0	4.5	4.4
0.5	3	10	5	16.6	14.5	12.7	11.0	11.0
0.5	3	20	5	28.2	26.0	21.8	20.0	20.0

TABLE 7

MAXIMUM STRESS AT FIRST INTERFACE IN TOP LAYER

H1/A	H2/A	E1/E2	E2/E3	NY1 = 0.5 NY2 = 0.5 NY3 = 0.5	NY1 = 0.5 NY2 = 0.3 NY3 = 0.5	NY1 = 0.3 NY2 = 0.5 NY3 = 0.5	NY1 = 0.3 NY2 = 0.3 NY3 = 0.5	NY1 = 0.3 NY2 = 0.3 NY3 = 0.3
2.0	2.0	5	5	4.0	3.7	3.1	2.9	2.8
2.0	2.0	10	5	6.3	6.0	4.8	4.6	4.5
2.0	2.0	20	5	8.7	8.5	6.8	6.6	6.4

second layer also has a measurable influence, whereas the Poisson's ratio for the third layer does not seem to be of much importance. NY1 stands for Poisson's ratio in the top layer, etc.

It follows from Tables 6 and 7 that the stresses calculated with Poisson's ratio equal to 0.5 in all three layers can be about 50 percent higher than the stresses found with a Poisson's ratio of 0.3 in all layers. Because of this variation, supplementary tables have been calculated for Poisson's ratio equal to 0.4 in all three layers (Appendix B). Tables for Poisson's ratio equal to 0.3 are given in Appendix C. It is thus possible to find intermediate values by interpolation.

CONCLUSIONS

Tables for the radial stresses in the top layer in a three-layer system have been calculated for distances from the axis of the load up to four times the radius of the loaded area. For thick pavements the radial stresses caused by dual wheels are considerably smaller than the stresses caused by the equivalent single wheel load. In thin pavement the maximum radial stress is found as the stress caused by a single wheel load equal to one-fourth of the axle load.

Furthermore, it is shown that Poisson's ratio has an important influence on the radial stresses.

REFERENCES

1. Acum, W. E. A., and Fox, L. Computation of Load Stresses in a Three-Layer Elastic System. Geotechnique, No. 2, pp. 293-300, 1951.
2. Jones, A. Tables of Stresses in Three-Layer Elastic Systems. HRB Bull. 342, pp. 176-214, 1962.
3. Burmister, D. M. The General Theory of Stresses and Displacements in Layered Systems. Jour. of Applied Physics, Vol. 16, pp. 89-94, 126-127, 296-302, 1945.

Appendix A

RATIO OF RADIAL STRESS TO SURFACE PRESSURE—POISSON'S RATIO EQUAL TO 0.5 IN ALL THREE LAYERS[a]

TABLE 8

H1/A = 0.25   H2/A = 1.00   Z/H1 = 0.00

E1/E2	E2/E3	R/A=0.0	R/A=0.5	R/A=1.0	R/A=1.5	R/A=2.0	R/A=2.5	R/A=3.0	R/A=3.5	R/A=4.0
2	5	-0.69	-0.54	-0.54	-0.41	-0.16	-0.06	-0.01	0.02	0.03
5	5	0.31	0.47	-0.31	-0.72	-0.34	-0.16	-0.07	-0.03	-0.00
10	5	2.11	2.06	0.22	-0.98	-0.58	-0.32	-0.19	-0.11	-0.06
20	5	5.29	4.76	1.34	-1.10	-0.91	-0.59	-0.40	-0.28	-0.20
50	5	12.10	10.54	4.39	-0.44	-1.22	-1.13	-0.92	-0.73	-0.57
100	5	19.13	16.72	8.33	1.27	-0.83	-1.37	-1.40	-1.26	-1.09
500	5	39.68	35.63	23.02	11.13	5.08	1.70	-0.24	-1.33	-1.91
2	10	-0.88	-0.72	-0.70	-0.52	-0.24	-0.10	-0.03	0.01	0.04
5	10	0.18	0.34	-0.43	-0.83	-0.42	-0.22	-0.11	-0.05	-0.00
10	10	2.18	2.12	0.24	-1.00	-0.62	-0.37	-0.23	-0.14	-0.09
20	10	5.75	5.18	1.65	-0.91	-0.82	-0.58	-0.41	-0.31	-0.24
50	10	13.43	11.81	5.43	0.32	-0.72	-0.84	-0.78	-0.69	-0.61
100	10	21.44	18.92	10.24	2.80	0.29	-0.62	-0.94	-1.03	-1.03
500	10	44.75	40.60	27.67	15.31	8.69	4.71	2.18	0.54	-0.54

H1/A = 0.25   H2/A = 1.00   Z/H1 = 1.00

R1/R2	E2/E3	R/A=0.0	R/A=0.5	R/A=1.0	R/A=1.5	R/A=2.0	R/A=2.5	R/A=3.0	R/A=3.5	R/A=4.0
2	5	-2.07	-2.02	-1.07	-0.17	-0.05	0.03	0.08	0.09	0.09
5	5	-3.38	-3.28	-1.56	-0.08	-0.00	0.08	0.12	0.14	0.14
10	5	-5.27	-4.95	-2.21	0.02	0.14	0.17	0.21	0.21	0.21
20	5	-8.38	-7.58	-3.37	0.03	0.38	0.39	0.38	0.30	0.33
50	5	-14.83	-13.06	-6.31	-0.69	0.60	0.68	0.84	0.77	0.68
100	5	-21.49	-18.90	-10.07	-2.37	0.17	1.03	1.26	1.25	1.16
500	5	-41.05	-36.93	-24.16	-11.94	-5.65	-2.08	-0.01	1.19	1.85
2	10	-2.53	-2.45	-1.41	-0.41	-0.20	-0.04	0.05	0.09	0.11
5	10	-4.08	-3.94	-2.09	-0.46	-0.24	-0.06	0.06	0.13	0.16
10	10	-6.24	-5.85	-2.94	-0.50	-0.20	-0.03	0.10	0.18	0.22
20	10	-9.73	-8.84	-4.40	-0.73	-0.12	0.09	0.22	0.30	0.34
50	10	-16.98	-15.09	-8.04	-2.01	-0.33	0.25	0.50	0.61	0.65
100	10	-24.49	-21.77	-12.58	-4.41	-1.35	-0.04	0.58	0.88	1.01
500	10	-46.48	-42.23	-29.13	-16.40	-9.51	-5.31	-2.60	-0.81	0.37

H1/A = 0.25   H2/A = 2.00   Z/H1 = 0.00

E1/E2	E2/E3	R/A=0.0	R/A=0.5	R/A=1.0	R/A=1.5	R/A=2.0	R/A=2.5	R/A=3.0	R/A=3.5	R/A=4.0
2	5	-0.58	-0.44	-0.50	-0.42	-0.21	-0.12	-0.07	-0.04	-0.02
5	5	0.19	0.36	-0.39	-0.78	-0.40	-0.24	-0.15	-0.09	-0.05
10	5	1.56	1.58	-0.11	-1.15	-0.65	-0.35	-0.21	-0.14	-0.10
20	5	4.06	3.67	0.61	-1.45	-1.00	-0.56	-0.34	-0.23	-0.16
50	5	9.50	8.20	2.71	-1.37	-1.52	-1.06	-0.68	-0.46	-0.34
100	5	15.33	13.24	5.66	-0.38	-1.57	-1.46	-1.11	-0.82	-0.62
500	5	34.05	30.28	18.41	-7.56	2.63	0.26	-0.85	-1.33	-1.50
2	10	-0.69	-0.56	-0.61	-0.51	-0.29	-0.19	-0.12	-0.08	-0.05
5	10	0.05	0.22	-0.53	-0.91	-0.51	-0.32	-0.22	-0.15	-0.10
10	10	1.44	1.47	-0.22	-1.26	-0.75	-0.45	-0.30	-0.22	-0.16
20	10	4.00	3.62	0.54	-1.52	-1.08	-0.64	-0.41	-0.29	-0.22
50	10	9.70	8.39	2.86	-1.26	-1.45	-1.03	-0.68	-0.48	-0.37
100	10	15.90	13.78	6.15	0.03	-1.24	-1.22	-0.95	-0.72	-0.57
500	10	36.32	32.51	20.53	9.51	4.36	1.75	0.41	-0.30	-0.68

H1/A = 0.25   H2/A = 2.00   Z/H1 = 1.00

E1/E2	E2/E3	R/A=0.0	R/A=0.5	R/A=1.0	R/A=1.5	R/A=2.0	R/A=2.5	R/A=3.0	R/A=3.5	R/A=4.0
2	5	-1.53	-1.57	-0.81	-0.11	-0.13	-0.09	-0.05	-0.02	-0.00
5	5	-2.48	-2.52	-1.12	0.02	-0.12	-0.12	-0.08	-0.04	-0.01
10	5	-3.95	-3.82	-1.54	0.20	-0.00	-0.10	-0.11	-0.04	-0.00
20	5	-6.44	-5.90	-2.32	0.39	0.25	-0.03	-0.06	-0.01	0.02
50	5	-11.74	-10.32	-4.42	0.20	0.68	0.45	0.26	0.17	0.16
100	5	-17.40	-15.18	-7.31	-0.80	0.69	0.81	0.65	0.51	0.42
500	5	-35.54	-31.70	-19.72	-8.57	-3.43	-0.89	0.36	0.96	1.23
2	10	-1.70	-1.73	-0.96	-0.24	-0.24	-0.20	-0.12	-0.07	-0.04
5	10	-2.78	-2.82	-1.40	-0.23	-0.30	-0.27	-0.20	-0.13	-0.07
10	10	-4.32	-4.18	-1.87	-0.08	-0.24	-0.30	-0.24	-0.16	-0.09
20	10	-6.94	-6.38	-2.76	0.01	-0.07	-0.23	-0.23	-0.17	-0.10
50	10	-12.51	-11.06	-5.11	-0.39	0.19	0.06	-0.05	-0.06	-0.02
100	10	-18.52	-16.27	-8.32	-1.68	-0.05	0.22	0.18	0.15	0.15
500	10	-38.23	-34.35	-22.24	-10.90	-5.51	-2.70	-1.18	-0.31	0.20

[a]A negative sign indicates compression.

Z/H1 = 0 indicates tables of stresses at the interface.

Z/H1 = 1 indicates tables of stresses at the surface.

TABLE 9

H1/λ = 0.25   H2/λ = 3.00   Z/H1 = 0.00

E1/E2	E2/E3	R/λ=0.0	R/λ=0.5	R/λ=1.0	R/λ=1.5	R/λ=2.0	R/λ=2.5	R/λ=3.0	R/λ=3.5	R/λ=4.0
2	5	-0.49	-0.37	-0.44	-0.58	-0.19	-0.12	-0.09	-0.06	-0.04
5	5	0.26	0.43	-0.34	-0.75	-0.38	-0.23	-0.16	-0.12	-0.09
10	5	1.57	1.59	-0.09	-1.14	-0.64	-0.36	-0.23	-0.17	-0.13
20	5	3.89	3.52	0.48	-1.54	-1.05	-0.59	-0.35	-0.24	-0.18
50	5	8.90	7.65	2.24	-1.70	-1.71	-1.14	-0.70	-0.44	-0.30
100	5	14.21	12.18	4.76	-1.05	-1.99	-1.67	-1.17	-0.78	-0.53
500	5	31.26	27.58	15.98	5.53	1.06	-0.84	-1.52	-1.63	-1.53
2	10	-0.56	-0.43	-0.51	-0.44	-0.25	-0.17	-0.13	-0.10	-0.08
5	10	0.16	0.33	-0.43	-0.84	-0.47	-0.31	-0.23	-0.18	-0.14
10	10	1.45	1.48	-0.20	-1.24	-0.74	-0.45	-0.32	-0.24	-0.20
20	10	3.79	3.42	0.38	-1.63	-1.14	-0.68	-0.44	-0.32	-0.25
50	10	8.88	7.62	2.21	-1.74	-1.76	-1.20	-0.76	-0.50	-0.37
100	10	14.35	12.32	4.88	-0.95	-1.91	-1.62	-1.14	-0.76	-0.53
500	10	32.32	28.61	16.97	6.46	1.90	-0.09	-0.87	-1.09	-1.07

H1/λ = 0.25   H2/λ = 3.00   Z/H1 = 1.00

E1/E2	E2/E3	R/λ=0.0	R/λ=0.5	R/λ=1.0	R/λ=1.5	R/λ=2.0	R/λ=2.5	R/λ=3.0	R/λ=3.5	R/λ=4.0
2	5	-1.36	-1.41	-0.69	-0.03	-0.09	-0.09	-0.07	-0.05	-0.04
5	5	-2.21	-2.27	-0.92	0.15	-0.05	-0.12	-0.11	-0.09	-0.07
10	5	-3.56	-3.47	-1.26	0.39	0.09	-0.09	-0.13	-0.11	-0.09
20	5	-5.88	-5.38	-1.91	0.66	0.39	0.05	-0.09	-0.11	-0.09
50	5	-10.78	-9.42	-3.70	0.71	0.96	0.53	0.19	0.03	-0.02
100	5	-15.97	-13.83	-6.18	0.02	1.19	1.02	0.64	0.34	0.18
500	5	-32.80	-28.89	-17.20	-6.48	-1.85	0.17	0.96	1.17	1.15
2	10	-1.45	-1.50	-0.77	-0.11	-0.16	-0.15	-0.12	-0.10	-0.07
5	10	-2.35	-2.42	-1.06	0.02	-0.17	-0.22	-0.21	-0.17	-0.13
10	10	-3.76	-3.66	-1.45	0.21	0.04	-0.24	-0.26	-0.22	-0.18
20	10	-6.15	-5.64	-2.15	0.43	0.18	-0.14	-0.25	-0.25	-0.21
50	10	-11.17	-9.80	-4.c	0.37	0.65	0.26	-0.04	-0.17	-0.19
100	10	-16.52	-14.37	-6.49	-0.45	0.76	0.64	0.31	0.07	-0.05
500	10	-34.03	-30.28	-18.54	-7.75	-3.01	-0.88	0.03	0.37	0.46

H1/λ = 0.50   H2/λ = 1.00   Z/H1 = 0.00

E1/E2	E2/E3	R/λ=0.0	R/λ=0.5	R/λ=1.0	R/λ=1.5	R/λ=2.0	R/λ=2.5	R/λ=3.0	R/λ=3.5	R/λ=4.0
2	5	0.09	0.09	-0.18	-0.31	-0.19	-0.10	-0.06	-0.03	-0.02
5	5	1.48	1.30	0.36	-0.31	-0.30	-0.22	-0.16	-0.11	-0.08
10	5	3.13	2.72	1.16	-0.08	-0.30	-0.31	-0.27	-0.22	-0.18
20	5	5.22	4.58	2.39	0.52	-0.09	-0.30	-0.35	-0.34	-0.31
50	5	8.43	7.52	4.62	1.96	0.75	0.12	-0.21	-0.37	-0.44
100	5	11.00	9.95	6.65	3.52	1.88	0.90	0.29	-0.09	-0.32
500	5	16.81	15.58	11.79	8.01	5.70	4.09	2.91	2.02	1.34
2	10	0.07	0.07	-0.20	-0.33	-0.20	-0.12	-0.07	-0.04	-0.02
5	10	1.60	1.41	0.45	-0.25	-0.26	-0.20	-0.15	-0.11	-0.09
10	10	3.43	3.01	1.41	0.12	-0.08	-0.21	-0.21	-0.19	-0.17
20	10	5.78	5.12	2.88	0.95	0.23	-0.05	-0.18	-0.23	-0.25
50	10	9.41	8.48	5.52	2.76	1.44	0.69	0.24	-0.03	-0.20
100	10	12.30	11.22	7.87	4.64	2.88	1.77	1.03	0.53	0.17
500	10	18.62	17.38	13.55	9.71	7.32	5.62	4.33	3.34	2.54

H1/λ = 0.50   H2/λ = 1.00   Z/H1 = 1.00

E1/E2	E2/E3	R/λ=0.0	R/λ=0.5	R/λ=1.0	R/λ=1.5	R/λ=2.0	R/λ=2.5	R/λ=3.0	R/λ=3.5	R/λ=4.0
2	5	-2.02	-1.90	-1.03	-0.19	-0.06	0.00	0.04	0.06	0.07
5	5	-3.40	-3.09	-1.60	-0.31	-0.03	0.06	0.10	0.12	0.12
10	5	-4.90	-4.39	-2.46	-0.58	-0.07	0.11	0.17	0.20	0.20
20	5	-6.63	-5.92	-3.46	-1.16	-0.31	0.07	0.22	0.29	0.31
50	5	-9.49	-8.55	-5.49	-2.52	-1.13	-0.38	0.03	0.28	0.40
100	5	-11.83	-10.76	-7.37	-3.98	-2.21	-1.13	-0.47	-0.03	0.25
500	5	-17.28	-16.05	-12.23	-8.27	-5.90	-4.24	-3.04	-2.12	-1.41
2	10	-2.34	-2.21	-1.28	-0.39	-0.20	-0.09	-0.01	0.04	0.06
5	10	-3.81	-3.48	-1.99	-0.61	-0.26	-0.09	-0.00	0.06	0.10
10	10	-5.43	-4.90	-2.89	-1.02	-0.41	-0.13	0.02	0.10	0.15
20	10	-7.48	-6.75	-4.20	-1.79	-0.81	-0.32	-0.05	0.10	0.20
50	10	-10.68	-9.71	-6.57	-3.49	-1.96	-1.06	-0.51	-0.14	-0.06
100	10	-13.26	-12.17	-8.71	-5.22	-3.32	-2.10	-1.29	-0.70	-0.29
500	10	-19.13	-17.89	-14.03	-10.01	-7.55	-5.80	-4.50	-3.46	-2.64

TABLE 10

H1/A = 0.50   H2/A = 2.00   Z/H1 = 0.00

E1/E2	E2/E3	R/A=0.0	R/A=0.5	R/A=1.0	R/A=1.5	R/A=2.0	R/A=2.5	R/A=3.0	R/A=3.5	R/A=4.0
2	5	0.00	0.01	-0.25	-0.37	-0.23	-0.14	-0.09	-0.05	-0.03
5	5	1.15	0.99	0.12	-0.47	-0.39	-0.25	-0.16	-0.11	-0.07
10	5	2.51	2.16	0.71	-0.38	-0.47	-0.37	-0.26	-0.18	-0.13
20	5	4.29	3.71	1.67	0.01	-0.40	-0.44	-0.37	-0.29	-0.23
50	5	7.16	6.32	3.58	1.16	0.19	-0.21	-0.36	-0.38	-0.37
100	5	9.63	8.63	5.48	2.55	1.14	0.39	-0.02	-0.23	-0.34
500	5	15.75	14.54	10.81	7.13	4.94	3.46	2.40	1.64	1.06
2	10	-0.05	-0.04	-0.30	-0.42	-0.27	-0.17	-0.11	-0.08	-0.05
5	10	1.12	0.96	0.09	-0.50	-0.41	-0.28	-0.19	-0.13	-0.10
10	10	2.54	2.18	0.73	-0.37	-0.46	-0.37	-0.27	-0.19	-0.14
20	10	4.42	3.84	1.79	0.11	-0.32	-0.38	-0.33	-0.26	-0.21
50	10	7.53	6.68	3.92	1.47	0.46	0.02	-0.16	-0.23	-0.25
100	10	10.25	9.24	6.07	3.10	1.65	0.84	0.38	0.11	-0.06
500	10	17.06	15.84	12.09	8.37	6.13	4.59	3.47	2.63	1.97

H1/A = 0.50   H2/A = 2.00   Z/H1 = 1.00

E1/E2	E2/E3	R/A=0.0	R/A=0.5	R/A=1.00	R/A=1.5	R/A=2.0	R/A=2.5	R/A=3.0	R/A=3.5	R/A=4.0
2	5	-1.65	-1.58	-0.81	-0.10	-0.07	-0.06	-0.04	-0.02	-0.01
5	5	-2.74	-2.50	-1.23	-0.13	-0.01	-0.03	-0.04	-0.03	-0.01
10	5	-3.99	-3.56	-1.81	-0.28	0.02	0.05	0.06	0.03	0.04
20	5	-5.61	-4.98	-2.72	-0.69	-0.09	0.09	0.11	0.12	0.11
50	5	-8.25	-7.38	-4.51	-1.80	-0.67	-0.16	0.07	0.18	0.23
100	5	-10.54	-9.53	-6.29	-3.12	-1.59	-0.74	-0.27	0.02	0.18
500	5	-16.31	-15.11	-11.35	-7.49	-5.23	-3.70	-2.62	-1.81	-1.20
2	10	-1.78	-1.70	-0.93	-0.21	-0.16	-0.14	-0.10	-0.07	-0.04
5	10	-2.68	-2.69	-1.41	-0.29	-0.15	-0.13	-0.12	-0.09	-0.06
10	10	-4.26	-3.83	-2.06	-0.50	-0.17	-0.11	-0.10	-0.07	-0.04
20	10	-5.99	-5.35	-3.07	-1.00	-0.36	-0.14	-0.08	-0.04	-0.01
50	10	-8.83	-7.95	-5.06	-2.30	-1.12	-0.55	-0.27	-0.10	-0.00
100	10	-11.34	-10.32	-7.05	-3.81	-2.24	-1.33	-0.75	-0.43	-0.20
500	10	-17.71	-16.50	-12.72	-8.82	-6.51	-4.91	-3.76	-2.87	-2.18

H1/A = 0.50   H2/A = 3.00   Z/H1 = 0.00

E1/E2	E2/E3	R/A=0.0	R/A=0.5	R/A=1.0	R/A=1.5	R/A=2.0	R/A=2.5	R/A=3.0	R/A=3.5	R/A=4.0
2	5	0.02	0.03	-0.24	-0.36	-0.23	-0.14	-0.09	-0.06	-0.05
5	5	1.11	0.96	0.09	-0.50	-0.41	-0.27	-0.18	-0.12	-0.08
10	5	2.37	2.02	0.60	-0.47	-0.53	-0.41	-0.29	-0.19	-0.14
20	5	4.00	3.44	1.43	-0.19	-0.54	-0.53	-0.42	-0.31	-0.23
50	5	6.63	5.81	3.12	0.77	-0.11	-0.43	-0.49	-0.45	-0.39
100	5	8.92	7.94	4.81	2.10	0.69	0.04	-0.27	-0.39	-0.42
500	5	14.87	13.67	9.99	6.36	4.25	2.86	1.89	1.22	0.73
2	10	-0.02	-0.01	-0.27	-0.40	-0.26	-0.17	-0.12	-0.09	-0.07
5	10	1.07	0.91	0.05	-0.54	-0.45	-0.31	-0.21	-0.15	-0.12
10	10	2.35	2.00	0.57	-0.50	-0.56	-0.44	-0.32	-0.22	-0.16
20	10	4.29	3.45	1.45	-0.18	-0.53	-0.53	-0.43	-0.32	-0.24
50	10	6.78	5.95	3.25	0.89	-0.01	-0.33	-0.41	-0.39	-0.34
100	10	9.28	8.30	5.19	2.26	0.93	0.27	-0.07	-0.21	-0.27
500	10	15.75	14.55	10.84	7.20	5.06	3.63	2.62	1.90	1.37

H1/A = 0.50   H2/A = 3.00   Z/H1 = 1.00

E1/E2	E2/E3	R/A=0.0	R/A=0.5	R/A=1.0	R/A=1.5	R/A=2.0	R/A=2.5	R/A=3.0	R/A=3.5	R/A=4.0
2	5	-1.53	-1.46	-0.71	-0.04	-0.03	-0.05	-0.05	-0.04	-0.03
5	5	-2.54	-2.31	-1.07	-0.01	0.06	0.01	-0.03	-0.04	-0.04
10	5	-3.70	-3.16	-1.58	-0.11	0.13	0.10	0.03	0.00	-0.01
20	5	-5.19	-4.55	-2.38	-0.42	0.09	0.18	0.14	0.09	0.05
50	5	-7.64	-6.79	-3.98	-1.36	-0.35	0.01	0.18	0.21	0.19
100	5	-9.78	-8.80	-5.62	-2.63	-1.13	-0.41	-0.05	0.14	0.21
500	5	-15.46	-14.27	-10.55	-6.76	-4.58	-3.14	-2.15	-1.43	-0.91
2	10	-1.60	-1.53	-0.78	-0.10	-0.09	-0.10	-0.09	-0.08	-0.07
5	10	-2.65	-2.41	-1.18	-0.11	-0.03	-0.07	-0.10	-0.10	-0.09
10	10	-3.85	-3.43	-1.72	-0.16	0.10	-0.01	-0.06	-0.08	-0.09
20	10	-5.40	-4.78	-2.57	-0.61	-0.08	0.03	0.00	-0.02	-0.05
50	10	-7.96	-7.11	-4.29	-1.66	-0.62	-0.19	-0.04	0.02	0.03
100	10	-10.25	-9.26	-6.07	-2.98	-1.53	-0.77	-0.38	-0.16	-0.05
500	10	-16.45	-15.25	-11.52	-7.70	-5.49	-4.01	-2.97	-2.20	-1.64

TABLE 11

H1/A = 1.00   H2/A = 1.00   Z/H1 = 0.00

E1/E2	E2/E3	R/λ=0.0	R/λ=0.5	R/λ=1.0	R/λ=1.5	R/λ=2.0	R/λ=2.5	R/λ=3.0	R/λ=3.5	R/λ=4.0
2	5	0.42	0.34	0.12	-0.05	-0.09	-0.08	-0.06	-0.05	-0.04
5	5	1.32	1.14	0.64	0.20	0.02	-0.04	-0.07	-0.08	-0.08
10	5	2.09	1.84	1.17	0.55	0.24	0.08	-0.00	-0.05	-0.08
20	5	2.87	2.57	1.77	1.00	0.57	0.32	0.17	0.06	-0.02
50	5	3.85	3.51	2.61	1.71	1.16	0.80	0.55	0.36	0.22
100	5	4.53	4.18	3.23	2.27	1.66	1.24	0.94	0.70	0.51
500	5	5.94	5.57	4.57	3.55	2.87	2.39	2.02	1.71	1.45
2	10	0.48	0.40	0.17	-0.01	-0.05	-0.05	-0.04	-0.04	-0.04
5	10	1.46	1.27	0.77	0.32	0.12	0.04	-0.00	-0.03	-0.04
10	10	2.31	2.06	1.38	0.74	0.41	0.23	0.12	0.05	0.00
20	10	3.18	2.88	2.07	1.28	0.83	0.55	0.37	0.23	0.13
50	10	4.25	3.92	3.00	2.09	1.51	1.14	0.86	0.65	0.48
100	10	4.98	4.63	3.67	2.70	2.07	1.64	1.32	1.06	0.84
500	10	6.44	6.08	5.07	4.05	3.36	2.87	2.49	2.16	1.89

H1/A = 1.00   H2/A = 1.00   Z/H1 = 1.00

E1/E2	E2/E3	R/λ=0.0	R/λ=0.5	R/λ=1.0	R/λ=1.5	R/λ=2.0	R/λ=2.5	R/λ=3.0	R/λ=3.5	R/λ=4.0
2	5	-1.64	-1.58	-0.92	-0.25	-0.13	-0.06	-0.01	0.01	0.03
5	5	-2.30	-2.17	-1.35	-0.51	-0.27	-0.12	-0.03	0.02	0.05
10	5	-2.89	-2.72	-1.79	-0.83	-0.47	-0.25	-0.11	-0.02	0.03
20	5	-3.52	-3.31	-2.30	-1.23	-0.78	-0.48	-0.33	-0.14	-0.04
50	5	-4.31	-4.11	-3.02	-1.86	-1.32	-0.93	-0.65	-0.44	-0.28
100	5	-4.95	-4.70	-3.58	-2.38	-1.79	-1.35	-1.02	-0.77	-0.57
500	5	-6.27	-6.01	-4.86	-3.60	-2.96	-2.46	-2.06	-1.75	-1.48
2	10	-1.82	-1.75	-1.08	-0.39	-0.24	-0.15	-0.08	-0.03	-0.00
5	10	-2.55	-2.41	-1.58	-0.71	-0.44	-0.26	-0.15	-0.07	-0.02
10	10	-3.25	-3.07	-2.13	-1.14	-0.71	-0.45	-0.28	-0.16	-0.08
20	10	-3.88	-3.67	-2.65	-1.56	-1.08	-0.75	-0.52	-0.35	-0.22
50	10	-4.78	-4.54	-3.44	-2.27	-1.70	-1.29	-0.98	-0.74	-0.55
100	10	-5.42	-5.17	-4.04	-2.82	-2.22	-1.76	-1.41	-1.13	-0.91
500	10	-6.78	-6.52	-5.36	-4.10	-3.45	-2.94	-2.54	-2.21	-1.93

H1/A = 1.00   H2/A = 2.00   Z/H1 = 0.00

E1/E2	E2/E3	R/λ=0.0	R/λ=0.5	R/λ=1.0	R/λ=1.5	R/λ=2.0	R/λ=2.5	R/λ=3.0	R/λ=3.5	R/λ=4.0
2	5	0.30	0.23	0.02	-0.14	-0.15	-0.11	-0.08	-0.06	-0.04
5	5	1.08	0.91	0.44	0.04	-0.10	-0.12	-0.11	-0.10	-0.08
10	5	1.78	1.55	0.91	0.33	0.07	-0.04	-0.08	-0.09	-0.10
20	5	2.53	2.25	1.47	0.75	0.36	0.16	0.05	-0.02	-0.06
50	5	3.53	3.21	2.32	1.45	0.93	0.61	0.40	0.25	0.14
100	5	4.27	3.92	2.98	2.04	1.45	1.07	0.79	0.58	0.42
500	5	5.82	5.45	4.45	3.44	2.77	2.29	1.93	1.63	1.38
2	10	0.29	0.22	0.01	-0.14	-0.15	-0.12	-0.09	-0.06	-0.05
5	10	1.11	0.94	0.47	0.07	-0.05	-0.10	-0.09	-0.08	-0.07
10	10	1.87	1.63	0.99	0.40	0.13	0.02	-0.03	-0.05	-0.06
20	10	2.68	2.39	1.62	0.88	0.49	0.28	0.16	0.07	0.02
50	10	3.79	3.46	2.57	1.69	1.16	0.83	0.61	0.44	0.31
100	10	4.60	4.25	3.31	2.36	1.76	1.37	1.08	0.85	0.67
500	10	6.27	5.91	4.91	3.89	3.21	2.73	2.36	2.04	1.79

H1/A = 1.00   H2/A = 2.00   Z/H1 = 1.00

E1/E2	E2/E3	R/λ=0.0	R/λ=0.5	R/λ=1.0	R/λ=1.5	R/λ=2.0	R/λ=2.5	R/λ=3.0	R/λ=3.5	R/λ=4.0
2	5	-1.45	-1.40	-0.80	-0.18	-0.09	-0.06	-0.04	-0.02	-0.01
5	5	-2.07	-1.95	-1.17	-0.39	-0.20	-0.10	-0.05	-0.03	-0.01
10	5	-2.64	-2.47	-1.58	-0.67	-0.38	-0.20	-0.11	-0.05	-0.01
20	5	-3.22	-3.03	-2.04	-1.02	-0.62	-0.37	-0.21	-0.11	-0.04
50	5	-4.08	-3.85	-2.79	-1.65	-1.14	-0.79	-0.54	-0.36	-0.23
100	5	-4.73	-4.49	-3.38	-2.20	-1.63	-1.21	-0.91	-0.68	-0.50
500	5	-6.17	-5.91	-4.76	-3.51	-2.87	-2.38	-1.99	-1.68	-1.43
2	10	-1.54	-1.49	-0.87	-0.24	-0.16	-0.11	-0.09	-0.06	-0.05
5	10	-2.18	-2.06	-1.28	-0.49	-0.29	-0.17	-0.11	-0.08	-0.05
10	10	-2.78	-2.62	-1.72	-0.80	-0.49	-0.30	-0.19	-0.12	-0.08
20	10	-3.45	-3.25	-2.26	-1.22	-0.82	-0.54	-0.37	-0.25	-0.17
50	10	-4.39	-4.16	-3.08	-1.94	-1.42	-1.05	-0.79	-0.59	-0.44
100	10	-5.10	-4.86	-3.74	-2.55	-1.97	-1.54	-1.22	-0.98	-0.78
500	10	-6.64	-6.38	-5.23	-3.97	-3.32	-2.82	-2.43	-2.11	-1.84

TABLE 12

H1/A = 1.00   H2/A = 3.00   Z/H1 = 0.00

E1/E2	E2/E3	R/A=0.0	R/A=0.5	R/A=1.0	R/A=1.5	R/A=2.0	R/A=2.5	R/A=3.0	R/A=3.5	R/A=4.0
2	5	0.28	0.20	-0.00	-0.16	-0.16	-0.13	-0.09	-0.07	-0.05
5	5	1.01	0.84	0.38	-0.01	-0.14	-0.16	-0.14	-0.12	-0.09
10	5	1.66	1.43	0.80	0.23	-0.02	-0.11	-0.13	-0.13	-0.12
20	5	2.36	2.08	1.32	0.61	0.24	0.06	-0.03	-0.08	-0.10
50	5	3.33	3.00	2.12	1.27	0.77	0.47	0.28	0.15	0.06
100	5	4.06	3.71	2.78	1.85	1.28	0.91	0.65	0.46	0.32
500	5	5.68	5.31	4.32	3.31	2.64	2.17	1.82	1.52	1.28
2	10	0.26	0.19	-0.02	-0.17	-0.18	-0.14	-0.10	-0.08	-0.06
5	10	1.01	0.84	0.38	-0.01	-0.14	-0.16	-0.14	-0.12	-0.10
10	10	1.69	1.46	0.83	0.26	0.01	-0.08	-0.11	-0.11	-0.11
20	10	2.46	2.17	1.41	0.69	0.32	0.12	0.02	-0.03	-0.06
50	10	3.48	3.16	2.27	1.41	0.91	0.60	0.41	0.27	0.17
100	10	4.34	3.99	3.05	2.12	1.54	1.16	0.90	0.70	0.50
500	10	6.07	5.70	4.71	3.69	3.02	2.55	2.19	1.89	1.64

H1/A = 1.00   H2/A = 3.00   Z/H1 = 1.00

E1/E2	E2/E3	R/A=0.0	R/A=0.5	R/A=1.0	R/A=1.5	R/A=2.0	R/A=2.5	R/A=3.0	R/A=3.5	R/A=4.0
2	5	-1.38	-1.33	-0.72	-0.12	-0.06	-0.03	-0.03	-0.02	-0.02
5	5	-1.94	-1.83	-1.06	-0.29	-0.12	-0.04	-0.01	-0.00	-0.00
10	5	-2.46	-2.30	-1.43	-0.53	-0.26	-0.11	-0.04	-0.01	0.01
20	5	-3.05	-2.85	-1.88	-0.68	-0.50	-0.27	-0.14	-0.06	-0.01
50	5	-3.88	-3.66	-2.60	-1.48	-1.00	-0.66	-0.44	-0.28	-0.17
100	5	-4.54	-4.30	-3.20	-2.03	-1.47	-1.07	-0.79	-0.58	-0.42
500	5	-6.05	-5.79	-4.64	-3.39	-2.76	-2.27	-1.90	-1.60	-1.35
2	10	-1.43	-1.38	-0.77	-0.16	-0.10	-0.07	-0.06	-0.06	-0.05
5	10	-2.02	-1.91	-1.14	-0.37	-0.20	-0.11	-0.08	-0.06	-0.05
10	10	-2.57	-2.42	-1.54	-0.64	-0.36	-0.21	-0.13	-0.09	-0.06
20	10	-3.19	-3.00	-2.02	-1.01	-0.65	-0.41	-0.27	-0.18	-0.12
50	10	-4.12	-3.90	-2.84	-1.72	-1.22	-0.88	-0.64	-0.48	-0.36
100	10	-4.81	-4.57	-3.47	-2.29	-1.73	-1.32	-1.03	-0.81	-0.64
500	10	-6.46	-6.20	-5.05	-3.80	-3.16	-2.67	-2.29	-1.98	-1.72

H1/A = 1.50   H2/A = 1.00   Z/H1 = 0.00

E1/E2	E2/E3	R/A=0.0	R/A=0.5	R/A=1.0	R/A=1.5	R/A=2.0	R/A=2.5	R/A=3.0	R/A=3.5	R/A=4.0
2	5	0.37	0.32	0.19	0.06	0.00	-0.02	-0.03	-0.03	-0.03
5	5	0.91	0.81	0.55	0.31	0.15	0.07	0.03	0.01	-0.00
10	5	1.35	1.22	0.90	0.50	0.33	0.21	0.13	0.07	0.03
20	5	1.70	1.55	1.19	0.82	0.56	0.39	0.28	0.19	0.13
50	5	2.15	1.99	1.59	1.18	0.88	0.68	0.53	0.42	0.33
100	5	2.49	2.32	1.92	1.49	1.17	0.95	0.75	0.62	0.51
500	5	3.05	2.89	2.47	2.02	1.69	1.45	1.27	1.13	1.00
2	10	0.43	0.37	0.24	0.11	0.04	0.02	0.01	0.00	-0.01
5	10	1.02	0.91	0.66	0.40	0.24	0.15	0.10	0.06	0.03
10	10	1.46	1.33	1.01	0.68	0.46	0.32	0.23	0.16	0.11
20	10	1.88	1.73	1.36	0.98	0.72	0.54	0.42	0.33	0.25
50	10	2.40	2.24	1.79	1.38	1.07	0.86	0.71	0.59	0.49
100	10	2.66	2.50	2.09	1.65	1.33	1.11	0.95	0.81	0.70
500	10	3.28	3.11	2.69	2.25	1.91	1.67	1.50	1.35	1.22

H1/A = 1.50   H2/A = 1.00   Z/H1 = 1.00

E1/E2	E2/E3	R/A=0.0	R/A=0.5	R/A=1.0	R/A=1.5	R/A=2.0	R/A=2.5	R/A=3.0	R/A=3.5	R/A=4.0
2	5	-1.39	-1.37	-0.80	-0.23	-0.15	-0.10	-0.05	-0.03	-0.01
5	5	-1.74	-1.70	-1.08	-0.43	-0.30	-0.19	-0.12	-0.07	-0.03
10	5	-2.03	-1.97	-1.32	-0.64	-0.46	-0.32	-0.22	-0.14	-0.08
20	5	-2.32	-2.25	-1.58	-0.87	-0.66	-0.49	-0.36	-0.26	-0.18
50	5	-2.69	-2.62	-1.93	-1.18	-0.95	-0.75	-0.60	-0.47	-0.37
100	5	-3.00	-2.92	-2.23	-1.47	-1.23	-0.97	-0.80	-0.66	-0.55
500	5	-3.53	-3.45	-2.74	-1.98	-1.72	-1.50	-1.31	-1.16	-1.03
2	10	-1.50	-1.48	-0.91	-0.32	-0.24	-0.17	-0.11	-0.07	-0.04
5	10	-1.89	-1.84	-1.22	-0.56	-0.42	-0.30	-0.21	-0.15	-0.10
10	10	-2.20	-2.14	-1.49	-0.79	-0.61	-0.46	-0.34	-0.25	-0.18
20	10	-2.51	-2.45	-1.77	-1.05	-0.83	-0.65	-0.51	-0.40	-0.31
50	10	-2.90	-2.83	-2.14	-1.39	-1.15	-0.95	-0.78	-0.65	-0.54
100	10	-3.17	-3.10	-2.40	-1.64	-1.39	-1.18	-1.00	-0.86	-0.74
500	10	-3.76	-3.68	-2.97	-2.21	-1.95	-1.72	-1.53	-1.38	-1.24

TABLE 13

H1/A = 1.50   H2/A = 2.00   Z/H1 = 0.00

E1/E2	E2/E3	R/A=0.0	R/A=0.5	R/A=1.0	R/A=1.5	R/A=2.0	R/A=2.5	R/A=3.0	R/A=3.5	R/A=4.0
2	5	0.27	0.22	0.10	-0.01	-0.06	-0.06	-0.06	-0.05	-0.04
5	5	0.77	0.67	0.43	0.20	0.06	-0.00	-0.02	-0.04	-0.04
10	5	1.18	1.06	0.75	0.44	0.25	0.14	0.06	0.02	-0.00
20	5	1.55	1.41	1.05	0.69	0.45	0.30	0.20	0.13	0.08
50	5	2.03	1.87	1.48	1.07	0.78	0.59	0.46	0.36	0.28
100	5	2.36	2.20	1.79	1.36	1.05	0.84	0.69	0.57	0.47
500	5	3.02	2.85	2.43	1.99	1.66	1.42	1.25	1.10	0.98
2	10	0.28	0.23	0.11	-0.00	-0.05	-0.06	-0.05	-0.04	-0.03
5	10	0.82	0.72	0.48	0.24	0.11	0.04	0.02	0.00	-0.01
10	10	1.24	1.11	0.80	0.49	0.29	0.18	0.12	0.07	0.04
20	10	1.66	1.52	1.16	0.80	0.55	0.39	0.29	0.22	0.16
50	10	2.19	2.03	1.64	1.23	0.93	0.74	0.60	0.49	0.41
100	10	2.54	2.38	1.97	1.54	1.23	1.02	0.86	0.73	0.63
500	10	3.24	3.07	2.65	2.20	1.87	1.64	1.46	1.31	1.19

H1/A = 1.50   H2/A = 2.00   Z/H1 = 1.00

E1/E2	E2/E3	R/A=0.0	R/A=0.5	R/A=1.0	R/A=1.5	R/A=2.0	R/A=2.5	R/A=3.0	R/A=3.5	R/A=4.0
2	5	-1.29	-1.27	-0.72	-0.16	-0.11	-0.08	-0.05	-0.03	-0.02
5	5	-1.62	-1.58	-0.98	-0.35	-0.24	-0.15	-0.10	-0.06	-0.03
10	5	-1.91	-1.85	-1.22	-0.54	-0.39	-0.26	-0.18	-0.12	-0.07
20	5	-2.21	-2.14	-1.48	-0.77	-0.58	-0.43	-0.31	-0.22	-0.16
50	5	-2.60	-2.53	-1.84	-1.11	-0.88	-0.70	-0.55	-0.43	-0.34
100	5	-2.89	-2.81	-2.12	-1.37	-1.13	-0.92	-0.76	-0.63	-0.52
500	5	-3.50	-3.42	-2.72	-1.96	-1.70	-1.48	-1.29	-1.14	-1.01
2	10	-1.35	-1.33	-0.78	-0.22	-0.16	-0.12	-0.09	-0.07	-0.05
5	10	-1.71	-1.67	-1.06	-0.43	-0.31	-0.22	-0.16	-0.11	-0.08
10	10	-2.02	-1.97	-1.32	-0.65	-0.49	-0.36	-0.26	-0.20	-0.15
20	10	-2.35	-2.28	-1.62	-0.91	-0.71	-0.55	-0.42	-0.33	-0.26
50	10	-2.78	-2.70	-2.02	-1.28	-1.05	-0.86	-0.70	-0.58	-0.48
100	10	-3.08	-3.01	-2.31	-1.56	-1.32	-1.11	-0.94	-0.80	-0.69
500	10	-3.72	-3.64	-2.94	-2.18	-1.92	-1.69	-1.51	-1.35	-1.22

H1/A = 1.50   H2/A = 3.00   Z/H1 = 0.00

E1/E2	E2/E3	R/A=0.0	R/A=0.5	R/A=1.0	R/A=1.5	R/A=2.0	R/A=2.5	R/A=3.0	R/A=3.5	R/A=4.0
2	5	0.24	0.19	0.07	-0.03	-0.08	-0.08	-0.07	-0.06	-0.05
5	5	0.71	0.61	0.40	0.15	0.02	-0.04	-0.05	-0.06	-0.06
10	5	1.09	0.96	0.66	0.36	0.17	0.06	0.01	-0.02	-0.02
20	5	1.46	1.32	0.97	0.61	0.37	0.23	0.13	0.08	0.04
50	5	1.94	1.79	1.40	0.99	0.71	0.52	0.40	0.30	0.23
100	5	2.28	2.12	1.72	1.29	0.98	0.78	0.63	0.51	0.42
500	5	2.98	2.81	2.40	1.95	1.62	1.39	1.22	1.07	0.95
2	10	0.24	0.19	0.07	-0.03	-0.08	-0.08	-0.07	-0.06	-0.05
5	10	0.74	0.64	0.40	0.16	0.03	-0.02	-0.04	-0.05	-0.05
10	10	1.13	1.00	0.70	0.39	0.21	0.11	0.05	0.01	-0.01
20	10	1.54	1.40	1.05	0.69	0.44	0.30	0.21	0.15	0.10
50	10	2.06	1.90	1.51	1.10	0.82	0.63	0.50	0.40	0.32
100	10	2.43	2.27	1.86	1.44	1.12	0.92	0.77	0.65	0.55
500	10	3.19	3.02	2.60	2.15	1.82	1.59	1.41	1.27	1.14

H1/A = 1.50   H2/A = 3.00   Z/H1 = 1.00

E1/E2	E2/E3	R/A=0.0	R/A=0.5	R/A=1.0	R/A=1.5	R/A=2.0	R/A=2.5	R/A=3.0	R/A=3.5	R/A=4.0
2	5	-1.24	-1.22	-0.68	-0.13	-0.08	-0.06	-0.04	-0.03	-0.02
5	5	-1.56	-1.52	-0.92	-0.30	-0.20	-0.12	-0.07	-0.04	-0.03
10	5	-1.83	-1.78	-1.14	-0.48	-0.33	-0.22	-0.14	-0.09	-0.05
20	5	-2.13	-2.06	-1.40	-0.70	-0.52	-0.37	-0.26	-0.18	-0.13
50	5	-2.52	-2.45	-1.77	-1.04	-0.82	-0.64	-0.49	-0.38	-0.30
100	5	-2.82	-2.75	-2.05	-1.31	-1.07	-0.87	-0.71	-0.58	-0.48
500	5	-3.47	-3.39	-2.69	-1.93	-1.67	-1.45	-1.26	-1.11	-0.99
2	10	-1.28	-1.26	-0.72	-0.16	-0.12	-0.09	-0.07	-0.05	-0.04
5	10	-1.62	-1.58	-0.98	-0.36	-0.25	-0.17	-0.12	-0.09	-0.07
10	10	-1.92	-1.87	-1.23	-0.56	-0.41	-0.30	-0.22	-0.16	-0.12
20	10	-2.25	-2.18	-1.52	-0.80	-0.61	-0.46	-0.35	-0.27	-0.20
50	10	-2.66	-2.59	-1.91	-1.17	-0.95	-0.76	-0.62	-0.50	-0.41
100	10	-2.99	-2.91	-2.22	-1.47	-1.23	-1.03	-0.86	-0.73	-0.62
500	10	-3.68	-3.60	-2.89	-2.13	-1.87	-1.65	-1.47	-1.31	-1.18

TABLE 14

H1/A = 2.00   H2/A = 1.00   Z/H1 = 0.00

E1/E2	E2/E3	R/λ=0.0	R/λ=0.5	R/λ=1.0	R/λ=1.5	R/λ=2.0	R/λ=2.5	R/λ=3.0	R/λ=3.5	R/λ=4.0
2	5	0.29	0.26	0.18	0.10	0.05	0.02	0.00	-0.01	-0.01
5	5	0.63	0.58	0.44	0.30	0.19	0.11	0.07	0.04	0.02
10	5	0.88	0.81	0.65	0.46	0.32	0.22	0.16	0.11	0.08
20	5	1.10	1.02	0.84	0.63	0.47	0.35	0.27	0.21	0.16
50	5	1.35	1.27	1.07	0.85	0.66	0.53	0.44	0.36	0.31
100	5	1.51	1.43	1.23	1.00	0.81	0.67	0.57	0.49	0.42
500	5	1.85	1.77	1.56	1.32	1.13	0.98	0.87	0.79	0.72
2	10	0.34	0.30	0.23	0.15	0.09	0.05	0.03	0.02	0.01
5	10	0.71	0.65	0.52	0.37	0.25	0.18	0.13	0.09	0.07
10	10	0.98	0.91	0.74	0.56	0.41	0.31	0.24	0.19	0.15
20	10	1.21	1.14	0.95	0.74	0.57	0.45	0.37	0.30	0.25
50	10	1.47	1.39	1.19	0.97	0.78	0.65	0.55	0.47	0.41
100	10	1.64	1.56	1.35	1.12	0.93	0.79	0.69	0.61	0.54
500	10	1.98	1.90	1.69	1.45	1.25	1.11	1.00	0.91	0.84

H1/A = 2.00   H2/A = 1.00   Z/H1 = 1.00

E1/E2	E2/E3	R/λ=0.0	R/λ=0.5	R/λ=1.0	R/λ=1.5	R/λ=2.0	R/λ=2.5	R/λ=3.0	R/λ=3.5	R/λ=4.0
2	5	-1.26	-1.26	-0.73	-0.18	-0.14	-0.10	-0.07	-0.05	-0.03
5	5	-1.47	-1.45	-0.90	-0.33	-0.26	-0.20	-0.14	-0.10	-0.07
10	5	-1.64	-1.61	-1.05	-0.47	-0.38	-0.29	-0.22	-0.17	-0.12
20	5	-1.80	-1.77	-1.20	-0.61	-0.50	-0.41	-0.33	-0.26	-0.20
50	5	-2.00	-1.97	-1.40	-0.79	-0.68	-0.57	-0.48	-0.40	-0.34
100	5	-2.15	-2.12	-1.54	-0.93	-0.81	-0.70	-0.61	-0.52	-0.45
500	5	-2.46	-2.43	-1.85	-1.23	-1.12	-1.01	-0.90	-0.81	-0.74
2	10	-1.33	-1.32	-0.79	-0.25	-0.20	-0.16	-0.12	-0.09	-0.06
5	10	-1.56	-1.54	-0.99	-0.42	-0.34	-0.27	-0.21	-0.16	-0.12
10	10	-1.74	-1.72	-1.16	-0.57	-0.47	-0.39	-0.31	-0.25	-0.20
20	10	-1.94	-1.91	-1.34	-0.74	-0.61	-0.51	-0.43	-0.36	-0.30
50	10	-2.12	-2.10	-1.52	-0.91	-0.80	-0.69	-0.60	-0.51	-0.45
100	10	-2.27	-2.24	-1.67	-1.06	-0.94	-0.83	-0.73	-0.64	-0.57
500	10	-2.59	-2.56	-1.98	-1.37	-1.25	-1.13	-1.03	-0.94	-0.86

H1/A = 2.00   H2/A = 2.00   Z/H1 = 0.00

E1/E2	E2/E3	R/λ=0.0	R/λ=0.5	R/λ=1.0	R/λ=1.5	R/λ=2.0	R/λ=2.5	R/λ=3.0	R/λ=3.5	R/λ=4.0
2	5	0.21	0.18	0.12	0.04	-0.00	-0.02	-0.03	-0.03	-0.02
5	5	0.54	0.49	0.36	0.22	0.12	0.06	0.03	0.01	-0.00
10	5	0.79	0.72	0.56	0.39	0.25	0.16	0.11	0.07	0.05
20	5	1.02	0.95	0.77	0.57	0.41	0.30	0.22	0.17	0.13
50	5	1.29	1.21	1.02	0.80	0.62	0.49	0.40	0.33	0.28
100	5	1.47	1.39	1.19	0.96	0.77	0.64	0.54	0.46	0.40
500	5	1.84	1.75	1.55	1.31	1.11	0.97	0.86	0.78	0.71
2	10	0.23	0.20	0.13	0.06	0.01	-0.01	-0.01	-0.02	-0.02
5	10	0.58	0.53	0.40	0.26	0.16	0.09	0.06	0.04	0.03
10	10	0.86	0.79	0.63	0.45	0.32	0.23	0.17	0.13	0.10
20	10	1.10	1.03	0.85	0.64	0.48	0.37	0.29	0.24	0.20
50	10	1.40	1.32	1.12	0.90	0.72	0.59	0.50	0.42	0.37
100	10	1.59	1.51	1.30	1.08	0.89	0.75	0.65	0.57	0.51
500	10	1.96	1.88	1.67	1.44	1.24	1.09	0.99	0.90	0.83

H1/A = 2.00   H2/A = 2.00   Z/H1 = 1.00

E1/E2	E2/E3	R/λ=0.0	R/λ=0.5	R/λ=1.0	R/λ=1.5	R/λ=2.0	R/λ=2.5	R/λ=3.0	R/λ=3.5	R/λ=4.0
2	5	-1.20	-1.19	-0.67	-0.14	-0.11	-0.08	-0.06	-0.04	-0.03
5	5	-1.40	-1.38	-0.84	-0.28	-0.22	-0.16	-0.12	-0.08	-0.06
10	5	-1.57	-1.55	-0.99	-0.41	-0.33	-0.26	-0.20	-0.15	-0.11
20	5	-1.74	-1.72	-1.15	-0.56	-0.46	-0.37	-0.30	-0.23	-0.18
50	5	-1.96	-1.94	-1.36	-0.76	-0.65	-0.55	-0.46	-0.38	-0.32
100	5	-2.12	-2.09	-1.51	-0.91	-0.79	-0.68	-0.59	-0.51	-0.44
500	5	-2.46	-2.43	-1.85	-1.23	-1.11	-1.00	-0.89	-0.81	-0.73
2	10	-1.24	-1.23	-0.71	-0.18	-0.15	-0.12	-0.09	-0.07	-0.06
5	10	-1.46	-1.45	-0.90	-0.34	-0.28	-0.22	-0.18	-0.14	-0.11
10	10	-1.66	-1.64	-1.08	-0.50	-0.42	-0.34	-0.28	-0.22	-0.18
20	10	-1.84	-1.81	-1.24	-0.65	-0.55	-0.46	-0.38	-0.31	-0.26
50	10	-2.07	-2.04	-1.47	-0.87	-0.75	-0.65	-0.56	-0.48	-0.42
100	10	-2.24	-2.21	-1.63	-1.02	-0.91	-0.80	-0.70	-0.62	-0.54
500	10	-2.58	-2.55	-1.97	-1.36	-1.24	-1.12	-1.02	-0.93	-0.85

TABLE 15

H1/A = 2.00   H2/A = 3.00   Z/H1 = 0.00

E1/E2	E2/E3	R/λ=0.0	R/λ=0.5	R/λ=1.0	R/λ=1.5	R/λ=2.0	R/λ=2.5	R/λ=3.0	R/λ=3.5	R/λ=4.0
2	5	0.19	0.16	0.09	0.02	-0.02	-0.04	-0.04	-0.04	-0.03
5	5	0.51	0.45	0.33	0.19	0.09	0.04	0.01	-0.01	-0.01
10	5	0.74	0.68	0.52	0.34	0.21	0.13	0.08	0.04	0.02
20	5	0.97	0.90	0.72	0.52	0.36	0.25	0.18	0.14	0.10
50	5	1.25	1.17	0.98	0.76	0.58	0.45	0.36	0.30	0.25
100	5	1.44	1.36	1.16	0.93	0.74	0.61	0.51	0.44	0.38
500	5	1.82	1.74	1.53	1.30	1.10	0.96	0.85	0.77	0.69
2	10	0.19	0.16	0.09	0.02	-0.02	-0.04	-0.04	-0.04	-0.03
5	10	0.52	0.47	0.34	0.21	0.11	0.05	0.02	0.01	-0.00
10	10	0.78	0.72	0.56	0.38	0.25	0.16	0.11	0.08	0.06
20	10	1.02	0.95	0.77	0.57	0.41	0.31	0.23	0.18	0.15
50	10	1.33	1.25	1.06	0.84	0.66	0.53	0.44	0.37	0.32
100	10	1.54	1.46	1.26	1.03	0.84	0.70	0.61	0.53	0.47
500	10	1.94	1.86	1.65	1.42	1.22	1.08	0.97	0.88	0.81

H1/A = 2.00   H2/A = 3.00   Z/H1 = 1.00

E1/E2	E2/E3	R/λ=0.0	R/λ=0.5	R/λ=1.0	R/λ=1.5	R/λ=2.0	R/λ=2.5	R/λ=3.0	R/λ=3.5	R/λ=4.0
2	5	-1.16	-1.16	-0.64	-0.11	-0.09	-0.06	-0.05	-0.03	-0.03
5	5	-1.36	-1.35	-0.81	-0.25	-0.19	-0.14	-0.10	-0.07	-0.05
10	5	-1.53	-1.51	-0.96	-0.30	-0.30	-0.23	-0.18	-0.13	-0.10
20	5	-1.71	-1.69	-1.12	-0.53	-0.44	-0.35	-0.28	-0.22	-0.18
50	5	-1.93	-1.90	-1.33	-0.73	-0.62	-0.52	-0.43	-0.36	-0.30
100	5	-2.09	-2.06	-1.49	-0.88	-0.77	-0.66	-0.56	-0.48	-0.42
500	5	-2.44	-2.41	-1.83	-1.22	-1.10	-0.99	-0.88	-0.80	-0.72
2	10	-1.20	-1.19	-0.67	-0.15	-0.12	-0.09	-0.07	-0.06	-0.05
5	10	-1.41	-1.40	-0.85	-0.30	-0.24	-0.19	-0.14	-0.11	-0.09
10	10	-1.58	-1.56	-1.01	-0.43	-0.35	-0.28	-0.22	-0.17	-0.14
20	10	-1.77	-1.75	-1.18	-0.59	-0.50	-0.41	-0.33	-0.27	-0.22
50	10	-2.01	-1.99	-1.42	-0.82	-0.71	-0.60	-0.52	-0.44	-0.38
100	10	-2.20	-2.17	-1.59	-0.98	-0.87	-0.76	-0.66	-0.58	-0.51
500	10	-2.57	-2.54	-1.96	-1.34	-1.22	-1.11	-1.00	-0.92	-0.84

Appendix B

RATIO OF RADIAL STRESS TO SURFACE PRESSURE—POISSON'S RATIO EQUAL TO 0.4 IN ALL THREE LAYERS[a]

TABLE 16

H1/A = 0.25   H2/A = 1.00   Z/H1 = 0.00

E1/E2	E2/E3	R/A=0.0	R/A=0.5	R/A=1.0	R/A=1.5	R/A=2.0	R/A=2.5	R/A=3.0	R/A=3.5	R/A=4.0
2	5	-0.72	-0.57	-0.53	-0.36	-0.14	-0.04	-0.01	0.02	0.03
5	5	-0.00	0.17	-0.43	-0.69	-0.32	-0.15	-0.07	-0.03	-0.00
10	5	1.43	1.45	-0.09	-1.00	-0.56	-0.31	-0.18	-0.11	-0.07
20	5	4.08	3.69	0.73	-1.27	-0.93	-0.59	-0.39	-0.27	-0.19
50	5	9.96	8.63	3.11	-1.05	-1.45	-1.20	-0.92	-0.71	-0.55
100	5	16.22	14.07	6.37	0.13	-1.42	-1.64	-1.50	-1.28	-1.07
500	5	35.13	31.31	19.35	8.33	3.03	0.24	-1.25	-2.00	-2.34
2	10	-0.89	-0.73	-0.66	-0.46	-0.20	-0.08	-0.02	0.02	0.04
5	10	-0.12	0.06	-0.54	-0.78	-0.39	-0.20	-0.10	-0.04	-0.01
10	10	1.48	1.49	-0.08	-1.03	-0.60	-0.35	-0.22	-0.14	-0.09
20	10	4.46	4.03	0.98	-1.12	-0.88	-0.59	-0.42	-0.31	-0.24
50	10	11.12	9.72	4.00	-0.41	-1.06	-1.00	-0.85	-0.72	-0.62
100	10	18.27	16.00	8.04	1.43	-0.50	-1.06	-1.18	-1.16	-1.09
500	10	39.80	35.86	23.58	12.08	6.21	2.83	0.76	-0.52	-1.33

H1/A = 0.25   H2/A = 1.00   Z/H1 = 1.00

E1/E2	E2/E3	R/A=0.0	R/A=0.5	R/A=1.0	R/A=1.5	R/A=2.0	R/A=2.5	R/A=3.0	R/A=3.5	R/A=4.0
2	5	-1.79	-1.74	-0.91	-0.16	-0.04	0.04	0.07	0.08	0.08
5	5	-2.95	-2.86	-1.36	-0.06	0.01	0.07	0.11	0.12	0.12
10	5	-4.55	-4.32	-1.84	0.08	0.14	0.16	0.18	0.18	0.18
20	5	-7.19	-6.50	-2.74	0.20	0.40	0.36	0.34	0.31	0.28
50	5	-12.76	-11.19	-5.08	-0.14	0.79	0.87	0.79	0.70	0.60
100	5	-18.67	-16.30	-8.19	-1.33	0.70	1.24	1.30	1.21	1.07
500	5	-36.57	-32.67	-20.61	-9.30	-3.73	-0.74	0.91	1.78	2.20
2	10	-2.20	-2.12	-1.21	-0.35	-0.16	-0.02	0.05	0.09	0.11
5	10	-3.57	-3.43	-1.78	-0.37	-0.19	-0.03	0.07	0.13	0.15
10	10	-5.38	-5.05	-2.46	-0.35	-0.13	0.01	0.12	0.18	0.20
20	10	-8.35	-7.58	-3.62	-0.43	0.01	0.14	0.23	0.29	0.32
50	10	-14.63	-12.94	-6.55	-1.25	0.05	0.42	0.56	0.62	0.64
100	10	-21.31	-18.82	-10.38	-3.06	-0.56	0.41	0.82	0.99	1.04
500	10	-41.53	-37.50	-25.10	-13.29	-7.11	-3.49	-1.24	0.19	1.10

H1/A = 0.25   H2/A = 2.00   Z/H1 = 0.00

E1/E2	E2/E3	R/A=0.0	R/A=0.5	R/A=1.0	R/A=1.5	R/A=2.0	R/A=2.5	R/A=3.0	R/A=3.5	R/A=4.0
2	5	-0.61	-0.48	-0.48	-0.37	-0.17	-0.09	-0.06	-0.03	-0.01
5	5	-0.07	0.11	-0.48	-0.74	-0.36	-0.20	-0.12	-0.07	-0.04
10	5	1.03	1.10	-0.31	-1.12	-0.60	-0.32	-0.20	-0.13	-0.09
20	5	3.14	2.86	0.18	-1.53	-0.99	-0.55	-0.33	-0.22	-0.15
50	5	7.91	6.79	1.79	-1.75	-1.65	-1.09	-0.69	-0.45	-0.33
100	5	13.11	11.22	4.21	-1.18	-1.96	-1.63	-1.19	-0.84	-0.62
500	5	30.05	26.49	15.22	5.17	0.91	-0.94	-1.66	-1.86	-1.83
2	10	-0.72	-0.58	-0.58	-0.46	-0.25	-0.16	-0.10	-0.06	-0.03
5	10	-0.20	-0.02	-0.60	-0.84	-0.45	-0.28	-0.19	-0.12	-0.08
10	10	0.92	0.99	-0.43	-1.23	-0.70	-0.41	-0.27	-0.19	-0.14
20	10	3.08	2.80	0.11	-1.60	-1.06	-0.62	-0.39	-0.28	-0.21
50	10	8.06	6.93	1.91	-1.66	-1.60	-1.08	-0.69	-0.48	-0.36
100	10	13.58	11.67	4.61	-0.84	-1.70	-1.45	-1.07	-0.77	-0.59
500	10	32.04	28.43	17.06	6.85	2.39	0.32	-0.62	-1.03	-1.19

H1/A = 0.25   H2/A = 2.00   Z/H1 = 1.00

E1/E2	E2/E3	R/A=0.0	R/A=0.5	R/A=1.0	R/A=1.5	R/A=2.0	R/A=2.5	R/A=3.0	R/A=3.5	R/A=4.0
2	5	-1.34	-1.36	-0.69	-0.10	-0.11	-0.07	-0.05	-0.02	0.01
5	5	-2.23	-2.25	-0.98	0.02	-0.09	-0.11	-0.07	-0.03	0.00
10	5	-3.52	-3.40	-1.33	0.22	0.01	-0.09	-0.07	-0.03	0.00
20	5	-5.69	-5.21	-1.95	0.45	0.27	0.06	-0.01	-0.00	0.02
50	5	-10.32	-9.02	-3.60	0.53	0.80	0.49	0.26	0.15	0.15
100	5	-15.33	-13.27	-5.96	-0.09	1.06	0.99	0.73	0.53	0.41
500	5	-31.61	-27.97	-16.63	-6.31	-1.80	0.25	1.13	1.46	1.53
2	10	-1.49	-1.51	-0.83	-0.23	-0.21	-0.16	-0.10	-0.06	-0.02
5	10	-2.50	-2.50	-1.19	-0.17	-0.25	-0.22	-0.16	-0.10	-0.05
10	10	-3.84	-3.71	-1.61	-0.03	-0.10	-0.24	-0.19	-0.13	-0.07
20	10	-6.11	-5.61	-2.31	0.14	0.02	-0.16	-0.18	-0.13	-0.07
50	10	-10.97	-9.65	-4.17	0.04	0.41	0.19	0.03	-0.01	0.01
100	10	-16.27	-14.19	-6.81	-0.82	0.45	0.50	0.35	0.25	0.10
500	10	-33.96	-30.27	-18.82	-8.32	-3.58	-1.28	-0.15	0.43	0.72

[a] A negative sign indicates compression.
Z/H1 = 0 indicates tables of stresses at the interface.
Z/H1 = 1 indicates tables of stresses at the surface.

TABLE 17

H1/A = 0.? H2/A = 1.00 Z/H1 = 1.00

E1/E2	E2/E'	R/A=0.0	R/A=0.5	R/A=1.0	R/A=1.5	R/A=2.0	R/A=2.5	R/A=3.0	R/A=3.5	R/A=4.0
2	5	-0.41	-0.41	-0.43	-0.33	-0.16	-0.10	-0.07	-0.05	-0.03
5	5	-0.00	0.11	-0.43	-0.70	-0.34	-0.20	-0.13	-0.08	-0.07
10	5	1.0	1.11	-0.70	1.11	-0.60	-0.33	-0.21	-0.15	-0.11
20	5	3.03	2.74	0.01	-1.58	-1.02	-0.56	-0.34	-0.23	-0.17
50	5	7.47	6.78	1.46	-1.99	-1.73	-1.16	-0.70	-0.44	-0.30
100	5	12.29	10.42	2.54	-1.68	-2.27	-1.79	-1.22	-0.80	-0.54
500	5	27.79	24.31	13.26	3.54	-0.35	-1.80	-2.17	-2.07	-1.81
2	10	-0.59	-0.47	-0.48	-0.38	-0.21	-0.14	-0.10	-0.08	-0.06
5	10	-0.03	0.08	-0.51	-0.78	-0.42	-0.27	-0.19	-0.15	-0.11
10	10	0.94	1.02	-0.40	-1.20	-0.69	-0.41	-0.28	-0.22	-0.17
20	10	2.93	2.66	-0.00	-1.68	-1.11	-0.65	-0.42	-0.30	-0.24
50	10	7.45	6.36	1.43	-2.02	-1.82	-1.20	-0.74	-0.48	-0.35
100	10	12.40	10.52	3.63	-1.60	-2.21	-1.75	-1.20	-0.80	-0.55
500	10	28.67	25.17	14.09	4.48	0.35	-1.19	-1.64	-1.62	-1.45

H1/A = 0.25 H2/A = 3.00 Z/H1 = 1.00

E1/E2	E2/E3	R/A=0.0	R/A=0.5	R/A=1.0	R/A=1.5	R/A=2.0	R/A=2.5	R/A=3.0	R/A=3.5	R/A=4.0
2	5	-1.20	-1.23	-0.59	-0.03	-0.07	-0.07	-0.06	-0.04	-0.03
5	5	-2.01	-2.04	-0.82	0.13	-0.04	-0.09	-0.09	-0.07	-0.05
10	5	-3.22	-3.12	-1.10	0.36	0.09	-0.07	-0.10	-0.09	-0.07
20	5	-5.26	-4.80	-1.62	0.67	0.39	0.07	-0.05	-0.08	-0.07
50	5	-9.60	-8.35	-3.05	0.91	1.02	0.57	0.23	0.06	0.00
100	5	-14.25	-12.35	-5.11	0.53	1.43	1.14	0.71	0.39	0.21
500	5	-29.25	-25.69	-14.60	-4.63	-0.52	1.09	1.59	1.59	1.42
2	10	-1.28	-1.14	-0.67	-.10	-0.13	-0.12	-0.10	-0.08	-0.06
5	10	-2.15	-2.17	-0.94	0.01	-0.14	-0.19	-0.17	-0.14	-0.11
10	10	-3.40	-3.29	-1.27	0.21	0.06	-0.19	-0.21	-0.18	-0.15
20	10	-5.49	-5.03	-1.83	0.47	0.21	-0.09	-0.19	-0.20	-0.17
50	10	-9.93	-8.67	-3.36	0.63	0.77	0.34	0.04	-0.10	-0.14
100	10	-14.70	-12.70	-5.54	0.14	1.08	0.83	0.44	0.17	0.02
500	10	-30.45	-26.87	-15.74	-5.70	-1.51	0.21	0.82	0.93	0.86

H1/A = 0.50 H2/A = 1.00 Z/H1 = 0.00

E1/E2	E2/E3	R/A=0.0	R/A=0.5	R/A=1.0	R/A=1.5	R/A=2.0	R/A=2.5	R/A=3.0	R/A=3.5	R/A=4.0
2	5	-0.00	0.01	-0.21	-0.30	-0.17	-0.09	-0.05	-0.03	-0.02
5	5	1.12	0.98	0.18	-0.37	-0.31	-0.22	-0.15	-0.11	-0.08
10	5	2.52	2.18	0.80	-0.25	-0.38	-0.34	-0.28	-0.22	-0.17
20	5	4.37	3.81	1.81	0.17	-0.16	-0.40	-0.41	-0.37	-0.32
50	5	7.31	6.47	3.76	1.34	0.32	-0.17	-0.40	-0.49	-0.52
100	5	9.72	8.73	5.60	2.70	1.25	0.43	-0.06	-0.34	-0.50
500	5	15.26	14.07	10.42	6.83	4.69	3.23	2.17	1.39	0.80
2	10	-0.02	-0.01	-0.23	-0.32	-0.19	-0.11	-0.06	-0.04	-0.02
5	10	1.22	1.07	0.25	-0.32	-0.28	-0.17	-0.15	-0.12	-0.09
10	10	2.79	2.44	1.02	-0.08	-0.26	-0.26	-0.24	-0.21	-0.18
20	10	4.88	4.30	2.25	0.53	-0.01	-0.21	-0.28	-0.29	-0.29
50	10	8.22	7.36	4.58	2.06	0.92	0.32	-0.03	-0.22	-0.34
100	10	10.93	9.91	6.73	3.72	2.15	1.20	0.79	0.17	-0.11
500	10	16.97	15.77	12.07	8.41	6.20	4.64	3.47	2.50	1.87

H1/A = 0.50 H2/A = 1.00 Z/H1 = 1.00

E1/E2	E2/E3	R/A=0.0	R/A=0.5	R/A=1.0	R/A=1.5	R/A=2.0	R/A=2.5	R/A=3.0	R/A=3.5	R/A=4.0
2	5	-1.71	-1.59	-0.85	-0.16	-0.05	0.01	0.04	0.06	0.06
5	5	-2.81	-2.54	-1.32	-0.23	-0.00	0.07	0.09	0.11	0.11
10	5	-4.08	-3.62	-1.93	-0.41	0.00	0.14	0.18	0.19	0.18
20	5	-5.71	-5.06	-2.86	-0.85	-0.13	0.15	0.26	0.30	0.30
50	5	-8.31	-7.43	-4.64	-1.97	-0.75	-0.12	0.19	0.37	0.45
100	5	-10.48	-9.47	-6.33	-3.24	-1.64	-0.71	-0.16	0.19	0.40
500	5	-15.64	-14.46	-10.86	-7.17	-4.95	-3.44	-2.36	-1.53	-0.92
2	10	-1.97	-1.85	-1.08	-0.33	-0.16	-0.06	0.00	0.04	0.07
5	10	-3.23	-2.94	-1.66	-0.49	-0.19	-0.05	0.02	0.07	0.10
10	10	-4.64	-4.16	-2.40	-0.79	-0.28	-0.06	0.05	0.12	0.16
20	10	-6.47	-5.79	-3.52	-1.40	-0.56	-0.16	0.04	0.16	0.23
50	10	-9.39	-8.48	-5.61	-2.82	-1.47	-0.70	-0.25	0.04	0.10
100	10	-11.81	-10.77	-7.56	-4.36	-2.63	-1.56	-0.86	-0.37	-0.03
500	10	-17.38	-16.18	-12.54	-8.79	-6.48	-4.87	-3.68	-2.74	-2.00

TABLE 18

H1/A = 0.50   H2/A = 2.00   Z/H1 = 0.00

E1/E2	E2/E3	R/A=0.0	R/A=0.5	R/A=1.0	R/A=1.5	R/A=2.0	R/A=2.5	R/A=3.0	R/A=3.5	R/A=4.0
2	5	-0.06	-0.05	-0.26	-0.34	-0.20	-0.12	-0.07	-0.04	-0.03
5	5	0.86	0.74	-0.01	-0.49	-0.37	-0.24	-0.15	-0.10	-0.07
10	5	2.02	1.72	0.44	-0.48	-0.50	-0.37	-0.26	-0.18	-0.13
20	5	3.59	3.08	1.22	-0.24	-0.52	-0.49	-0.40	-0.30	-0.23
50	5	6.19	5.41	2.85	0.65	-0.15		-0.49	-0.46	-0.41
100	5	8.45	7.51	4.53	1.82	0.60	-0.00	-0.30	-0.43	-0.47
500	5	14.17	13.00	9.42	5.93	3.92	2.59	1.67	1.01	0.54
2	10	-0.12	-0.10	-0.30	-0.38	-0.24	-0.15	-0.09	-0.06	-0.04
5	10	0.83	0.71	-0.04	-0.52	-0.40	-0.26	-0.18	-0.12	-0.09
10	10	2.04	1.74	0.46	-0.48	-0.46	-0.37	-0.27	-0.19	-0.14
20	10	3.70	3.18	1.32	-0.16	-0.46	-0.44	-0.36	-0.28	-0.22
50	10	6.51	5.72	3.15	0.92	0.09	-0.23	-0.33	-0.34	-0.32
100	10	9.00	8.06	5.05	2.31	1.04	0.38	0.16	-0.15	-0.24
500	10	15.37	14.20	10.59	7.07	5.01	3.62	2.63	1.90	1.34

H1/A = 0.50   H2/A = 2.00   Z/H1 = 1.00

E1/E2	E2/E3	R/A=0.0	R/A=0.5	R/A=1.0	R/A=1.5	R/A=2.0	R/A=2.5	R/A=3.0	R/A=3.5	R/A=4.0
2	5	-1.38	-1.31	-0.67	-0.09	-0.06	-0.05	-0.04	-0.02	-0.00
5	5	-2.33	-2.12	-1.03	-0.10	-0.00	-0.01	-0.03	-0.01	0.01
10	5	-3.43	-3.04	-1.50	-0.19	0.05	0.06	0.03	0.02	0.02
20	5	-4.84	-4.26	-2.24	-0.48	0.02	0.13	0.14	0.13	0.11
50	5	-7.21	-6.39	-3.77	-1.34	-0.36	0.05	0.20	0.26	0.27
100	5	-9.29	-8.33	-5.33	-2.45	-1.09	-0.37	-0.01	0.20	0.30
500	5	-14.64	-13.48	-9.95	-6.37	-4.27	-2.88	-1.93	-1.22	-0.71
2	10	-1.51	-1.44	-0.79	-0.20	-0.14	-0.11	-0.09	-0.06	-0.03
5	10	-2.50	-2.28	-1.18	-0.23	-0.11	-0.10	-0.10	-0.07	-0.04
10	10	-3.65	-3.26	-1.71	-0.37	-0.10	-0.06	-0.06	-0.05	-0.03
20	10	-5.17	-4.58	-2.54	-0.73	-0.19	-0.04	-0.01	0.01	0.02
50	10	-7.72	-6.89	-4.24	-1.77	-0.75	-0.28	-0.08	0.03	0.08
100	10	-1.00	-9.03	-6.00	-3.08	-1.65	-0.88	-0.45	-0.17	-0.01
500	10	-15.92	-14.76	-11.20	-7.57	-5.42	-3.97	-2.94	-2.16	-1.57

H1/A = 0.50   H2/A = 3.00   Z/H1 = 0.00

E1/E2	E2/E3	R/A=0.0	R/A=0.5	R/A=1.0	R/A=1.5	R/A=2.0	R/A=2.5	R/A=3.0	R/A=3.5	R/A=4.0
2	5	-0.04	-0.03	-0.24	-0.33	-0.20	-0.12	-0.07	-0.05	-0.04
5	5	0.83	0.71	-0.03	-0.51	-0.38	-0.25	-0.16	-0.11	-0.07
10	5	1.92	1.62	0.36	-0.55	-0.54	-0.40	-0.27	-0.18	-0.13
20	5	3.37	2.87	1.04	-0.39	-0.63	-0.56	-0.43	-0.31	-0.22
50	5	5.76	5.00	2.48	0.34	-0.39	-1.07	-0.59	-0.51	-0.42
100	5	7.86	6.93	4.00	1.36	0.23	-0.29	-0.50	-0.55	-0.53
500	5	13.35	12.20	8.65	5.22	3.29	2.04	1.21	0.64	0.25
2	10	-0.08	-0.06	-0.28	-0.37	-0.23	-0.15	-0.10	-0.07	-0.06
5	10	-0.79	0.67	-0.06	-0.54	-0.42	-0.28	-0.19	-0.14	-0.10
10	10	1.90	1.60	0.33	-0.58	-0.57	-0.43	-0.30	-0.21	-0.15
20	10	3.39	2.88	1.05	-0.38	-0.62	-0.56	-0.43	-0.32	-0.23
50	10	5.88	5.11	2.59	0.44	-0.20	-1.07	-0.53	-0.46	-0.38
100	10	8.17	7.24	4.30	1.59	0.44	-0.10	-0.33	-0.40	-0.40
500	10	14.14	12.98	9.42	5.97	4.01	2.73	1.85	1.24	0.80

H1/A = 0.50   H2/A = 3.00   Z/H1 = 1.00

E1/E2	E2/E3	R/A=0.0	R/A=0.5	R/A=1.0	R/A=1.5	R/A=2.0	R/A=2.5	R/A=3.0	R/A=3.5	R/A=4.0
2	5	-1.27	-1.21	-0.59	-0.03	-0.03	-0.04	-0.04	-0.03	-0.03
5	5	-2.16	-1.96	-0.89	0.00	0.09	0.02	-0.02	-0.03	-0.03
10	5	-3.19	-2.81	-1.31	-0.04	0.15	0.11	0.04	0.01	-0.01
20	5	-4.52	-3.91	-1.98	-0.26	0.17	0.22	0.16	0.11	0.06
50	5	-6.72	-5.92	-3.35	-0.99	-0.11	0.21	0.28	0.27	0.23
100	5	-8.66	-7.72	-4.78	-1.98	-0.76	-0.10	0.17	0.29	0.32
500	5	-13.85	-12.71	-9.22	-5.69	-3.67	-2.36	-1.50	-0.88	-0.45
2	10	-1.34	-1.28	-0.65	-0.09	-0.08	-0.09	-0.08	-0.07	-0.05
5	10	-2.26	-2.05	-0.99	-0.06	-0.02	-0.05	-0.08	-0.08	-0.07
10	10	-3.32	-2.94	-1.43	-0.07	0.13		-0.04	-0.06	-0.07
20	10	-4.69	-4.13	-2.14	-0.41	0.03	0.10	0.05	0.01	-0.03
50	10	-6.99	-6.19	-3.61	-1.24	-0.32	0.01	0.10	0.11	0.09
100	10	-9.06	-8.11	-5.16	-2.34	-1.05	-0.41	-0.11	0.04	0.10
500	10	-14.73	-13.58	-10.07	-6.52	-4.47	-3.13	-2.22	-1.56	-1.08

TABLE 19

H1/A = 1.00   H2/A = 1.00   Z/H1 = 0.00

E1/E2	E2/E3	R/A=0.0	R/A=0.5	R/A=1.0	R/A=1.5	R/A=2.0	R/A=2.5	R/A=3.0	R/A=3.5	R/A=4.0
2	5	0.37	0.26	0.07	-0.08	-0.10	-0.08	-0.06	-0.05	-0.04
5	5	1.09	0.93	0.49	0.11	-0.04	-0.08	-0.09	-0.09	-0.09
10	5	1.79	1.56	0.94	0.38	0.12	-0.00	-0.06	-0.10	-0.11
20	5	2.51	2.24	1.49	0.78	0.40	0.19	0.06	-0.03	-0.04
50	5	3.45	3.13	2.26	1.42	0.91	0.60	0.38	0.22	0.10
100	5	4.10	3.76	2.85	1.94	1.37	1.00	0.73	0.51	0.35
500	5	5.46	5.10	4.14	3.16	2.52	2.07	1.72	1.44	1.20
2	10	0.40	0.33	0.13	-0.02	-0.05	-0.09	-0.05	-0.04	-0.04
5	10	1.22	1.06	0.61	0.21	0.05	-0.01	-0.04	-0.06	-0.06
10	10	2.00	1.77	1.14	0.56	0.28	0.13	0.08	0.03	-0.05
20	10	2.81	2.53	1.77	1.04	0.63	0.39	0.24	0.13	0.05
50	10	3.83	3.51	2.63	1.77	1.24	0.90	0.66	0.47	0.33
100	10	4.63	4.19	4.27	2.35	1.76	1.37	1.07	0.84	0.65
500	10	5.94	5.58	4.61	3.63	2.98	2.52	2.17	1.87	1.62

H1/A = 1.00   H2/A = 1.00   Z/H1 = 1.00

E1/E2	E2/E3	R/A=0.0	R/A=0.5	R/A=1.0	R/A=1.5	R/A=2.0	R/A=2.5	R/A=3.0	R/A=3.5	R/A=4.0
2	5	-1.35	-1.29	-0.76	-0.21	-0.11	-0.04	-0.01	0.02	0.03
5	5	-1.93	-1.81	-1.12	-0.42	-0.21	-0.08	-0.01	0.03	0.05
10	5	-2.46	-2.30	-1.51	-0.68	-0.37	-0.18	-0.06	0.01	0.03
20	5	-3.04	-2.84	-1.96	-1.04	-0.63	-0.36	-0.23	-0.07	0.01
50	5	-3.82	-3.60	-2.64	-1.61	-1.11	-0.75	-0.50	-0.31	-0.18
100	5	-4.40	-4.16	-3.16	-2.09	-1.54	-1.13	-0.83	-0.60	-0.42
500	5	-5.66	-5.41	-4.37	-3.25	-2.63	-2.16	-1.79	-1.50	-1.25
2	10	-1.51	-1.45	-0.90	-0.33	-0.20	-0.12	-0.06	-0.03	0.01
5	10	-2.15	-2.03	-1.32	-0.60	-0.36	-0.22	-0.13	-0.04	0.00
10	10	-2.78	-2.61	-1.80	-0.96	-0.58	-0.35	-0.20	-0.10	-0.03
20	10	-3.38	-3.18	-2.28	-1.34	-0.90	-0.60	-0.39	-0.25	-0.14
50	10	-4.22	-4.00	-3.03	-1.99	-1.46	-1.07	-0.79	-0.58	-0.41
100	10	-4.84	-4.60	-3.59	-2.51	-1.94	-1.51	-1.18	-0.93	-0.73
500	10	-6.13	-5.88	-4.85	-3.71	-3.09	-2.61	-2.23	-1.92	-1.67

H1/A = 1.00   H2/A = 2.00   Z/H1 = 0.00

E1/E2	E2/E3	R/A=0.0	R/A=0.5	R/A=1.0	R/A=1.5	R/A=2.0	R/A=2.5	R/A=3.0	R/A=3.5	R/A=4.0
2	5	0.23	0.16	-0.02	-0.14	-0.08	-0.11	-0.08	-0.05	-0.04
5	5	0.89	0.74	0.32	-0.03	-0.13	-0.18	-0.12	-0.10	-0.08
10	5	1.55	1.34	0.75	0.19	-0.02	-0.10	-0.12	-0.12	-0.11
20	5	2.20	1.93	1.21	0.54	0.21	0.04	-0.04	-0.08	-0.11
50	5	3.13	2.82	1.98	1.16	0.69	0.42	0.24	0.12	0.03
100	5	3.83	3.50	2.59	1.71	1.16	0.82	0.58	0.39	0.26
500	5	5.32	4.96	4.00	3.03	2.39	1.96	1.62	1.35	1.12
2	10	0.22	0.16	-0.02	-0.15	-0.15	-0.11	-0.08	-0.06	-0.04
5	10	0.92	0.76	0.34	-0.00	-0.11	-0.19	-0.10	-0.09	-0.07
10	10	1.60	1.39	0.80	0.27	0.05	-0.05	-0.07	-0.08	-0.08
20	10	2.33	2.06	1.34	0.66	0.32	0.15	0.06	-0.00	-0.04
50	10	3.37	3.05	2.20	1.38	0.90	0.61	0.42	0.28	0.18
100	10	4.14	3.81	2.90	2.00	1.45	1.09	0.84	0.64	0.49
500	10	5.75	5.39	4.42	3.45	2.81	2.36	2.02	1.74	1.50

H1/A = 1.00   H2/A = 2.00   Z/H1 = 1.00

E1/E2	E2/E3	R/A=0.0	R/A=0.5	R/A=1.0	R/A=1.5	R/A=2.0	R/A=2.5	R/A=3.0	R/A=3.5	R/A=4.0
2	5	-1.19	-1.15	-0.65	-0.15	-0.08	-0.05	-0.03	-0.02	-0.01
5	5	-1.72	-1.61	-0.96	-0.31	-0.15	-0.07	-0.03	-0.01	0.01
10	5	-2.22	-2.07	-1.31	-0.54	-0.28	-0.13	-0.06	-0.01	0.02
20	5	-2.76	-2.58	-1.73	-0.84	-0.48	-0.26	-0.13	-0.05	0.00
50	5	-3.55	-3.34	-2.40	-1.40	-0.93	-0.61	-0.39	-0.24	-0.13
100	5	-4.17	-3.93	-2.95	-1.90	-1.37	-0.99	-0.71	-0.51	-0.36
500	5	-5.53	-5.28	-4.26	-3.14	-2.53	-2.06	-1.71	-1.42	-1.19
2	10	-1.27	-1.22	-0.72	-0.21	-0.14	-0.10	-0.07	-0.05	-0.04
5	10	-1.82	-1.72	-1.06	-0.40	-0.23	-0.13	-0.09	-0.06	-0.04
10	10	-2.35	-2.20	-1.44	-0.66	-0.38	-0.23	-0.14	-0.08	-0.05
20	10	-2.96	-2.77	-1.92	-1.02	-0.65	-0.42	-0.27	-0.17	-0.10
50	10	-3.83	-3.61	-2.67	-1.67	-1.18	-0.85	-0.61	-0.44	-0.32
100	10	-4.51	-4.27	-3.29	-2.22	-1.68	-1.29	-1.00	-0.78	-0.60
500	10	-5.97	-5.72	-4.69	-3.57	-2.95	-2.48	-2.11	-1.82	-1.57

TABLE 20

H1/A = 1.00   H2/H3 = 3.00   Z/H1 = 0.00

E1/E2	E2/E3	R/A=0.0	R/A=0.5	R/A=1.0	R/A=1.5	R/A=2.0	R/A=2.5	R/A=3.0	R/A=3.5	R/A=4.0
2	5	0.21	0.15	-0.03	-0.16	-0.16	-0.12	-0.08	-0.06	-0.04
5	5	0.83	0.68	0.27	-0.07	-0.17	-0.18	-0.14	-0.11	-0.09
10	5	1.41	1.20	0.62	0.11	-0.09	-0.15	-0.15	-0.14	-0.13
20	5	2.05	1.79	1.07	0.42	0.10	-0.04	-0.10	-0.13	-0.14
50	5	2.99	2.68	1.84	1.04	0.59	0.29	0.13	0.03	-0.04
100	5	3.63	3.30	2.41	1.53	1.00	0.67	0.45	0.29	0.17
500	5	5.17	4.81	3.85	2.89	2.26	1.83	1.50	1.24	1.02
2	10	0.20	0.14	-0.04	-0.17	-0.17	-0.13	-0.09	-0.07	-0.05
5	10	0.83	0.68	0.27	-0.07	-0.17	-0.18	-0.14	-0.12	-0.09
10	10	1.44	1.22	0.64	0.14	-0.07	-0.13	-0.14	-0.13	-0.12
20	10	2.13	1.87	1.16	0.50	0.16	0.01	-0.06	-0.09	-0.10
50	10	3.08	2.77	1.93	1.13	0.67	0.41	0.25	0.13	0.06
100	10	3.88	3.55	2.65	1.77	1.24	0.90	0.67	0.50	0.37
500	10	5.54	5.18	4.22	3.25	2.62	2.18	1.85	1.57	1.35

H1/A = 1.00   H2/A = 3.00   Z/H1 = 1.00

E1/E2	E2/E3	R/A=0.0	R/A=0.5	R/A=1.0	R/A=1.5	R/A=2.0	R/A=2.5	R/A=3.0	R/A=3.5	R/A=4.0
2	5	-1.12	-1.08	-0.59	-0.10	-0.05	-0.03	-0.02	-0.02	-0.02
5	5	-1.61	-1.51	-0.87	-0.24	-0.09	-0.03	-0.00	0.00	0.00
10	5	-2.08	-1.93	-1.19	-0.43	-0.19	-0.06	-0.01	0.02	0.02
20	5	-2.61	-2.43	-1.59	-0.72	-0.38	-0.18	-0.07	-0.01	0.02
50	5	-3.37	-3.16	-2.23	-1.25	-0.80	-0.50	-0.30	-0.17	-0.08
100	5	-3.98	-3.75	-2.78	-1.74	-1.20	-0.86	-0.60	-0.42	-0.28
500	5	-5.40	-5.15	-4.13	-3.01	-2.41	-1.95	-1.60	-1.33	-1.10
2	10	-1.17	-1.13	-0.64	-0.14	-0.06	-0.07	-0.06	-0.05	-0.04
5	10	-1.68	-1.58	-0.94	-0.30	-0.15	-0.08	-0.05	-0.04	-0.04
10	10	-2.17	-2.03	-1.28	-0.52	-0.27	-0.14	-0.08	-0.05	-0.04
20	10	-2.74	-2.56	-1.72	-0.86	-0.50	-0.30	-0.18	-0.11	-0.07
50	10	-3.58	-3.37	-2.44	-1.45	-0.99	-0.68	-0.48	-0.34	-0.24
100	10	-4.23	-4.00	-3.02	-1.98	-1.45	-1.08	-0.81	-0.62	-0.47
500	10	-5.78	-5.53	-4.51	-3.39	-2.78	-2.32	-1.96	-1.67	-1.44

H1/A = 1.50   H2/A = 1.00   Z/H1 = 0.00

E1/E2	E2/E3	R/A=0.0	R/A=0.5	R/A=1.0	R/A=1.5	R/A=2.0	R/A=2.5	R/A=3.0	R/A=3.5	R/A=4.0
2	5	0.30	0.25	0.14	0.03	-0.02	-0.07	-0.06	-0.04	-0.05
5	5	0.77	0.69	0.43	0.23	0.09	0.03	-0.01	-0.03	-0.04
10	5	1.19	1.06	0.76	0.46	0.27	0.16	0.07	0.02	0.01
20	5	1.51	1.37	1.03	0.69	0.44	0.23	0.20	0.12	0.07
50	5	1.94	1.79	1.41	1.02	0.74	0.55	0.42	0.32	0.24
100	5	2.27	2.11	1.72	1.30	1.01	0.81	0.66	0.54	0.43
500	5	2.82	2.65	2.25	1.82	1.50	1.28	1.12	0.98	0.87
2	10	0.36	0.31	0.19	0.09	0.03	0.00	-0.00	-0.01	-0.01
5	10	0.90	0.80	0.55	0.32	0.17	0.10	0.05	0.02	0.00
10	10	1.29	1.17	0.87	0.56	0.36	0.24	0.16	0.11	0.06
20	10	1.68	1.54	1.20	0.84	0.59	0.43	0.33	0.24	0.15
50	10	2.18	2.02	1.64	1.24	0.96	0.77	0.63	0.48	0.39
100	10	2.44	2.29	1.88	1.47	1.17	0.96	0.81	0.69	0.55
500	10	3.04	2.87	2.46	2.03	1.72	1.49	1.33	1.19	1.07

H1/A = 1.50   H2/A = 1.00   Z/H1 = 1.00

E1/E2	E2/E3	R/A=0.0	R/A=0.5	R/A=1.0	R/A=1.5	R/A=2.0	R/A=2.5	R/A=3.0	R/A=3.5	R/A=4.0
2	5	-1.14	-1.11	-0.66	-0.19	-0.13	-0.08	-0.05	-0.02	0.00
5	5	-1.45	-1.41	-0.90	-0.38	-0.26	-0.17	-0.10	-0.04	-0.01
10	5	-1.71	-1.66	-1.12	-0.55	-0.39	-0.26	-0.17	-0.10	-0.05
20	5	-1.99	-1.92	-1.36	-0.76	-0.56	-0.41	-0.29	-0.20	-0.13
50	5	-2.34	-2.27	-1.68	-1.05	-0.83	-0.65	-0.50	-0.39	-0.30
100	5	-2.62	-2.55	-1.96	-1.32	-1.09	-0.89	-0.69	-0.56	-0.46
500	5	-3.13	-3.06	-2.46	-1.81	-1.56	-1.34	-1.17	-1.02	-0.90
2	10	-1.25	-1.23	-0.77	-0.29	-0.20	-0.14	-0.09	-0.06	-0.03
5	10	-1.58	-1.54	-1.03	-0.49	-0.36	-0.25	-0.17	-0.11	-0.07
10	10	-1.87	-1.82	-1.27	-0.69	-0.52	-0.38	-0.28	-0.20	-0.14
20	10	-2.17	-2.10	-1.54	-0.93	-0.72	-0.56	-0.43	-0.33	-0.25
50	10	-2.57	-2.50	-1.92	-1.28	-1.02	-0.83	-0.67	-0.55	-0.45
100	10	-2.80	-2.72	-2.13	-1.49	-1.25	-1.04	-0.88	-0.74	-0.63
500	10	-3.35	-3.27	-2.67	-2.02	-1.77	-1.55	-1.37	-1.23	-1.10

145

TABLE 21

H1/A = 1.50   H2/A = 2.00   Z/H1 = 0.00

E1/E2	E2/E3	R/A=0.0	R/A=0.5	R/A=1.0	R/A=1.5	R/A=2.0	R/A=2.5	R/A=3.0	R/A=3.5	R/A=4.0
2	5	0.22	0.17	0.07	-0.03	-0.06	-0.07	-0.06	-0.05	-0.04
5	5	0.64	0.55	0.34	0.13	0.02	-0.03	-0.05	-0.05	-0.05
10	5	1.02	0.90	0.62	0.34	0.17	0.08	0.03	0.00	-0.01
20	5	1.37	1.23	0.90	0.56	0.34	0.20	0.13	0.07	0.03
50	5	1.82	1.67	1.30	0.91	0.64	0.46	0.35	0.26	0.10
100	5	2.17	2.02	1.63	1.22	0.93	0.73	0.60	0.45	0.36
500	5	2.78	2.61	2.21	1.78	1.47	1.25	1.09	0.95	0.84
2	10	0.23	0.18	0.08	-0.02	-0.05	-0.06	-0.05	-0.04	-0.03
5	10	0.69	0.60	0.38	0.18	0.06	0.01	-0.01	-0.02	-0.02
10	10	1.07	0.95	0.67	0.38	0.21	0.11	0.06	0.03	0.01
20	10	1.47	1.33	1.00	0.66	0.43	0.29	0.21	0.15	0.10
50	10	1.97	1.82	1.44	1.05	0.78	0.60	0.48	0.39	0.31
100	10	2.31	2.15	1.76	1.35	1.06	0.86	0.72	0.61	0.51
500	10	2.99	2.82	2.42	1.99	1.67	1.45	1.29	1.15	1.03

H1/A = 1.50   H2/A = 2.00   Z/H1 = 1.00

E1/E2	E2/E3	R/A=0.0	R/A=0.5	R/A=1.0	R/A=1.5	R/A=2.0	R/A=2.5	R/A=3.0	R/A=3.5	R/A=4.0
2	5	-1.05	-1.04	-0.59	-0.14	-0.09	-0.06	-0.04	-0.03	-0.02
5	5	-1.34	-1.30	-0.81	-0.29	-0.19	-0.12	-0.07	-0.04	-0.02
10	5	-1.59	-1.55	-1.02	-0.46	-0.32	-0.21	-0.13	-0.08	-0.04
20	5	-1.87	-1.81	-1.26	-0.67	-0.49	-0.35	-0.24	-0.16	-0.11
50	5	-2.24	-2.17	-1.60	-0.97	-0.76	-0.59	-0.45	-0.34	-0.26
100	5	-2.51	-2.44	-1.86	-1.22	-0.99	-0.80	-0.64	-0.52	-0.42
500	5	-3.10	-3.03	-2.43	-1.78	-1.53	-1.32	-1.14	-1.00	-0.88
2	10	-1.10	-1.08	-0.64	-0.19	-0.14	-0.10	-0.08	-0.06	-0.04
5	10	-1.41	-1.38	-0.88	-0.36	-0.26	-0.18	-0.13	-0.09	-0.06
10	10	-1.70	-1.65	-1.12	-0.55	-0.41	-0.29	-0.21	-0.15	-0.11
20	10	-2.00	-1.94	-1.39	-0.79	-0.60	-0.46	-0.34	-0.26	-0.20
50	10	-2.40	-2.34	-1.76	-1.13	-0.91	-0.73	-0.59	-0.48	-0.39
100	10	-2.70	-2.62	-2.04	-1.40	-1.16	-0.97	-0.81	-0.68	-0.58
500	10	-3.31	-3.23	-2.64	-1.98	-1.73	-1.52	-1.34	-1.20	-1.07

H1/A = 1.50   H2/A = 3.00   Z/H1 = 0.00

E1/E2	E2/E3	R/A=0.0	R/A=0.5	R/A=1.0	R/A=1.5	R/A=2.0	R/A=2.5	R/A=3.0	R/A=3.5	R/A=4.0
2	5	0.20	0.15	0.05	-0.05	-0.08	-0.08	-0.07	-0.05	-0.04
5	5	0.60	0.51	0.29	0.11	-0.02	-0.06	-0.07	-0.07	-0.06
10	5	0.94	0.82	0.54	0.26	0.09	0.01	-0.03	-0.05	-0.06
20	5	1.28	1.15	0.82	0.49	0.27	0.14	0.07	0.03	-0.00
50	5	1.74	1.58	1.21	0.83	0.57	0.40	0.29	0.21	0.14
100	5	2.09	1.93	1.55	1.14	0.85	0.63	0.50	0.40	0.31
500	5	2.73	2.57	2.17	1.74	1.42	1.21	1.05	0.92	0.80
2	10	0.19	0.15	0.04	-0.05	-0.08	-0.08	-0.07	-0.06	-0.05
5	10	0.62	0.53	0.31	0.12	-0.01	-0.05	-0.06	-0.06	-0.06
10	10	0.98	0.86	0.58	0.30	0.14	0.05	0.01	-0.01	-0.02
20	10	1.36	1.22	0.89	0.55	0.33	0.21	0.13	0.08	0.05
50	10	1.84	1.69	1.32	0.93	0.67	0.50	0.38	0.30	0.23
100	10	2.20	2.04	1.65	1.25	0.96	0.76	0.63	0.52	0.43
500	10	2.93	2.76	2.36	1.93	1.61	1.40	1.23	1.10	0.99

H1/A = 1.50   H2/A = 3.00   Z/H1 = 1.00

E1/E2	E2/E3	R/A=0.0	R/A=0.5	R/A=1.0	R/A=1.5	R/A=2.0	R/A=2.5	R/A=3.0	R/A=3.5	R/A=4.0
2	5	-1.00	-0.99	-0.55	-0.11	-0.07	-0.05	-0.03	-0.02	-0.02
5	5	-1.28	-1.24	-0.76	-0.25	-0.16	-0.09	-0.05	-0.03	-0.02
10	5	-1.53	-1.48	-0.96	-0.41	-0.27	-0.17	-0.10	-0.06	-0.03
20	5	-1.79	-1.74	-1.19	-0.60	-0.43	-0.29	-0.20	-0.13	-0.08
50	5	-2.17	-2.10	-1.52	-0.91	-0.70	-0.53	-0.40	-0.30	-0.23
100	5	-2.45	-2.38	-1.79	-1.16	-0.93	-0.74	-0.59	-0.48	-0.38
500	5	-3.06	-2.99	-2.39	-1.74	-1.49	-1.28	-1.11	-0.97	-0.85
2	10	-1.04	-1.03	-0.59	-0.14	-0.10	-0.08	-0.06	-0.05	-0.04
5	10	-1.33	-1.30	-0.81	-0.30	-0.21	-0.14	-0.10	-0.07	-0.05
10	10	-1.60	-1.55	-1.03	-0.48	-0.34	-0.24	-0.17	-0.12	-0.09
20	10	-1.90	-1.84	-1.29	-0.70	-0.53	-0.39	-0.27	-0.20	-0.15
50	10	-2.29	-2.22	-1.65	-1.03	-0.82	-0.64	-0.51	-0.41	-0.33
100	10	-2.60	-2.53	-1.94	-1.30	-1.08	-0.88	-0.73	-0.61	-0.51
500	10	-3.26	-3.18	-2.59	-1.93	-1.68	-1.47	-1.30	-1.15	-1.03

TABLE 22

H1/A = 2.00   H2/A = 1.00   Z/H1 = 0.00

E1/E2	E2/E3	R/A=0.0	R/A=0.5	R/A=1.0	R/A=1.5	R/A=2.0	R/A=2.5	R/A=3.0	R/A=3.5	R/A=4.0
2	5	0.24	0.21	0.15	0.08	0.03	0.01	-0.01	-0.01	-0.01
5	5	0.56	0.51	0.39	0.25	0.15	0.08	0.04	0.02	-0.00
10	5	0.77	0.71	0.56	0.39	0.26	0.17	0.11	0.07	0.04
20	5	0.98	0.91	0.74	0.54	0.39	0.28	0.21	0.16	0.12
50	5	1.25	1.17	0.98	0.74	0.57	0.45	0.36	0.30	0.24
100	5	1.38	1.30	1.11	0.89	0.71	0.58	0.49	0.41	0.35
500	5	1.71	1.63	1.43	1.20	1.01	0.88	0.78	0.70	0.63
2	10	0.30	0.27	0.20	0.13	0.07	0.04	0.02	0.01	-0.00
5	10	0.62	0.57	0.44	0.31	0.20	0.13	0.09	0.06	0.04
10	10	0.87	0.81	0.65	0.48	0.34	0.25	0.18	0.14	0.11
20	10	1.11	1.04	0.86	0.67	0.51	0.40	0.32	0.26	0.22
50	10	1.34	1.27	1.08	0.86	0.68	0.56	0.47	0.40	0.34
100	10	1.51	1.43	1.23	1.01	0.83	0.69	0.60	0.52	0.46
500	10	1.83	1.75	1.55	1.32	1.13	1.00	0.90	0.82	0.75

H1/A = 2.00   H2/A = 1.00   Z/H1 = 1.00

E1/E2	E2/E3	R/A=0.0	R/A=0.5	R/A=1.0	R/A=1.5	R/A=2.0	R/A=2.5	R/A=3.0	R/A=3.5	R/A=4.0
2	5	-1.03	-1.02	-0.60	-0.16	-0.13	-0.09	-0.06	-0.04	-0.02
5	5	-1.21	-1.20	-0.75	-0.29	-0.22	-0.16	-0.12	-0.08	-0.05
10	5	-1.37	-1.34	-0.89	-0.41	-0.33	-0.25	-0.19	-0.13	-0.10
20	5	1.52	-1.50	-1.03	-0.54	-0.44	-0.35	-0.28	-0.21	-0.16
50	5	-1.71	-1.69	-1.21	-0.71	-0.61	-0.51	-0.42	-0.35	-0.29
100	5	-1.85	-1.82	-1.35	-0.84	-0.73	-0.63	-0.53	-0.46	-0.39
500	5	-2.15	-2.13	-1.65	-1.14	-1.02	-0.91	-0.81	-0.73	-0.66
2	10	-1.09	-1.08	-0.66	-0.22	-0.17	-0.13	-0.10	-0.07	-0.05
5	10	-1.30	-1.28	-0.84	-0.37	-0.30	-0.23	-0.18	-0.13	-0.10
10	10	-1.47	-1.45	-0.99	-0.50	-0.42	-0.33	-0.26	-0.21	-0.16
20	10	-1.65	-1.63	-1.16	-0.66	-0.56	-0.47	-0.39	-0.30	-0.25
50	10	-1.83	-1.80	-1.33	-0.83	-0.72	-0.62	-0.52	-0.45	-0.38
100	10	-1.97	-1.94	-1.47	-0.96	-0.85	-0.74	-0.65	-0.57	-0.50
500	10	-2.28	-2.25	-1.77	-1.26	-1.14	-1.03	-0.93	-0.85	-0.77

H1/A = 2.00   H2/A = 2.00   Z/H1 = 0.00

E1/E2	E2/E3	R/A=0.0	R/A=0.5	R/A=1.0	R/A=1.5	R/A=2.0	R/A=2.5	R/A=3.0	R/A=3.5	R/A=4.0
2	5	0.18	0.16	0.10	0.03	-0.01	-0.03	-0.03	-0.03	-0.02
5	5	0.47	0.42	0.30	0.18	0.09	0.04	0.01	0.00	-0.01
10	5	0.69	0.63	0.48	0.31	0.19	0.11	0.07	0.04	0.02
20	5	0.91	0.84	0.67	0.48	0.33	0.23	0.16	0.12	0.09
50	5	1.17	1.09	0.90	0.69	0.52	0.41	0.32	0.26	0.21
100	5	1.34	1.26	1.07	0.85	0.67	0.55	0.46	0.39	0.33
500	5	1.69	1.61	1.41	1.18	1.00	0.86	0.76	0.68	0.62
2	10	0.19	0.16	0.10	0.04	0.00	-0.01	-0.02	-0.02	-0.02
5	10	0.50	0.45	0.33	0.20	0.11	0.06	0.03	0.02	0.01
10	10	0.75	0.69	0.54	0.37	0.25	0.17	0.12	0.09	0.07
20	10	1.00	0.93	0.76	0.57	0.40	0.30	0.23	0.18	0.14
50	10	1.27	1.19	1.00	0.79	0.62	0.50	0.41	0.35	0.30
100	10	1.45	1.37	1.18	0.96	0.78	0.65	0.56	0.49	0.43
500	10	1.81	1.73	1.53	1.30	1.12	0.98	0.88	0.80	0.73

H1/A = 2.00   H2/A = 2.00   Z/H1 = 1.00

E1/E2	E2/E3	R/A=0.0	R/A=0.5	R/A=1.0	R/A=1.5	R/A=2.0	R/A=2.5	R/A=3.0	R/A=3.5	R/A=4.0
2	5	-0.97	-0.96	-0.54	-0.12	-0.09	-0.07	-0.05	-0.03	-0.02
5	5	-1.15	-1.13	-0.69	-0.24	-0.18	-0.13	-0.10	-0.07	-0.04
10	5	-1.30	-1.28	-0.83	-0.36	-0.28	-0.21	-0.16	-0.11	-0.08
20	5	-1.46	-1.44	-0.98	-0.49	-0.40	-0.32	-0.25	-0.19	-0.15
50	5	-1.67	-1.65	-1.17	-0.68	-0.57	-0.47	-0.39	-0.32	-0.26
100	5	-1.82	-1.79	-1.32	-0.82	-0.71	-0.60	-0.51	-0.44	-0.37
500	5	-2.14	-2.11	-1.64	-1.13	-1.01	-0.90	-0.80	-0.72	-0.65
2	10	-1.01	-1.00	-0.58	-0.16	-0.13	-0.10	-0.08	-0.06	-0.05
5	10	-1.21	-1.19	-0.75	-0.30	-0.24	-0.19	-0.15	-0.11	-0.09
10	10	-1.38	-1.36	-0.91	-0.44	-0.36	-0.29	-0.23	-0.18	-0.14
20	10	-1.55	-1.53	-1.06	-0.57	-0.48	-0.40	-0.32	-0.26	-0.21
50	10	-1.77	-1.75	-1.28	-0.78	-0.67	-0.57	-0.49	-0.41	-0.35
100	10	-1.93	-1.90	-1.43	-0.93	-0.81	-0.71	-0.62	-0.54	-0.47
500	10	-2.26	-2.23	-1.76	-1.25	-1.13	-1.02	-0.92	-0.83	-0.76

TABLE 23

H1/A = 2.00   H2/A = 3.00   Z/H1 = 0.00

E1/E2	E2/E3	R/A=0.0	R/A=0.5	R/A=1.0	R/A=1.5	R/A=2.0	R/A=2.5	R/A=3.0	R/A=3.5	R/A=4.0
2	5	0.15	0.13	0.07	0.01	-0.02	-0.04	-0.04	-0.04	-0.0*
5	5	0.43	0.35	0.27	0.14	0.06	0.01	-0.01	-0.02	-0.0?
10	5	0.64	0.55	0.43	0.27	0.15	0.08	0.04	0.01	-0.00
20	5	0.86	0.74	0.62	0.43	0.26	0.17	0.12	0.07	0.06
50	5	1.12	1.05	0.86	0.65	0.43	0.30	0.24	0.12	0.19
100	5	1.31	1.17	1.03	0.82	0.64	0.51	0.42	0.36	0.70
500	5	1.67	1.59	1.39	1.17	0.98	0.84	0.75	0.67	0.60
2	10	0.16	0.13	0.07	0.02	-0.02	-0.04	-0.04	-0.04	-0.03
5	10	0.44	0.40	0.28	0.16	0.07	0.02	0.00	-0.01	-0.01
10	10	0.68	0.62	0.47	0.31	0.19	0.11	0.07	0.04	0.0?
20	10	0.91	0.84	0.67	0.48	0.33	0.24	0.17	0.13	0.10
50	10	1.20	1.12	0.94	0.73	0.56	0.44	0.36	0.30	0.25
100	10	1.40	1.32	1.13	0.91	0.73	0.60	0.51	0.44	0.39
500	10	1.79	1.71	1.51	1.28	1.09	0.96	0.86	0.79	0.71

H1/A = 2.00   H2/A = 3.00   Z/H1 = 1.00

E1/E2	E2/E3	R/A=0.0	R/A=0.5	R/A=1.0	R/A=1.5	R/A=2.0	R/A=2.5	R/A=3.0	R/A=3.5	R/A=4.0
2	5	-0.94	-0.93	-0.52	-0.10	-0.07	-0.05	-0.04	-0.03	-0.02
5	5	-1.11	-1.10	-0.66	-0.21	-0.16	-0.11	-0.08	-0.05	-0.04
10	5	-1.27	-1.25	-0.79	-0.33	-0.25	-0.19	-0.14	-0.10	-0.07
20	5	-1.43	-1.41	-0.94	-0.46	-0.37	-0.29	-0.23	-0.17	-0.13
50	5	-1.63	-1.61	-1.14	-0.64	-0.54	-0.44	-0.36	-0.30	-0.24
100	5	-1.79	-1.76	-1.29	-0.79	-0.68	-0.58	-0.49	-0.41	-0.35
500	5	-2.13	-2.10	-1.62	-1.11	-1.00	-0.89	-0.79	-0.71	-0.67
2	10	-0.97	-0.96	-0.55	-0.12	-0.10	-0.08	-0.06	-0.05	-0.04
5	10	-1.16	-1.14	-0.70	-0.25	-0.20	-0.15	-0.12	-0.09	-0.07
10	10	-1.31	-1.29	-0.84	-0.37	-0.30	-0.23	-0.18	-0.14	-0.11
20	10	-1.49	-1.46	-1.00	-0.52	-0.43	-0.35	-0.28	-0.22	-0.18
50	10	-1.72	-1.69	-1.22	-0.73	-0.62	-0.53	-0.44	-0.37	-0.32
100	10	-1.89	-1.86	-1.39	-0.89	-0.77	-0.67	-0.58	-0.50	-0.44
500	10	-2.24	-2.21	-1.74	-1.23	-1.11	-1.00	-0.90	-0.82	-0.75

Appendix C

RATIO OF RADIAL STRESS TO SURFACE PRESSURE—POISSON'S RATIO EQUAL TO 0.3 IN ALL THREE LAYERS[a]

TABLE 24

H1/A = 0.25   H2/A = 1.00   Z/H1 = 0.00

E1/E2	E2/E3	R/A=0.0	R/A=0.5	R/A=1.0	R/A=1.5	R/A=2.0	R/A=2.5	R/A=3.0	R/A=3.5	R/A=4.0
2	5	-0.69	-0.55	-0.48	-0.30	-0.10	-0.02	0.01	0.03	0.03
5	5	-0.18	-0.01	-0.48	-0.64	-0.28	-0.13	-0.06	-0.02	0.00
10	5	0.96	1.03	-0.27	-0.98	-0.52	-0.28	-0.16	-0.10	-0.06
20	5	3.17	2.89	0.30	-1.35	-0.92	-0.56	-0.36	-0.25	-0.18
50	5	8.24	7.59	2.12	-1.47	-1.58	-1.22	-0.90	-0.68	-0.52
100	5	13.79	11.85	4.77	-0.75	-1.84	-1.81	-1.54	-1.26	-1.03
500	5	31.03	27.42	16.08	5.88	1.28	-0.98	-2.07	-2.54	-2.67
2	10	-0.85	-0.70	-0.60	-0.39	-0.16	-0.05	-0.00	0.03	0.04
5	10	-0.29	-0.11	-0.57	-0.72	-0.34	-0.17	-0.09	-0.03	0.00
10	10	1.00	1.06	-0.27	-1.01	-0.57	-0.33	-0.20	-0.13	-0.08
20	10	3.49	3.18	0.51	-1.24	+0.88	-0.57	-0.40	-0.30	-0.23
50	10	9.26	8.05	2.88	-0.95	-1.28	-1.08	-0.88	-0.73	-0.62
100	10	15.61	13.57	6.23	0.35	-1.10	-1.38	-1.36	-1.25	-1.13
500	10	35.30	31.57	19.90	9.21	4.04	1.19	-0.46	-1.43	-1.99

H1/A = 0.25   H2/A = 1.00   Z/H1 = 1.00

E1/E2	E2/E3	R/A=0.0	R/A=0.5	R/A=1.0	R/A=1.5	R/A=2.0	R/A=2.5	R/A=3.0	R/A=3.5	R/A=4.0
2	5	-1.51	-1.45	-0.76	-0.11	-0.02	0.05	0.07	0.08	0.08
5	5	-2.55	-2.46	-1.10	-0.02	0.03	0.08	0.11	0.12	0.12
10	5	-3.89	-3.65	-1.50	-0.12	0.17	0.16	0.18	0.18	0.17
20	5	-6.16	-5.53	-2.22	0.35	0.45	0.37	0.33	0.30	0.26
50	5	-10.95	-9.54	-4.01	0.31	0.97	0.91	0.78	0.66	0.57
100	5	-16.16	-14.00	-6.56	-0.45	1.13	1.42	1.35	1.20	1.03
500	5	-32.44	-28.73	-17.37	-6.93	-2.02	0.45	1.71	2.30	2.52
2	10	-1.88	-1.79	-1.01	-0.28	-0.11	0.01	0.07	0.10	0.11
5	10	-3.07	-2.94	-1.49	-0.28	-0.12	0.01	0.10	0.14	0.16
10	10	-4.61	-4.31	-2.02	-0.21	-0.05	0.06	0.15	0.19	0.21
20	10	-7.13	-6.46	-2.92	-0.16	0.14	0.21	0.28	0.32	0.32
50	10	-12.57	-11.06	-5.26	-0.60	0.38	0.59	0.65	0.66	0.65
100	10	-18.50	-16.21	-8.45	-1.90	0.12	0.80	1.04	1.11	1.10
500	10	-36.94	-33.12	-21.40	-10.45	-4.95	-1.86	-0.02	1.10	1.77

H1/A = 0.25   H2/A = 2.00   Z/H1 = 0.00

E1/E2	E2/E3	R/A=0.0	R/A=0.5	R/A=1.0	R/A=1.5	R/A=2.0	R/A=2.5	R/A=3.0	R/A=3.5	R/A=4.0
2	5	-0.59	-0.47	-0.44	-0.31	-0.14	-0.07	-0.04	-0.01	0.00
5	5	-0.22	-0.04	-0.51	-0.66	-0.35	-0.16	-0.09	-0.05	-0.02
10	5	0.66	0.77	-0.44	-1.06	-0.55	-0.29	-0.13	-0.11	-0.07
20	5	2.43	2.24	-0.13	-1.54	-0.94	-0.51	-0.30	-0.19	-0.14
50	5	6.58	5.62	1.08	-1.99	-1.69	-1.08	-0.66	-0.43	-0.31
100	5	11.21	9.48	3.01	-1.78	-2.20	-1.71	-1.20	-0.83	-0.60
500	5	26.49	23.12	12.43	3.15	-0.49	-1.87	-2.26	-2.23	-2.04
2	10	-0.69	-0.56	-0.52	-0.38	-0.20	-0.12	-0.07	-0.03	-0.01
5	10	-0.34	-0.15	-0.61	-0.76	-0.39	-0.23	-0.15	-0.09	0.21
10	10	0.56	0.66	-0.54	-1.16	-0.63	-0.36	-0.23	-0.16	-0.11
20	10	2.38	2.19	-0.18	-1.60	-1.00	-0.57	-0.35	-0.24	-0.18
50	10	6.71	5.74	1.18	-1.92	-1.65	-1.07	-0.67	-0.46	-0.34
100	10	11.61	9.87	3.35	-1.50	-1.99	-1.57	-1.11	-0.78	-0.59
500	10	28.23	24.82	14.04	-4.60	0.77	-0.81	-1.41	-1.57	-1.56

H1/A = 0.25   H2/A = 2.00   Z/H1 = 1.00

E1/E2	E2/E3	R/A=0.0	R/A=0.5	R/A=1.0	R/A=1.5	R/A=2.0	R/A=2.5	R/A=3.0	R/A=3.5	R/A=4.0
2	5	-1.12	-1.13	-0.57	-0.08	-0.08	-0.06	-0.03	-0.01	0.01
5	5	-1.94	-1.94	-0.82	0.04	-0.06	-0.07	-0.05	-0.01	0.01
10	5	-3.07	-2.95	-1.09	0.24	0.04	-0.04	-0.04	-0.01	0.01
20	5	-4.93	-4.54	-1.55	0.54	0.32	0.09	0.02	0.02	0.04
50	5	-8.97	-7.79	-2.84	0.81	0.93	0.56	0.31	0.20	0.16
100	5	-13.38	-11.49	-4.74	0.52	1.35	1.13	0.79	0.55	0.42
500	5	-27.99	-24.54	-13.85	-4.33	-0.41	1.19	1.75	1.85	1.77
2	10	-1.26	-1.26	-0.69	-0.18	-0.16	-0.12	-0.07	-0.03	-0.01
5	10	-2.17	-2.16	-1.00	-0.12	-0.19	-0.17	-0.12	-0.07	-0.03
10	10	-3.34	-2.82	-1.33	0.03	-0.12	-0.18	-0.14	-0.09	-0.04
20	10	-5.29	-4.84	-1.87	0.27	0.09	-0.09	-0.11	-0.08	-0.03
50	10	-9.51	-8.32	-3.32	0.40	0.59	0.30	0.11	0.05	0.05
100	10	-14.19	-12.27	-5.45	-0.06	0.84	0.73	0.49	0.34	0.27
500	10	-30.04	-26.55	-15.75	-6.06	-1.93	-0.10	0.70	1.02	1.14

[a] A negative sign indicates compression.
Z/H1 = 0 indicates tables of stresses at the interface.
Z/H1 = 1 indicates tables of stresses at the surface.

TABLE 25

H1/A = 0.25   H2/A = 3.00   Z/H1 = 0.00

E1/E2	E2/E3	R/A=0.0	R/A=0.5	R/A=1.0	R/A=1.5	R/A=2.0	R/A=2.5	R/A=3.0	R/A=3.5	R/A=4.0
2	5	-0.53	-0.41	-0.39	-0.27	-0.12	-0.07	-0.04	-0.03	-0.02
5	5	-0.16	0.02	-0.46	-0.63	-0.29	-0.16	-0.10	-0.07	-0.05
10	5	0.68	0.79	-0.43	-1.05	-0.54	-0.29	-0.18	-0.12	-0.09
20	5	2.36	2.17	-0.18	-1.57	-0.96	-0.52	-0.30	-0.20	-0.15
50	5	6.25	5.31	0.83	-2.17	-1.79	-1.12	-0.66	-0.41	-0.28
100	5	10.56	8.87	2.50	-2.15	-2.44	-1.82	-1.21	-0.78	-0.52
500	5	24.61	21.31	10.82	1.81	-1.50	-2.55	-2.64	-2.35	-1.97
2	10	-0.58	-0.46	0.44	-0.32	-0.16	-0.11	-0.08	-0.05	-0.03
5	10	-0.24	-0.07	-0.54	-0.70	-0.36	-0.22	-0.16	-0.12	-0.09
10	10	0.59	0.69	-0.52	-1.14	-0.62	-0.36	+0.14	-0.18	-0.14
20	10	2.27	2.09	-0.27	-1.65	-1.04	-0.59	-0.37	-0.26	-0.20
50	10	6.23	5.29	0.80	-2.20	-1.83	-1.16	-0.71	-0.45	-0.32
100	10	10.65	8.95	2.57	-2.09	-2.39	-1.79	-1.20	-0.78	-0.53
500	10	25.37	22.05	11.52	2.61	-0.91	-2.03	-2.20	-1.99	-1.68

H1/A = 0.25   H2/A = 3.00   Z/H1 = 1.00

E1/E2	E2/E3	R/A=0.0	R/A=0.5	R/A=1.0	R/A=1.5	R/A=2.0	R/A=2.5	R/A=3.0	R/A=3.5	R/A=4.0
2	5	-0.91	-0.93	-0.48	-0.03	-0.06	-0.05	-0.05	-0.03	-0.02
5	5	-1.76	-1.77	-0.68	0.13	-0.02	-0.07	-0.06	-0.05	-0.03
10	5	-2.83	-2.72	-0.91	0.36	0.10	-0.04	-0.07	-0.06	-0.05
20	5	-4.59	-4.18	-1.30	0.70	0.40	0.10	-0.02	-0.05	-0.04
50	5	-8.40	-7.26	-2.41	1.11	1.08	0.60	0.26	0.09	0.03
100	5	-12.54	-10.69	-4.07	1.00	1.63	1.23	0.75	0.42	0.24
500	5	-26.04	-22.66	-12.17	-3.04	0.60	1.84	2.07	1.91	1.61
2	10	-1.08	-1.09	-0.55	-0.08	-0.11	-0.10	-0.09	-0.07	-0.04
5	10	-1.88	-1.89	-0.79	0.02	-0.11	-0.15	-0.13	-0.11	-0.08
10	10	-2.98	-2.87	-1.06	0.23	-0.02	-0.14	-0.16	-0.14	-0.11
20	10	-4.79	-4.38	-1.48	0.53	0.24	-0.04	-0.14	-0.15	-0.13
50	10	-8.68	-7.54	-2.67	0.87	0.87	0.40	0.09	-0.05	-0.09
100	10	-12.92	-11.07	-4.33	0.67	1.34	0.97	0.53	0.24	0.09
500	10	-27.06	-23.67	-13.14	-3.87	-0.22	1.10	1.43	1.36	1.16

H1/A = 0.50   H2/A = 1.00   Z/H1 = 0.00

E1/E2	E2/E3	R/A=0.0	R/A=0.5	R/A=1.0	R/A=1.5	R/A=2.0	R/A=2.5	R/A=3.0	R/A=3.5	R/A=4.0
2	5	-0.05	-0.03	-0.21	-0.28	-0.15	-0.08	-0.04	-0.02	-0.01
5	5	0.86	0.75	0.06	-0.39	-0.31	-0.21	-0.14	-0.10	-0.07
10	5	2.06	1.77	0.54	-0.36	-0.42	-0.35	-0.27	-0.21	-0.17
20	5	3.69	3.18	1.36	-0.09	-0.42	-0.75	-0.43	-0.38	-0.32
50	5	6.35	5.57	3.03	0.83	-0.02	-0.39	-0.54	-0.58	-0.56
100	5	8.58	7.64	4.68	1.99	0.72	0.04	-0.34	-0.54	-0.64
500	5	13.78	12.64	9.12	5.71	3.75	2.43	1.49	0.82	0.31
2	10	-0.06	-0.04	-0.23	-0.29	-0.17	-0.09	-0.05	-0.03	-0.02
5	10	0.95	0.84	0.12	-0.35	-0.28	-0.20	-0.15	-0.11	-0.09
10	10	2.30	2.00	0.73	-0.22	-0.33	-0.29	-0.25	-0.21	-0.18
20	10	4.15	3.62	1.75	0.22	-0.20	-0.32	-0.35	-0.34	-0.32
50	10	7.18	6.38	3.77	1.47	0.50	0.01	-0.25	-0.38	-0.45
100	10	9.69	8.73	5.70	2.91	1.52	0.70	0.19	-0.13	-0.35
500	10	15.38	14.22	10.66	7.18	5.13	3.71	2.66	1.86	1.24

H1/A = 0.50   H2/A = 1.00   Z/H1 = 1.00

E1/E2	E2/E3	R/A=0.0	R/A=0.5	R/A=1.0	R/A=1.5	R/A=2.0	R/A=2.5	R/A=3.0	R/A=3.5	R/A=4.0
2	5	-1.38	-1.28	-0.69	-0.13	-0.03	0.02	0.04	0.06	0.06
5	5	-2.34	-2.10	-1.06	-0.16	0.03	0.08	0.09	0.11	0.10
10	5	-3.43	-3.03	-1.55	-0.27	0.07	0.17	0.18	0.19	0.18
20	5	-4.87	-4.28	-2.33	-0.58	0.02	0.24	0.29	0.32	0.30
50	5	-7.23	-6.40	-3.86	-1.47	-0.41	0.10	0.33	0.45	0.49
100	5	-9.23	-8.27	-5.37	-2.57	-1.13	-0.34	0.11	0.39	0.53
500	5	-14.05	-12.91	-9.53	-6.11	-4.05	-2.67	-1.70	-0.98	-0.45
2	10	-1.63	-1.52	-0.88	-0.27	-0.12	-0.03	0.02	0.05	0.07
5	10	-2.71	-2.44	-1.35	-0.38	-0.12	-0.01	0.05	0.09	0.11
10	10	-3.93	-3.50	-1.96	-0.59	-0.15	0.02	0.09	0.15	0.17
20	10	-5.55	-4.93	-2.90	-1.05	-0.33	-0.02	0.13	0.22	0.27
50	10	-8.21	-7.35	-4.73	-2.23	-1.03	-0.38	-0.02	0.21	0.25
100	10	-10.44	-9.45	-6.48	-3.57	-2.00	-1.06	-0.47	-0.06	0.21
500	10	-15.66	-14.51	-11.09	-7.60	-5.45	-3.96	-2.88	-2.04	-1.39

TABLE 26

H1/A = 0.50　　H2/A = 2.00　　Z/H1 = 0.00

E1/E2	E2/E3	R/A=0.0	R/A=0.5	R/A=1.0	R/A=1.5	R/A=2.0	R/A=2.5	R/A=3.0	R/A=3.5	R/A=4.0
2	5	-0.09	-0.07	-0.25	-0.31	-0.17	-0.10	-0.05	-0.03	-0.02
5	5	0.65	0.56	-0.09	-0.48	-0.34	-0.21	-0.13	-0.08	-0.06
10	5	1.64	1.39	0.24	-0.55	-0.50	-0.36	-0.24	-0.16	-0.11
20	5	3.02	2.56	0.87	-0.42	-0.60	-0.52	-0.40	-0.29	-0.22
50	5	5.36	4.63	2.24	0.24	-0.58	-0.58	-0.51	-0.51	-0.43
100	5	7.42	6.53	3.71	1.21	0.16	-0.31	-0.51	-0.57	-0.57
500	5	12.71	11.59	8.14	4.85	3.01	1.83	1.03	0.48	0.09
2	10	-0.14	-0.11	-0.29	-0.34	-0.20	-0.12	-0.07	-0.05	-0.03
5	10	0.63	0.53	-0.11	-0.51	-0.37	-0.24	-0.16	-0.10	-0.07
10	10	1.66	1.40	0.26	-0.54	-0.50	-0.36	-0.25	-0.17	-0.13
20	10	3.12	2.65	0.95	-0.35	-0.54	-0.48	-0.37	-0.28	-0.21
50	10	5.64	4.91	2.50	0.47	-0.20	-0.41	-0.45	-0.41	-0.36
100	10	8.01	7.12	4.27	1.74	0.65	0.13	-0.23	-0.34	-0.27
500	10	13.81	12.69	9.22	5.88	3.99	2.75	1.88	1.25	0.79

H1/A = 0.50　　H2/A = 2.00　　Z/H1 = 1.00

E1/E2	E2/E3	R/A=0.0	R/A=0.5	R/A=1.0	R/A=1.5	R/A=2.0	R/A=2.5	R/A=3.0	R/A=3.5	R/A=4.0
2	5	-1.11	-1.05	-0.54	-0.08	-0.05	-0.04	-0.03	-0.01	0.00
5	5	-1.94	-1.74	-0.82	-0.05	0.02	0.01	-0.00	0.00	0.00
10	5	-2.89	-2.53	-1.20	-0.09	0.10	0.10	0.06	0.05	0.04
20	5	-4.15	-3.61	-1.82	-0.27	0.13	0.20	0.16	0.15	0.12
50	5	-6.25	-5.49	-3.10	-0.94	-0.10	0.22	0.30	0.32	0.30
100	5	-8.14	-7.23	-4.47	-1.87	-0.65	-0.06	0.21	0.35	0.40
500	5	-13.06	-11.95	-8.64	-5.32	-3.39	-2.14	-1.30	-0.70	-0.27
2	10	-1.22	-1.15	-0.63	-0.16	-0.11	-0.09	-0.07	-0.04	-0.02
5	10	-2.09	-1.89	-0.96	-0.17	-0.08	-0.07	-0.07	-0.05	-0.02
10	10	-3.08	-2.73	-1.38	-0.24	-0.03	-0.01	-0.03	-0.02	-0.00
20	10	-4.42	-3.88	-2.07	-0.49	-0.05	0.05	0.05	0.05	0.05
50	10	-6.70	-5.92	-3.51	-1.31	-0.43	-0.06	0.07	0.14	0.16
100	10	-8.76	-7.84	-5.06	-2.41	-1.14	-0.49	-0.16	0.05	0.16
500	10	-14.23	-13.11	-9.78	-6.41	-4.42	-3.11	-2.20	-1.52	-1.01

H1/A = 0.50　　H2/A = 3.00　　Z/H1 = 0.00

E1/E2	E2/E3	R/A=0.0	R/A=0.5	R/A=1.0	R/A=1.5	R/A=2.0	R/A=2.5	R/A=3.0	R/A=3.5	R/A=4.0
2	5	-0.07	-0.05	-0.23	-0.30	-0.17	-0.10	-0.05	-0.04	-0.03
5	5	0.63	0.54	0.02	-0.50	-0.35	-0.22	-0.14	-0.09	-0.06
10	5	1.57	1.31	0.18	-0.60	-0.54	-0.38	-0.25	-0.17	-0.11
20	5	2.85	2.40	0.72	-0.53	-0.69	-0.57	-0.42	-0.30	-0.21
50	5	5.01	4.30	1.94	-0.01	-0.59	-0.71	-0.65	-0.54	-0.43
100	5	6.92	6.04	3.26	0.97	-0.15	-0.66	-0.65	-0.54	-0.59
500	5	11.96	10.86	7.45	4.20	2.44	1.34	0.62	0.16	-0.15
2	10	-0.11	-0.08	-0.26	-0.33	-0.20	-0.12	-0.08	-0.06	-0.04
5	10	0.60	0.51	0.02	-0.53	-0.39	-0.25	-0.17	-0.11	-0.08
10	10	1.54	1.29	0.16	-0.62	-0.56	-0.40	-0.27	-0.19	-0.13
20	10	2.86	2.41	0.73	-0.53	-0.68	-0.57	-0.43	-0.30	-0.22
50	10	5.11	4.40	2.03	0.08	-0.51	-0.64	-0.60	-0.49	-0.40
100	10	7.19	6.32	3.53	1.02	0.03	-0.38	-0.53	-0.54	-0.50
500	10	12.67	11.56	8.13	4.87	3.08	1.94	1.19	0.68	0.33

H1/A = 0.50　　H2/A = 3.00　　Z/H1 = 1.00

E1/E2	E2/E3	R/A=0.0	R/A=0.5	R/A=1.0	R/A=1.5	R/A=2.0	R/A=2.5	R/A=3.0	R/A=3.5	R/A=4.0
2	5	-1.02	-0.97	-0.47	-0.03	-0.02	-0.03	-0.03	-0.03	-0.02
5	5	-1.80	-1.62	-0.72	0.02	0.10	0.02	-0.01	-0.02	-0.02
10	5	-2.70	-2.36	-1.05	0.03	0.17	0.12	0.05	0.02	0.01
20	5	-3.88	-3.31	-1.60	-0.10	0.25	0.26	0.18	0.12	0.07
50	5	-5.85	-5.10	-2.76	-0.66	0.11	0.34	0.36	0.32	0.26
100	5	-7.60	-6.71	-4.00	-1.47	-0.37	0.16	0.35	0.41	0.40
500	5	-12.35	-11.24	-7.97	-4.71	-2.84	-1.68	-0.92	-0.40	-0.06
2	10	-1.08	-1.03	-0.53	-0.08	-0.07	-0.07	-0.07	-0.06	-0.04
5	10	-1.89	-1.70	-0.80	-0.05	-0.00	-0.04	-0.07	-0.06	-0.06
10	10	-2.81	-2.47	-1.16	0.01	0.07	0.04	-0.02	-0.04	-0.05
20	10	-4.03	-3.51	-1.74	-0.24	0.12	0.15	0.08	0.04	0.00
50	10	-6.08	-5.33	-2.85	-0.87	-0.09	0.17	0.21	0.17	0.13
100	10	-7.95	-7.05	-4.33	-1.78	-0.63	-0.11	0.11	0.20	0.22
500	10	-13.13	-12.02	-8.74	-5.45	-3.55	-2.35	-1.55	-0.99	-0.59

TABLE 27

H1/A = 1.00   H2/A = 1.00   Z/H1 = 0.00

E1/E2	E2/E3	R/A=0.0	R/A=0.5	R/A=1.0	R/A=1.5	R/A=2.0	R/A=2.5	R/A=3.0	R/A=3.5	R/A=4.0
2	5	0.27	0.21	0.04	-0.09	-0.10	-0.08	-0.06	-0.05	-0.04
5	5	0.95	0.81	0.41	0.08	-0.08	-0.11	-0.10	-0.10	-0.09
10	5	1.54	1.33	0.76	0.25	0.03	-0.06	-0.10	-0.12	-0.13
20	5	2.20	1.94	1.24	0.59	0.25	0.07	-0.03	-0.09	-0.13
50	5	3.08	2.77	1.95	1.15	0.69	0.42	0.23	0.09	-0.00
100	5	3.70	3.37	2.40	1.63	1.11	0.77	0.53	0.34	0.20
500	5	4.99	4.64	3.71	2.77	2.17	1.76	1.44	1.18	0.96
2	10	0.33	0.27	0.09	-0.06	-0.06	-0.08	-0.05	-0.05	-0.04
5	10	1.04	0.89	0.48	0.13	-0.01	-0.05	-0.06	-0.07	-0.09
10	10	1.73	1.52	0.94	0.41	0.17	0.05	-0.01	-0.02	-0.08
20	10	2.48	2.22	1.50	0.82	0.46	0.26	0.13	0.04	-0.03
50	10	3.44	3.13	2.30	1.48	1.00	0.70	0.48	0.32	0.19
100	10	4.10	3.78	2.89	2.01	1.47	1.11	0.85	0.63	0.47
500	10	5.44	5.09	4.15	3.21	2.60	2.18	1.85	1.57	1.35

H1/A = 1.00   H2/A = 1.00   Z/H1 = 1.00

E1/E2	E2/E3	R/A=0.0	R/A=0.5	R/A=1.0	R/A=1.5	R/A=2.0	R/A=2.5	R/A=3.0	R/A=3.5	R/A=4.0
2	5	-1.07	-1.02	-0.60	-0.18	-0.09	-0.03	0.00	0.02	0.03
5	5	-1.58	-1.47	-0.91	-0.34	-0.15	-0.05	0.01	0.04	0.06
10	5	-2.05	-1.90	-1.24	-0.56	-0.28	-0.11	-0.01	0.04	0.06
20	5	-2.58	-2.40	-1.65	-0.86	-0.49	-0.25	-0.13	-0.01	0.06
50	5	-3.31	-3.10	-2.27	-1.38	-0.91	-0.58	-0.36	-0.20	-0.08
100	5	-3.85	-3.62	-2.76	-1.82	-1.29	-0.92	-0.64	-0.44	-0.28
500	5	-5.04	-4.80	-3.89	-2.89	-2.31	-1.86	-1.52	-1.25	-1.03
2	10	-1.22	-1.16	-0.73	-0.28	-0.17	-0.09	-0.05	-0.01	0.02
5	10	-1.78	-1.67	-1.09	-0.50	-0.28	-0.16	-0.08	-0.01	0.03
10	10	-2.31	-2.18	-1.51	-0.80	-0.49	-0.26	-0.13	-0.05	0.01
20	10	-2.90	-2.71	-1.94	-1.13	-0.73	-0.46	-0.28	-0.15	-0.06
50	10	-3.69	-3.47	-2.63	-1.72	-1.23	-0.87	-0.62	-0.43	-0.28
100	10	-4.26	-4.03	-3.16	-2.20	-1.66	-1.26	-0.97	-0.74	-0.55
500	10	-5.49	-5.24	-4.33	-3.33	-2.73	-2.28	-1.93	-1.64	-1.40

H1/A = 1.00   H2/A = 2.00   Z/H1 = 0.00

E1/E2	E2/E3	R/A=0.0	R/A=0.5	R/A=1.0	R/A=1.5	R/A=2.0	R/A=2.5	R/A=3.0	R/A=3.5	R/A=4.0
2	5	0.18	0.13	-0.03	-0.14	-0.13	-0.10	-0.07	-0.05	-0.03
5	5	0.74	0.60	0.23	-0.07	-0.15	-0.15	-0.12	-0.10	-0.08
10	5	1.29	1.09	0.55	0.13	-0.09	-0.14	-0.14	-0.13	-0.12
20	5	1.91	1.66	0.99	0.37	0.08	-0.04	-0.10	-0.13	-0.14
50	5	2.78	2.48	1.68	0.91	0.49	0.26	0.11	0.01	-0.06
100	5	3.43	3.11	2.24	1.41	0.91	0.60	0.39	0.24	0.12
500	5	4.83	4.49	3.56	2.63	2.04	1.64	1.33	1.08	0.88
2	10	0.18	0.12	-0.04	-0.15	-0.14	-0.11	-0.07	-0.05	-0.04
5	10	0.77	0.63	0.25	-0.05	-0.14	-0.13	-0.11	-0.09	-0.07
10	10	1.37	1.17	0.63	0.15	-0.04	-0.09	-0.10	-0.10	-0.10
20	10	2.03	1.78	1.10	0.48	0.19	0.05	-0.02	-0.06	-0.08
50	10	2.99	2.69	1.89	1.11	0.68	0.43	0.27	0.16	0.08
100	10	3.72	3.40	2.53	1.68	1.17	0.85	0.63	0.45	0.32
500	10	5.24	4.89	3.96	3.03	2.43	2.02	1.70	1.44	1.23

H1/A = 1.00   H2/A = 2.00   Z/H1 = 1.00

E1/E2	E2/E3	R/A=0.0	R/A=0.5	R/A=1.0	R/A=1.5	R/A=2.0	R/A=2.5	R/A=3.0	R/A=3.5	R/A=4.0
2	5	-0.94	-0.90	-0.51	-0.12	-0.07	-0.04	0.02	0.01	-0.00
5	5	-1.39	-1.30	-0.77	-0.25	-0.11	-0.04	-0.00	0.01	0.02
10	5	-1.83	-1.70	-1.07	-0.43	-0.20	-0.08	-0.02	0.02	0.04
20	5	-2.33	-2.15	-1.43	-0.69	-0.36	-0.17	-0.06	0.00	0.04
50	5	-3.05	-2.85	-2.04	-1.18	-0.74	-0.46	-0.27	-0.14	-0.05
100	5	-3.62	-3.40	-2.55	-1.63	-1.13	-0.78	-0.54	-0.36	-0.22
500	5	-4.91	-4.67	-3.76	-2.77	-2.19	-1.76	-1.43	-1.17	-0.95
2	10	-1.00	-0.96	-0.57	-0.18	-0.11	-0.08	-0.06	-0.04	-0.03
5	10	-1.48	-1.39	-0.86	-0.33	-0.18	-0.10	-0.06	-0.04	-0.02
10	10	-1.95	-1.82	-1.18	-0.53	-0.29	-0.15	-0.09	-0.04	-0.02
20	10	-2.50	-2.33	-1.60	-0.85	-0.51	-0.30	-0.18	-0.10	-0.05
50	10	-3.31	-3.10	-2.28	-1.41	-0.97	-0.66	-0.46	-0.31	-0.21
100	10	-3.94	-3.71	-2.85	-1.92	-1.42	-1.05	-0.79	-0.59	-0.44
500	10	-5.32	-5.08	-4.17	-3.17	-2.59	-2.14	-1.80	-1.53	-1.30

TABLE 28

H1/A = 1.00   H2/A = 3.00   Z/H1 = 0.00

E1/E2	E2/E3	R/A=0.0	R/A=0.5	R/A=1.0	R/A=1.5	R/A=2.0	R/A=2.5	R/A=3.0	R/A=3.5	R/A=4.0
2	5	0.18	0.12	-0.04	-0.15	-0.14	-0.11	-0.07	-0.05	-0.04
5	5	0.69	0.56	0.19	-0.11	-0.18	-0.17	-0.13	-0.11	-0.08
10	5	1.21	1.01	0.48	0.02	-0.10	-0.18	-0.17	-0.15	-0.13
20	5	1.83	1.58	0.87	0.27	-0.00	-0.11	-0.15	-0.16	-0.16
50	5	2.65	2.35	1.56	0.81	0.40	0.18	0.06	-0.06	-0.11
100	5	3.24	2.93	2.07	1.24	0.76	0.47	0.28	0.14	0.04
500	5	4.69	4.34	3.42	2.49	1.90	1.51	1.22	0.98	0.78
2	10	0.16	0.11	-0.06	-0.16	-0.16	-0.12	-0.08	-0.06	-0.05
5	10	0.69	0.56	0.19	-0.11	-0.18	-0.17	-0.14	-0.11	-0.09
10	10	1.23	1.03	0.50	0.04	-0.13	-0.16	-0.16	-0.14	-0.12
20	10	1.86	1.61	0.94	0.34	0.04	-0.07	-0.11	-0.13	-0.13
50	10	2.73	2.44	1.64	0.88	0.47	0.25	0.12	0.03	-0.03
100	10	3.43	3.12	2.26	1.42	0.94	0.64	0.44	0.32	0.22
500	10	5.03	4.69	3.76	2.83	2.24	1.84	1.53	1.28	1.08

H1/A = 1.00   H2/A = 3.00   Z/H1 = 1.00

E1/E2	E2/E3	R/A=0.0	R/A=0.5	R/A=1.0	R/A=1.5	R/A=2.0	R/A=2.5	R/A=3.0	R/A=3.5	R/A=4.0
2	5	-0.88	-0.84	-0.46	-0.08	-0.04	-0.02	-0.02	-0.01	-0.01
5	5	-1.30	-1.21	-0.70	-0.19	-0.06	-0.01	0.01	0.01	0.01
10	5	-1.72	-1.58	-0.96	-0.34	-0.13	-0.02	0.02	0.03	0.03
20	5	-2.19	-2.02	-1.31	-0.58	-0.28	-0.10	-0.01	0.03	0.05
50	5	-2.89	-2.69	-1.89	-1.04	-0.62	-0.35	-0.19	-0.08	-0.01
100	5	-3.45	-3.23	-2.38	-1.48	-1.00	-0.66	-0.44	-0.27	-0.16
500	5	-4.78	-4.53	-3.63	-2.65	-2.08	-1.65	-1.33	-1.07	-0.87
2	10	-0.92	-0.89	-0.50	-0.12	-0.07	-0.05	-0.05	-0.04	-0.03
5	10	-1.37	-1.27	-0.76	-0.24	-0.11	-0.05	-0.04	-0.03	-0.02
10	10	-1.80	-1.67	-1.04	-0.42	-0.20	-0.09	-0.04	-0.02	-0.01
20	10	-2.31	-2.14	-1.42	-0.69	-0.38	-0.20	-0.10	-0.05	-0.02
50	10	-3.07	-2.87	-2.06	-1.21	-0.79	-0.51	-0.34	-0.22	-0.14
100	10	-3.68	-3.45	-2.60	-1.69	-1.20	-0.86	-0.62	-0.45	-0.33
500	10	-5.13	-4.89	-3.98	-2.99	-2.42	-1.98	-1.65	-1.39	-1.18

H1/A = 1.50   H2/A = 1.00   Z/H1 = 0.00

E1/E2	E2/E3	R/A=0.0	R/A=0.5	R/A=1.0	R/A=1.5	R/A=2.0	R/A=2.5	R/A=3.0	R/A=3.5	R/A=4.0
2	5	0.27	0.23	0.13	0.03	-0.03	-0.04	-0.04	-0.04	-0.04
5	5	0.66	0.58	0.37	0.17	0.05	-0.01	-0.03	-0.04	-0.05
10	5	1.01	0.89	0.62	0.34	0.19	0.10	0.05	-0.01	-0.04
20	5	1.34	1.21	0.89	0.56	0.34	0.21	0.12	0.06	0.02
50	5	1.75	1.60	1.24	0.87	0.61	0.44	0.32	0.23	0.16
100	5	2.03	1.87	1.49	1.10	0.82	0.64	0.54	0.43	0.35
500	5	2.58	2.42	2.03	1.62	1.32	1.12	0.96	0.84	0.73
2	10	0.30	0.26	0.15	0.05	0.01	-0.01	-0.01	-0.02	-0.02
5	10	0.78	0.69	0.48	0.27	0.14	0.06	0.02	-0.00	-0.02
10	10	1.14	1.02	0.74	0.46	0.28	0.17	0.11	0.06	0.02
20	10	1.51	1.37	1.04	0.71	0.48	0.34	0.24	0.17	0.11
50	10	1.94	1.79	1.42	1.04	0.81	0.63	0.51	0.41	0.33
100	10	2.22	2.07	1.69	1.29	1.01	0.82	0.68	0.57	0.47
500	10	2.79	2.63	2.24	1.82	1.52	1.31	1.16	1.03	0.92

H1/A = 1.50   H2/A = 1.00   Z/H1 = 1.00

E1/E2	E2/E3	R/A=0.0	R/A=0.5	R/A=1.0	R/A=1.5	R/A=2.0	R/A=2.5	R/A=3.0	R/A=3.5	R/A=4.0
2	5	-0.89	-0.87	-0.52	-0.17	-0.11	-0.07	-0.03	-0.01	0.01
5	5	-1.16	-1.13	-0.74	-0.32	-0.21	-0.13	-0.07	-0.02	0.00
10	5	-1.43	-1.38	-0.93	-0.47	-0.32	-0.21	-0.12	-0.06	-0.02
20	5	-1.66	-1.60	-1.15	-0.66	-0.48	-0.33	-0.22	-0.14	-0.08
50	5	-1.99	-1.92	-1.45	-0.93	-0.72	-0.55	-0.41	-0.31	-0.22
100	5	-2.25	-2.18	-1.70	-1.17	-0.95	-0.76	-0.61	-0.49	-0.37
500	5	-2.74	-2.67	-2.18	-1.63	-1.39	-1.19	-1.02	-0.89	-0.77
2	10	-0.99	-0.97	-0.62	-0.25	-0.17	-0.11	-0.07	-0.04	-0.02
5	10	-1.29	-1.25	-0.85	-0.42	-0.30	-0.20	-0.13	-0.08	-0.04
10	10	-1.56	-1.50	-1.07	-0.60	-0.44	-0.31	-0.22	-0.15	-0.09
20	10	-1.83	-1.77	-1.31	-0.81	-0.62	-0.47	-0.35	-0.25	-0.18
50	10	-2.21	-2.14	-1.66	-1.14	-0.92	-0.74	-0.60	-0.45	-0.36
100	10	-2.42	-2.35	-1.86	-1.33	-1.10	-0.91	-0.75	-0.63	-0.53
500	10	-2.94	-2.87	-2.38	-1.83	-1.59	-1.38	-1.22	-1.08	-0.96

TABLE 29

H1/A = 1.50   H2/A = 2.00   Z/H1 = 0.00

E1/E2	E2/E3	R/A=0.0	R/A=0.5	R/A=1.0	R/A=1.5	R/A=2.0	R/A=2.5	R/A=3.0	R/A=3.5	R/A=4.0
2	5	0.18	0.14	0.05	-0.03	-0.07	-0.07	-0.05	-0.04	-0.04
5	5	0.57	0.48	0.29	0.08	-0.02	-0.05	-0.06	-0.06	-0.06
10	5	0.89	0.78	0.51	0.25	0.10	0.03	-0.01	-0.02	-0.03
20	5	1.20	1.08	0.76	0.45	0.25	0.13	0.06	0.02	-0.01
50	5	1.63	1.49	1.13	0.76	0.51	0.36	0.26	0.18	0.12
100	5	1.96	1.81	1.43	1.05	0.77	0.60	0.47	0.38	0.30
500	5	2.54	2.38	1.99	1.58	1.28	1.08	0.93	0.81	0.70
2	10	0.19	0.15	0.05	-0.03	-0.05	-0.06	-0.05	-0.04	-0.03
5	10	0.59	0.51	0.31	0.12	0.02	-0.02	-0.03	-0.03	-0.03
10	10	0.93	0.82	0.56	0.30	0.14	0.06	0.02	-0.00	-0.02
20	10	1.30	1.17	0.85	0.54	0.33	0.21	0.14	0.09	0.05
50	10	1.80	1.65	1.29	0.93	0.67	0.51	0.37	0.29	0.22
100	10	2.09	1.94	1.57	1.18	0.90	0.72	0.59	0.49	0.40
500	10	2.73	2.58	2.18	1.77	1.47	1.27	1.12	0.99	0.88

H1/A = 1.50   H2/A = 2.00   Z/H1 = 1.00

E1/E2	E2/E3	R/A=0.0	R/A=0.5	R/A=1.0	R/A=1.5	R/A=2.0	R/A=2.5	R/A=3.0	R/A=3.5	R/A=4.0
2	5	-0.81	-0.80	-0.46	-0.12	-0.08	-0.05	-0.03	-0.02	-0.01
5	5	-1.06	-1.03	-0.65	-0.24	-0.16	-0.09	-0.05	-0.02	-0.01
10	5	-1.30	-1.25	-0.83	-0.39	-0.26	-0.16	-0.09	-0.05	-0.02
20	5	-1.55	-1.49	-1.05	-0.57	-0.40	-0.27	-0.18	-0.11	-0.07
50	5	-1.89	-1.83	-1.36	-0.85	-0.65	-0.48	-0.36	-0.27	-0.19
100	5	-2.18	-2.11	-1.63	-1.10	-0.88	-0.70	-0.53	-0.42	-0.33
500	5	-2.70	-2.63	-2.14	-1.60	-1.36	-1.16	-0.99	-0.86	-0.75
2	10	-0.86	-0.85	-0.51	-0.16	-0.12	-0.09	-0.06	-0.05	-0.03
5	10	-1.13	-1.10	-0.71	-0.31	-0.21	-0.15	-0.10	-0.07	-0.04
10	10	-1.39	-1.34	-0.92	-0.47	-0.34	-0.23	-0.16	-0.11	-0.07
20	10	-1.67	-1.61	-1.16	-0.68	-0.51	-0.37	-0.27	-0.20	-0.16
50	10	-2.04	-1.98	-1.51	-0.99	-0.79	-0.62	-0.49	-0.39	-0.31
100	10	-2.32	-2.25	-1.77	-1.24	-1.02	-0.83	-0.69	-0.57	-0.47
500	10	-2.90	-2.82	-2.33	-1.79	-1.55	-1.35	-1.18	-1.04	-0.93

H1/A = 1.50   H2/A = 3.00   Z/H1 = 0.00

E1/E2	E2/E3	R/A=0.0	R/A=0.5	R/A=1.0	R/A=1.5	R/A=2.0	R/A=2.5	R/A=3.0	R/A=3.5	R/A=4.0
2	5	0.17	0.13	0.03	-0.05	-0.08	-0.06	-0.06	-0.05	-0.04
5	5	0.51	0.42	0.23	0.07	-0.04	-0.08	-0.08	-0.07	-0.06
10	5	0.81	0.70	0.44	0.19	0.04	-0.03	-0.05	-0.07	-0.07
20	5	1.15	1.02	0.71	0.40	0.20	0.10	0.02	-0.02	-0.04
50	5	1.55	1.40	1.05	0.69	0.44	0.29	0.20	0.13	0.08
100	5	1.88	1.73	1.36	0.97	0.70	0.53	0.41	0.32	0.25
500	5	2.49	2.33	1.94	1.53	1.24	1.03	0.89	0.77	0.67
2	10	0.16	0.12	0.03	-0.05	-0.08	-0.06	-0.07	-0.05	-0.04
5	10	0.52	0.44	0.25	0.07	-0.03	-0.07	-0.07	-0.06	-0.06
10	10	0.85	0.74	0.48	0.23	0.08	0.01	-0.02	-0.03	-0.04
20	10	1.19	1.06	0.75	0.44	0.24	0.13	0.07	0.03	0.01
50	10	1.65	1.50	1.15	0.78	0.54	0.38	0.28	0.21	0.15
100	10	1.98	1.83	1.46	1.07	0.80	0.62	0.50	0.41	0.33
500	10	2.67	2.51	2.12	1.71	1.41	1.21	1.06	0.94	0.83

H1/A = 1.50   H2/A = 3.00   Z/H1 = 1.00

E1/E2	E2/E3	R/A=0.0	R/A=0.5	R/A=1.0	R/A=1.5	R/A=2.0	R/A=2.5	R/A=3.0	R/A=3.5	R/A=4.0
2	5	-0.77	-0.76	-0.43	-0.09	-0.06	-0.04	-0.02	-0.02	-0.01
5	5	-1.01	-0.98	-0.60	-0.21	-0.12	-0.07	-0.03	-0.02	-0.01
10	5	-1.24	-1.19	-0.78	-0.34	-0.22	-0.13	-0.07	-0.03	-0.01
20	5	-1.48	-1.42	-0.98	-0.51	-0.35	-0.23	-0.14	-0.09	-0.05
50	5	-1.82	-1.76	-1.29	-0.78	-0.59	-0.43	-0.31	-0.23	-0.17
100	5	-2.08	-2.01	-1.54	-1.01	-0.80	-0.62	-0.48	-0.38	-0.30
500	5	-2.66	-2.59	-2.10	-1.56	-1.32	-1.12	-0.96	-0.83	-0.72
2	10	-0.81	-0.79	-0.46	-0.12	-0.09	-0.06	-0.05	-0.04	-0.03
5	10	-1.06	-1.03	-0.65	-0.25	-0.17	-0.11	-0.07	-0.05	-0.04
10	10	-1.30	-1.25	-0.84	-0.40	-0.28	-0.18	-0.12	-0.08	-0.06
20	10	-1.57	-1.51	-1.07	-0.60	-0.43	-0.31	-0.22	-0.16	-0.10
50	10	-1.93	-1.87	-1.40	-0.89	-0.69	-0.53	-0.41	-0.32	-0.25
100	10	-2.22	-2.15	-1.67	-1.15	-0.93	-0.75	-0.61	-0.50	-0.41
500	10	-2.84	-2.77	-2.28	-1.74	-1.50	-1.30	-1.13	-1.00	-0.89

TABLE 30

H1/A = 2.00   H2/A = 1.00   Z/H1 = 0.00

E1/E2	E2/E3	R/A=0.0	R/A=0.5	R/A=1.0	R/A=1.5	R/A=2.0	R/A=2.5	R/A=3.0	R/A=3.5	R/A=4.0
2	5	0.20	0.18	0.12	0.06	0.02	-0.00	-0.01	-0.02	-0.02
5	5	0.48	0.44	0.33	0.20	0.11	0.06	0.03	-0.00	-0.02
10	5	0.68	0.62	0.48	0.32	0.20	0.12	0.07	0.04	0.02
20	5	0.88	0.81	0.65	0.46	0.32	0.22	0.16	0.11	0.08
50	5	1.13	1.06	0.88	0.67	0.51	0.40	0.32	0.26	0.19
100	5	1.26	1.18	1.00	0.78	0.61	0.50	0.41	0.34	0.29
500	5	1.57	1.50	1.30	1.08	0.90	0.77	0.68	0.60	0.54
2	10	0.26	0.23	0.17	0.10	0.05	0.03	0.01	0.01	-0.01
5	10	0.54	0.49	0.38	0.25	0.16	0.10	0.06	0.04	0.02
10	10	0.77	0.71	0.57	0.40	0.28	0.19	0.14	0.10	0.07
20	10	1.00	0.93	0.76	0.58	0.43	0.33	0.26	0.21	0.17
50	10	1.22	1.15	0.96	0.76	0.59	0.48	0.39	0.33	0.28
100	10	1.38	1.30	1.11	0.90	0.72	0.60	0.51	0.44	0.39
500	10	1.68	1.61	1.41	1.19	1.01	0.88	0.79	0.72	0.65

H1/A = 2.00   H2/A = 1.00   Z/H1 = 1.00

E1/E2	E2/E3	R/A=0.0	R/A=0.5	R/A=1.0	R/A=1.5	R/A=2.0	R/A=2.5	R/A=3.0	R/A=3.5	R/A=4.0
2	5	-0.80	-0.79	-0.47	-0.14	-0.00	-0.08	-0.05	-0.03	-0.01
5	5	-0.96	-0.95	-0.60	-0.25	-0.19	-0.14	-0.09	-0.06	-0.03
10	5	-1.10	-1.08	-0.73	-0.36	-0.28	-0.21	-0.15	-0.10	-0.07
20	5	-1.25	-1.22	-0.86	-0.47	-0.38	-0.30	-0.23	-0.17	-0.13
50	5	-1.45	-1.42	-1.05	-0.64	-0.53	-0.44	-0.36	-0.29	-0.23
100	5	-1.56	-1.53	-1.16	-0.76	-0.65	-0.55	-0.46	-0.39	-0.33
500	5	-1.84	-1.82	-1.44	-1.04	-0.92	-0.82	-0.72	-0.64	-0.58
2	10	-0.86	-0.85	-0.52	-0.19	-0.00	-0.11	-0.08	-0.06	-0.04
5	10	-1.04	-1.03	-0.68	-0.32	-0.26	-0.20	-0.15	-0.11	-0.07
10	10	-1.20	-1.18	-0.82	-0.44	-0.36	-0.28	-0.22	-0.17	-0.13
20	10	-1.37	-1.34	-0.98	-0.59	-0.49	-0.41	-0.33	-0.27	-0.22
50	10	-1.54	-1.51	-1.14	-0.74	-0.64	-0.54	-0.46	-0.38	-0.32
100	10	-1.67	-1.64	-1.27	-0.87	-0.76	-0.66	-0.57	-0.49	-0.43
500	10	-1.96	-1.93	-1.55	-1.15	-1.04	-0.93	-0.83	-0.75	-0.68

H1/A = 2.00   H2/A = 2.00   Z/H1 = 0.00

E1/E2	E2/E3	R/A=0.0	R/A=0.5	R/A=1.0	R/A=1.5	R/A=2.0	R/A=2.5	R/A=3.0	R/A=3.5	R/A=4.0
2	5	0.16	0.13	0.08	0.02	-0.02	-0.03	-0.03	-0.03	-0.03
5	5	0.40	0.36	0.25	0.14	0.06	0.02	-0.00	-0.01	-0.02
10	5	0.60	0.54	0.40	0.25	0.14	0.07	0.03	0.01	-0.00
20	5	0.80	0.74	0.58	0.40	0.26	0.17	0.11	0.08	0.05
50	5	1.07	1.00	0.82	0.62	0.46	0.35	0.28	0.20	0.16
100	5	1.22	1.14	0.96	0.75	0.58	0.46	0.38	0.31	0.26
500	5	1.55	1.47	1.28	1.06	0.88	0.75	0.66	0.59	0.53
2	10	0.16	0.14	0.08	0.03	-0.01	-0.02	-0.02	-0.02	-0.02
5	10	0.43	0.38	0.27	0.16	0.08	0.03	0.01	0.00	-0.01
10	10	0.66	0.60	0.46	0.31	0.19	0.12	0.08	0.06	0.04
20	10	0.89	0.82	0.66	0.48	0.34	0.25	0.19	0.15	0.12
50	10	1.14	1.07	0.89	0.69	0.53	0.42	0.34	0.28	0.24
100	10	1.32	1.24	1.06	0.85	0.68	0.56	0.47	0.41	0.35
500	10	1.66	1.59	1.39	1.17	0.99	0.87	0.77	0.70	0.64

H1/A = 2.00   H2/A = 2.00   Z/H1 = 1.00

E1/E2	E2/E3	R/A=0.0	R/A=0.5	R/A=1.0	R/A=1.5	R/A=2.0	R/A=2.5	R/A=3.0	R/A=3.5	R/A=4.0
2	5	-0.74	-0.74	-0.42	-0.10	-0.00	-0.06	-0.04	-0.03	-0.02
5	5	-0.90	-0.89	-0.55	-0.20	-0.15	-0.11	-0.08	-0.05	-0.03
10	5	-1.04	-1.02	-0.67	-0.31	-0.24	-0.18	-0.13	-0.09	-0.06
20	5	-1.19	-1.17	-0.81	-0.43	-0.34	-0.26	-0.20	-0.15	-0.12
50	5	-1.39	-1.36	-0.99	-0.60	-0.50	-0.41	-0.33	-0.27	-0.21
100	5	-1.53	-1.50	-1.13	-0.73	-0.62	-0.53	-0.44	-0.37	-0.31
500	5	-1.83	-1.80	-1.43	-1.02	-0.91	-0.80	-0.71	-0.63	-0.56
2	10	-0.78	-0.78	-0.46	-0.13	-0.00	-0.09	-0.07	-0.05	-0.04
5	10	-0.96	-0.94	-0.61	-0.25	-0.20	-0.16	-0.12	-0.09	-0.07
10	10	-1.11	-1.10	-0.75	-0.38	-0.30	-0.24	-0.19	-0.14	-0.11
20	10	-1.27	-1.25	-0.89	-0.50	-0.42	-0.34	-0.27	-0.21	-0.18
50	10	-1.48	-1.46	-1.09	-0.69	-0.59	-0.50	-0.42	-0.35	-0.29
100	10	-1.63	-1.60	-1.23	-0.83	-0.72	-0.62	-0.54	-0.46	-0.40
500	10	-1.94	-1.91	-1.54	-1.13	-1.02	-0.91	-0.82	-0.74	-0.67

TABLE 31

H1/A = 2.00   H2/A = 3.00   Z/R1 = 0.00

E1/E2	E2/E3	R/A=0.0	R/A=0.5	R/A=1.0	R/A=1.5	R/A=2.0	R/A=2.5	R/A=3.0	R/A=3.5	R/A=4.0
2	5	0.13	0.11	0.05	0.00	-0.02	-0.04	-0.04	-0.04	-0.03
5	5	0.37	0.33	0.22	0.11	0.03	-0.01	-0.03	-0.04	-0.04
10	5	0.57	0.51	0.38	0.23	0.12	0.06	0.02	-0.01	-0.02
20	5	0.76	0.69	0.53	0.36	0.22	0.14	0.08	0.05	0.02
50	5	1.02	0.95	0.77	0.57	0.42	0.31	0.24	0.17	0.13
100	5	1.18	1.10	0.92	0.71	0.54	0.43	0.35	0.28	0.24
500	5	1.53	1.45	1.26	1.04	0.86	0.74	0.65	0.57	0.51
2	10	0.14	0.11	0.06	0.00	-0.02	-0.04	-0.04	-0.04	-0.03
5	10	0.38	0.34	0.23	0.12	0.04	0.00	-0.01	-0.02	-0.02
10	10	0.59	0.54	0.40	0.25	0.14	0.07	0.04	0.02	0.01
20	10	0.82	0.75	0.59	0.41	0.28	0.19	0.14	0.10	0.07
50	10	1.08	1.01	0.83	0.63	0.47	0.36	0.29	0.23	0.19
100	10	1.27	1.19	1.01	0.80	0.63	0.51	0.43	0.37	0.31
500	10	1.64	1.56	1.37	1.15	0.97	0.84	0.75	0.68	0.62

H1/A = 2.00   H2/A = 3.00   Z/H1 = 1.00

E1/E2	E2/E3	R/A=0.0	R/A=0.5	R/A=1.0	R/A=1.5	R/A=2.0	R/A=2.5	R/A=3.0	R/A=3.5	R/A=4.0
2	5	-0.72	-0.71	-0.40	-0.08	-0.00	-0.04	-0.03	-0.02	-0.02
5	5	-0.87	-0.86	-0.52	-0.18	-0.13	-0.09	-0.06	-0.04	-0.03
10	5	-1.01	-0.99	-0.64	-0.28	-0.21	-0.15	-0.11	-0.07	-0.05
20	5	-1.16	-1.13	-0.78	-0.40	-0.32	-0.24	-0.18	-0.13	-0.10
50	5	-1.35	-1.32	-0.96	-0.56	-0.47	-0.38	-0.30	-0.24	-0.19
100	5	-1.49	-1.47	-1.10	-0.70	-0.60	-0.50	-0.42	-0.35	-0.29
500	5	-1.81	-1.79	-1.41	-1.01	-0.89	-0.79	-0.70	-0.62	-0.55
2	10	-0.75	-0.74	-0.43	-0.11	-0.00	-0.07	-0.05	-0.04	-0.03
5	10	-0.91	-0.89	-0.56	-0.21	-0.17	-0.12	-0.09	-0.07	-0.05
10	10	-1.06	-1.04	-0.69	-0.33	-0.26	-0.19	-0.14	-0.11	-0.08
20	10	-1.21	-1.19	-0.82	-0.45	-0.37	-0.30	-0.23	-0.18	-0.14
50	10	-1.43	-1.40	-1.03	-0.64	-0.54	-0.45	-0.37	-0.31	-0.26
100	10	-1.59	-1.56	-1.19	-0.79	-0.68	-0.59	-0.50	-0.43	-0.37
500	10	-1.92	-1.89	-1.52	-1.11	-1.00	-0.89	-0.80	-0.72	-0.65